MODULATION OF NETWORK OSCILLATIONS BY BRAIN STIMULATION

Stephen L. Schmidt

A dissertation submitted to the faculty of the University of North Carolina at Chapel Hill in partial fulfillment of the requirements for the degree of Doctor of Philosophy in the Biomedical Engineering Department.

Chapel Hill
2016

Approved by:

Flavio Frohlich

Shawn Gomez

Angel Peterchev

Anne Taylor

Hae Won Shin

ABSTRACT

Stephen L. Schmidt: Modulation of network oscillations by brain stimulation
(Under the direction of Flavio Frohlich)

Finding new and effective treatments for mental illness represents one of the largest challenges of our time due the large number of people affected. Despite long and careful study there have been few recent breakthroughs in pharmacological treatments of mental illness. To address this, the National Institute of Mental Health (NIMH) has recently begun to focus on the investigation of network level correlates of mental illnesses. Patients with mental illness often exhibit aberrant neural oscillatory activity, thus making the network level a promising scale for the identification of measureable neural correlates of mental illnesses. At the network level, neural activity is primarily in the form of cortical oscillations which may be recorded noninvasively with electroencephalography (EEG). Such EEG oscillations are the result of synchronized activity from many cells in the neocortex. However the exact mechanisms of how oscillations arise and spread throughout the brain remain unknown. Non-invasive brain stimulation is a promising treatment modality because it specifically targets activity of brain networks. Unlike pharmacological treatments, stimulation with electric and magnetic fields directly targets electrical activity of many cells in a network. In particular, transcranial alternating current stimulation appears to be especially suited for targeting oscillations in brain networks. Despite the promise of these brain stimulation techniques, the underlying mechanisms remain unknown.

The studies presented in this dissertation address two critical gaps in the treatment of mental illnesses. (1) How does rhythmic network activity arise from cellular and synaptic components? And (2) how does brain stimulation interact with ongoing network activity? Only by understanding how network activity arises and how it interacts with brain stimulation we may begin to design brain stimulation paradigms for treatment of mental illness.

ACKNOWLEDGEMENTS

First I would like to thank my mentor and advisor, Flavio Frohlich who taught me many things including how to perform scientific experiments and how to make bananas flambé. Flavio took a chance on someone with a questionable academic record; I like to think it has turned out pretty well for both of us.

I would like to thank my committee: Angel Peterchev, Anne Taylor, Hae Won Shin and Shawn Gomez for their valuable input. Charlene Santos and Mark Ross have provided countless hours of managing the animal colony, Vladimir Ghukasyan for providing the microscopy core, and Hyung Kim for genotyping results in less than 48 hours.

I also thank all current and past members of the Frohlich Lab for their scientific input and making the lab a fun place to work. In particular I would like to thank Apoorva Iyengar, Alban Foulser, Chris Dorsett, Davis Bennet, Erin Chew, Ehsan Negahbani, Mohammad Hammad, Nadia Mishal and Sarah Schoenrock who performed many of the *in vitro* experiments. Also I want to thank Sankar Alagapan who took some ECoG recordings from the beginning of a project and turned it into something really special.

I also thank my parents for teaching me the value of hard work. Finally I thank Elizabeth McSweeney for her endless support and for convincing me that pursuing science was an option for me in the first place.

PREFACE

All the work presented here was part of a group effort. I have been extremely lucky to work with capable and affable colleagues. In this preface I list the work performed by each contributor. Chapter 2: Flavio Frohlich and Stephen L. Schmidt designed experiments, analyzed the data and wrote the paper; Davis V. Bennet, Erin Y. Chew, Mohamad A. Hammad and Flavio Frohlich performed the experiments. Chapter 3: Flavio Frohlich and Stephen L. Schmidt designed the experiments and wrote the paper. Stephen L. Schmidt analyzed the data. Apoorva K. Iyengar, Christopher R. Dorsett, and Stephen L. Schmidt performed the experiments. Chapter 4: Flavio Frohlich and Stephen L. Schmidt designed the experiments and wrote the paper. A. Alban Foulser, Apoorva K Iyengar and Stephen L. Schmidt performed the experiments. Stephen L. Schmidt analyzed the data. Michael R. Boyle validated the analysis code. Chapter 5: Flavio Frohlich, Hae Won Shin, Sankaraleengam Alagapan and Stephen L. Schmidt designed the experiments. Eldad Hadar, Hae Won Shin, Sankaraleengam Alagapan, and Stephen L. Schmidt performed the experiments. Sankaraleengam Alagapan analyzed the data. Flavio Frohlich, Hae Won Shin, Jeremie Lefebvre, Sankaraleengam Alagapan and Stephen L Schmidt wrote the paper. Jeremie Lefebvre developed and analyzed the network model. Flavio Frohlich and Sankaraleengam Alagapan developed the summation model. Chapter 6 is a section of a book chapter written by Flavio Frohlich, Sankaraleengam Alagapan, Michael R. Boyle, Franz Hamilton, Guoshi Li, Caroline Lustenberger and Stephen L. Schmidt. The section included as Chapter 6 was written by Flavio Frohlich and Stephen L. Schmidt.

TABLE OF CONTENTS

LIST OF TABLES

LIST OF FIGURES

LIST OF ABBREVIATIONS

AC	Alternating current
ACh	Acetylcholine
aCSF	Artificial cerebral spinal fluid
AMPA	α-amino-3-hydroxy-5-methyl-4-isoxazolepropionic acid
ANOVA	Analysis of variance
ApEn	Approximate entropy
BDNF	Brain-derived neurotropic factor
CA3	Cornu Ammonis region 3
CCEP	Cortico-cortical evoked potential
CCh	Carbachol
ChR2	Channelrhodopsin 2
DC	Direct current
DSM	Diagnostic and Statistical Manual of Mental Disorders
ECoG	Electrocorticography
EEG	Electroencephalogram
EF	Electric Field
eYFP	Enhanced yellow fluorescent protein
FDA	Food and Drug Administration
FR	Firing rate
GABA	γ-aminobutyric acid
HCN	Hyperpolarization-activated cyclic nucleotide-gated
IAF	Individualized alpha frequency
Kv7	Voltage-gated slowly inactivating potassium
LTD	Long term depression
LTP	Long term potentiation
LV PYs	Layer 5 pyramidal cells

MEA	Multi-electrode array
MI	Modulation index
mPFC	Medial prefrontal cortex
MU	Multiunit
NE	Norepinephrine
NIMH	National Institute of Mental Health
NMDA	N-methyl-D-aspartic acid
PCA	Principal component analysis
PPF	Paired pulse facilitation
PSD	Power spectral density
PV	Parvalbumin
RDoC	Research Domain Criteria
SU	Single unit
tACS	Transcranial alternating current stimulation
tCS	Transcranial current stimulation
tDCS	Transcranial direct current stimulation
Thy1	Thy-1 cell surface antigen
TMS	Transcranial magnetic stimulation
V1	Primary visual cortex
ZAP	Impedance amplitude profile

CHAPTER 1: INTRODUCTION

In the US, mental illness affects as much as 32.4 percent of the population (Bagalman & Napili, 2015). The cost of treatment, disability benefits, and lost wages total in the US $317.6 billion annually (T. R. Insel, 2008). Despite the large sum spent on mental health, patients with mental illness have a higher mortality rate; 1.2 to 4.9 times that of healthy individuals (Colton & Manderscheid, 2006). Together these data demonstrate that mental health is widely recognized issue but that there is a need for improved treatment of disease. The lack of clear diagnoses is a large contributing factor to the state of mental health treatment. A recent study found that nine of twenty-three types of mental illnesses were diagnosed with questionable or unacceptable consistency between clinicians in the same academic center (Regier et al., 2013). Incorrect diagnosis often results in ineffective treatment. Such variability in diagnoses is due in part to the lack of defined measureable indicators of disease, for most mental illnesses. To address this issue, the National Institute of Mental Health has recently adopted the research domain criteria (RDoC) project. Using RDoC, network brain activity correlates of disease may be identified using electrophysiological or functional neuroimaging methods (T. Insel et al., 2010). The use of quantifiable measures in disease identification should reduce diagnostic variability between clinicians, limiting dollars spent on ineffective treatments and improving patient health. This new paradigm of diagnosis and treatments based on aberrant network activity rather than behavioral criteria alone is still in its early stages.

The RDoC framework specifically aims to identify pathological network activity which can be measured in patients with mental illness. The scale of networks was specifically chosen because it can be measured in both healthy participants and in patients with mental illness *in situ*. However the brain is a complex system which spans many spatial scales (Frohlich, 2014) across ten orders of magnitude from organic and inorganic molecules, measured in Å, to behavior on the scale of meters. Molecules interact with receptors and ion channels to affect the activity of cells in the brain, neurons and glia. Neurons

organize into networks comprised of a few to hundreds of cells (Buzsáki, 2006). Small networks can control the most rudimentary of behaviors such as automatic breath expiration control. However for complex behaviors, networks organize into brain areas which work together to integrate multi-sensory stimuli and memory into responses (Prabhakaran, Smith, Desmond, Glover, & Gabrieli, 1997). In addition to the broad spatial scale of neural activity, the brain functions both as an electrical and chemical system. For example, molecules which bind to the receptors in cell membrane may simply open a channel allowing ions to flow down their concentration gradient causing a change in the voltage across the cell membrane or start a signaling cascade which alters the biochemistry within the cell. Such complexity means that fully described disease pathology and treatment should be understood at the levels of genes and proteins through biomolecular and electrical activities of cells to electrical activities of networks and brain areas finally to output behaviors. The RDoC framework specifically aims to find correlates of disease at the level of networks, particularly those which can be measured with non-invasive measures. Such network activity may represent a middle ground to bridge the gap between behavior and biomolecular activity. In addition to aiding diagnosis in future versions of the DSM, the RDoC approach aims to relate aberrant network-level activity to the underlying biomolecular changes.

In line with the RDoC framework, the work presented here focuses on electrical activity of networks of neurons. At the scale of networks, neural activity is often measured in the form of network oscillations. Such oscillations are rhythmic fluctuations in electric fields generated by neurons. Cortical oscillations were first discovered by measuring small changes in voltages as measured by EEG (Berger, 1929). To date there is only one EEG oscillation based diagnostic aid for certain types of ADHD (Snyder, Rugino, Hornig, & Stein, 2015) however there are numerous possible disease correlates under test based on EEG oscillations. Network oscillations are typically recorded in frequencies between 0.1 Hz to 100 Hz. Such oscillations arise from the average of synaptic activity in a small area (Buzsaki, Anastassiou, & Koch, 2012). When many neurons are synchronized an oscillating electric field is formed. However, cortical oscillations are not simply the output of synchronized activity; they play a functional role as well. Electric fields similar to those caused by cortical oscillations have been shown to influence the activity of networks (Frohlich & McCormick, 2010) and individual cells within the network (Radman, Su, An, Parra, & Bikson, 2007). These studies provide evidence that network oscillations perturb the ongoing network

activity and recruit more cells to the oscillation. Such oscillations facilitate neuronal interaction by bringing neurons closer to action potential threshold simultaneously (Steriade, Nunez, & Amzica, 1993), which allows communication between the cells in the network (Womelsdorf, Valiante, Sahin, Miller, & Tiesinga, 2014). Network oscillations therefore synchronize cells within a network and between networks to facilitate information transfer.

To date, most interventions for mental illness have focused on behavioral therapy or pharmacological interventions. Behavioral therapy can help patients change pathological behavior but does not directly address the underlying brain activity causing the behaviors. Conversely, pharmacological interventions aim to address the underlying neurobiology but can have limited or off-target effects. For example, as many as 60% of patients who receive pharmacological treatment for depression do not have an adequate response to antidepressants (Fava, 2003). However, non-invasive brain stimulation has recently emerged as a network-level intervention for the treatment of psychiatric diseases. Such non-invasive stimulation affects networks or regions within the brain to change electrical activity. Network-level interventions are particularly appealing for treatment of disease for two reasons. First, network electrical activity has been correlated with behavior (Wang, 2010). Second, network activity may be directly measured both in healthy participants and patients with mental illness with EEG. In particular, transcranial magnetic stimulation (TMS) has been approved by the FDA for the treatment of depression (O'Reardon et al., 2007). TMS provides a supra-threshold stimulus to neurons in a relatively small region in the brain via targeted magnetic fields. Non-invasive stimulation with weak electrical currents has also shown promise as a safe and effective intervention for modulating network neural activity. Transcranial direct current stimulation (tDCS) is the application of constant current to the brain though electrodes on the scalp. In contrast to TMS, tDCS provides a subthreshold change in the resting membrane potential over a large area of the neocortex. Such change in polarization can be measured indirectly with motor evoke potentials. Indeed tDCS can modulate the excitability of neurons as measured by motor evoked potentials (Nitsche & Paulus, 2000). While individual studies have found cognitive effects of tDCS, a recent review has found that across 59 studies of the effect of tDCS on cognition, tDCS has yet to produce reliable effects on cognition in healthy participants (Horvath, Forte, & O, 2015). By comparison, transcranial alternating current stimulation (tACS) applies sinusoidal current with a given

frequency for the targeted manipulation of cortical oscillations. TACS has been shown to modulate such complex behaviors as creativity (Lustenberger, Boyle, Foulser, Mellin, & Frohlich, 2015) and lucid dreaming (Voss et al., 2014). While behavioral effects can be seen in human participants, recording EEG during tACS stimulation is difficult. The current from tACS produces voltages across the scalp which are then recorded by the EEG. If the neural activity is entrained by the stimulation, the artifact from tACS should be frequency matched to the underlying neural activity. Due to this and to the modulation of the stimulation artifact by physiological signals such as heartbeat and breathing (Noury, Hipp, & Siegel, 2016) the stimulation artifact may not be easily removed by filtering. Therefore invasive electrophysiological and neuroimaging studies using animal models have provided insights into the mechanism of action of transcranial current stimulation. The tACS artifact may be removed from invasive electrophysiological recordings because action potentials may be recorded. Action potentials lie in a different frequency band from most frequencies used in most tACS paradigms and therefore the artifact may be removed by high pass filtering. By removal of the tACS artifact, invasive electrophysiology may elucidate the mechanism by which weak electric fields influence neural activity.

Work conducted using *in vitro* electrophysiology has provided a putative mechanism of action for stimulation with weak electric fields. When applied in parallel to the somato-dendritic axis of a cell, the cell membrane becomes slightly depolarized making the cell more likely to fire (Chan, Hounsgaard, & Nicholson, 1988). The depolarization caused by transcranial current stimulation is not large enough to evoke spiking activity in a cell at rest, however over a large population, many cells will be near the threshold for firing and the small depolarization from stimulation can cause the cells to fire (Bikson et al., 2004). Recent work has suggested that such mechanism of the effect of direct current stimulation may be too simplified (Rahman et al., 2013) and that glia, in addition to neurons may contribute to the effect of stimulation in the intact animal (Monai et al., 2016). Indeed the effect of tDCS in humans is dependent on the pharmacological tone of the subject (Nitsche et al., 2003). Nitsche and colleagues therefore suggest that plastic mechanisms are recruited either directly or indirectly by tDCS. *In vitro* examination of stimulation with dynamic electric fields mimicking tACS was shown to synchronize firing of cells within a network (Radman et al., 2007); however the strength of the effect was reduced as the frequency of stimulation was increased (Deans, Powell, & Jefferys, 2007). This work has led to the hypothesis that

transcranial current stimulation entrains networks. In this case several criteria must be met (Thut, Schyns, & Gross, 2011). First the stimulation must directly affect the network. Secondly, the stimulation must not instantaneously reset the phase of the ongoing oscillation but subtly change it to match the frequency of the stimulation over time. Once entrained, the network will match the frequency of the stimulation with some constant phase delay. Computational models have suggested that sinusoidal stimulation results in entrainment of networks by demonstrating an Arnold tongue response (Ali, Sellers, & Frohlich, 2013). An Arnold tongue is a property of coupled harmonic oscillators where an oscillator can become entrained to a periodic stimulus based on the amplitude and frequency of the stimulus. For small amplitude stimuli, entrainment occurs only when the frequency is matched to the endogenous frequency of the oscillator. As stimulus amplitude increases, the range of frequencies which entrain the oscillator become larger. Very high amplitude stimuli are therefore able to entrain the network to any frequency, but this amplitude is likely much greater than the subthreshold stimulus given by tACS. When tACS is applied it is generally assumed that the stimulus is near enough to the endogenous oscillation to entrain it to match the frequency of the stimulation. To date the hypothesis that tACS can entrain the ongoing neural oscillation has only been tested with visual stimulus (Notbohm, Kurths, & Herrmann, 2016) or indirectly with tACS by comparing short bursts of stimulation to stimulation with longer duration (Vossen, Gross, & Thut, 2015).

In addition to identification of pathological network level activity, the RDoC framework places value on relating network phenomena to the underlying cellular mechanisms and ultimately to the genetic and epigenetic underpinnings of disease. By regulation of translation the number and location of membrane bound proteins may be controlled. Such proteins change the electrical activities of cells which in turn effect the entire network. Here, I present two studies relating network activity to the underlying activation of receptors and ion channels. Neurons express a large variety of receptors and ion channels which are exposed on both sides of the cell membrane. Receptors may be broadly classified into two groups, metabotropic and ionotropic receptors. Metabotropic receptors do not allow molecules or ions to pass the cell membrane; instead extracellular molecules bind to metabotropic receptors which start a signaling cascade on the intracellular side of the cell. For example acetylcholine receptors may bind any cholinergic agonist which causes a number of downstream effects such as suppression of the slowly inactivating inward potassium current (Brown & Adams, 1980). There are a wide variety of metabotropic

receptors, many of which have unknown functions in the central nervous system (Jassal et al., 2010). Metabotropic receptors are the targets of roughly half of all prescription drugs (Gudermann, Nurnberg, & Schultz, 1995). Conversely, ion channels (including ionotropic receptors) allow ions to pass through the cell membrane along their concentration gradient. Ion channels can be voltage gated, opening and closing based on the voltage across the cell membrane; ligand gated, opening only when a molecule is bound to the channel; or both. For example the hyperpolarization activated cyclic nucleotide gated (HCN) channel requires the binding of cyclic adenosine monophosphate (cAMP) and a sufficiently hyperpolarized membrane potential to allow the flow of K^+ ions into the cell (Robinson & Siegelbaum, 2003). Such ion channel and receptor activity sets the state of the neurons in a network. For example noradrenergic activation can set network activity to awake state activity from resting state activity (Constantinople & Bruno, 2011).

Much of the work I present here was performed in cortical slices. In this method, live sections of neocortex are isolated and the supra-threshold spiking activity recorded. The slices are provided nutrients through a continuous flow of artificial cerebral spinal fluid (aCSF) into the recording chamber. Pharmacological agents may be added to the aCSF allowing the examination of the effect of the agent on neurons. Multielectrode array (MEA) recordings record spiking activity of cells within a short distance from the electrode. Technological advances have made it possible to record from acute cortical slices rather than cultures grown directly on electrodes (Egert, Heck, & Aertsen, 2002). Slices of extracted tissue offer an advantage over experiments with neuron cultures grown directly on the recording electrodes. Specifically connectivity of neural cell cultures grown directly on electrodes is often non-physiological and results in seizure-like activity patterns (Gluckman, Nguyen, Weinstein, & Schiff, 2001). Because the activity on any electrode may originate from several cells, it is termed multiunit (MU) activity. Traditionally, each action potential is considered an all-or-none event, indicating that each action potential from a given cell should have the same waveform but waveforms should differ between cells. However, for comparison between individual cells single units (SU) may be isolated by examination of the shape of the spikes using a clustering algorithm (Fee, Mitra, & Kleinfeld, 1996). Each SU is presumed to be an individual cell within the network of the slice. Acute cortical slices preserve the connectivity of the *in vivo* network in two dimensions; however the experimental conditions of a typical slice preparation suppress spontaneous

activity so that the dynamics of individual cells may be studied in isolation (Sanchez-Vives & McCormick, 2000). To overcome this lack of spontaneous activity, artificial cerebral spinal fluid (aCSF) which more closely resembles the ion concentrations found in the cerebral spinal fluid *in vivo* has been used. Critically, the magnesium and calcium ion concentrations are reduced from 2 mM in found in most slice preparations to 1 mM which has been shown to lead to spontaneous activity in the form of slow oscillations (Sanchez-Vives & McCormick, 2000). Such spontaneous activity is critical for evaluation of the effect of stimulation on networks.

Optogenetic stimulation provides an interesting avenue to study the mechanisms of network activity and brain stimulation in animal models (Frohlich & Schmidt, 2013). With this technique, a gene is inserted into the genome of a specific type of neuron or specific region which cause the cells to express a light sensitive ion channel, Channelrhodopsin-2 (ChR2). When stimulated with blue light (460 nm), the ChR2 channel opens and allows ions to flow out of the cell, which depolarizes the cell (Zhang, Wang, Boyden, & Deisseroth, 2006). With sufficient light intensity at the cell soma, such depolarizations can be great enough to evoke supra-threshold spiking activity in the cells which are stimulated. Here, I have utilized Thy1-ChR2 mouse line which expresses ChR2 in a large portion of layer 5 pyramidal cells (L5 PYs) throughout the neocortex (Arenkiel et al., 2007). When stimulated with blue light, many L5 cells depolarize and fire spikes in response to the stimulation. Such cell type specificity allows the dissection of the role of individual cell types within the network. For example, L5 PYs are critical to slow oscillations in neocortex and have been shown to fire first during the UP (or depolarized) phase of the oscillation (Chauvette, Volgushev, & Timofeev, 2010; Sanchez-Vives & McCormick, 2000). However with optogenetic activation of many of these cells, UP states may be triggered which are similar to naturally occurring UP states, demonstrating that stimulation of these cells is sufficient for the cortical UP state (Beltramo et al., 2013). This finding provided the basis for recruitment of network oscillations *in vitro* presented here. While the aCSF allowed for spontaneous activity, without optogenetic stimulation cells within the network remained relatively independent. However, with optogenetic stimulus many cells were recruited to the network oscillation which are often lacking from *in vitro* preparations.

The work presented here is conceptually divided into two parts: (1) study of the contribution of individual ion channel species on network activity with a focus on rhythmic activity, and (2) the effect of

brain stimulation on cortical networks. First, I present a study concerned with network dynamics in response to activation of cholinergic and noradrenergic signaling (Chapter 2). Chapter 3 focuses on the interaction of ion channels and synaptic transmission in the resonant response of networks to supra-threshold stimulation of L5 PYs. I then present two studies regarding the effect of brain stimulation on cortical networks. In Chapter 4, I present a study which examines the effect of stimulation with electric fields on a network with an endogenous oscillation evoked by optogenetic stimulus. I then further examine the interaction of endogenous oscillations and brain stimulation in human participants (Chapter 5). I provide a review of animal experiments focusing on the mechanisms which underlie the effects of electric field stimulation (Chapter 6). Finally, I provide a brief discussion in Chapter 7.

REFERENCES

Ali, M. M., Sellers, K. K., & Frohlich, F. (2013). Transcranial alternating current stimulation modulates large-scale cortical network activity by network resonance. *The Journal of neuroscience : the official journal of the Society for Neuroscience, 33*(27), 11262-11275. doi:10.1523/JNEUROSCI.5867-12.2013

Arenkiel, B. R., Peca, J., Davison, I. G., Feliciano, C., Deisseroth, K., Augustine, G. J., . . . Feng, G. (2007). In vivo light-induced activation of neural circuitry in transgenic mice expressing channelrhodopsin-2. *Neuron, 54*(2), 205-218. doi:10.1016/j.neuron.2007.03.005

Bagalman, E., & Napili, A. (2015). *Prevalence of Mental Illness in the United States: Data Sources and Estimates*. Retrieved from

Beltramo, R., D'Urso, G., Dal Maschio, M., Farisello, P., Bovetti, S., Clovis, Y., . . . Fellin, T. (2013). Layer-specific excitatory circuits differentially control recurrent network dynamics in the neocortex. *Nature neuroscience, 16*(2), 227-234. doi:10.1038/nn.3306

Berger, H. (1929). Über das Elektrenkephalogramm des Menschen. *Archiv für Psychiatrie und Nervenkrankheiten, 87*(1), 527-570.

Bikson, M., Inoue, M., Akiyama, H., Deans, J. K., Fox, J. E., Miyakawa, H., & Jefferys, J. G. (2004). Effects of uniform extracellular DC electric fields on excitability in rat hippocampal slices in vitro. *The Journal of physiology, 557*(Pt 1), 175-190. doi:10.1113/jphysiol.2003.055772

Brown, D. A., & Adams, P. R. (1980). Muscarinic suppression of a novel voltage-sensitive K+ current in a vertebrate neurone. *Nature, 283*(5748), 673-676.

Buzsáki, G. (2006). *Rhythms of the brain*. Oxford ; New York: Oxford University Press.

Buzsaki, G., Anastassiou, C. A., & Koch, C. (2012). The origin of extracellular fields and currents--EEG, ECoG, LFP and spikes. *Nat Rev Neurosci, 13*(6), 407-420. doi:10.1038/nrn3241

Chan, C. Y., Hounsgaard, J., & Nicholson, C. (1988). Effects of electric fields on transmembrane potential and excitability of turtle cerebellar Purkinje cells in vitro. *The Journal of physiology, 402*, 751-771.

Chauvette, S., Volgushev, M., & Timofeev, I. (2010). Origin of active states in local neocortical networks during slow sleep oscillation. *Cerebral cortex, 20*(11), 2660-2674. doi:10.1093/cercor/bhq009

Colton, C. W., & Manderscheid, R. W. (2006). Congruencies in increased mortality rates, years of potential life lost, and causes of death among public mental health clients in eight states. *Prev Chronic Dis, 3*(2), A42.

Constantinople, C. M., & Bruno, R. M. (2011). Effects and mechanisms of wakefulness on local cortical networks. *Neuron, 69*(6), 1061-1068. doi:10.1016/j.neuron.2011.02.040

Deans, J. K., Powell, A. D., & Jefferys, J. G. (2007). Sensitivity of coherent oscillations in rat hippocampus to AC electric fields. *The Journal of physiology, 583*(Pt 2), 555-565. doi:10.1113/jphysiol.2007.137711

Egert, U., Heck, D., & Aertsen, A. (2002). Two-dimensional monitoring of spiking networks in acute brain slices. *Experimental brain research. Experimentelle Hirnforschung. Experimentation cerebrale, 142*(2), 268-274. doi:10.1007/s00221-001-0932-5

Fava, M. (2003). Diagnosis and definition of treatment-resistant depression. *Biological psychiatry, 53*(8), 649-659.

Fee, M. S., Mitra, P. P., & Kleinfeld, D. (1996). Automatic sorting of multiple unit neuronal signals in the presence of anisotropic and non-Gaussian variability. *Journal of neuroscience methods, 69*(2), 175-188. doi:10.1016/S0165-0270(96)00050-7

Frohlich, F. (2014). Endogenous and exogenous electric fields as modifiers of brain activity: rational design of noninvasive brain stimulation with transcranial alternating current stimulation. *Dialogues in clinical neuroscience, 16*(1), 93-102.

Frohlich, F., & McCormick, D. A. (2010). Endogenous electric fields may guide neocortical network activity. *Neuron, 67*(1), 129-143. doi:10.1016/j.neuron.2010.06.005

Frohlich, F., & Schmidt, S. L. (2013). Rational design of transcranial current stimulation (TCS) through mechanistic insights into cortical network dynamics. *Frontiers in human neuroscience, 7*, 804. doi:10.3389/fnhum.2013.00804

Gluckman, B. J., Nguyen, H., Weinstein, S. L., & Schiff, S. J. (2001). Adaptive electric field control of epileptic seizures. *The Journal of neuroscience : the official journal of the Society for Neuroscience, 21*(2), 590-600.

Gudermann, T., Nurnberg, B., & Schultz, G. (1995). Receptors and G proteins as primary components of transmembrane signal transduction. Part 1. G-protein-coupled receptors: structure and function. *J Mol Med (Berl), 73*(2), 51-63.

Horvath, J., Forte, C., & O, C. (2015). Quantitative Review Finds No Evidence of Cognitive Effects in Healthy Populations From Single-session Transcranial Direct Current Stimulation (tDCS). *Brain stimulation*. doi:10.1016/j.brs.2015.01.400

Insel, T., Cuthbert, B., Garvey, M., Heinssen, R., Pine, D. S., Quinn, K., . . . Wang, P. (2010). Research domain criteria (RDoC): toward a new classification framework for research on mental disorders. *The American journal of psychiatry, 167*(7), 748-751. doi:10.1176/appi.ajp.2010.09091379

Insel, T. R. (2008). Assessing the economic costs of serious mental illness. *The American journal of psychiatry, 165*(6), 663-665. doi:10.1176/appi.ajp.2008.08030366

Jassal, B., Jupe, S., Caudy, M., Birney, E., Stein, L., Hermjakob, H., & D'Eustachio, P. (2010). The systematic annotation of the three main GPCR families in Reactome. *Database (Oxford), 2010*, baq018. doi:10.1093/database/baq018

Lustenberger, C., Boyle, M. R., Foulser, A. A., Mellin, J. M., & Frohlich, F. (2015). Functional role of frontal alpha oscillations in creativity. *Cortex; a journal devoted to the study of the nervous system and behavior, 67*, 74-82. doi:10.1016/j.cortex.2015.03.012

Monai, H., Ohkura, M., Tanaka, M., Oe, Y., Konno, A., Hirai, H., . . . Hirase, H. (2016). Calcium imaging reveals glial involvement in transcranial direct current stimulation-induced plasticity in mouse brain. *Nat Commun, 7*, 11100. doi:10.1038/ncomms11100

Nitsche, M. A., Fricke, K., Henschke, U., Schlitterlau, A., Liebetanz, D., Lang, N., . . . Paulus, W. (2003). Pharmacological modulation of cortical excitability shifts induced by transcranial direct current stimulation in humans. *The Journal of physiology, 553*(Pt 1), 293-301. doi:10.1113/jphysiol.2003.049916

Nitsche, M. A., & Paulus, W. (2000). Excitability changes induced in the human motor cortex by weak transcranial direct current stimulation. *The Journal of physiology, 527 Pt 3*, 633-639.

Notbohm, A., Kurths, J., & Herrmann, C. S. (2016). Modification of Brain Oscillations via Rhythmic Light Stimulation Provides Evidence for Entrainment but Not for Superposition of Event-Related Responses. *Frontiers in human neuroscience, 10*, 10. doi:10.3389/fnhum.2016.00010

Noury, N., Hipp, J. F., & Siegel, M. (2016). Physiological processes non-linearly affect electrophysiological recordings during transcranial electric stimulation. *NeuroImage*. doi:10.1016/j.neuroimage.2016.03.065

O'Reardon, J. P., Solvason, H. B., Janicak, P. G., Sampson, S., Isenberg, K. E., Nahas, Z., . . . Sackeim, H. A. (2007). Efficacy and safety of transcranial magnetic stimulation in the acute treatment of major depression: a multisite randomized controlled trial. *Biological psychiatry, 62*(11), 1208-1216. doi:10.1016/j.biopsych.2007.01.018

Prabhakaran, V., Smith, J. A., Desmond, J. E., Glover, G. H., & Gabrieli, J. D. (1997). Neural substrates of fluid reasoning: an fMRI study of neocortical activation during performance of the Raven's Progressive Matrices Test. *Cogn Psychol, 33*(1), 43-63. doi:10.1006/cogp.1997.0659

Radman, T., Su, Y., An, J. H., Parra, L. C., & Bikson, M. (2007). Spike timing amplifies the effect of electric fields on neurons: implications for endogenous field effects. *The Journal of neuroscience : the official journal of the Society for Neuroscience, 27*(11), 3030-3036. doi:10.1523/JNEUROSCI.0095-07.2007

Rahman, A., Reato, D., Arlotti, M., Gasca, F., Datta, A., Parra, L. C., & Bikson, M. (2013). Cellular effects of acute direct current stimulation: somatic and synaptic terminal effects. *The Journal of physiology, 591*(10), 2563-2578. doi:10.1113/jphysiol.2012.247171

Regier, D. A., Narrow, W. E., Clarke, D. E., Kraemer, H. C., Kuramoto, S. J., Kuhl, E. A., & Kupfer, D. J. (2013). DSM-5 field trials in the United States and Canada, Part II: test-retest reliability of selected categorical diagnoses. *The American journal of psychiatry, 170*(1), 59-70. doi:10.1176/appi.ajp.2012.12070999

Robinson, R. B., & Siegelbaum, S. A. (2003). Hyperpolarization-activated cation currents: from molecules to physiological function. *Annual review of physiology, 65*, 453-480. doi:10.1146/annurev.physiol.65.092101.142734

Sanchez-Vives, M. V., & McCormick, D. A. (2000). Cellular and network mechanisms of rhythmic recurrent activity in neocortex. *Nature neuroscience, 3*(10), 1027-1034. doi:10.1038/79848

Snyder, S. M., Rugino, T. A., Hornig, M., & Stein, M. A. (2015). Integration of an EEG biomarker with a clinician's ADHD evaluation. *Brain Behav, 5*(4), e00330. doi:10.1002/brb3.330

Steriade, M., Nunez, A., & Amzica, F. (1993). Intracellular analysis of relations between the slow (< 1 Hz) neocortical oscillation and other sleep rhythms of the electroencephalogram. *The Journal of neuroscience : the official journal of the Society for Neuroscience, 13*(8), 3266-3283.

Thut, G., Schyns, P. G., & Gross, J. (2011). Entrainment of perceptually relevant brain oscillations by non-invasive rhythmic stimulation of the human brain. *Frontiers in psychology, 2*, 170. doi:10.3389/fpsyg.2011.00170

Voss, U., Holzmann, R., Hobson, A., Paulus, W., Koppehele-Gossel, J., Klimke, A., & Nitsche, M. A. (2014). Induction of self awareness in dreams through frontal low current stimulation of gamma activity. *Nature neuroscience, 17*(6), 810-812. doi:10.1038/nn.3719

Vossen, A., Gross, J., & Thut, G. (2015). Alpha Power Increase After Transcranial Alternating Current Stimulation at Alpha Frequency (alpha-tACS) Reflects Plastic Changes Rather Than Entrainment. *Brain stimulation, 8*(3), 499-508. doi:10.1016/j.brs.2014.12.004

Wang, X. J. (2010). Neurophysiological and computational principles of cortical rhythms in cognition. *Physiological reviews, 90*(3), 1195-1268. doi:10.1152/physrev.00035.2008

Womelsdorf, T., Valiante, T. A., Sahin, N. T., Miller, K. J., & Tiesinga, P. (2014). Dynamic circuit motifs underlying rhythmic gain control, gating and integration. *Nature neuroscience, 17*(8), 1031-1039. doi:10.1038/nn.3764

Zhang, F., Wang, L. P., Boyden, E. S., & Deisseroth, K. (2006). Channelrhodopsin-2 and optical control of excitable cells. *Nat Methods, 3*(10), 785-792. doi:10.1038/nmeth936

Ali, M. M., Sellers, K. K., & Frohlich, F. (2013). Transcranial alternating current stimulation modulates large-scale cortical network activity by network resonance. *The Journal of neuroscience : the official journal of the Society for Neuroscience, 33*(27), 11262-11275. doi:10.1523/JNEUROSCI.5867-12.2013

Arenkiel, B. R., Peca, J., Davison, I. G., Feliciano, C., Deisseroth, K., Augustine, G. J., . . . Feng, G. (2007). In vivo light-induced activation of neural circuitry in transgenic mice expressing channelrhodopsin-2. *Neuron, 54*(2), 205-218. doi:10.1016/j.neuron.2007.03.005

Bagalman, E., & Napili, A. (2015). *Prevalence of Mental Illness in the United States: Data Sources and Estimates*. Retrieved from

Beltramo, R., D'Urso, G., Dal Maschio, M., Farisello, P., Bovetti, S., Clovis, Y., . . . Fellin, T. (2013). Layer-specific excitatory circuits differentially control recurrent network dynamics in the neocortex. *Nature neuroscience, 16*(2), 227-234. doi:10.1038/nn.3306

Berger, H. (1929). Über das Elektrenkephalogramm des Menschen. *Archiv für Psychiatrie und Nervenkrankheiten, 87*(1), 527-570.

Bikson, M., Inoue, M., Akiyama, H., Deans, J. K., Fox, J. E., Miyakawa, H., & Jefferys, J. G. (2004). Effects of uniform extracellular DC electric fields on excitability in rat hippocampal slices in vitro. *The Journal of physiology, 557*(Pt 1), 175-190. doi:10.1113/jphysiol.2003.055772

Brown, D. A., & Adams, P. R. (1980). Muscarinic suppression of a novel voltage-sensitive K+ current in a vertebrate neurone. *Nature, 283*(5748), 673-676.

Buzsáki, G. (2006). *Rhythms of the brain*. Oxford ; New York: Oxford University Press.

Buzsaki, G., Anastassiou, C. A., & Koch, C. (2012). The origin of extracellular fields and currents--EEG, ECoG, LFP and spikes. *Nat Rev Neurosci, 13*(6), 407-420. doi:10.1038/nrn3241

Chan, C. Y., Hounsgaard, J., & Nicholson, C. (1988). Effects of electric fields on transmembrane potential and excitability of turtle cerebellar Purkinje cells in vitro. *The Journal of physiology, 402*, 751-771.

Chauvette, S., Volgushev, M., & Timofeev, I. (2010). Origin of active states in local neocortical networks during slow sleep oscillation. *Cerebral cortex, 20*(11), 2660-2674. doi:10.1093/cercor/bhq009

Colton, C. W., & Manderscheid, R. W. (2006). Congruencies in increased mortality rates, years of potential life lost, and causes of death among public mental health clients in eight states. *Prev Chronic Dis, 3*(2), A42.

Constantinople, C. M., & Bruno, R. M. (2011). Effects and mechanisms of wakefulness on local cortical networks. *Neuron, 69*(6), 1061-1068. doi:10.1016/j.neuron.2011.02.040

Deans, J. K., Powell, A. D., & Jefferys, J. G. (2007). Sensitivity of coherent oscillations in rat hippocampus to AC electric fields. *The Journal of physiology, 583*(Pt 2), 555-565. doi:10.1113/jphysiol.2007.137711

Egert, U., Heck, D., & Aertsen, A. (2002). Two-dimensional monitoring of spiking networks in acute brain slices. *Experimental brain research. Experimentelle Hirnforschung. Experimentation cerebrale, 142*(2), 268-274. doi:10.1007/s00221-001-0932-5

Fava, M. (2003). Diagnosis and definition of treatment-resistant depression. *Biological psychiatry, 53*(8), 649-659.

Fee, M. S., Mitra, P. P., & Kleinfeld, D. (1996). Automatic sorting of multiple unit neuronal signals in the presence of anisotropic and non-Gaussian variability. *Journal of neuroscience methods, 69*(2), 175-188. doi:10.1016/S0165-0270(96)00050-7

Frohlich, F. (2014). Endogenous and exogenous electric fields as modifiers of brain activity: rational design of noninvasive brain stimulation with transcranial alternating current stimulation. *Dialogues in clinical neuroscience, 16*(1), 93-102.

Frohlich, F., & McCormick, D. A. (2010). Endogenous electric fields may guide neocortical network activity. *Neuron, 67*(1), 129-143. doi:10.1016/j.neuron.2010.06.005

Frohlich, F., & Schmidt, S. L. (2013). Rational design of transcranial current stimulation (TCS) through mechanistic insights into cortical network dynamics. *Frontiers in human neuroscience, 7*, 804. doi:10.3389/fnhum.2013.00804

Gluckman, B. J., Nguyen, H., Weinstein, S. L., & Schiff, S. J. (2001). Adaptive electric field control of epileptic seizures. *The Journal of neuroscience : the official journal of the Society for Neuroscience, 21*(2), 590-600.

Gudermann, T., Nurnberg, B., & Schultz, G. (1995). Receptors and G proteins as primary components of transmembrane signal transduction. Part 1. G-protein-coupled receptors: structure and function. *J Mol Med (Berl), 73*(2), 51-63.

Horvath, J., Forte, C., & O, C. (2015). Quantitative Review Finds No Evidence of Cognitive Effects in Healthy Populations From Single-session Transcranial Direct Current Stimulation (tDCS). *Brain stimulation*. doi:10.1016/j.brs.2015.01.400

Insel, T., Cuthbert, B., Garvey, M., Heinssen, R., Pine, D. S., Quinn, K., . . . Wang, P. (2010). Research domain criteria (RDoC): toward a new classification framework for research on mental disorders. *The American journal of psychiatry, 167*(7), 748-751. doi:10.1176/appi.ajp.2010.09091379

Insel, T. R. (2008). Assessing the economic costs of serious mental illness. *The American journal of psychiatry, 165*(6), 663-665. doi:10.1176/appi.ajp.2008.08030366

Jassal, B., Jupe, S., Caudy, M., Birney, E., Stein, L., Hermjakob, H., & D'Eustachio, P. (2010). The systematic annotation of the three main GPCR families in Reactome. *Database (Oxford), 2010*, baq018. doi:10.1093/database/baq018

Lustenberger, C., Boyle, M. R., Foulser, A. A., Mellin, J. M., & Frohlich, F. (2015). Functional role of frontal alpha oscillations in creativity. *Cortex; a journal devoted to the study of the nervous system and behavior, 67*, 74-82. doi:10.1016/j.cortex.2015.03.012

Monai, H., Ohkura, M., Tanaka, M., Oe, Y., Konno, A., Hirai, H., . . . Hirase, H. (2016). Calcium imaging reveals glial involvement in transcranial direct current stimulation-induced plasticity in mouse brain. *Nat Commun, 7*, 11100. doi:10.1038/ncomms11100

Nitsche, M. A., Fricke, K., Henschke, U., Schlitterlau, A., Liebetanz, D., Lang, N., . . . Paulus, W. (2003). Pharmacological modulation of cortical excitability shifts induced by transcranial direct current stimulation in humans. *The Journal of physiology, 553*(Pt 1), 293-301. doi:10.1113/jphysiol.2003.049916

Nitsche, M. A., & Paulus, W. (2000). Excitability changes induced in the human motor cortex by weak transcranial direct current stimulation. *The Journal of physiology, 527 Pt 3*, 633-639.

Notbohm, A., Kurths, J., & Herrmann, C. S. (2016). Modification of Brain Oscillations via Rhythmic Light Stimulation Provides Evidence for Entrainment but Not for Superposition of Event-Related Responses. *Frontiers in human neuroscience, 10*, 10. doi:10.3389/fnhum.2016.00010

Noury, N., Hipp, J. F., & Siegel, M. (2016). Physiological processes non-linearly affect electrophysiological recordings during transcranial electric stimulation. *NeuroImage*. doi:10.1016/j.neuroimage.2016.03.065

O'Reardon, J. P., Solvason, H. B., Janicak, P. G., Sampson, S., Isenberg, K. E., Nahas, Z., . . . Sackeim, H. A. (2007). Efficacy and safety of transcranial magnetic stimulation in the acute treatment of major depression: a multisite randomized controlled trial. *Biological psychiatry, 62*(11), 1208-1216. doi:10.1016/j.biopsych.2007.01.018

Prabhakaran, V., Smith, J. A., Desmond, J. E., Glover, G. H., & Gabrieli, J. D. (1997). Neural substrates of fluid reasoning: an fMRI study of neocortical activation during performance of the Raven's Progressive Matrices Test. *Cogn Psychol, 33*(1), 43-63. doi:10.1006/cogp.1997.0659

Radman, T., Su, Y., An, J. H., Parra, L. C., & Bikson, M. (2007). Spike timing amplifies the effect of electric fields on neurons: implications for endogenous field effects. *The Journal of neuroscience : the official journal of the Society for Neuroscience, 27*(11), 3030-3036. doi:10.1523/JNEUROSCI.0095-07.2007

Rahman, A., Reato, D., Arlotti, M., Gasca, F., Datta, A., Parra, L. C., & Bikson, M. (2013). Cellular effects of acute direct current stimulation: somatic and synaptic terminal effects. *The Journal of physiology, 591*(10), 2563-2578. doi:10.1113/jphysiol.2012.247171

Regier, D. A., Narrow, W. E., Clarke, D. E., Kraemer, H. C., Kuramoto, S. J., Kuhl, E. A., & Kupfer, D. J. (2013). DSM-5 field trials in the United States and Canada, Part II: test-retest reliability of selected categorical diagnoses. *The American journal of psychiatry, 170*(1), 59-70. doi:10.1176/appi.ajp.2012.12070999

Robinson, R. B., & Siegelbaum, S. A. (2003). Hyperpolarization-activated cation currents: from molecules to physiological function. *Annual review of physiology, 65*, 453-480. doi:10.1146/annurev.physiol.65.092101.142734

Sanchez-Vives, M. V., & McCormick, D. A. (2000). Cellular and network mechanisms of rhythmic recurrent activity in neocortex. *Nature neuroscience, 3*(10), 1027-1034. doi:10.1038/79848

Snyder, S. M., Rugino, T. A., Hornig, M., & Stein, M. A. (2015). Integration of an EEG biomarker with a clinician's ADHD evaluation. *Brain Behav, 5*(4), e00330. doi:10.1002/brb3.330

Steriade, M., Nunez, A., & Amzica, F. (1993). Intracellular analysis of relations between the slow (< 1 Hz) neocortical oscillation and other sleep rhythms of the electroencephalogram. *The Journal of neuroscience : the official journal of the Society for Neuroscience, 13*(8), 3266-3283.

Thut, G., Schyns, P. G., & Gross, J. (2011). Entrainment of perceptually relevant brain oscillations by non-invasive rhythmic stimulation of the human brain. *Frontiers in psychology, 2*, 170. doi:10.3389/fpsyg.2011.00170

Voss, U., Holzmann, R., Hobson, A., Paulus, W., Koppehele-Gossel, J., Klimke, A., & Nitsche, M. A. (2014). Induction of self awareness in dreams through frontal low current stimulation of gamma activity. *Nature neuroscience, 17*(6), 810-812. doi:10.1038/nn.3719

Vossen, A., Gross, J., & Thut, G. (2015). Alpha Power Increase After Transcranial Alternating Current Stimulation at Alpha Frequency (alpha-tACS) Reflects Plastic Changes Rather Than Entrainment. *Brain stimulation, 8*(3), 499-508. doi:10.1016/j.brs.2014.12.004

Wang, X. J. (2010). Neurophysiological and computational principles of cortical rhythms in cognition. *Physiological reviews, 90*(3), 1195-1268. doi:10.1152/physrev.00035.2008

Womelsdorf, T., Valiante, T. A., Sahin, N. T., Miller, K. J., & Tiesinga, P. (2014). Dynamic circuit motifs underlying rhythmic gain control, gating and integration. *Nature neuroscience, 17*(8), 1031-1039. doi:10.1038/nn.3764

Zhang, F., Wang, L. P., Boyden, E. S., & Deisseroth, K. (2006). Channelrhodopsin-2 and optical control of excitable cells. *Nat Methods, 3*(10), 785-792. doi:10.1038/nmeth936

CHAPTER 2: DIFFERENTIAL EFFECTS OF CHOLINERGIC AND NORADRENERGIC NEUROMODULATIONON SPONTANEOUS CORTICAL NETWORK DYNAMICS[1]

INTRODUCTION

Cortical networks exhibit a broad range of different activity states that range from slow, rhythmic discharges during slow-wave sleep to fully desynchronized activity patterns during periods of behavioral arousal and focused attention (Steriade & Amzica, 1998; Steriade, Timofeev, & Grenier, 2001). The neuromodulators acetylcholine and norepinephrine play a key role in controlling this activation which leads to desynchronization of cortical network dynamics (Armitage, Hall, & Sellers, 1969; Celesia & Jasper, 1966; Constantinople & Bruno, 2011; Jouvet, 1969; Kalmbach, Hedrick, & Waters, 2012). However, phasic release of these neuromodulators also occurs in the awake state in response to different behavioral triggers. Acetylcholine appears to be tightly linked to attentional processing and learning whereas norepinephrine is released under circumstances of substantial changes in the environment that need overall behavioral adjustment (Baxter & Chiba, 1999; Dalley et al., 2001; Vankov, Herve-Minvielle, & Sara, 1995; Yu & Dayan, 2005). Both neuromodulators target a wide-range of cellular targets that affect intrinsic and synaptic excitability in a complex way (Armstrong-James & Fox, 1983; Giocomo & Hasselmo, 2005; Hasselmo, Linster, Patil, Ma, & Cekic, 1997; Sato, Fox, & Daw, 1989; Sillito & Kemp, 1983). Furthermore, both acetylcholine (ACh) and norepinephrine (NE) have the potential to introduce long-term circuit modification due to their ability to alter the rules by which synaptic weights are altered during experimentally-induced long-term potentiation (LTP) and long-term depression (LTD) (Huerta & Lisman, 1995; Kirkwood, Rozas, Kirkwood, Perez, & Bear, 1999; Seol et al., 2007; Thomas, Moody, Makhinson, & O'Dell, 1996). Despite this growing understanding of context-dependent release of ACh and NE and the

[1] This chapter previously appeared as an article in Neuropharmacology; doi:10.1016/j.neuropharm.2013.04.045 (http://www.sciencedirect.com/science/article/pii/S0028390813001913). The original citation is as follows: **Stephen L. Schmidt**, Erin Y. Chew, Davis V. Bennett, Mohamed A. Hammad, Flavio Frohlich (2013). Differential effects of cholinergic and noradrenergic neuromodulation on spontaneous cortical network dynamics. Neuropharmacology, 72: 259-273.

corresponding cellular targets, very little is known about the direct effect of these neuromodulators on cortical network dynamics. We here examined what the net effects of neuromodulation on cortical networks are in absence of experimental and potentially unphysiological stimulation paradigms. To this purpose, we studied how spontaneous, desynchronized cortical network dynamics are modulated by using multichannel electrophysiology in acute cortical slices combined with quantitative strategies from information theory (Pincus & Goldberger, 1994) and network science (Tononi & Sporns, 2003) to elucidate the effects on the spatiotemporal network dynamics.

METHODS

Ethical Statement

All animal procedures were approved by the Institute of Animal Use and Care of the University of North Carolina – Chapel Hill and were in compliance with the National Institutes of Health guide for the care and use of Laboratory animals (NIH Publications No. 8023, revised 1978). All efforts were made to minimize animal suffering, to reduce the number of animals used, and to utilize alternative approaches where available.

Solutions

All chemicals were purchased from Sigma (St. Louis, MO). Sucrose solution: 83.0mM NaCl, 2.5mM KCl, 0.5mM CaCl2, 3.3mM MgSO4, 1.0mM NaH2PO4, 26.2mM NaHCO3, 22.0mM Dextrose Anhydrose, 72.0mM Sucrose. Artificial cerebral spinal fluid (aCSF): 119.0mM NaCl, 2.5mM KCl, 1.0mM NaH2PO4, 26.2mM NaHCO3, 22.0mM glucose, 1.0mM MgSO4, and 1.0mM CaCl2. Incubation solution: aCSF modified to contain 2.0mM MgsSO4 and 2.0mM CaCl2. Control aCSF: aCSF with added KCl to a final concentration of 3.5mM KCl. Nicotine aCSF: control aCSF with 10μM nicotine added. Pirenzipine aCSF: control aCSF with 50μM pirenzepine added. L-Phenylephrine aCSF: control aCSF with 50μM L-Phenylephrine. Clonidine aCSF: control aCSF with 50μM clonidine. Isoproterenol aCSF: control aCSF with 40μM isoproterenol added. Prazosin aCSF: control aCSF with 20μM prazosin added. Yohimbine aCSF: control aCSF with 40μM yohimbine. Propranolol aCSF: control aCSF with 40μM propranolol added.

Slice Preparation

Adolescent (p15-p36) C57BL/6J mice were deeply anesthetized with Euthasol and decapitated. Brains were removed and quickly placed in ice-cold sucrose solution bubbled with carbogen (95% O_2, 5% CO_2) and 200µm coronal slices were then cut from the primary visual cortex (V1) using a VT1000S (Leica Microsystems, Wetzlar, Germany). Slices recovered in incubation solution bubbled with carbogen for at least 45 minutes at 34°C before placement on the array.

Drug Application and Experiment Design

Slices were placed on a MEA 2100 (Multichannel Systems, Reutlingen, Germany) with perforated arrays of 59 electrodes of 30µm diameter and 200µm x 200µm spacing. The array was perfused from both sides with control aCSF bubbled with carbogen at 36°C (Figure 2.1A). After a 1800s control epoch the perfusion was switched to control aCSF with 1µM, 10µM, 50µM, or 100µM of carbachol (CCh) or NE which was then followed by a 1800s washout epoch with control aCSF. Providing oxygenated aCSF to both sides of the slice together with a high perfusion flow rate (>4 mL/min) in a relatively small chamber around the array enabled the occurrence of spontaneous activity without any pharmacological manipulations in control conditions. Control aCSF differed from the aCSF commonly used in slice experiments by containing only 1mM Mg^{2+} and 1mM Ca^{2+}. Reduced Mg^{2+} and Ca^{2+} concentration more closely resembles the concentration of CSF *in vivo* (Sanchez-Vives & McCormick, 2000). We found that switching to the higher, standard concentrations reduced spontaneous activity in our preparation (logarithm of firing-rate ratio: -0.29459 + 0.034543, n = 206).

To determine the receptor subtypes responsible for the effects studied here, we used specific receptor agonists and antagonists. The cholinergic signaling was dissected by nicotine as a selective agonist for nicotinic cholinergic receptors and M1-specific muscarinic antagonist pirenzepine. We isolated the three noradrenergic receptor subtypes α_1, α_2, and β by agonist L-phenylephrine, clonidine, isoproterenol, respectively, and antagonist prazosin, yohimbine, and propranolol, respectively. Agonists were applied to the aCSF instead of CCh or NE; antagonists were added to the aCSF for the entire experiment in addition to 50µM of CCh or NE that were applied after 1800 s. To ensure the measured

response was indeed mediated by the applied compound and not an artifact of the perfusion system or the experimental setup, we conducted control experiments where the perfusion was switched between two beakers of control aCSF ("placebo").

Histology and Electrode Locations

Typically, about half of the electrodes (channels) were positioned over V1. Electrode locations were determined by superimposing the image of the slice on the array to that of the array alone (Figure 2.1B). Cortical layers were then mapped to the electrodes by measuring the relative position between pia and white matter and comparing to Nissl-stained reference sections of age-matched mice (Figure 2.1C).

Multiunit and Single Unit Data Acquisition

Raw traces were recorded from 59 channels simultaneously, sampled at 25 kHz (Figure 2.1D-E, example traces for the entire array, many channels show robust action potential firing, enlarged individual traces show prototypic action potential waveforms, spikes) with MC_Rack (Multichannel Systems, Reutlingen, Germany). The raw data was high-pass filtered with a 300Hz – 4^{th} order Butterworth filter and the noise level determined by calculating the standard deviation of the recorded signal on each channel. Spikes were identified by crossing -4 times the noise level of that channel (with 1 ms dead time after each threshold crossing). As described in section 2.5, the location of each channel was determined by percentage depth from pia (Figure 2.1F, average firing rate by depth shows higher activity in deep layers as typically seen in *in vivo* recordings of cortex). To identify single units, spike-sorting was performed for each channel using a random subset of 3000 spikes which were over-clustered using the kmeans algorithm. Clusters were manually combined after examining wave shape and the distance between individual clusters determined by linkage analysis (Fee, Mitra, & Kleinfeld, 1996) as shown in Figure 2.2A. After spike-sorting, reference waveforms were determined by averaging the waveforms for each unit. All spikes from the corresponding electrode were then assigned to one of the reference units by determining the minimal distance between the actual spike and the reference waveform (template matching). The resulting units had to contain a minimum of 100 spikes and the distribution of the negative peak values of the spikes had to resemble a normal distribution (Hill, Mehta, & Kleinfeld, 2011). Figure 2.2B displays a

representative subset of units from 8 channels (clusters from the same channel are displayed in the same color, different slice from Figure 2.2A). On average, 52 clusters were isolated from each slice or 2.97 units per channel.

Data Analysis

The data were analyzed using custom-written scripts in Matlab (Mathworks, Natick, MA). Only electrodes in V1 were spike-sorted and therefore data from other brain regions were not included in the single unit data. Raster plots were created by sorting units by their distance from pia and plotting the last 20s of each epoch ("control", "drug application", "washout"). Multiunit channels were identified as stable and included if 3 of 5 evenly spaced overlapping lines fitted to the firing-rate time-course had a slope of less than .006 spikes per second in the control epoch. Channels that had no spikes for a period of at least 600s were excluded. The time courses for each electrode were built by counting spikes in 3s bins for the duration of the experiment. The time-courses of each channel were then z-scored which removed biases from our calculations of medians due to different intrinsic firing rate levels across channels. Furthermore, the z-score also normalized the standard deviation. Then, the median of all channels in V1 was computed for each 3s bin. The last 300s of all three 1800s intervals (control, drug applied, and washout) were used for all subsequent analysis and discrete spike trains were constructed for each channel by binning spike times (1ms bins). To determine if the application of neuromodulators caused a significant increase or decrease of the firing rate (FR), respectively, we created a shuffle control in which the FRs of both the control and neuromodulator epochs were split into 5s windows and recombined randomly to make two new shuffled modulation indices. The modulation index was then calculated as follows:

$$\textit{Modulation Index} = (FR(NM) - FR(Ctrl))/(FR(NM) + FR(Ctrl))$$

where FR(NM) denotes the FR during neuromodulator application and FR(Ctrl) denotes the FR during the preceding control epoch. The modulation index of the measured firing rate was compared to the modulation-index distribution of the 500 shuffles: our significance criterion required that the true modulation index was significantly different from the median of the shuffled value ($p < .05$ after a Bonferroni correction for the number of channels being compared). Channels not in V1 were then excluded using the method described in section 2.4.

We calculated the average FR of each single unit for each epoch window. The effect of the neuromodulator was determined by dividing the neuromodulator epoch FR by the control epoch FR. Similar to the neuromodulator effect, the plasticity effect of each neuron was calculated by dividing the washout epoch FR by the control epoch FR. Single units where this ratio was either zero or undefined due to the complete absence of spikes in either of the epochs were excluded. These ratios are reported on a $\log_{10}$ scale (i.e. no effect corresponds to a value of zero). We determined skewness of effect distributions using the skewness function of Matlab. We calculated the standard error of skewness using SES = sqrt(6/n), any distribution with a skewness greater than 2*SES was considered significantly skewed. The correlation between effect and plasticity of was determined using the corrcoef function of Matlab on all cells that had a non-zero FR for all epochs. To examine the change caused by neuromodulators as a function of cortical depth we then grouped units in layers I-IV and layers V-VI.

Approximate entropy (ApEn) is a measure of signal irregularity based on how frequently individual temporal patterns reoccur in the data (Pincus & Goldberger, 1994). ApEn was calculated using an additional script for Matlab written by Kijoon Lee based on (Chon, Scully, & Lu, 2009). ApEn requires three input parameters: *m*, *r*, and *N*; the length of the pattern, a tolerance threshold, and the length of the data to be analyzed. Briefly, the algorithm that determines ApEn scans the data and looks for approximate matches for every pattern detected. Tolerance threshold *r* determines how close this match must be. For each pattern, all matches are then evaluated by considering their first subsequent data point. If this data point is different from the first subsequent data point of the original pattern, ApEn is accordingly increased. In order to minimize the number of bins with zeros spikes while still fulfilling the minimum data-length requirement (Pincus & Goldberger, 1994) of the ApEn algorithm (typically n >= 1000), spike trains were binned with 300ms resolution. The following parameter values were used: $m = 2$, $r = 0.1*\text{std(FR)}$, and $N = 1000$. Pairwise correlation was calculated using the corrcoef matlab function using spike trains binned with 100ms resolution. This correlation coefficient was computed for each pair of multiunit channels. Compensated power spectral densities (PSDs) of single units were calculated using Thomson's multitaper method and compared to a shuffle control as in (Rivlin-Etzion, Ritov, Heimer, Bergman, & Bar-Gad, 2006). Briefly, the frequency spectrum of each single unit was calculated from the discrete spike train using with the Matlab function pmtm. The raw frequency spectrum was divided by the

average spectrum of 20 ISI shuffled versions of the spike train. Principal component analysis (PCA) was performed on z-scored 10ms binned spike trains and then broken into 5s non-overlapping windows using the princomp function in Matlab. PCA transformed the binned FR of all units in a slice to decorrelated component dimensions. We then sorted the component dimensions by percent variance accounted and determined the number of dimensions required to account for 50% of the total variance. Due to the discretization of this measure, we used bootstrapping on the windowed results to estimate the mean percent of total dimensions for each epoch. We then examined change in the percentage of total dimensions to account for 50% of the variance between neuromodulator applied and control epochs to assess the effect of the neuromodulators.

Statistics

All data are expressed as median values ± SEM unless otherwise noted. Medians of data shown on $\log_{10}$ scale were taken as the $\log_{10}$ of the median, while SEM for data on $\log_{10}$ scale was determined by

$$SEM = std(\log_{10}(data))/sqrt(n)$$

In general, FR data are typically not normally distributed (Shafi et al., 2007); we confirmed that effect size did not follow a normal distribution and therefore statistical significance was determined using Kruskal-Wallace tests in conjunction with Tukey's multiple comparison tests at $p < 0.05$, unless otherwise noted. These test compute confidence intervals at $p = 0.05$, if the confidence intervals of two groups do not overlap then $p < 0.05$. However, exact p values for each comparison were not computed.

RESULTS

Neuromodulators CCh and NE Increase Spontaneous Activity

To assess the effects of cholinergic and noradrenergic neuromodulators on network dynamics in sensory cortex, we performed multi-electrode array recordings from slices of mouse visual cortex maintained in an environment that mimicked the ion concentrations of the cerebral spinal fluid. We found that the slices exhibited sparse spontaneous action potential firing. We first asked whether CCh and NE modulated this spontaneous activity. To this end, we recorded a stable control baseline of 1800s and

added either CCh or NE to the bath for an additional 1800s before switching back to control for another 1800s to probe for long-term network effects that outlast the presence of the neuromodulators. Raster plots of individual units (n = 726 units pooled from 13 slices for CCh, and n = 512 units from 10 slices for NE) for initial control, neuromodulator application, and subsequent washout showed that application of 50μM CCh increased the spontaneous activity which returned to baseline after washout (Figure 2.2B, Top, left to right). In the case of 50μM NE, activity also increased upon application but remained elevated after washout (Figure 2.2B, bottom, left to right). Given these distinct effects of CCh and NE on spontaneous network dynamics, we next examined the concentration-dependence of the time-course of action of CCh and NE.

Temporal Response Profile

We determined the effect of the neuromodulators CCh and NE on network dynamics (z-scored time-course of average firing rate) as a function of time and concentration (1, 10, 50 and 100μM for both CCh and NE). For CCh experiments (Figure 2.3A 1, 10, 50 and 100μM CCh from top to bottom. n = 10, 13, 13 and 15 slices), the FR increased and remained elevated for the duration of CCh present in the bath. For higher concentrations (50 and 100μM CCh), the initial transient of the FR response to CCh became steeper and exhibited an overshoot in comparison to the steady-state response. In summary, application of CCh caused a pronounced, reversible increase in spontaneous activity.

Similarly, NE also caused an FR increase for all concentrations (Figure 2.3B, 1, 10, 50 and 100μM NE from top to bottom. n = 13, 11, 10 and 14 slices) with a pronounced overshoot only for 50μM NE. When the perfusion was returned to control aCSF, we found different responses as a function of concentration: 1μM NE allowed a quick return to baseline, 10 and 100μM NE concentrations caused a slower return to baseline, whereas 50μM NE caused an outlasting, stable elevation of the FR for the remaining 1800s of the experiment. Thus, spontaneous activity markedly increased with application of NE; higher concentrations caused FR increases that outlasted the application of NE. This sustained elevation of spontaneous activity motivated the further consideration of not only the control and neuromodulator data but also the washout (“plasticity”) epoch.

Concentration Dependent Modulation of Spatial Spread of Spontaneous Activity

Based on the time-course plots (Figure 2.3), we next analyzed the last 300s before the end of each epoch to quantify the steady-state response to the neuromodulators. All subsequent analysis was limited to these analysis windows. We first asked if individual channels (locations in the slice) exhibited a significant FR increase or decrease with the application of neuromodulators as measure of the spatial spread of the effect. An increase in channels with altered FR indicated that a larger fraction/area of the network exhibited a response to the applied neuromodulator. The percentages of channels on each slice were then calculated for each of the three neuromodulator effect types (Figure 2.4, increase, no effect, decrease; CCh left, NE right). We first applied this measure to multiunit channels of control ("placebo") slices where no neuromodulators were applied to exclude false positives (all values are mean % ± SEM): 20.5 ± 2.81% with significant increase and 4.2 ± 0.60% with significant decrease. As expected, the majority of channels failed to show a significant effect (75.2 ± 2.55 % for control slices; dotted horizontal lines in Figure 2.4; n = 8 slices). In contrast to the control slices, CCh mediated a concentration-dependent effect where concentrations up to 50μM raised the percentage of channels with a significant FR increase, and only 100μM caused a lower percentage of channels to exhibit a FR increase in comparison to 10 and 50μM (33.7 ± 1.37 for 1μM, 47.3 ± 2.06 for 10μM, 68.6 ± 1.42 for 50μM, and 40.3 ± 1.72 for 100μM; all values are mean % ± SEM; n = 10, 13, 13 and 15 slices). This concentration-dependent increase of channels with elevated FR in response to CCh was likely mediated by recruitment of additional network locations that failed to exhibit a significant modulation by CCh for lower concentrations (50.4 ± 1.75 for 1μM, 42.1 ± 1.86 for 10μM, 24.2 ± 1.07 for 50μM, and 49.4 ± 1.94 for 100μM, all values are mean % ± SEM). The percentage of channels with a FR increase was significantly larger than those of control slices for 10, 50 and 100μM CCh. All concentrations of CCh had significantly fewer channels with no effect than control slices (ANOVA and post-hoc Tukey's test $p < 0.05$). Of the four concentrations of CCh used, only 1μM had significantly more channels with a FR decrease than control (15.9 ± 1.41 for 1μM, 10.7 ± 0.50 for 10μM, 07.2 ± 0.50 for 50μM, and 10.2 ± 0.67 for 100μM; all values are mean % ± SEM). Therefore, overall, CCh increased the spatial spread of the spontaneous activity by (1) increasing the number of locations in the network (i.e. channels) that exhibited activity and (2) preventing network locations from becoming silent.

NE had a more complex effect on the spatial spread of activity; as for CCh, we found that for all concentrations NE had fewer channels with no effect than the control slices (51.5 ± 1.30 for 1μM, 49.6 ± 1.56 for 10μM, 52.8 ± 1.74 for 50μM, and 44.8 ± 1.90 for 100μM; n = 10, 13, 13 and 15 slices). However in contrast to the CCh experiments, slices did not exhibit significantly more channels with FR increases than the control slices (32.6 ± 1.44 for 1μM, 36.4 ± 1.72 for 10μM, 31.3 ± 1.49 for 50μM, and 32.7 ± 2.07 for 100μM). Only 100μM NE had significantly more channels with a FR decrease (15.9 ± 1.29 for 1μM, 13.9 ± 0.90 for 10μM, 15.9 ± 1.19 for 50μM, and 22.4 ± 1.73 for 100μM). Therefore, NE modulated the network dynamics compared to control yet the effects on the FR were bidirectional.

Magnitude of Neuromodulator and Plasticity Effects

The above analysis examined the effect of the neuromodulators on overall multiunit firing rate which consists of the action potential firing of all neurons close to the recording electrode site. We next sorted the action potential waveforms into single units (presumed individual neurons) to test for concentration-dependent effects on the FR of individual neurons. We defined neuromodulator effect as the FR in presence of neuromodulator divided by the control FR for each single unit. The range of neuromodulator effect sizes covered six orders of magnitude since many units were very quiet during control. Figure 2.5A shows a histogram of the logarithmic effect size for increasing concentration from left to right. FR of cells in slices exposed to CCh exhibited large increases for all concentrations (0.327 ± 0.0407 for 1μM, 0.612 ± 0.0389 for 10μM, 1.39 ± 0.0433 for 50μM, and 0.730 ± 0.0450 for 100μM (all values $\log_{10}$); n = 395, 581, 635 and 655 units across 9, 13, 13 and 14 slices; all significantly different from each other with the exception of the comparison of 10μM to 100μM CCh). This result is in close agreement with the above-shown time course and multiunit FR data. Since the multiunit data for NE failed to show a significant increase in the number of channels with increased FR, we predicted that the effect of NE at the level of single units would be bidirectional such that some units had a FR increase whereas others had a FR decrease. Indeed, FR in units of NE-exposed slices displayed smaller median logarithmic effect sizes (0.168 ± 0.0328 1μM, 0.398 ± 0.0342 for 10μM, 0.416 ± 0.0438 for 50μM, and 0.280 ± 0.0393 100μM; n = 685, 650, 472 and 470 units across 13, 11, 10 and 15 slices). Some concentration dependence existed for this measure: 1μM NE was significantly different from 10μM NE as

well as 10μM from 100μM NE. To determine the uniformity of the neuromodulator effects, we next examined the skewness of the effect distributions in Figure 2.5A. For this measure, if the effect of the neuromodulator increases the spontaneous activity by some factor (with some Gaussian noise) the effect size distribution is normal with a skewness of zero. We found that the effect size distributions of 10, 50 and 100μM concentrations of CCh had a significant negative skewness (0.148 ± 0.123 for 1μM, -0.228 ± 0.102 for 10μM, -0.459 ± 0.097 for 50μM, and -0.319 ± 0.096 for 100μM). Skewness of NE effect size distributions varied by concentration with significant positive skewness for the effect of 1μM NE and negative skewness for 50μM NE. (0.431 ± 0.094 for 1μM, 0.191 ± 0.096 for 10μM, -0.623 ± 0.113 for 50μM, and -0.137 ± 0.113 for 100μM). Therefore, a simple model of neuromodulator effect on cellular excitability cannot explain the experimentally determined effects.

Due to the observed outlasting effect of NE application on multiunit firing rate, we next determined the single unit behavior for the last 300s of the "wash out" epoch after drug application. We defined the "plasticity effect" by calculating the change of the washout epoch FR relative to (divided by) the control epoch FR. We first examined the correlation between the neuromodulator effect size and the plasticity effect (Figure 2.5C). For CCh, correlation coefficients between neuromodulator effect and plasticity were low (0.066 to 0.261 for 1μM, 0.310 to .463 for 10μM, 0.306 to 0.445 for 50μM, and 0.222 to 0.369 for 100μM (95% confidence interval); n = 384, 474, 561 and 581 single units across 9, 13, 13 and 14 slices). This result further confirms that CCh had little plasticity effect for any concentration. Conversely, NE had higher correlation for concentrations greater than 1μM (0.165 to 0.308 for 1μM, 0.549 to 0.653 for 10μM, 0.603 to 0.708 for 50μM, and 0.485 to 0.616 for 100μM (95% confidence interval); n = 659, 567, 456 and 432 units across 13, 11, 10 and 15 slices). The higher correlation for 10, 50 and 100μM indicated that the plasticity effect seen in the time-courses (Figure 2.3) was mediated by neurons continuing to maintain their increased FR rather than different neurons responding to washout of NE. We next examined the plasticity size in terms of effect size for all units. We here show the neuromodulator effect versus the plasticity effect for all single unit channels (Figure 2.5D, increasing concentration from left to right). This plot visualizes whether the increased FR during the washout epoch was mediated by units maintaining their neuromodulator-epoch FR or by different units becoming active after the washout. In the case of maintained FR, we would expect many points on the unity line of the plot. However, if different cells

responded to washout, we would expect the data to contain two groups; the first group would contain cells that increased their FR with NE but exhibited a FR decrease after wash-out (above unity line in Figure 2.5D) and the second group would contain cells that failed to directly respond to NE application with an increase in FR yet exhibited a delayed response after NE wash-out (below unity line). For the NE concentrations that appeared to have an outlasting effect as determined by the time-course data (Figure 2.3), we noted an increased number of cells on the unity line (blue dots, 3 rightmost panels), further supporting that the units which directly responded to NE were the ones to exhibit an outlasting FR increase.

After we determined that the FR of slices subjected to higher concentrations of NE remained elevated for the remaining 1800s of the experiments after washout of the drug, we wanted to determine how long this plasticity can remain in effect. To do so we performed 9000s experiments using 1800s of control, then 1800s with 100μM NE, followed by 5400s of washout. We then examined 300s windows at the end of control epoch (1800s), end of the NE epoch (3600s), and 5 washout epochs (5400s, 6000s, 7000s, 8000s, and 9000s). We compared the distribution of FRs of each of the washout epochs to that of the same channels in control. We found that the plasticity effect was detectable for least 40 minutes after switching to control aCSF (data not shown).

Effects of Neuromodulators by Cortical Depth

Having described the effects of both neuromodulators on average FR, we further divided the data to examine if these results depended on cortical depth. We used histological methods to determine the cortical layer of each electrode and by extension each cell recorded from that electrode. We separated cells into superficial (layers I to IV) and deep layers (V and VI) to examine the differential effect of CCh and NE between superficial and deep layers of cortex. In Figure 2.6A, we display the median neuromodulator effect size of both superficial and deep layers for CCh (top) and NE (bottom) for all concentrations (increasing left to right). Only 1 and 100μM concentrations showed a significant difference between superficial and deep layers (Table 2.1, two leftmost columns). However, for all concentrations of CCh the data trended towards deeper layers exhibiting a larger response. When examining NE slices, we found that for both 1 and 50μM NE concentrations the median neuromodulator effect size of deep layers

was significantly larger than that of superficial layers. As with CCh slices, all concentrations of NE trended towards a larger effect in deeper layers, however the bidirectional modulation of FR by NE obscured the results. Deeper layers of cortex exhibited a greater response to 1 and 50μM NE than those in superficial layers.

We were interested in examining both the neuromodulator and washout epochs of our experiment to determine if the response observed during the neuromodulator epoch was reversible by washout. We examined the median plasticity size of both CCh (top) and NE (bottom) for all concentrations (increasing from left to right) in Figure 2.6B. We found that when evaluating washout, single units for all CCh concentrations return to, or undershoot baseline established by the control epoch (Table 2.1, two rightmost columns). The small difference between control and washout FR confirmed the return to baseline observed in Figure 2.2B and Figure 2.3A. Additionally, the layer dependence of the neuromodulator effect observed in the neuromodulator epoch was not present during the washout epoch for all concentrations. After washout of CCh, there was no significant difference between superficial and deep layers for any of the concentrations studied. Having established that the same cells stay active during the plasticity epoch after washout of NE (Figure 2.5B), we expected to see one or both layer-groups remain at an elevated FR for higher concentrations of NE. Indeed, after washout of 10 or 50μM NE FR of neurons in deep layers remained significantly elevated in comparison to those in superficial layers. This indicates that the elevated spontaneous activity visible in the plasticity epoch of the time courses for these concentrations was mediated by cells in deeper layers of cortex.

Network Dynamics

So far, we have presented analysis of the changes in FR induced by a wide-range of CCh and NE concentrations. However, signaling in cortex is assumed to rely on more sophisticated temporal and spatial features of network activity. We therefore employed four additional approaches to provide more detailed insights into cholinergic and noradrenergic modulation of spontaneous cortical network dynamics with regards to temporal and spatial activity structure. In particular, it has been shown that information processing in cortex is dependent on not only the number of spikes but the timing of those spikes (Gerstner, Kreiter, Markram, & Herz, 1997). To investigate the amount of information contained in the

spontaneous activity we examined the ApEn of each channel. ApEn is a nonlinear measure of variance that when applied to a spike train measures the amount of information that can be contained in that spike train. When we plotted the change in ApEn versus the neuromodulator effect size (the change in FR) (Figure 2.7A, CCh top, NE bottom, increasing concentration from left to right), we found that ApEn is not correlated with neuromodulator effect size and therefore indeed a measure for temporal structure and not simply of activity levels (-0.0114 for 1μM CCh, 0.212 for 10μM CCh, 0.0271 for 50μM CCh, 0.0742 for 100μM CCh, 0.290 for 1μM NE, 0.0553 for 10μM NE, 0.164 for 50μM NE and 0.319 for 100μM NE; n = 167, 225, 225, 283, 195, 272, 187 and 210 channels from 9, 13, 12, 14, 10, 11, 9 and 13 slices). We next examined the median change in ApEn (rightmost panel of Figure 2.7A for each concentration of CCh, top, and NE, bottom). We additionally validated our results against control slices (0.027 ± 0.0121, n = 150 from 6 slices) and confirm that with the exception of 100μM NE all concentrations tested significantly increased ApEn. Despite the lack of correlation between neuromodulator effect size and change in ApEn, the median change in ApEn was similar in shape to the neuromodulator effect size (0.113 ± 0.0348 for 1μM CCh, 0.449 ± 0.0353 for 10μM CCh, 0.869 ± 0.0321 for 50μM CCh, 0.492 ± 0.0355 for 100μM CCh, 0.113 ± 0.0293 for 1μM NE, 0.172 ± 0.0286 for 10μM NE, 0.146 ± 0.0332 for 50μM NE, and 0.103 ± 0.0320 for 100μM NE; n = 167, 226, 226, 285, 195, 272, 187 and 210 channels from 9, 13, 12, 14, 10, 11, 9 and 13 slices). These results imply that overall the information content of spontaneous activity increases together with overall FR yet at the level of individual network locations the modulation of these two features (ApEn and FR) are uncorrelated and possibly mediated by distinct mechanisms.

After we determined that individual channels contain more information with application of neuromodulators, we examined the change in spatial network dynamics by measuring pairwise correlations coefficients of all pairs of multiunit channels per slice. In essence, each channel on each slice was compared to each of the other channels on that slice for all epochs. We display here a typical result showing that application of 10μM CCh decreased correlation between channel pairs (Figure 2.7B Left). We then combined the results of all slices of CCh (top) and NE (bottom) by concentration (increasing from left to right) and found that with the possible exception of 50 and 100μM CCh, both neuromodulators generally decreased the correlation between multiunit channels. We then compared the median change correlation (-0.0185 ± 0.0034 for 1μM CCh, -0.0124 ± 0.0041 for 10μM CCh, 0.0070 ± 0.0022 for 50μM

CCh, 0.0004 ± 0.0012 for 100μM CCh, -0.00842 ± 0.00152 for 1μM NE, -0.01241 ± 0.00406 for 10μM NE, -0.025794 ± 0.00482 for 50μM NE, -0.0166 ± 0.00319 for 100μM NE, and 0.0272 ± 0.0121 for control slices; n = 3558, 4042, 4734, 6252, 3896, 6884, 3946, 3608, and 3676 electrode pairs from 9, 13, 12, 14, 10, 11, 9, 13 and 6 slices). Because most channel pairs were already decorrelated in control condition, the change in correlation was smaller than we expected, indeed when we excluded channel pairs that had a correlation value of less than 0.1 for both epochs we found a much larger effect (-0.245 ± 0.009 for 1μM CCh, -0.355 ± 0.010 for 10μM CCh, 0.108 ± 0.009 for 50μM CCh, -0.178 ± 0.008 for 100μM CCh, -0.172 ± 0.009 for 1μM NE, -0.211 ± 0.005 for 10μM NE, -0.548 ± 0.008 for 50μM NE, -0.298 ± 0.007 for 100μM NE and -0.131 ± 0.014 for control slices; n = 1006, 1348, 1282, 604, 392, 1554, 1368, 972 and 368). 1 and 10μM CCh both significantly decorrelated the network while 50μM had a smaller but significant increase in correlation. All concentrations of NE significantly decreased correlations, indicating that neural activity on different channels became more independent with application of NE. This decorrelation led us to conclude that the temporal and spatial patterning of the spontaneous activity increased the complexity of the network dynamics within the slices.

We next examined the effect of CCh and NE on the power spectrum since these neuromodulators typically reduce low frequency oscillations *in vivo* yet the effect of CCh, only in presence of blocked synaptic inhibition, has been reported to enhance rhythmic neocortical activity *in vitro* (Lukatch & MacIver, 1997). We examined the compensated power spectral densities (PSDs) of the discrete spike trains of single units obtained in each epoch. Figure 2.8A displays the median compensated PSD of single units in neuromodulator minus the control compensated PSD. Both neuromodulators in all concentrations decrease the power in low frequencies (up to ~8Hz) as indicated by a negative difference between neuromodulator and control.

Since we were able to simultaneously record spikes from over 50 units per slice on average, we were able to use measures of the dynamics of the slice as a whole which can uncover fundamental changes in the network dynamics (Schiff, Huang, & Wu, 2007). To examine the complexity of the network as a whole we performed PCA on the spike trains of all single units that together form time-dependent activity vectors (5s non-overlapping windows). As applied here PCA uses singular value decomposition to transform spike trains of measured single units into theoretical activity generators, each of which explain

some amount of the variance of the original activity vectors. We first examined percent variance explained by each component dimension and determined the percent of total dimensions required to explain at least 50% of the total variance (Figure 2.8B top left; variable dimensions black, less variable dimensions gray). The mean of all windows was determined for both control and neuromodulator epochs and the difference calculated (Figure 2.8B bottom left; green percent of total dimensions for each window in control, red in 50μCCh). From the increased temporal and spatial complexity of multiunit channels as measured by ApEn and correlation coefficients, we expected addition of neuromodulators to increase the spatiotemporal complexity of the whole-slice network dynamics. Indeed, for all concentrations of both neuromodulators the data trended towards increased complexity. When we applied CCh the percentage of total dimensions needed to explain 50% of the variance was significantly increased for 50 and 100μM concentrations (5.16 ± 1.17 for 1μM CCh, 6.72 ± 1.42 for 10μM CCh, 15.80 ± 1.59 for 50μM CCh, 7.30 ± 1.49 for 100μM CCh; n = 9, 13, 13 and 13 slices). Similarly 1 and 10μM concentrations of NE caused a significant increase in dimensionality (5.37 ± 1.23 for 1μM NE, 4.00 ± 0.86 for 10μM NE, 6.16 ± 2.11 for 50μM NE, and 3.59 ± 1.47 for 100μM NE; n = 13, 11, 10 and 14 slices). The increase in the number of dimensions required to explain 50% of the variance indicates that the complexity of the network as a whole is increased when CCh or NE was applied.

Pharmacological Agents Identify Receptor Specific Effects

Thus far we have characterized the effects of CCh and NE on overall cortical network dynamics in visual cortex. We next used selective agonist and antagonists to determine the receptor types involved in these responses. Based on the literature (Kirkwood et al., 1999; Metherate, Ashe, & Weinberger, 1990), we expected that muscarinic M1 receptors mediated the increase in FR by the cholinergic agonist CCh. Indeed, we found that the muscarinic M1 receptor antagonist pirenzepine completely blocked the CCh (50μM) mediated enhancement of spontaneous activity (5μM; -logarithmic effect size: 0.085 ± 0.043, n = 5 slices; Figure 2.9A, left). In addition, we also did not find a response to nicotine (10μM, -0.052 +0.019 n = 12, Figure 2.8A, right). Together, in agreement with the literature, these experiments suggest that the CCh response was predominantly mediated by M1 muscarinic receptors.

We dissected the response to NE by using both selective agonists and antagonists (in presence of 50μM NE) for α_1, α_2, and β receptors. Inspection of the z-scored time-courses for the agonists supported a potential role of both α_1 and β signaling in mediating the outlasting increase in FR (Figure 2.9B, left, top to bottom). We found that application of the α_1 agonist L-Phenylephrine slowly increased FR which remained elevated after washout (10μM; 0.245 ± 0.048, n = 7 slices). Clonidine, a α_2 agonist, caused a small reduction in the spontaneous FR (-0.044 ± 0.022, n = 6 slices). Using a β agonist, isoproterenol (40μM; 0.104 ± 0.048, n = 5 slices), we observed an initial transient response to the agent similar to that of 50μM NE (Figure 2.3B, 3rd from top) and again an outlasting response. We then used selective antagonists (Figure 2.8B, right, top to bottom) together with 50μM NE to further verify these results. Indeed, blocking α_1 and α_2 receptors did not suppress the enhancing effect of NE based on the time-course but the application of the α_2 antagonist caused an overall run down of the activity which lead to decrease in FR in our measure (20μM, 40μM; 0.040 +0.030, -0.044 +0.025 n = 6 and 8 slices, respectively). However, the β antagonist propranolol completely blocked the enhancement which suggests that the NE response shown in this study was mostly mediated by this receptor type (40μM; -0.0335 +0.0261, n = 7 slices). The activated yet delayed response to the α_1 agonist, however, hints at extra complexity that may warrant further future studies with techniques complementary to the ones used here.

DISCUSSION

Summary of Findings

In this study, we compared the concentration-dependent network effects of cholinergic and noradrenergic neuromodulators that are associated both with determining overall cortical state and with synaptic plasticity. We found that application of CCh greatly increased spontaneous activity of most active cells predominately via modulation of muscarinic M1 receptors. In contrast, the effect of NE was more diverse with cells increasing or decreasing their firing rate. Overall, NE mediated only a modest instantaneous increase in network activity when compared to CCh. However, NE induced plastic reorganization of the network (particularly in infragranular layers) that was maintained after wash-out for at least 40 minutes. We found this plasticity to be mediated by beta noradrenergic receptors with a

potential (smaller) role for α_1 receptors. Interestingly, we found significant effects of even just 1μM for both CCh and NE, concentrations which are likely close to physiological concentrations *in vivo*. Changes in activity level were accompanied by changes in the complexity of the spatiotemporal structure of the network activity. Both neuromodulators increased temporal complexity of individual channels as measured by ApEn. As would be expected for neuromodulators responsible desynchronizing networks (Armitage et al., 1969; Celesia & Jasper, 1966; Constantinople & Bruno, 2011; Jouvet, 1969; Kalmbach et al., 2012), lower concentrations of CCh and all concentrations of NE increased the spatial complexity by causing a decrease in the pairwise correlation between activity in different network locations. Similarly, measurements of dimensionality of the whole-slice network dynamics by principal component analysis also indicated an increase in complexity. Together, these results indicate that there are fewer similarities between network locations and more complexity in each individual location and in the overall spatio-temporal structure. Therefore, we concluded that both cholinergic and adrenergic neuromodulation increases overall network complexity yet CCh had a more pronounced, instantaneous effect whereas NE had a more moderate but outlasting effect.

Studying Network Dynamics *In Vitro* with Multielectrode Arrays

To our knowledge, this is the first study that combined the use of a multielectrode array with sophisticated network-level analysis strategies to investigate the role of neuromodulation in acute cortical slices. The study of spontaneous network dynamics in acute cortical slices has emerged as a promising approach to understanding the synaptic mechanisms of rhythmic activity in cortex (Frohlich & McCormick, 2010; Sanchez-Vives & McCormick, 2000; Traub, Jefferys, & Whittington, 1994). Here, we used similar adaptions to the aCSF to make the conditions more *in vivo*-like and found robust yet sparse spontaneous activity in control conditions. Importantly, the spontaneous activity in our slices exhibited a layer-dependent FR profile very similar to what is typically found *in vivo* (Ruthazer, Baker, & Stryker, 1999; Schroeder & Foxe, 2002). Oxygenation of slices had been reported to be of particular importance for the generation and maintenance of spontaneous activity in slice (Hajos et al., 2009; Hajos & Mody, 2009) and the perfusion system in our MEA experiments likely provided enhanced oxygenation in comparison to the standard submerge slice chamber. The new generation of MEAs (Boppart, Wheeler, & Wallace, 1992;

Huang, Williams, & Johnson, 2012; Stett et al., 2003) has provided important insight into the genesis of hypersynchronized, epileptiform activity patterns in acute hippocampal and cortical slices (Beggs & Plenz, 2003; Gonzalez-Sulser et al., 2011; Motamedi, Gonzalez-Sulser, Dzakpasu, & Vicini, 2012; Motamedi et al., 2006; H. Yang, Shew, Roy, & Plenz, 2012). Previously, MEA studies mostly focused on cultured neuronal networks due to the better signal quality to be obtained from neurons directly grown on the MEA (Becchetti et al., 2012; Beggs & Plenz, 2004; Egert et al., 1998; Gullo, Maffezzoli, Dossi, & Wanke, 2009; Nikonenko, Jourdain, & Muller, 2003; Okawara et al., 2007; Petrozzino, Pozzo Miller, & Connor, 1995; Sullivan, Leu, Taylor, Fahlman, & Bickler, 2002). Given the confidence with which we succeeded in extracting on average more than 50 well-isolated single units per slice, we believe that the experimental approach taken here can be applied to the study of other modulatory pharmacological manipulations including both endogenous ligands and exogenous, pharmacological compounds for drug testing (Gholmieh et al., 2001; Gross, Rhoades, Azzazy, & Wu, 1995).

Neuromodulation in Acute Cortical Slices

The literature on the effects of the neuromodulators ACh and NE on cellular and synaptic excitability is inhomogeneous. Most recently (Favero, Varghese, & Castro-Alamancos, 2012) have noted that ACh caused a decrease in excitability of excitatory cells of layers II/III and IV of somatosensory cortex *in vitro*. Conversely, (Eggermann & Feldmeyer, 2009) uncovered an excitatory effect of acetylcholine in layer II/III and V while confirming a decrease in excitability of layer IV spiny neurons. Earlier, pioneering studies have already pointed to how both increases and decreases of excitability can occur in response to acetylcholine *in vitro* (McCormick & Prince, 1986). Adding to this complexity, studies *in vivo* have yielded a wide range in percentage of neurons excited by cholinergic modulation (Bassant, Baleyte, & Lamour, 1990; Lamour, Dutar, & Jobert, 1982; Lamour, Dutar, Jobert, & Dykes, 1988; McKenna, Ashe, Hui, & Weinberger, 1988; Metherate et al., 1990; Metherate, Tremblay, & Dykes, 1988; Muller & Singer, 1989; Sillito & Kemp, 1983). We have shown here that the net effect of CCh acting on cholinergic receptors is an increase of overall spontaneous activity. For NE, previous work (Favero et al., 2012) suggests a decrease in excitability of excitatory cells accompanied by an increase in excitability of fast-spiking interneurons. This result, which is in agreement with (Kawaguchi & Shindou, 1998) may

explain the diversity of changes in FR when we applied NE to the slices in this study. When NE is applied, the FR of interneurons would increase while postsynaptic excitatory cells would decrease their FR, and indeed we noted that 100μM NE caused a significant number of channels with a FR decrease (Figure 2.4, bottom right). However a recent human study, administration of a NE reuptake inhibitor (thereby increasing extracellular NE) was shown to increase excitability in visual cortex (Hoffken, Lenz, Hockelmann, Dinse, & Tegenthoff, 2012). Therefore, no consensus has yet been reached on the net effect of NE on cortical network activity; our results support a net enhancement of the activity levels for the wide range of concentrations evaluated in our study. Some of the differences to these studies might be explained by differences in the methods used; in our study due to the arrangement of electrodes we performed a sampling of spontaneously activity cells and by means of extracellular recordings we did not perturb the intracellular milieu (and therefore signaling) as is the case for intracellular recordings. Extracellular recordings of action potentials also have potential biases towards (1) neurons with high spontaneous firing rates such as fast-spiking inhibitory interneurons (McCormick, Connors, Lighthall, & Prince, 1985) and (2) pyramidal cells that exhibit larger extracellular spike waveforms due to their cell morphology (Holt & Koch, 1999).

Response Dynamics

Despite the similarities in effect between the cholinergic and noradrenergic systems, there are important functional contrasts (Aston-Jones & Cohen, 2005; Baxter & Chiba, 1999; Bouret & Sara, 2005; Vankov et al., 1995; Yu & Dayan, 2005). In particular, the cholinergic system has been linked to tasks where there is an expected uncertainty, for example the state of a traffic light on a daily commute. On the other hand, NE is released in response to an unexpected uncertainty or object novelty, for example a new traffic light on the commute. Therefore, while both systems are tuned to enable privileged processing of incoming input by for example increasing the signal-to-noise ratio in primary sensory cortices, our results indicate that the modulation of spontaneous activity is different for the two systems, in particular with regards to the duration of the effect. An overall (and pronounced) increase in overall excitability as found for CCh may subserve the processing of weaker stimuli that otherwise would have remained subthreshold events. Scenarios that lead to an increase in NE release in the behaving animal are likely to be of

fundamental importance to the animal where a change to the circuitry beyond the presence of the increased NE release is beneficial and may correspond to the plasticity effect found in this study for NE. Importantly, we did not employ any artificial (electric) stimulation of the network to induce changes to the network or measure changes to evoked responses in the network with application of CCh or NE, rather we studied how the endogenously generated, spontaneous cortical activity was modulated.

Plasticity

Both cholinergic and noradrenergic systems have been implicated in learning and memory because both systems affect mechanisms of synaptic plasticity that cause long-term changes in synapse strength such as long-term potentiation (LTP) and long-term depression (LTD) for example by spike-time dependent plasticity (STDP) (Bear & Singer, 1986; Bi & Poo, 1998; Froemke & Dan, 2002; Fu et al., 2002; Kirkwood, Rioult, & Bear, 1996; Markram, Lubke, Frotscher, & Sakmann, 1997; Sjostrom & Nelson, 2002). Typically, synaptic plasticity is studied *in vitro* with different protocols of presynaptic and postsynaptic stimulation. Given that the detailed temporal structure of the pre-synaptic and postsynaptic spiking pattern determines synaptic plasticity (Froemke & Dan, 2002; Sjostrom & Nelson, 2002), our results on NE-induced plasticity are particularly intriguing since we did not apply any exogenous electrical stimulation. Rather, the spontaneous activity in our slice preparation was sufficient to support changes in its activity structure in response to NE application. Supportive of such an underlying mechanism are the findings that when neuromodulators are added, the temporal windows between pre- and postsynaptic action potentials for plasticity were increased in hippocampus (Lin, Min, Chiu, & Yang, 2003) and visual cortex (Seol et al., 2007). Alternatively, the plasticity effects in our study could also be explained by intrinsic plasticity. In this scenario, the increased firing rate caused by NE triggered a reorganization of intrinsic excitability (Desai, Rutherford, & Turrigiano, 1999).

While we do not have evidence for the specific role of synaptic or intrinsic plasticity in our experiments, possibly the most parsimonious explanation is indeed that CCh did not trigger synaptic plasticity but NE triggered LTP. Previous studies (Choi et al., 2005; Kirkwood et al., 1999; Seol et al., 2007) found LTD caused by cholinergic M1 receptors. At the level of spontaneous cortical network activity, we did not find any response indicative of LTD. Therefore, either the spontaneous activity was not

appropriately patterned to induce LTD or the synapses that were indeed subject to LTD played a minor role in the generation of the spontaneous activity. In contrast, it has been shown that NE causes LTP (Thomas et al., 1996; H. W. Yang, Lin, Yen, & Min, 2002), which is independent of the order of pre- and post-synaptic spikes (Lin et al., 2003). In the case of higher concentrations (in particular 10 and 50μM), we observed that the application of NE had an outlasting, enhancing effect on the spontaneous activity. This outlasting effect is likely caused by such LTP, where the temporal patterning of the spontaneous activity is not specific enough to induce a measurable change in activity levels but when the STDP rule is loosened such that any temporal order induces LTP, the same structure is sufficient to induce long-lasting changes to synaptic strength.

Conclusions and Outlook

Acetylcholine and norepinephrine are two well-studied neuromodulators due to their global importance in regulating synaptic and neuronal excitability as a function of behavioral state. Importantly, aberrations in these neuromodulatory systems have been implicated in a range of neuro-psychiatric disorders such as autism (Bodner, Beversdorf, Saklayen, & Christ, 2012; Deutsch, Urbano, Neumann, Burket, & Katz, 2010; Perry et al., 2001) and attention-deficit disorder (Michelson et al., 2003; Milberger, Biederman, Faraone, Chen, & Jones, 1997; Wilens et al., 1999). The vast number of different targets for these neuromodulators even just within cortex and the often seemingly contradicting findings on their effect on excitability has prevented an overall understanding of the effect on cortical network dynamics from emerging. Here we made use of recent technological innovation for the study of network dynamics with single-unit resolution *in vitro* (Egert, Heck, & Aertsen, 2002). We found that the cholinergic and the noradrenergic system both increased overall network complexity and activity levels with the important difference that the effects by norepinephrine outlasted the presence of the neuromodulators, indicative of a plastic reorganization of the underlying cortical circuit.

FIGURES AND TABLES

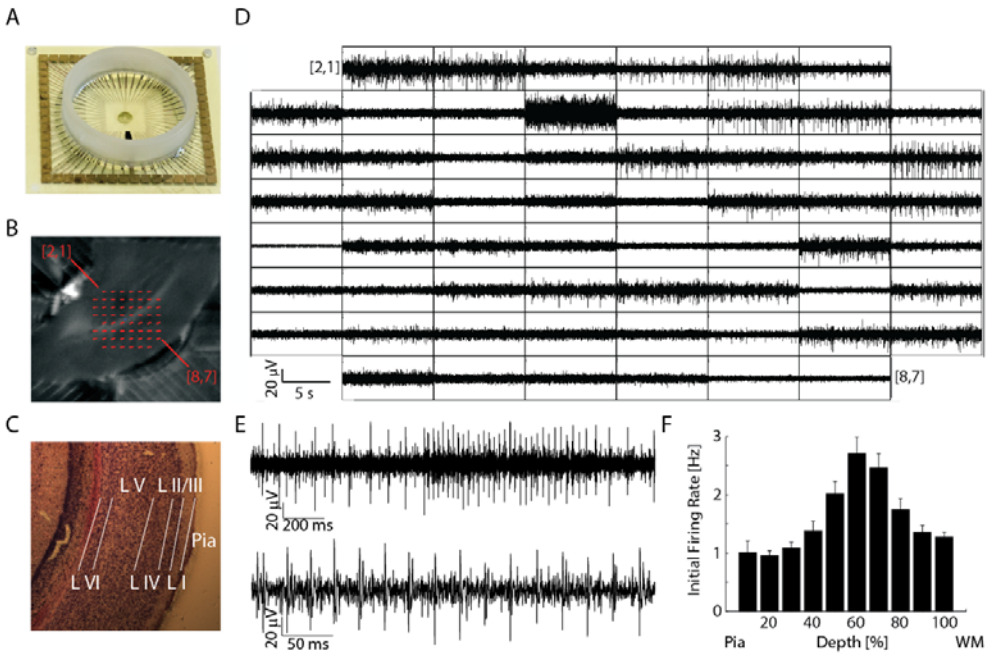

Figure 2.1. Use of a multielectrode array (MEA) allows simultaneous readings of neuronal activity on 59 channels.

(A). 200 µm x 200 µm MEA. (B). Cortical slice on the MEA with electrode locations superimposed (red); electrodes [2, 1] (top, leftmost) and [8, 7] (bottom, rightmost) indicated. (C). Nissl stained slice of mouse primary visual cortex with cortical layers and pia indicated. (D). A 10 s trace of all channels simultaneously recorded (top left: electrode [2, 1]; bottom right electrode [8, 7]). (E). Expanded traces from a single channel of panel (D) with many action potentials visible (Top: 1 s; Bottom: 250 ms). (F). Spontaneous activity (spikes per second) by cortical depth exhibited laminar profile with deeper layers more active than superficial layers.

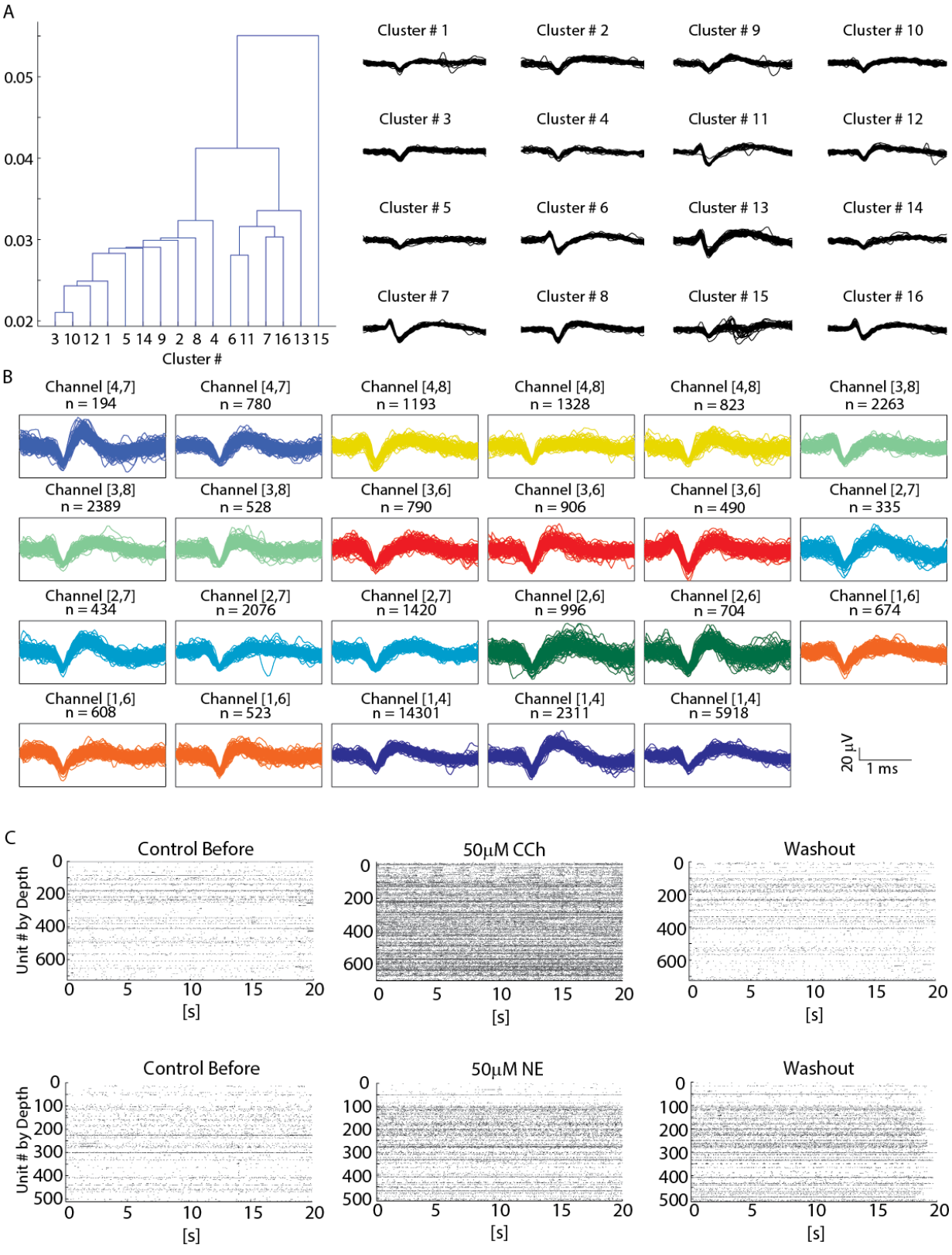
A
0.05
0.04
0.03
0.02
3 10 12 1 5 14 9 2 8 4 6 11 7 16 13 15
Cluster #
Cluster # 1
Cluster # 2
Cluster # 9
Cluster # 10
Cluster # 3
Cluster # 4
Cluster # 11
Cluster # 12
Cluster # 5
Cluster # 6
Cluster # 13
Cluster # 14
Cluster # 7
Cluster # 8
Cluster # 15
Cluster # 16
B
Channel [4,7] n = 194
Channel [4,7] n = 780
Channel [4,8] n = 1193
Channel [4,8] n = 1328
Channel [4,8] n = 823
Channel [3,8] n = 2263
Channel [3,8] n = 2389
Channel [3,8] n = 528
Channel [3,6] n = 790
Channel [3,6] n = 906
Channel [3,6] n = 490
Channel [2,7] n = 335
Channel [2,7] n = 434
Channel [2,7] n = 2076
Channel [2,7] n = 1420
Channel [2,6] n = 996
Channel [2,6] n = 704
Channel [1,6] n = 674
Channel [1,6] n = 608
Channel [1,6] n = 523
Channel [1,4] n = 14301
Channel [1,4] n = 2311
Channel [1,4] n = 5918
20 µV
1 ms
C
Control Before
50µM CCh
Washout
Unit # by Depth
[s]
Control Before
50µM NE
Washout
Unit # by Depth
[s]

Figure 2.2. Single Units

(A) Left: Dendrogram of similarity between combined clusters. Clusters are grouped by linkage analysis. Right: 16 clusters from 3000 spike waveforms. (B) Representative units from 8 channels of a representative example slice. Units from the same channel are in the same color; channel numbers and number of spikes (n) for each unit are indicated. (C) Raster plots of all single units isolated in 50 mM CCh (top) and 50 mM NE (bottom) for the final 20 s of control, neuromodulator, and washout epochs (left to right),indicating increased FR for 50 mM CCh, 50 mM NE, and NE washout epochs.

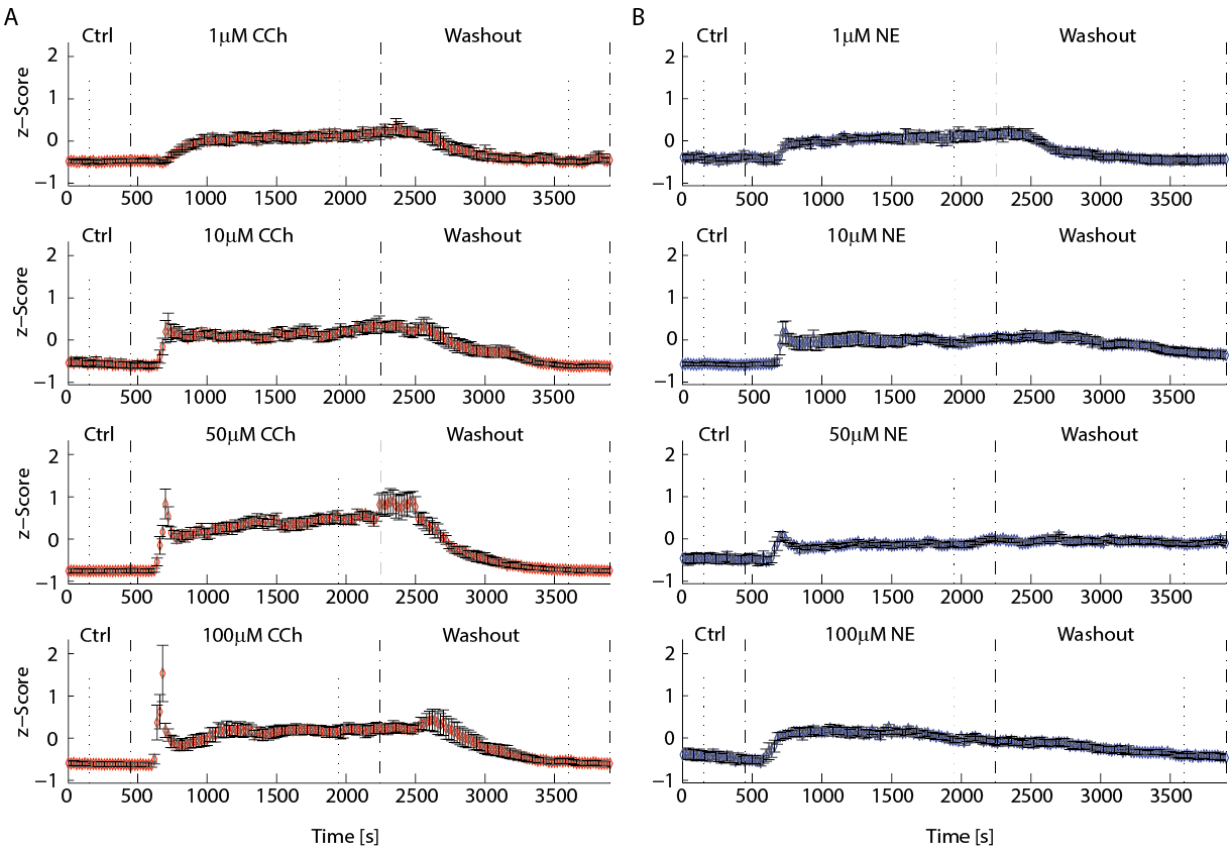

Figure 2.3 Time-courses of spontaneous activity in response to neuromodulator application.

(A). Time-course of median z-score of FR for all 1, 10, 50 and 100 mM CCh slices (top to bottom). Dashed lines indicate times of aCSF switches. Analysis windows were taken from last 300 s before aCSF switch (between dotted and dashed lines). CCh response begins with a large increase in FR around 700 s. After washout (about 2500 s here) the FR begins to return to baseline. By the washout analysis window all FRs have returned to baseline. (B) Time-course of median z-score of FR for all 1, 10, 50 and 100 mM NE slices (top to bottom). Around 700 s there is an increase in FR which remains until 2500 s where 1 mM NE slices return to baseline FR. 10, 50 mM NE slices do not return to baseline for the duration of the experiment (at least 1800 s washout).

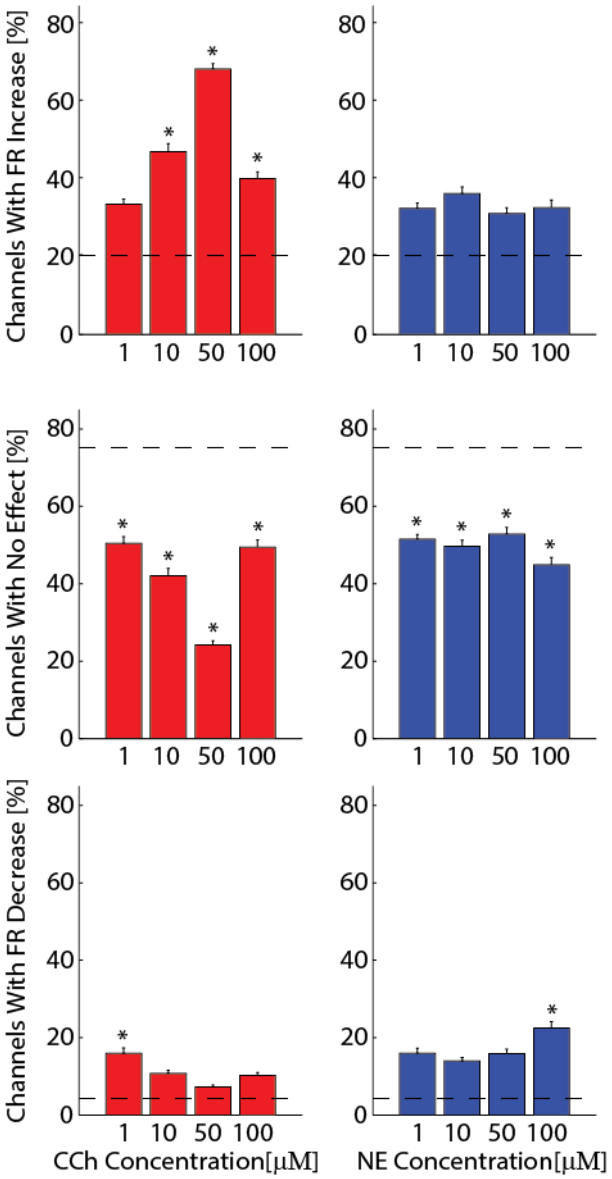

Figure 2.4. Effect types.

Percent of channels per slice for CCh (left) and NE (right) slices with a significant FR increase (top), no effect (middle), and significant FR decrease (bottom). Dashed line indicates mean for control slices. Only applications of 10, 50, and 100 mM CCh caused more channels to have a significant FR increase compared to control slices. However, all concentrations tested had fewer channels with no significant effect than control slices. Additionally 1 mM CCh and 100 mM NE caused more channels to have a significant decrease in FR than control slices (*$p < 0.05$ vs. control slices).

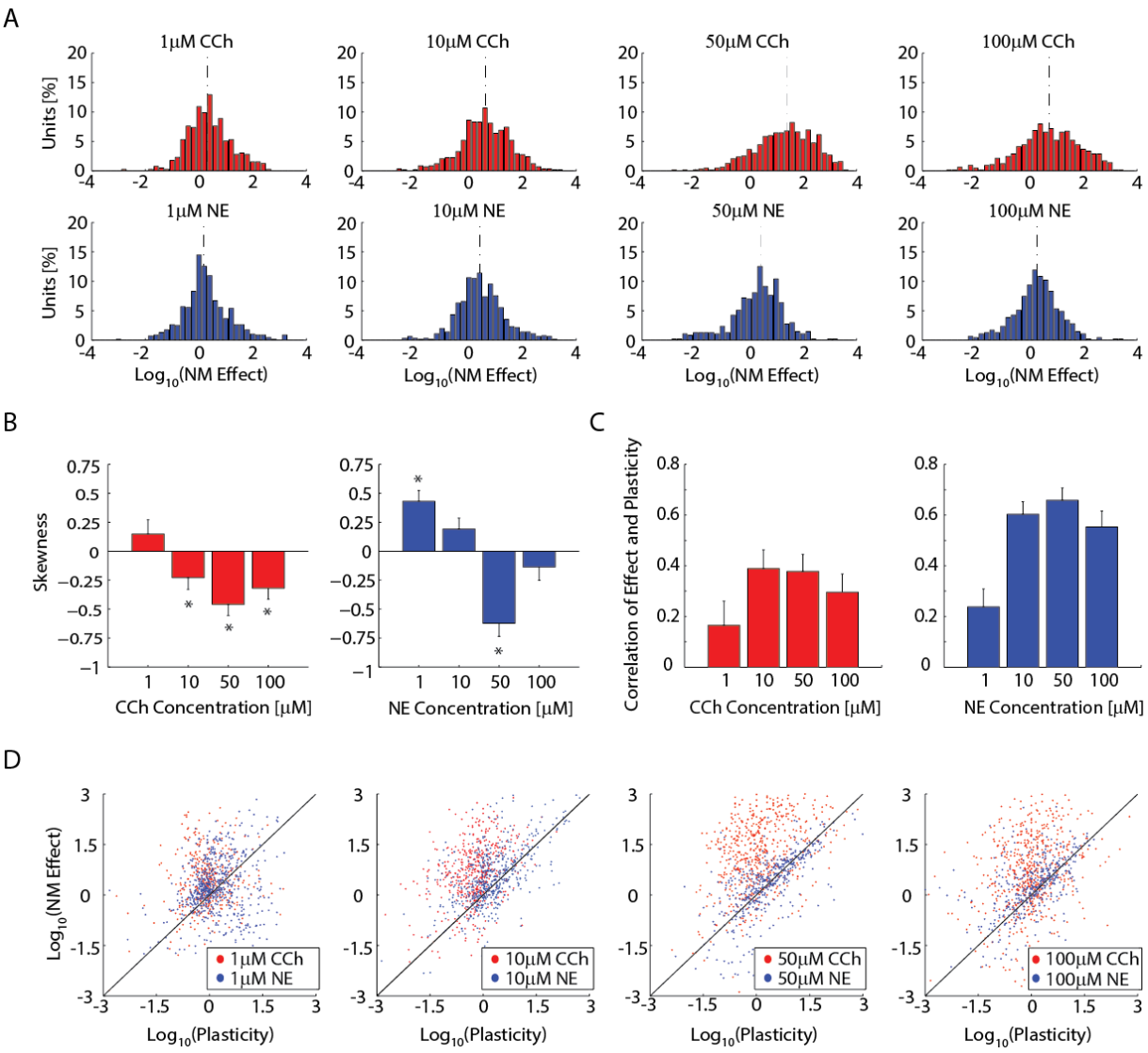

Figure 2.5. Neuromodulator effect and plasticity

(A) Distribution of neuromodulator effect on neurons for CCh (top) and NE (bottom) for increasing concentrations (left to right). Dashed line indicates median effect size. Application of CCh caused mostly increased FR (effect size greater than 0). Application of NE typically enhanced FR, however the median change was much smaller than for CCh. (B) Skewness of effect size distributions shown in (A) CCh (red, left) and NE (blue, right). Error bars indicate standard error of skewness. (C) Correlation of effect and plasticity size for CCh (red, left) and NE (blue, right). Error bars indicate 95% confidence interval. (D) Scatter plot of neuromodulator effect vs. plasticity for all neurons (CCh, red; NE, blue) for all concentrations (increasing left to right). Unity line (black) indicates no change in FR between neuromodulator and washout epoch. 1 mM data for CCh and NE both show low correlation between the

neuromodulator effect and plasticity. However, for higher concentrations of NE (10, 50 and 100 mM) the data lie on or near the unity line, indicating that the change in FR due to the application of NE continued after washout of the drug. CCh did not cause a similar outlasting effect. Less than 4% of data not plotted for visualization. (*$p < 0.05$ that distribution is skewed).

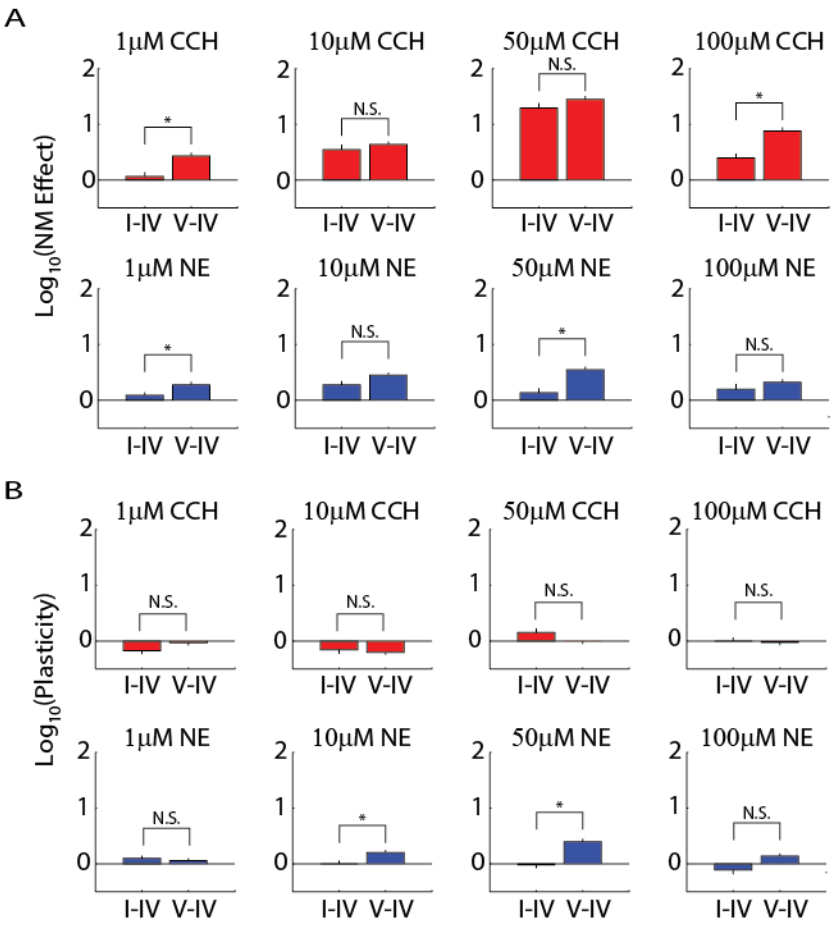

Figure 2.6. Effect by cortical depth.

(A) Median neuromodulator effect on layers I-IV and layers V-VI for single units (CCh, top; NE, bottom) for increasing concentrations (left to right). The data trend toward larger effects in layers V-VI for all concentrations (significant for 1 mM CCh, 100 mM CCh, 1 mM NE, 50 mM NE). (B) Median plasticity effect on layers I-IV and layers V-VI for CCh (top) and NE (bottom) for increasing concentrations (left to right). The FR of units after washout of any concentration of CCh returned to near baseline (zero plasticity effect) after washout with no layer dependence. However after the washout of 10 or 50 mM NE cells in deep layers remained significantly more active than those in layers I-IV (*$p < 0.05$, N.S: not significant).

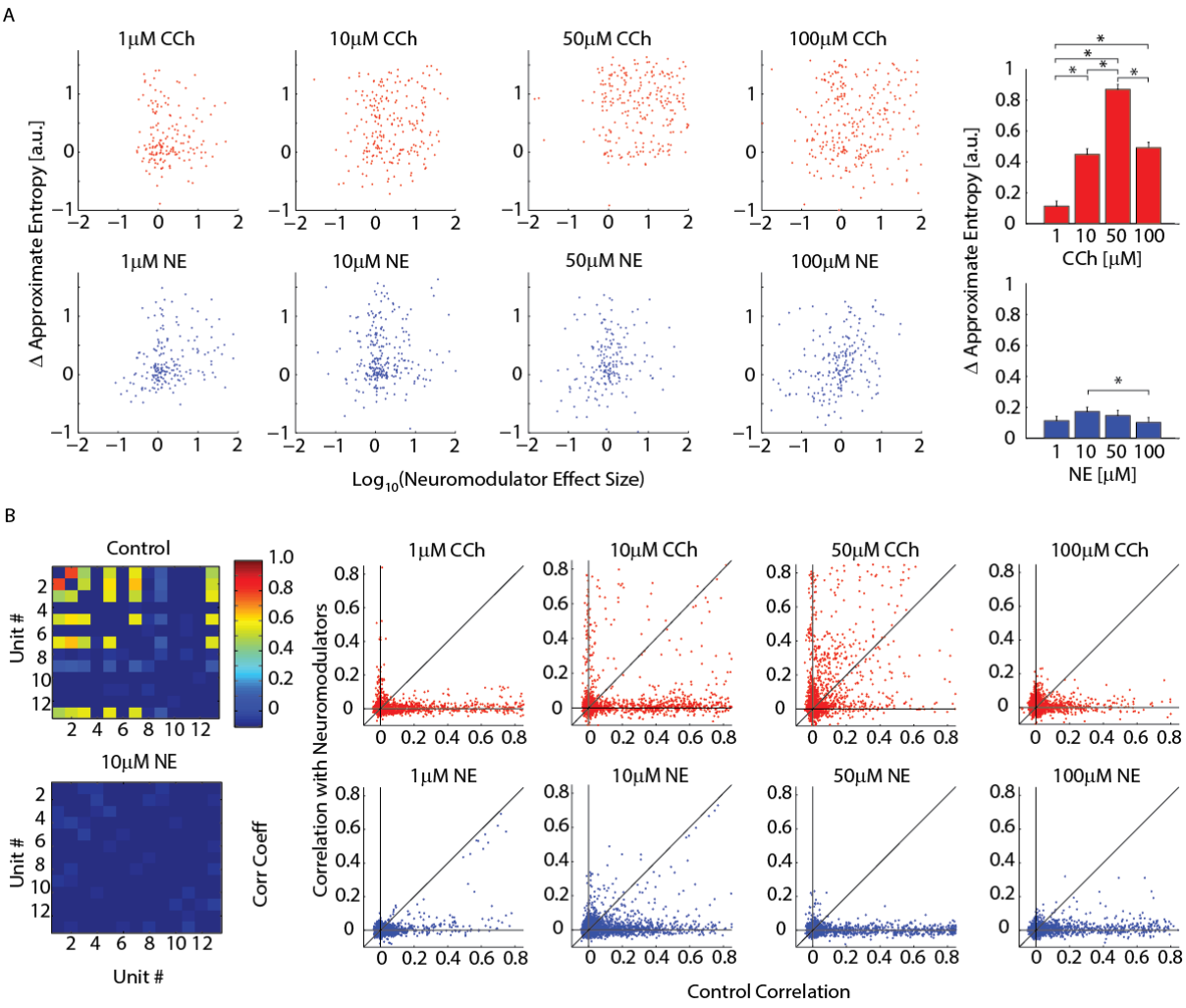

Figure 2.7. Network dynamics.

(A) Scatter plot of change in ApEn vs. neuromodulator effect (log_{10}) (left) of increasing concentrations (left to right) of CCh (top) and NE (bottom) for each channel. Both neuromodulators in all concentrations exhibited low correlation between ApEn and neuromodulator effect. Median change in ApEn by concentration for CCh (top) and NE (bottom) for increasing concentrations (left to right) displayed on the right. Applications of CCh up to 50 μM increased ApEn however application of 100 μM CCh caused an increase in ApEn that was significantly lower than 50 mM CCh. Channels in all concentrations of NE increased in complexity as measured by ApEn, however only 10 and 100 μM NE applications were significantly different from each other. (B) Left: Pairwise correlations multiunit activity in representative example slice in control aCSF (top) and 10 μM NE (bottom) displayed decorrelation. Right: Correlation of all electrode pairs per slice for all slices of CCh (top) and NE (bottom) for all concentrations

(increasing left to right). Application of either neuromodulator in most concentrations (with the exception of 50 and 100 μM CCh) caused a significant decorrelation of the network when compared to control slices. Application of 50 μM CCh caused a small but significant increase in correlation (*$p < 0.05$).

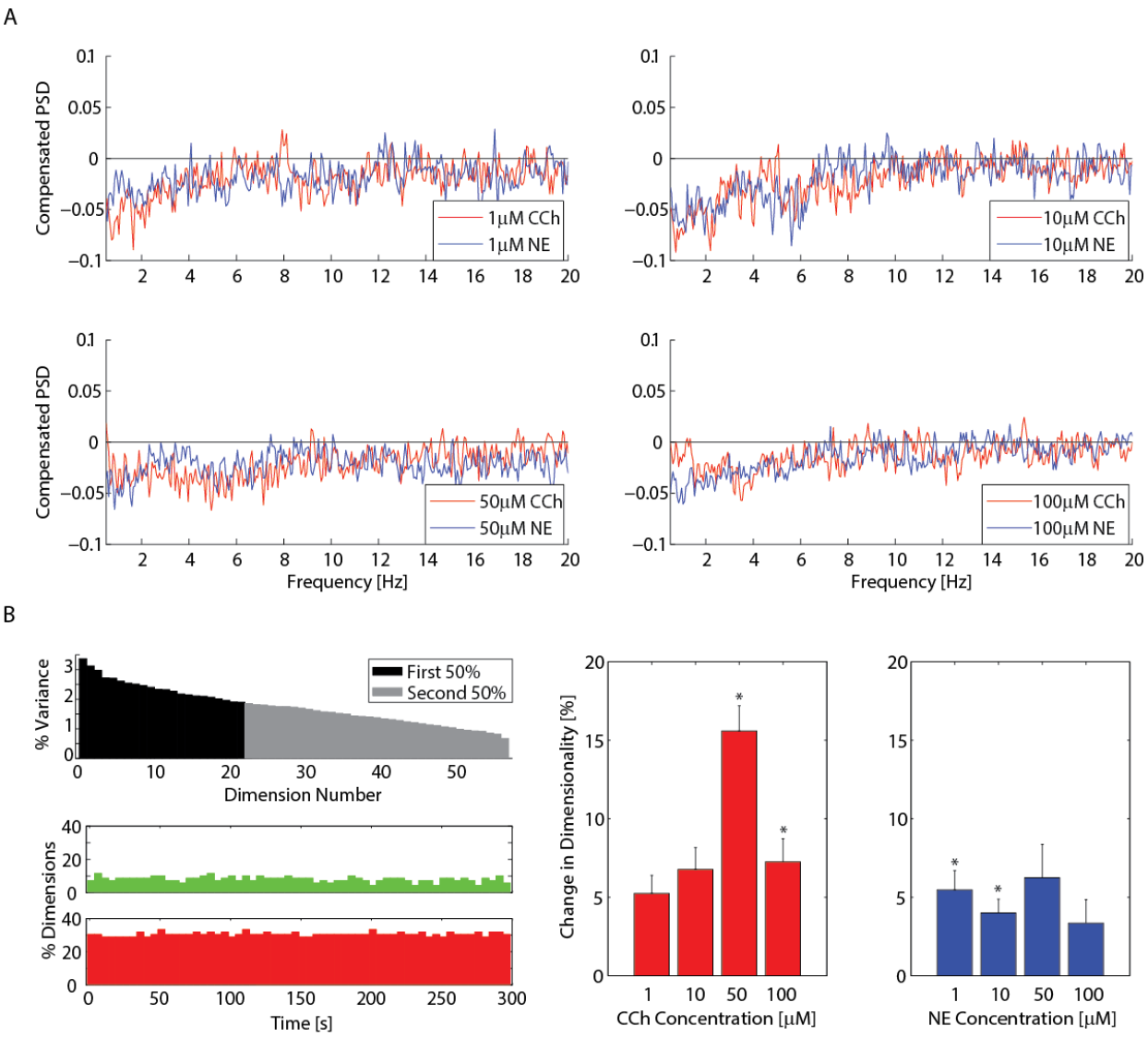

Figure 2.8. Frequency Analysis and PCA.

(A) Change in compensated PSDs between neuromodulator and control for 1, 10 (top, left to right), 50 and 100 µM (bottom, left to right) concentrations of CCh (red) and NE (blue). In all cases application of neuromodulators decreased low frequency power. (B) Left Top: component dimensions sorted by percent of variance explained for one window of one slice. Dimensions in black were the largest contributors to the overall variance (threshold at 50%). Left Bottom: percentage of total components required for explaining 50% of the variance for each 5 s window during the control (green, top) and 50 µM CCh (red, bottom) epochs of one slice. Right: Median change in dimensionality between neuromodulator and control epochs for CCh (red, left) and NE (blue, right). Positive values indicate increase in dimensionality and

therefore spatiotemporal complexity when the neuromodulator was applied. (*$p < 0.05$ neuromodulator vs control epochs).

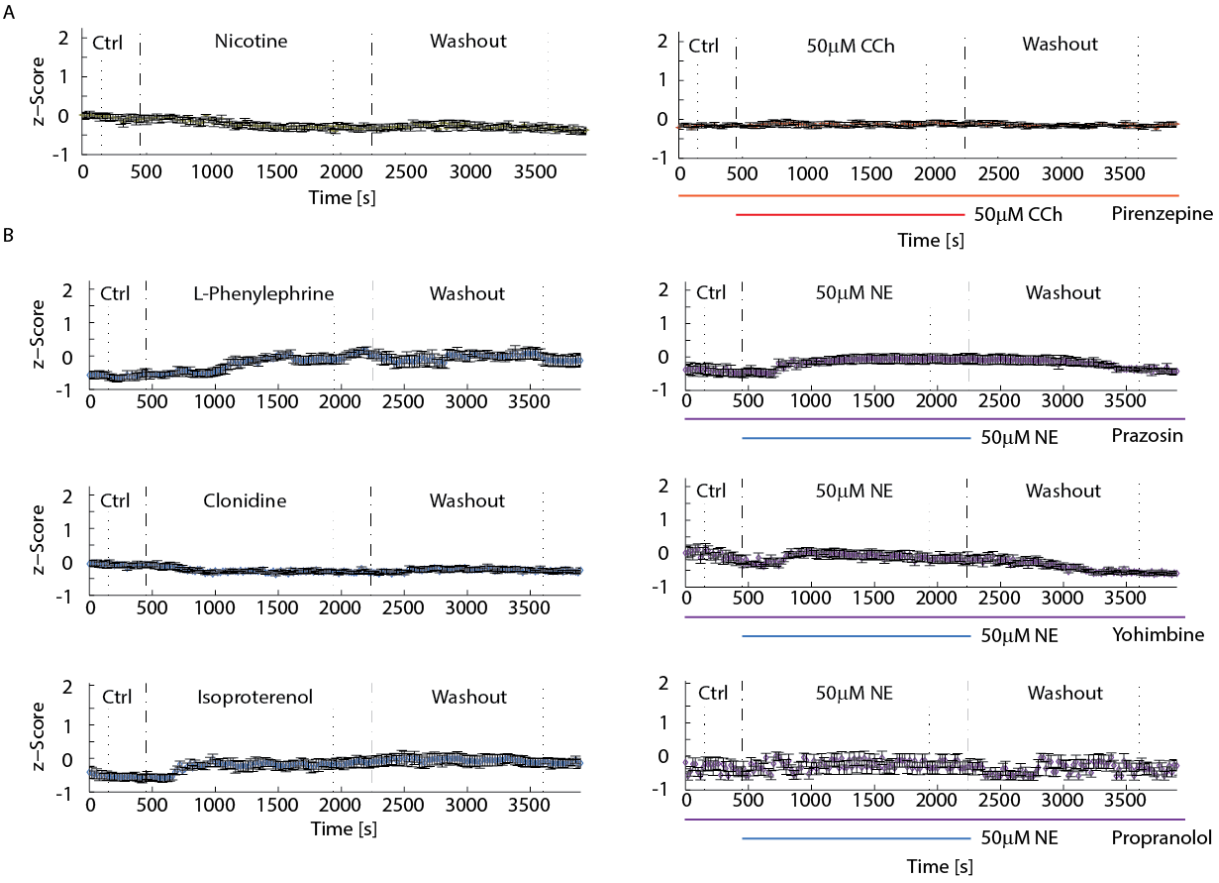

Figure 2.9. Time-course of response by receptor subtype.

(A) Z-scored time-courses for pirenzepine (left, M1 antagonist) and nicotine (right, nicotinic agonist) experiments. Blocking M1 receptors with pirenzepine completely abolished the effect of 50 mM CCh and nicotine had no significant effect. (B) Left: Z-Scored time-courses of L-Phenylephrine (α_1 agonist), Clonidine (α_2 agonist), Isoproterenol (β agonist) experiments. Increase of activity occurred for a_1 and b agonist, slight decrease occurred for α_2 agonist. Right: Z-Scored time-courses for α_1 (prazosin), α_2 (yohimbine) and b (propranolol) receptor antagonists. NE response was mostly unaffected for α_1 and α_2 antagonists. The b antagonist abolished the response.

	Effect I-IV	Effect V-IV	Plasticity I-IV	Plasticity V-VI
1μM CCh	0.065 ± 0.070; n = 120	0.433 ± 0.048; n = 278	-0.178 ± 0.051; n = 125	-0.032 ± 0.038; n = 276
10μM CCh	0.544 ± 0.081; n = 135	0.640 ± 0.044; n = 446	-0.160 ± 0.063; n = 126	-0.204 ± 0.033; n = 358
50μM CCh	1.290 ± 0.080; n = 194	1.449 ± 0.051; n = 438	0.150 ± 0.063; n = 179	-0.004 ± 0.041; n = 407
100μM CCh	0.398 ± 0.071; n = 194	0.879 ± 0.056; n = 462	0.000 ± 0.053; n = 184	-0.023 ± 0.040; n = 421
1μM NE	0.088 ± 0.046; n = 334	0.280 ± 0.046; n = 359	0.101 ± 0.036; n = 339	0.060 ± 0.034; n = 366
10μM NE	0.276 ± 0.059; n = 173	0.449 ± 0.041; n = 477	0.000 ± 0.053; n = 169	0.204 ± 0.039; n = 421
50μM NE	0.135 ± 0.077; n = 130	0.545 ± 0.051; n = 342	-0.015 ± 0.053; n = 137	0.398 ± 0.047; n = 343
100μM NE	0.199 ± 0.085; n = 109	0.322 ± 0.044; n = 361	-0.109 ± 0.070; n = 111	0.138 ± 0.042; n = 345

Table 2.1. Neuromodulator effect and plasticity by Cortical Depth.

Median values of effect and plasticity sizes for L I – L IV and L V – L VI. All values are on $\log_{10}$ scale.

REFERENCES

Armitage, A. K., Hall, G. H., & Sellers, C. M. (1969). Effects of nicotine on electrocortical activity and acetylcholine release from the cat cerebral cortex. *British journal of pharmacology, 35*(1), 152-160.

Armstrong-James, M., & Fox, K. (1983). Effects of ionophoresed noradrenaline on the spontaneous activity of neurones in rat primary somatosensory cortex. *The Journal of physiology, 335*, 427-447.

Aston-Jones, G., & Cohen, J. D. (2005). Adaptive gain and the role of the locus coeruleus-norepinephrine system in optimal performance. *The Journal of comparative neurology, 493*(1), 99-110. doi:10.1002/cne.20723

Bassant, M. H., Baleyte, J. M., & Lamour, Y. (1990). Effects of acetylcholine on single cortical somatosensory neurons in the unanesthetized rat. *Neuroscience, 39*(1), 189-197.

Baxter, M. G., & Chiba, A. A. (1999). Cognitive functions of the basal forebrain. *Current opinion in neurobiology, 9*(2), 178-183.

Bear, M. F., & Singer, W. (1986). Modulation of visual cortical plasticity by acetylcholine and noradrenaline. *Nature, 320*(6058), 172-176. doi:10.1038/320172a0

Becchetti, A., Gullo, F., Bruno, G., Dossi, E., Lecchi, M., & Wanke, E. (2012). Exact distinction of excitatory and inhibitory neurons in neural networks: a study with GFP-GAD67 neurons optically and electrophysiologically recognized on multielectrode arrays. *Frontiers in neural circuits, 6*, 63. doi:10.3389/fncir.2012.00063

Beggs, J. M., & Plenz, D. (2003). Neuronal avalanches in neocortical circuits. *The Journal of neuroscience : the official journal of the Society for Neuroscience, 23*(35), 11167-11177.

Beggs, J. M., & Plenz, D. (2004). Neuronal avalanches are diverse and precise activity patterns that are stable for many hours in cortical slice cultures. *The Journal of neuroscience : the official journal of the Society for Neuroscience, 24*(22), 5216-5229. doi:10.1523/JNEUROSCI.0540-04.2004

Bi, G. Q., & Poo, M. M. (1998). Synaptic modifications in cultured hippocampal neurons: dependence on spike timing, synaptic strength, and postsynaptic cell type. *The Journal of neuroscience : the official journal of the Society for Neuroscience, 18*(24), 10464-10472.

Bodner, K. E., Beversdorf, D. Q., Saklayen, S. S., & Christ, S. E. (2012). Noradrenergic moderation of working memory impairments in adults with autism spectrum disorder. *Journal of the International Neuropsychological Society : JINS, 18*(3), 556-564. doi:10.1017/S1355617712000070

Boppart, S. A., Wheeler, B. C., & Wallace, C. S. (1992). A flexible perforated microelectrode array for extended neural recordings. *IEEE transactions on bio-medical engineering, 39*(1), 37-42. doi:10.1109/10.108125

Bouret, S., & Sara, S. J. (2005). Network reset: a simplified overarching theory of locus coeruleus noradrenaline function. *Trends in neurosciences, 28*(11), 574-582. doi:10.1016/j.tins.2005.09.002

Celesia, G. G., & Jasper, H. H. (1966). Acetylcholine released from cerebral cortex in relation to state of activation. *Neurology, 16*(11), 1053-1063.

Choi, S. Y., Chang, J., Jiang, B., Seol, G. H., Min, S. S., Han, J. S., . . . Kirkwood, A. (2005). Multiple receptors coupled to phospholipase C gate long-term depression in visual cortex. *The Journal of neuroscience : the official journal of the Society for Neuroscience, 25*(49), 11433-11443. doi:10.1523/JNEUROSCI.4084-05.2005

Chon, K., Scully, C. G., & Lu, S. (2009). Approximate entropy for all signals. *IEEE engineering in medicine and biology magazine : the quarterly magazine of the Engineering in Medicine & Biology Society, 28*(6), 18-23. doi:10.1109/MEMB.2009.934629

Constantinople, C. M., & Bruno, R. M. (2011). Effects and mechanisms of wakefulness on local cortical networks. *Neuron, 69*(6), 1061-1068. doi:10.1016/j.neuron.2011.02.040

Dalley, J. W., McGaughy, J., O'Connell, M. T., Cardinal, R. N., Levita, L., & Robbins, T. W. (2001). Distinct changes in cortical acetylcholine and noradrenaline efflux during contingent and noncontingent performance of a visual attentional task. *Journal of Neuroscience, 21*(13), 4908-4914.

Desai, N. S., Rutherford, L. C., & Turrigiano, G. G. (1999). Plasticity in the intrinsic excitability of cortical pyramidal neurons. *Nature neuroscience, 2*(6), 515-520. doi:10.1038/9165

Deutsch, S. I., Urbano, M. R., Neumann, S. A., Burket, J. A., & Katz, E. (2010). Cholinergic abnormalities in autism: is there a rationale for selective nicotinic agonist interventions? *Clinical neuropharmacology, 33*(3), 114-120. doi:10.1097/WNF.0b013e3181d6f7ad

Egert, U., Heck, D., & Aertsen, A. (2002). Two-dimensional monitoring of spiking networks in acute brain slices. *Experimental brain research. Experimentelle Hirnforschung. Experimentation cerebrale, 142*(2), 268-274. doi:10.1007/s00221-001-0932-5

Egert, U., Schlosshauer, B., Fennrich, S., Nisch, W., Fejtl, M., Knott, T., . . . Hammerle, H. (1998). A novel organotypic long-term culture of the rat hippocampus on substrate-integrated multielectrode arrays. *Brain research. Brain research protocols, 2*(4), 229-242.

Eggermann, E., & Feldmeyer, D. (2009). Cholinergic filtering in the recurrent excitatory microcircuit of cortical layer 4. *Proceedings of the National Academy of Sciences of the United States of America, 106*(28), 11753-11758. doi:10.1073/pnas.0810062106

Favero, M., Varghese, G., & Castro-Alamancos, M. A. (2012). The state of somatosensory cortex during neuromodulation. *Journal of neurophysiology, 108*(4), 1010-1024. doi:10.1152/jn.00256.2012

Fee, M. S., Mitra, P. P., & Kleinfeld, D. (1996). Automatic sorting of multiple unit neuronal signals in the presence of anisotropic and non-Gaussian variability. *Journal of neuroscience methods, 69*(2), 175-188. doi:10.1016/S0165-0270(96)00050-7

Froemke, R. C., & Dan, Y. (2002). Spike-timing-dependent synaptic modification induced by natural spike trains. *Nature, 416*(6879), 433-438. doi:10.1038/416433a

Frohlich, F., & McCormick, D. A. (2010). Endogenous electric fields may guide neocortical network activity. *Neuron, 67*(1), 129-143. doi:10.1016/j.neuron.2010.06.005

Fu, Y. X., Djupsund, K., Gao, H., Hayden, B., Shen, K., & Dan, Y. (2002). Temporal specificity in the cortical plasticity of visual space representation. *Science, 296*(5575), 1999-2003. doi:10.1126/science.1070521

Gerstner, W., Kreiter, A. K., Markram, H., & Herz, A. V. (1997). Neural codes: firing rates and beyond. *Proceedings of the National Academy of Sciences of the United States of America, 94*(24), 12740-12741.

Gholmieh, G., Soussou, W., Courellis, S., Marmarelis, V., Berger, T., & Baudry, M. (2001). A biosensor for detecting changes in cognitive processing based on nonlinear systems analysis. *Biosensors & bioelectronics, 16*(7-8), 491-501.

Giocomo, L. M., & Hasselmo, M. E. (2005). Nicotinic modulation of glutamatergic synaptic transmission in region CA3 of the hippocampus. *The European journal of neuroscience, 22*(6), 1349-1356. doi:10.1111/j.1460-9568.2005.04316.x

Gonzalez-Sulser, A., Wang, J., Motamedi, G. K., Avoli, M., Vicini, S., & Dzakpasu, R. (2011). The 4-aminopyridine in vitro epilepsy model analyzed with a perforated multi-electrode array. *Neuropharmacology, 60*(7-8), 1142-1153. doi:10.1016/j.neuropharm.2010.10.007

Gross, G. W., Rhoades, B. K., Azzazy, H. M., & Wu, M. C. (1995). The use of neuronal networks on multielectrode arrays as biosensors. *Biosensors & bioelectronics, 10*(6-7), 553-567.

Gullo, F., Maffezzoli, A., Dossi, E., & Wanke, E. (2009). Short-latency cross- and autocorrelation identify clusters of interacting cortical neurons recorded from multi-electrode array. *Journal of neuroscience methods, 181*(2), 186-198. doi:10.1016/j.jneumeth.2009.05.003

Hajos, N., Ellender, T. J., Zemankovics, R., Mann, E. O., Exley, R., Cragg, S. J., . . . Paulsen, O. (2009). Maintaining network activity in submerged hippocampal slices: importance of oxygen supply. *The European journal of neuroscience, 29*(2), 319-327. doi:10.1111/j.1460-9568.2008.06577.x

Hajos, N., & Mody, I. (2009). Establishing a physiological environment for visualized in vitro brain slice recordings by increasing oxygen supply and modifying aCSF content. *Journal of neuroscience methods, 183*(2), 107-113. doi:10.1016/j.jneumeth.2009.06.005

Hasselmo, M. E., Linster, C., Patil, M., Ma, D., & Cekic, M. (1997). Noradrenergic suppression of synaptic transmission may influence cortical signal-to-noise ratio. *Journal of neurophysiology, 77*(6), 3326-3339.

Hill, D. N., Mehta, S. B., & Kleinfeld, D. (2011). Quality metrics to accompany spike sorting of extracellular signals. *The Journal of neuroscience : the official journal of the Society for Neuroscience, 31*(24), 8699-8705. doi:10.1523/JNEUROSCI.0971-11.2011

Hoffken, O., Lenz, M., Hockelmann, N., Dinse, H. R., & Tegenthoff, M. (2012). Noradrenergic modulation of human visual cortex excitability assessed by paired-pulse visual-evoked potentials. *Neuroreport, 23*(12), 707-711. doi:10.1097/WNR.0b013e3283565fb4

Holt, G. R., & Koch, C. (1999). Electrical interactions via the extracellular potential near cell bodies. *Journal of computational neuroscience, 6*(2), 169-184.

Huang, Y., Williams, J. C., & Johnson, S. M. (2012). Brain slice on a chip: opportunities and challenges of applying microfluidic technology to intact tissues. *Lab on a chip, 12*(12), 2103-2117. doi:10.1039/c2lc21142d

Huerta, P. T., & Lisman, J. E. (1995). Bidirectional synaptic plasticity induced by a single burst during cholinergic theta oscillation in CA1 in vitro. *Neuron, 15*(5), 1053-1063.

Jouvet, M. (1969). Biogenic amines and the states of sleep. *Science, 163*(3862), 32-41.

Kalmbach, A., Hedrick, T., & Waters, J. (2012). Selective optogenetic stimulation of cholinergic axons in neocortex. *Journal of neurophysiology, 107*(7), 2008-2019. doi:10.1152/jn.00870.2011

Kawaguchi, Y., & Shindou, T. (1998). Noradrenergic excitation and inhibition of GABAergic cell types in rat frontal cortex. *The Journal of neuroscience : the official journal of the Society for Neuroscience, 18*(17), 6963-6976.

Kirkwood, A., Rioult, M. C., & Bear, M. F. (1996). Experience-dependent modification of synaptic plasticity in visual cortex. *Nature, 381*(6582), 526-528. doi:10.1038/381526a0

Kirkwood, A., Rozas, C., Kirkwood, J., Perez, F., & Bear, M. F. (1999). Modulation of long-term synaptic depression in visual cortex by acetylcholine and norepinephrine. *The Journal of neuroscience : the official journal of the Society for Neuroscience, 19*(5), 1599-1609.

Lamour, Y., Dutar, P., & Jobert, A. (1982). Excitatory effect of acetylcholine on different types of neurons in the first somatosensory neocortex of the rat: laminar distribution and pharmacological characteristics. *Neuroscience, 7*(6), 1483-1494.

Lamour, Y., Dutar, P., Jobert, A., & Dykes, R. W. (1988). An iontophoretic study of single somatosensory neurons in rat granular cortex serving the limbs: a laminar analysis of glutamate and acetylcholine effects on receptive-field properties. *Journal of neurophysiology, 60*(2), 725-750.

Lin, Y. W., Min, M. Y., Chiu, T. H., & Yang, H. W. (2003). Enhancement of associative long-term potentiation by activation of beta-adrenergic receptors at CA1 synapses in rat hippocampal slices. *The Journal of neuroscience : the official journal of the Society for Neuroscience, 23*(10), 4173-4181.

Lukatch, H. S., & MacIver, M. B. (1997). Physiology, pharmacology, and topography of cholinergic neocortical oscillations in vitro. *Journal of neurophysiology, 77*(5), 2427-2445.

Markram, H., Lubke, J., Frotscher, M., & Sakmann, B. (1997). Regulation of synaptic efficacy by coincidence of postsynaptic APs and EPSPs. *Science, 275*(5297), 213-215.

McCormick, D. A., Connors, B. W., Lighthall, J. W., & Prince, D. A. (1985). Comparative electrophysiology of pyramidal and sparsely spiny stellate neurons of the neocortex. *Journal of neurophysiology, 54*(4), 782-806.

McCormick, D. A., & Prince, D. A. (1986). Mechanisms of action of acetylcholine in the guinea-pig cerebral cortex in vitro. *The Journal of physiology, 375*, 169-194.

McKenna, T. M., Ashe, J. H., Hui, G. K., & Weinberger, N. M. (1988). Muscarinic agonists modulate spontaneous and evoked unit discharge in auditory cortex of cat. *Synapse, 2*(1), 54-68. doi:10.1002/syn.890020109

Metherate, R., Ashe, J. H., & Weinberger, N. M. (1990). Acetylcholine modifies neuronal acoustic rate-level functions in guinea pig auditory cortex by an action at muscarinic receptors. *Synapse, 6*(4), 364-368. doi:10.1002/syn.890060409

Metherate, R., Tremblay, N., & Dykes, R. W. (1988). Transient and prolonged effects of acetylcholine on responsiveness of cat somatosensory cortical neurons. *Journal of neurophysiology, 59*(4), 1253-1276.

Michelson, D., Adler, L., Spencer, T., Reimherr, F. W., West, S. A., Allen, A. J., . . . Milton, D. (2003). Atomoxetine in adults with ADHD: two randomized, placebo-controlled studies. *Biological psychiatry, 53*(2), 112-120.

Milberger, S., Biederman, J., Faraone, S. V., Chen, L., & Jones, J. (1997). ADHD is associated with early initiation of cigarette smoking in children and adolescents. *Journal of the American Academy of Child and Adolescent Psychiatry, 36*(1), 37-44. doi:10.1097/00004583-199701000-00015

Motamedi, G. K., Gonzalez-Sulser, A., Dzakpasu, R., & Vicini, S. (2012). Cellular mechanisms of desynchronizing effects of hypothermia in an in vitro epilepsy model. *Neurotherapeutics : the journal of the American Society for Experimental NeuroTherapeutics, 9*(1), 199-209. doi:10.1007/s13311-011-0078-5

Motamedi, G. K., Salazar, P., Smith, E. L., Lesser, R. P., Webber, W. R., Ortinski, P. I., . . . Rogawski, M. A. (2006). Termination of epileptiform activity by cooling in rat hippocampal slice epilepsy models. *Epilepsy research, 70*(2-3), 200-210. doi:10.1016/j.eplepsyres.2006.05.001

Muller, C. M., & Singer, W. (1989). Acetylcholine-induced inhibition in the cat visual cortex is mediated by a GABAergic mechanism. *Brain research, 487*(2), 335-342.

Nikonenko, I., Jourdain, P., & Muller, D. (2003). Presynaptic remodeling contributes to activity-dependent synaptogenesis. *The Journal of neuroscience : the official journal of the Society for Neuroscience, 23*(24), 8498-8505.

Okawara, M., Katsuki, H., Kurimoto, E., Shibata, H., Kume, T., & Akaike, A. (2007). Resveratrol protects dopaminergic neurons in midbrain slice culture from multiple insults. *Biochemical pharmacology, 73*(4), 550-560. doi:10.1016/j.bcp.2006.11.003

Perry, E. K., Lee, M. L., Martin-Ruiz, C. M., Court, J. A., Volsen, S. G., Merrit, J., . . . Wenk, G. L. (2001). Cholinergic activity in autism: abnormalities in the cerebral cortex and basal forebrain. *The American journal of psychiatry, 158*(7), 1058-1066.

Petrozzino, J. J., Pozzo Miller, L. D., & Connor, J. A. (1995). Micromolar Ca2+ transients in dendritic spines of hippocampal pyramidal neurons in brain slice. *Neuron, 14*(6), 1223-1231.

Pincus, S. M., & Goldberger, A. L. (1994). Physiological time-series analysis: what does regularity quantify? *The American journal of physiology, 266*(4 Pt 2), H1643-1656.

Rivlin-Etzion, M., Ritov, Y., Heimer, G., Bergman, H., & Bar-Gad, I. (2006). Local shuffling of spike trains boosts the accuracy of spike train spectral analysis. *Journal of neurophysiology, 95*(5), 3245-3256. doi:10.1152/jn.00055.2005

Ruthazer, E. S., Baker, G. E., & Stryker, M. P. (1999). Development and organization of ocular dominance bands in primary visual cortex of the sable ferret. *The Journal of comparative neurology, 407*(2), 151-165.

Sanchez-Vives, M. V., & McCormick, D. A. (2000). Cellular and network mechanisms of rhythmic recurrent activity in neocortex. *Nature neuroscience, 3*(10), 1027-1034. doi:10.1038/79848

Sato, H., Fox, K., & Daw, N. W. (1989). Effect of electrical stimulation of locus coeruleus on the activity of neurons in the cat visual cortex. *Journal of neurophysiology, 62*(4), 946-958.

Schiff, S. J., Huang, X., & Wu, J. Y. (2007). Dynamical evolution of spatiotemporal patterns in mammalian middle cortex. *Physical review letters, 98*(17), 178102.

Schroeder, C. E., & Foxe, J. J. (2002). The timing and laminar profile of converging inputs to multisensory areas of the macaque neocortex. *Brain research. Cognitive brain research, 14*(1), 187-198.

Seol, G. H., Ziburkus, J., Huang, S., Song, L., Kim, I. T., Takamiya, K., . . . Kirkwood, A. (2007). Neuromodulators control the polarity of spike-timing-dependent synaptic plasticity. *Neuron, 55*(6), 919-929. doi:10.1016/j.neuron.2007.08.013

Shafi, M., Zhou, Y., Quintana, J., Chow, C., Fuster, J., & Bodner, M. (2007). Variability in neuronal activity in primate cortex during working memory tasks. *Neuroscience, 146*(3), 1082-1108. doi:10.1016/j.neuroscience.2006.12.072

Sillito, A. M., & Kemp, J. A. (1983). Cholinergic modulation of the functional organization of the cat visual cortex. *Brain research, 289*(1-2), 143-155.

Sjostrom, P. J., & Nelson, S. B. (2002). Spike timing, calcium signals and synaptic plasticity. *Current opinion in neurobiology, 12*(3), 305-314.

Steriade, M., & Amzica, F. (1998). Slow sleep oscillation, rhythmic K-complexes, and their paroxysmal developments. *Journal of sleep research, 7 Suppl 1*, 30-35.

Steriade, M., Timofeev, I., & Grenier, F. (2001). Natural waking and sleep states: a view from inside neocortical neurons. *Journal of neurophysiology, 85*(5), 1969-1985.

Stett, A., Egert, U., Guenther, E., Hofmann, F., Meyer, T., Nisch, W., & Haemmerle, H. (2003). Biological application of microelectrode arrays in drug discovery and basic research. *Analytical and bioanalytical chemistry, 377*(3), 486-495. doi:10.1007/s00216-003-2149-x

Sullivan, B. L., Leu, D., Taylor, D. M., Fahlman, C. S., & Bickler, P. E. (2002). Isoflurane prevents delayed cell death in an organotypic slice culture model of cerebral ischemia. *Anesthesiology, 96*(1), 189-195.

Thomas, M. J., Moody, T. D., Makhinson, M., & O'Dell, T. J. (1996). Activity-dependent beta-adrenergic modulation of low frequency stimulation induced LTP in the hippocampal CA1 region. *Neuron, 17*(3), 475-482.

Tononi, G., & Sporns, O. (2003). Measuring information integration. *BMC neuroscience, 4*, 31. doi:10.1186/1471-2202-4-31

Traub, R. D., Jefferys, J. G., & Whittington, M. A. (1994). Enhanced NMDA conductance can account for epileptiform activity induced by low Mg2+ in the rat hippocampal slice. *The Journal of physiology, 478 Pt 3*, 379-393.

Vankov, A., Herve-Minvielle, A., & Sara, S. J. (1995). Response to novelty and its rapid habituation in locus coeruleus neurons of the freely exploring rat. *The European journal of neuroscience, 7*(6), 1180-1187.

Wilens, T. E., Biederman, J., Spencer, T. J., Bostic, J., Prince, J., Monuteaux, M. C., . . . Polisner, D. (1999). A pilot controlled clinical trial of ABT-418, a cholinergic agonist, in the treatment of adults with attention deficit hyperactivity disorder. *The American journal of psychiatry, 156*(12), 1931-1937.

Yang, H., Shew, W. L., Roy, R., & Plenz, D. (2012). Maximal variability of phase synchrony in cortical networks with neuronal avalanches. *The Journal of neuroscience : the official journal of the Society for Neuroscience, 32*(3), 1061-1072. doi:10.1523/JNEUROSCI.2771-11.2012

Yang, H. W., Lin, Y. W., Yen, C. D., & Min, M. Y. (2002). Change in bi-directional plasticity at CA1 synapses in hippocampal slices taken from 6-hydroxydopamine-treated rats: the role of endogenous norepinephrine. *The European journal of neuroscience, 16*(6), 1117-1128.

Yu, A. J., & Dayan, P. (2005). Uncertainty, neuromodulation, and attention. *Neuron, 46*(4), 681-692. doi:10.1016/j.neuron.2005.04.026

CHAPTER 3: INTERACTION OF INTRINSIC AND SYNAPTIC CURRENTS MEDIATE NETWORK RESONANCE DRIVEN BY LAYER V PYRAMIDAL CELLS

INTRODUCTION

Cortical oscillations are periodic fluctuations in excitability and represent a fundamental organizational principle of neuronal activity in cortex (Buzsáki, 2006). Low frequency cortical oscillations (< 4 Hz) have been traditionally associated with sleep (Achermann & Borbely, 1997; Bazhenov, Timofeev, Steriade, & Sejnowski, 2002; Steriade, Timofeev, & Grenier, 2001) and deep anesthesia (Jameson & Sloan, 2006). However a broader role has recently emerged since pronounced slow rhythmic fluctuations in membrane voltage and local field potential have been also found in the awake, resting animal (Crochet & Petersen, 2006; Gentet, Avermann, Matyas, Staiger, & Petersen, 2010; Sellers, Bennett, & Frohlich, 2014). Functionally, low frequency cortical oscillations may play a key role in memory consolidation and synaptic scaling (Marshall, Helgadottir, Molle, & Born, 2006; Tononi & Cirelli, 2014). Mechanistically, layer 5 pyramidal cells (L5 PYs) have been associated with the genesis of low frequency oscillations in cortex, in particular in the slow (< 1 Hz) and delta frequency (1-4 Hz) bands. L5 PYs initiate individual UP states both *in vivo* (Chauvette, Volgushev, & Timofeev, 2010; Luczak, Bartho, Marguet, Buzsaki, & Harris, 2007) and *in vitro* (Sanchez-Vives & McCormick, 2000). Furthermore, low frequency, square-wave optogenetic stimulation of L5 PYs generated cortical UP and DOWN states *in vivo* that closely resembled those which occur during spontaneous, endogenous slow oscillations (Beltramo et al., 2013).

At the cellular level, L5 PYs cells express a large number of hyperpolarization-activated cyclic nucleotide-gated (HCN) channels (Lorincz, Notomi, Tamas, Shigemoto, & Nusser, 2002; Santoro et al., 2000; Ulrich, 2002). These channels mediate the hyperpolarization-activated depolarizing current, I_h, which acts as a pace-maker current in both cortical and thalamic cells (Luthi & McCormick, 1998). In particular, I_h is responsible for sub-threshold resonance, typically in the theta band but also outside of this

frequency range, *in vitro* in absence of network interactions for hyperpolarized membrane voltages in both pyramidal cells (Hu, Vervaeke, & Storm, 2002; Hutcheon, Miura, & Puil, 1996; Leung & Yu, 1998) and other excitatory cell types (Engel, Schimansky-Geier, Herz, Schreiber, & Erchova, 2008; Erchova, Kreck, Heinemann, & Herz, 2004b; Fransen, Alonso, Dickson, Magistretti, & Hasselmo, 2004; Haas & White, 2002; Yoshida, Giocomo, Boardman, & Hasselmo, 2011). However, the absence of HCN-mediated theta resonance for more depolarized membrane voltages (Hu et al., 2002) suggests that, in active networks, the role of I_h in generating rhythmic network activity may differ. Indeed, optogenetic stimulation *in vivo* confirmed a key role of I_h in theta resonance at the network level but surprisingly only for periodic stimulation of parvalbumin positive cells (presumed interneurons) and not stimulation of pyramidal cells, despite the presence of I_h in pyramidal cells (Stark et al., 2013). The number of HCN channels along the apical dendrite of L5 PYs increases exponentially with distance from the soma (Kole, Hallermann, & Stuart, 2006), implying a functional role of I_h in modulating synaptic integration in addition to somatic depolarization (Cuntz, Remme, & Torben-Nielsen, 2014; Magee, 2000; Zhuchkova, Remme, & Schreiber, 2013). Conversely, non-inactivating potassium current (I_M) mediates theta band resonance at depolarized membrane voltages in cells in isolation (Hu et al., 2002). Despite similar findings of theta band resonance *in vitro*, the resonant frequency of cells arising from I_M and I_h is dependent on a complex set of parameters and can vary with experimental conditions (Rotstein, 2015; Rotstein & Nadim, 2014). Indeed aside from regulation of the resting potential and mediation of somatic theta resonance, both I_h and I_M play a large role in dendritic integration (for review see: Magee, 2000). It has thus remained unclear if and how HCN- and Kv7- mediated single cell dynamics translate to networks driven by excitation of L5 PYs and to what extent these dynamics interact with synaptic activity.

To answer this question, we combined multichannel electrophysiology *in vitro* with optogenetic excitation of L5 PYs (Arenkiel et al., 2007). We hypothesized that the interaction of synaptic and cellular mechanisms plays a key role in network-wide supra-threshold frequency responses. To test this hypothesis, we applied frequency-sweep (chirp) stimulation to a large number of L5 PYs in acute cortical slices. Network activation of L5 PYs has been shown, for low frequency stimulation, to produce naturalistic network-wide activation *in vivo* (Beltramo et al., 2013). Used in conjunction with application of pharmacological agents and multielectrode array recordings, we were able to isolate synaptic from

cellular components of the network frequency response and discern the interactions which lead to the emergence of frequency-tuning of cortical networks. To account for differences in baseline excitability we introduce a metric of relative activity based on spiking activity across all stimulation frequencies. We utilize this metric to specifically examine network resonance. Using this measure resonance can be observed as greater spiking response across the network for a small set of stimulation frequencies which are not the lowest or highest stimulation frequencies (which would indicate a possible low-pass or high-pass response respectively).

METHODS

Solutions

All reagents were purchased from Fisher Scientific (Waltham, MA) with the exception of bicuculline and kynurenic acid (Sigma-Aldrich, St. Louis, MO) and ZD-7288 and XE-991 (Tocris Bioscience, Bristol, United Kingdom). Sucrose solution (in mM): 83.0 NaCl, 2.5 KCl, 0.5 $CaCl_2$, 3.3 $MgSO_4$, 1.0 NaH_2PO_4, 26.2 $NaHCO_3$, 22.0 Dextrose Anhydrose, and 72.0 Sucrose. Incubation solution: 119.0 NaCl, 2.5 KCl, 1.0 NaH_2PO_4, 26.2 $NaHCO_3$, 22.0 glucose, 2.0 $MgSO_4$, and 2.0 $CaCl_2$. Control artificial cerebral spinal fluid (control aCSF): 119.0 NaCl, 4.5 KCl, 1 NaH_2PO_4, 26.2 $NaHCO_3$, 22.0 glucose, 1.0 $MgSO_4$, and 1.0 $CaCl_2$. Kynurenic acid and bicuculline aCSF (Kyn + Bic aCSF): control aCSF with 1 mM kynurenic acid and 10 µM bicuculline added. XE aCSF: control aCSF with 10 µM XE-991. Kynurenic acid and Bicuculline with XE-991 aCSF (Kyn + Bic + XE aCSF): control aCSF with 1 mM kynurenic acid, 10 µM bicuculline, and 10 µM XE-991 added. ZD aCSF: control aCSF with 5 µM ZD-7288 added. Kynurenic acid and Bicuculline with ZD-7288 aCSF (Kyn + Bic + ZD aCSF): control aCSF with 1 mM kynurenic acid, 10 µM bicuculline, and 5 µM ZD-7288 added.

Slice Preparation

All animal procedures were performed in compliance with the National Institutes of Health guide for the care and use of laboratory animals (NIH Publications No. 8023, revised 1978) and approved by the Institute of Animal Use and Care of the University of North Carolina at Chapel Hill. Juvenile mice (p15-30) were deeply anesthetized with Euthasol (0.5 mL/kg, Virbac, Fort Worth, TX). The mice were then

decapitated and the brains quickly extracted and placed in ice cold sucrose solution. 200 μm coronal slices of medial prefrontal cortex (mPFC, including infralimbic and prelimbic cortex) were cut using a Vibratome VT1000s (Lecia Microsystems, Wetzlar, Germany) and allowed to recover for at least 1 hour in incubation solution at 34° Celsius. Details of this procedure have been previously described (Schmidt, Chew, Bennett, Hammad, & Frohlich, 2013).

Wide Field Fluorescence Imaging

A p28 mouse was anaesthetized with Euthasol and then transcardially perfused with PBS followed by 4% paraformaldehyde in PBS. 50 μm slices containing mPFC were cut using a CM 3050S (Leica Microsystems), mounted, stained with DAPI, and protected with coverslips. Images were acquired using an Eclipse 80i (Nikon Instruments, Tokyo, Japan) under 20x objective.

Patch Experimental Design

Slices were placed in the recording chamber and Kyn + Bic aCSF perfused at a rate of 1.2 mL/minute at 36 °C. MPFC was located under 4x objective and cells with ChR2/eYFP patched under 40x objective using a SliceScope (Scientifica, Uckfield, UK). Current clamp experiments were recorded in pClamp (Molecular Devices, Sunnyvale, CA) with a sampling rate of 5 kHz. Input and output were provided by a Digidata 1440A (Molecular Devices) and amplified by a MultiClamp 700B (Molecular Devices). Before each stimulation sweep a brief hyperpolarizing test pulse of -150 pA was applied for 100 ms. The current characterization protocol consisted of 1 second long current injections between – 500 and 900 pA (in steps of 50 pA). After the current characterization, increasing frequency ZAP current injections were performed by injecting current I_{inj} = 10 pA * sine ($\frac{\pi}{5} t^{2.5}$) for time *t* ranging from 0 to 30 seconds. Decreasing frequency ZAP current injections were made by decreasing *t* from 30 to 0 seconds. ZAP injections were performed in 5 sweeps in both directions at resting potential, with an injection of -100 pA, and with -200 pA injected current when possible.

Multi-electrode Array Experimental Design

MEA experiments were performed as in (Schmidt, Iyengar, Foulser, Boyle, & Frohlich, 2014). Briefly, slices were placed on a 6x10 perforated array of 30 μm electrodes (100 μm spacing) for a MEA2100 (MultiChannel Systems, Reutligen, Germany) and were perfused with aCSF at a rate of 7 mL/min. 59 simultaneous multiunit (MU) traces were recorded in MC_Rack (MultiChannel Systems). An optical fiber coupled to a LED460 (Prizmatix, Givat Shmuel, Israel) was placed over the slice so that 0.5 mW optogenetic stimulation was applied to the entire slice. Groups of 20 trials were applied, each trial consisted of optogenetic square-wave stimulation (50% duty cycle) of 0.25, 0.5, 1, 3, 5, 7, 9, 13, 17, 21, 25, 29 Hz for 3 s each (except 0.25 and 0.5 Hz stimui which were applied for 8 and 4 seconds respectively) in increasing or decreasing order. Increasing and decreasing trials were chosen in a random order. To account for the preferential response to the onset of stimulation, 50 s of 10 Hz stimulation was applied before the start of the first trial and during the 20 s between chirp stimuli. After the last trial, the perfusion was switched to a second type of aCSF based on the experiment. 20 additional chirp stimuli were applied 10 minutes after the switch of aCSF to allow the changes caused by the new aCSF to reach steady state. Fluorescence images of the slices on the MEA were captured using a Summit K2 (OptixCam, Roanoke, VA). EYFP within slices was excited and background light filtered using the SFA-Cyan (NightSea, Lexington, MA).

Data Analysis

All data were analyzed with custom-written Matlab scripts (The Mathworks, Natick, MA). The resting membrane voltage was calculated for each sweep before current injections by taking the median of membrane voltage occurring before the hyperpolarizing test pulse. The steady state response to current injections (V_{steady}) was determined by taking the median value of the membrane voltage during the last 20 ms of the 1 s pulses minus the resting state V_m in the current characterization protocol. For hyperpolarizing pules, V_{min} was calculated as the most negative voltage in response to a hyperpolarizing pulse minus the resting state voltage. The sag ratio was therefore calculated as V_{min}/V_{steady}.

For subthreshold ZAP current injections, any sweeps exhibiting deflections in V_m greater than 10 mV during the ZAP were excluded from analysis. Additionally if more than 2 of the sweeps for an

increasing or decreasing frequency ZAP experiment were excluded, the experiment was excluded from group analysis. The resting membrane voltage was calculated for each sweep before ZAP current injections by taking the median of membrane voltage occurring before the hyperpolarizing test pulse. Voltage and current power spectra were calculated from 0.5 to 50 Hz using the Chronux toolbox function mtspectrumc() in Matlab (Mitra & Bokil, 2008, chronux.org). A multi-taper method was used in preference to FFT due to the nonstationary nature of ZAP stimuli. The voltage and current signal power spectra were converted to amplitude spectra and divided following Ohm's law to yield impedance spectra. The resonant frequency was determined as the frequency with the maximum impedance between 0.5 Hz and 40 Hz. Q-value was calculated by dividing the amplitude of the impedance at the resonant frequency divided by that of the lowest frequency, 0.5 Hz (Hutcheon et al., 1996).

The MU traces recorded by the MEA were high pass filtered (300 Hz - 4^{th} order Butterworth) and spikes were extracted where the voltage crossed -4 times the standard deviation for that MU trace (1 ms deadtime). MU were included in subsequent analysis if the electrode was in mPFC and the average firing rate (FR) across the duration of the experiment was greater than 0.5 spikes/s. Time courses were calculated (1s bins) for each MU channel and z-scored by channel for the duration of the recording. Z-score was used to normalize the differences in FR dynamics across the MU in the slice. The mean of the z-scored data was plotted for each slice for purposes of visualizing the experiment only. Response to the conditioning stimulus for each trial was determined by the average FR of MU during the last 10 seconds of the conditioning stimulus before each trial. FR was calculated for each stimulation frequency as the total number of spikes divided by the duration of the stimulation for that frequency. The percentage of the total relative activity was calculated for each stimulation frequency *i* using:

$$Relative\ Activity = 100\% * \frac{FR_i}{\sum_{j=1}^{\#\ of\ stimulation\ frequncies} FR_j}$$

FR, rather than spike count, was used to account for the differences in stimulation duration. By subsequent normalization for the total FR of all stimulation frequencies, this metric compensated for the change in baseline excitability caused by pharmacological changes to the aCSF. The resonant frequency was determined by the stimulation frequency with the largest relative activity (across all layers) for each

chirp stimulus. A two-way ANOVA with factors of trial frequency direction and trial epoch (aCSF type) was used to determine statistical differences in resonant frequency.

To locate MU within L5 on the multielectrode array, the electrodes were superimposed over the fluorescence image of the slice on the array. Only electrodes within mPFC were included for analysis. Activity from electrodes was placed into one of two groups for analysis: MU within L5 (identified by the region of eYFP) and those outside of L5 (above or below the region of eYFP). Reported data in the text and error bars represent the 2.5% to 97.5% (2-sided 95%) confidence interval of the median using a 100 iteration bootstrapping algorithm. Statistical significance of the relative response to optogenetic stimuli in the MEA experiments was determined by a four-way ANOVA with factors frequency, chirp direction (increasing or decreasing frequency sweep), trial epoch and MU layer dimensions. Differences between MEA experiment types were determined by a three-way ANOVA with factors frequency, chirp frequency direction, and experiment type. Tukey's honestly significant difference criterion was used for correction of multiple comparisons where appropriate.

RESULTS

Networks Activated by L5 PYs Exhibited Resonance

We first probed the supra-threshold frequency response in multielectrode array experiments by utilizing a preparation of acute cortical slices of mPFC from the Thy1-ChR2 mouse line which expresses channelrhodopsin (ChR2) and eYFP in L5 PYs (Figure 3.1A, Left: EYFP image showing localization of ChR2 in L5 PYs, Right: inset displaying apical dendrites). Slices were placed on a MEA and activity from many layers of mPFC was simultaneously recorded (Figure 3.1B, green indicates ChR2 expression, electrodes are superimposed in cyan). We applied 20 chirps of increasing or decreasing frequency (10 each) square-wave (50% duty cycle) optogenetic stimulation in control aCSF (Figure 3.1C, example chirps). We observed a strong initial response to the optogenetic stimulation which quickly faded to a steady state response (Figure 3.1D, red arrow). To suppress this transient response during chirp stimuli, we applied a conditioning stimulus for 50s before the first trial and 20s between subsequent trials. Ten minutes after completing the first epoch of 20 trials a second epoch of stimulation was applied (Figure 3.1D, approximately 1300 s). During the second epoch the average firing rate (FR) response to the

conditioning stimulus was increased (median [95% confidence interval], L5: 3.85 [3.28 to 4.53] spikes/s in the 1st epoch of stimulation and 3.81 [3.60 to 4.65] spikes/s in the 2nd epoch of stimulation, other layers: 1.88 [1.65 to 2.05] spikes in the 1st epoch of stimulation and 2.33 [2.22 to 2.73] spikes/s in the 2nd epoch of stimulation, n = 180 trials, p = 0.132 and < 10^{-3} respectively, Wilcoxon signed rank). The relative activity by frequency was different between optogenetic sweeps of increasing and decreasing frequency ($p < 10^{-3}$ four-way ANOVA, see Methods). However, the relative activity was not different between epochs both for multiunits (MU) in L5 and MU in other layers (with the exception of L5 MU at 5 and 7 Hz for increasing frequency stims, p = 0.030 and 0.027 and 0.25 Hz for decreasing frequency chirps, p = 0.047, there were no significant differences for MU outside L5, n = 90 trials, Table 3.1-4, Figure 3.1E for MU within L5 and Figure 3.1F for MU outside of L5). We therefore examined increasing and decreasing frequency sweeps separately, but have demonstrated that our stimulation paradigm did not evoke a different response due to the time elapsed during the experiment. We next asked if the largest relative activity was evoked by the lowest stimulation frequency (a low pass filter response) or if larger relative activities were evoked by a few, slightly-higher frequencies of stimulation (resonant response). We observed a peak in the frequency response of the relative activity across the network in the delta to low-theta range (Resonant frequency for increasing frequency chirps: 3.01 [2.68 to 3.57] Hz for 1st control and 2.35 [2.07 to 2.56] Hz for 2nd control; resonant frequency for decreasing frequency chirps: 5.00 [4.57 to 5.50] Hz for 1st control and 4.43 [3.61 to 5.58] Hz for 2nd control; n = 90 trials for each condition; p = 0.251 and 0.502 respectively ANOVA). Due to the high-delta to low-theta resonant frequency, we hypothesized that intrinsic cellular resonance played a major role in the network response. We specifically targeted resonance mediated through I_M and I_h. Due to previous work on the effect of I_h on network oscillations (Giocomo & Hasselmo, 2009; Rotstein et al., 2005; Stark et al., 2013), we hypothesized that such currents play a critical role in the resonance phenomenon observed here at the network scale.

A Subset of eYFP labeled L5 PYs Exhibited Subthreshold Resonance

We next sought to confirm subthreshold resonance in eYFP labeled L5 PYs in the mPFC of the Thy1-ChR2 mouse line. These cells are activated by the application of blue light and therefore drive the response to optogenetic chirp experiments. To examine the subthreshold resonance of these cells, we

performed current clamp recordings at the somata of eYFP labeled L5 PYs with synaptic transmission suppressed (Kyn + Bic aCSF, aCSF with the addition of 10 μM bicuculline to block $GABA_A$ and 1mM kynurenic acid to block AMPA and NMDA transmission). We first observed the strength of I_h by applying hyperpolarizing current pulses and measuring V_{sag} (Figure 3.2A). The amplitude of V_{sag} varied between cells but was inversely correlated with V_{steady} for each cell ($r = -0.697$ Spearman's correlation for least correlated cell, $p < 0.05$, $n = 10$ cells). We next performed subthreshold frequency sweep current injections (ZAP stimuli) of both increasing and decreasing frequencies (Figure 3.2B, top: increasing frequency ZAP current in the time domain, bottom: ZAP current in the frequency domain). As in (Hu et al., 2002), the resonant frequency in response to ZAP stimuli did not differ between increasing and decreasing frequency stimuli ($p = 0.408$, $n = 19$ pairs of ZAP experiments). We observed both low pass and resonant frequency responses which varied between cells as observed in mPFC in (Dembrow, Chitwood, & Johnston, 2010, Figure 3.2C). We quantified deviation from a low-pass response by calculating Q value (Figure 3.2D left). In this metric, a value of 1 means that the amplitude at the resonant frequency was the same as that of the lowest frequency, indicating a low pass filter-like response. Finally we examined the correlation between sag ratio (see Methods) and resonant frequency (Figure 3.2D right). The sag ratio of the cells and therefore activation of I_h, was correlated to the resonant frequency ($r = 0.679$ Spearman correlation, $p < 10^{-3}$, median Vm: -71.4 [-77.8 -66.6] mV). We interpret these results to indicate that population of eYFP labeled cells consisted of both cells which do and cells which do not exhibit subthreshold resonance.

Resonant Frequency Shifted to Lower Frequencies with Synaptic Transmission Suppressed

Computational models and experiments with networks of chemical oscillators have demonstrated that the resonant frequency of networks of oscillators depend on the coupling between the oscillators (Ke, Tinsley, Steele, Wang, & Showalter, 2014; Lea-Carnall, Montemurro, Trujillo-Barreto, Parkes, & El-Deredy, 2016). To confirm these observations *in vitro*, we performed MEA experiments to examine the effect of suppressing synaptic transmission. If the effect of suppressing synaptic transmission was simply a reduction in FR we would expect to see the same relative activity as in control. However if the resonant profile is dependent on synaptic transmission, the distribution of the relative activity would be different

from control. To test for this effect, slices were given 20 optogenetic chirp stimuli (square-wave with 50% duty cycle) in control aCSF followed by 20 stimuli in Kyn + Bic aCSF (Figure 3.3A an example time course of the experiments). The response to the conditioning stimulus was decreased by suppressing synaptic transmission (MU inside L5: 8.66 [7.51 to 9.64] spikes/s in control aCSF and 3.14 [2.97 to 3.64] spikes/s in Kyn + Bic aCSF, MU outside of L5: 2.47 [2.35 to 2.60] spikes/s in control aCSF and 1.73 [1.62 to 1.87] spikes/s in Kyn + Bic aCSF, $p < 10^{-3}$ for both groups, Wilcoxon ranked sum). We next examined the change in relative activity by frequency, a metric which accounted for changes in baseline FR (see Methods). Within L5 the frequency response favored lower frequencies with synaptic transmission suppressed (Figure 3.3B). This shift was accomplished both by increased response to low frequency stimulation (0.25 Hz to 1 Hz for increasing frequency chirps and 0.25 Hz to 3 Hz for decreasing frequency chirps, four-way ANOVA, Table 3.1-2) and decreased response to stimulation in the middle of the frequency range (5 Hz to 13 Hz for increasing frequency chirps and 7 Hz to 13 Hz for decreasing frequency chirps). Outside of L5, there were few significant differences in frequency preference caused by the suppression of synaptic transmission (exceptions: increased response to 0.25 Hz and decreased response to 3 Hz to 5 Hz, for increasing frequency chirps only, four-way ANOVA, Table 3.3-4, Figure 3.3C). We observed a shift in the resonant frequency of the network due to the suppression of synaptic transmission in favor of low-frequency stimulation (increasing frequency sweeps: 3.09 [3.00 3.24] Hz for control aCSF and 1.94 [1.78 2.20] Hz for Kyn + Bic aCSF, decreasing frequency sweeps: 4.6 [4.29 4.93] Hz for control aCSF and 3.41 [2.98 4.17] Hz for Kyn + Bic aCSF, $p < 10^{-3}$ ANOVA, n = 90 trials for each condition). With synaptic transmission suppressed and therefore the number of post-synaptic potentials limited, the frequency response was shifted to favor lower frequency stimuli. These results support the hypothesis that synaptic transmission shapes the frequency response of neocortical networks activated by L5 PYs.

The Network Level Effect of I_M Was Largely Independent of Synaptic Transmission

We probed the contribution of depolarization activated current I_M by comparing the results of optogenetic stimulation during pharmacological blockade of Kv7 (Kv7.1, Kv7.2 and Kv7.3) channels to a preceding control epoch. To do so, we added 10 μM XE-991 to the aCSF (XE aCSF) used during the

second epoch of stimulation (Figure 3.4A, beginning at ~1900 s). As I_M returns depolarized cells to resting potential, we expected the blockade of I_M to increase the FR in response to the supra-threshold conditioning stimulus. Indeed, in response to the optogenetic conditioning stimulus in XE aCSF, the FR of L5 cells rose from 3.55 [2.98 to 4.14] spikes/s to 4.54 [3.88 to 4.91] spikes/s (n = 180 trials, p = 0.036 Wilcoxon ranked sum) however MU outside of L5 remained relatively constant (1.99 [1.90 to 2.09] spikes/s in control aCSF and 2.01 [1.92 to 2.10] spikes/s in XE aCSF, p = 0.12 Wilcoxon ranked sum). We observed an expected decrease in the L5 response to stimuli in the middle of the frequency range (5 to 9 Hz for increasing frequency chirps and 9 to 21 Hz for decreasing frequency chirps, $p < 0.05$, four-way ANOVA, Table 3.1-2, Figure 3.4B) as well as an increase in L5 response to low frequency stimuli (0.25 to 1 Hz for increasing frequency chirps and 0.25 to 3 Hz for decreasing frequency chirps). This result indicates that while the baseline FR activity has increased, the network preferentially responded to lower frequency stimuli when I_M was blocked. Importantly we observed similar effects in MU outside of L5 (Figure 3.4C, Tables 3.3-4). Specifically, the response to stimulus in the middle frequencies of the sweep was decreased (5 to 9 Hz for increasing frequency chirps and 7 to 17 Hz for decreasing frequency chirps). The response to low frequency stimuli was increased in MU outside of L5 as well (0.25 to 1 Hz for increasing frequency chirps and 0.25 to 3 Hz for decreasing frequency chirps). We next examined the change in the resonant frequency of the network. The blockade of I_M reduced the resonant frequency of the network (increasing frequency sweeps: 2.84 [2.68 2.96] Hz for control aCSF and 1.12 [0.994 1.31] Hz for XE aCSF, decreasing frequency sweeps: 5.07 [4.62 5.87] Hz for control aCSF and 2.92 [2.40 3.64] Hz for XE aCSF, $p < 10^{-3}$ ANOVA, n = 90 trials for each condition). These results indicate that the frequency response as a whole and, in particular, the resonant frequency of the network depended on I_M. Without I_M, the network preferentially responded to low frequency stimulus.

We next performed experiments to assess the interaction of I_M with synaptic transmission. To do so, we used aCSF with synaptic blockers (Kyn + Bic aCSF) during the entire experiment, during the 2nd epoch of stimulation we added XE-991 (Kyn + Bic + XE aCSF). The comparison of the two stimulation epochs exhibits the effect of I_M while synaptic transmission is suppressed (Figure 3.5A). With synaptic transmission suppressed the addition of XE reduced the response to the conditioning stimulus (Kyn + Bic aCSF: 4.86 [4.50 5.08] Hz, XE + Kyn + Bic aCSF: 3.43 [3.18 3.80] Hz, n = 160 trials, $p < 10^{-3}$ Wilcoxon

signed rank). Similar to experiments with XE alone, we observed a stronger relative activity for low frequencies (0.25 to 1 Hz) for MU in L5 as well as decrease in response to higher frequency stimulation (5 to 21 Hz) for both increasing and decreasing frequency sweeps (n = 80 trials each direction, $p < 10^{-3}$ four-way ANOVA, Tables 3.1-2, Figure 3.5B). MU outside of L5 were similarly affected by the blockade of XE with a greater response to low frequency stimulation (0.25 – 1 Hz for increasing frequency sweeps, 0.25 and 0.5 Hz for decreasing frequency sweeps) and a decreased response to middle frequency stimulation (3 – 9 Hz for increasing frequency sweeps, 5 – 13 Hz for decreasing frequency sweeps) compared to suppressed synaptic transmission alone (n = 80 sweeps for each condition, $p < 10^{-3}$ four way ANOVA, Tables 3.3-4, Figure 3.5C). The resonant frequency was decreased across the network with the blockade of I_M (increasing frequency sweeps: 2.47 [2.23 2.68] Hz for Kyn + Bic aCSF and 0.713 [0.638 0.813] Hz for Kyn + Bic + XE aCSF, decreasing frequency sweeps: 4.23 [3.85 4.55] Hz for Kyn + Bic aCSF and 1.35 [1.25 1.53] Hz for Kyn + Bic + XE aCSF, $p < 10^{-3}$, n = 80 trials for each condition).

We compared the difference in frequency response caused by the blockade of I_M in control to that of the blockade of I_M with suppressed synaptic transmission by summing the absolute value the difference in relative activity by frequency for all sweeps. The effect of the blockade of I_M was not different with synaptic transmission suppressed than the effect of the blockade of I_M with synaptic transmission intact (increasing frequency sweeps: 21.2 [19.3 22.9] % for XE aCSF and 19.35 [18.3 21.9] % Kyn + Bic + XE aCSF, decreasing frequency sweeps: 18.3 [17.1 18.9] % for XE aCSF and 20.4 [18.5 22.6] % for Kyn + Bic + XE aCSF, p = 0.988 for increasing frequency sweeps and 1.00 for decreasing frequency sweeps ANOVA, n = 90 trials for XE aCSF and 80 trials Kyn + Bic + XE aCSF in each direction frequency sweep). We interpret this result to indicate that the effect of I_M was largely independent of synaptic transmission. Taken together we observed I_M affects the frequency response of networks but those effects were not dependent of synaptic transmission.

The Network Level Effect of I_h Was Dependent on Synaptic Transmission

We next assessed the contribution of hyperpolarization activated depolarizing current I_h on networks driven by L5 pyramidal cells. In order to isolate the contribution of I_h to the frequency response, we performed experiments using HCN channel antagonist ZD-7288. The effect of blocking I_h was

determined by comparing trials of stimulation with ZD aCSF to trials of a previous within-slice control (Figure 3.6A: example time course of an experiment). With I_h blocked, the response to the 10 Hz conditioning stimulus was reduced across the network (L5: 7.54 [6.2 to 7.94] spikes/s in control aCSF and 4.60 [4.26 to 5.05] spikes/s in ZD aCSF, other layers: 2.64 [2.35 to 2.92] spikes/s in control aCSF and 2.08 [1.93 to 2.20] spikes/s in ZD aCSF, n = 180 trials, $p < 10^{-3}$, Wilcoxon ranked sum). Without I_h the MU in L5 were less responsive to middle frequency stimuli (n = 90 trials, 5 - 13 Hz for increasing frequency chirps and 7 - 17 Hz for decreasing frequency chirps, four-way ANOVA, Tables 3.1-2, Figure 3.6B). However, the MU in L5 also exhibited an increased response to low frequency stimuli (0.25 to 1 Hz for increasing and decreasing frequency chirps). This result indicates that by blocking I_h the response of the network was shifted to favor lower frequencies. MU outside of L5 also exhibited an increase response to low frequency stimulation (increased response to 0.25 and 0.5 Hz stimuli regardless of chirp direction and decreased response to 5 to 9 Hz for increasing frequency chirps and 9 to 13 Hz for decreasing frequency chirps, four-way ANOVA, Tables 3.3-4, Figure 3.6C). With I_h blocked, the resonant frequency of the network shifted towards lower frequencies (increasing frequency sweeps: 2.84 [2.71 3.00] Hz for control aCSF and 1.91 [1.64 2.18] Hz for ZD aCSF, decreasing frequency sweeps: 4.54 [4.31 4.82] Hz for control aCSF and 3.04 [2.56 3.83] Hz for ZD aCSF, $p = 0.005$ for increasing frequency sweeps and $p < 10^{-3}$ for decreasing frequency sweeps ANOVA, n = 90 trials for each condition). This result indicates that the change in the response of L5 cells propagated throughout the network to reduce the resonant frequency of the network.

We next considered how I_h interacts with synaptic transmission to contribute to the frequency response at the network scale. To separate these two components, we performed experiments with synaptic transmission suppressed for the duration of the experiment and examined the effect of blocking I_h in addition. With suppressed excitatory input from the network, the cells have a tendency to become hyperpolarized, meaning that I_h should be more active. Therefore the addition of ZD-7288 to Kyn + Bic aCSF during the 2nd epoch of trials (after a first epoch using Kyn + Bic aCSF) allowed us to assess the effect of I_h on the frequency response of the network in isolation (Figure 3.7A, time course of a typical experiment). Further blocking I_h did not significantly reduce the response to the conditioning stimulus for MU inside or outside of L5 (MU in L5: 2.69 [2.55 to 3.04] spikes/s in Kyn + Bic aCSF and 2.93 [2.60 to

3.19] spikes/s in Kyn + Bic + ZD aCSF, MU outside L5: 1.79 [1.67 to 1.90] spikes/s in Kyn + Bic aCSF and 1.76 [1.66 to 1.90] spikes/s in Kyn + Bic + ZD aCSF, n = 200 trials, p = 0.327 and 0.253 respectively, Wilcoxon ranked sum). With synaptic transmission suppressed, the L5 response to the chirp stimulus was only different for 0.5 Hz stimulus for increasing frequency chirps and 1 Hz for decreasing frequency chirps (n = 100 trials, p = 0.003 for 0.5 Hz for increasing frequency chirps, p = 0.0164 for 1 Hz decreasing frequency chirps, and p > 0.05 otherwise, four-way ANOVA, Tables 3.1-2, Figure 3.7B). Outside of L5, there were no significant effects of blocking I_h after suppressing synaptic transmission (n = 100 trials, p > 0.05, four-way ANOVA, Tables 3.3-4, Figure 3.7C). We next examined the effect of further blocking I_h on the resonant frequency of the network with synaptic transmission suppressed. With synaptic transmission suppressed, the addition ZD to the aCSF did not significantly modulate the resonant frequency (increasing frequency sweeps: 2.12 [1.85 2.50] Hz for Kyn + Bic aCSF and 1.57 [1.34 1.75] Hz for Kyn + Bic + ZD aCSF, decreasing frequency sweeps: 3.94 [3.48 4.48] Hz for Kyn + Bic aCSF and 3.34 [3.06 3.64] Hz for Kyn + Bic + ZD aCSF, p = 0.193 for increasing frequency sweeps and p = 0.110 for decreasing frequency sweeps ANOVA, n = 100 trials for each condition). Therefore, the effect of the addition of ZD-7288 once synaptic transmission has been suppressed was very limited. This result indicates that the effect of I_h was largely dependent on network activity.

We next directly compared the effect of blocking I_h in a slice with synaptic transmission intact to that of blocking I_h after synaptic transmission had been suppressed. To do so, we calculated the absolute change in relative activity caused by blocking I_h with synaptic transmission and with synaptic transmission suppressed. Across the entire network, the absolute change in activity levels caused by blocking I_h was greater when the network was intact (21.0 [18.5 to 22.7]% across all MU for blockade of I_h alone and 11.9 [11.0 to 12.5] % across all MU for blockade of I_h with synaptic transmission suppressed for increasing frequency chirps and 18.1 [16.9 to 21.1] % across all MU for blockade of I_h alone and 11.7 [10.4 to 12.8] % across all MU for blockade of I_h with synaptic transmission suppressed for decreasing frequency chirps, n = 90 pairs of trials for synaptic transmission intact and 100 pairs of trials for suppressed synaptic transmission, $p < 10^{-3}$ for both increasing and decreasing frequency chirps separately by Wilcoxon ranked sum, Figure 3.8A). Specifically, the increase in response to low frequency stimulation (0.25 - 1 Hz for both increasing and decreasing frequency chirps) and the decrease in response to middle frequency band (5

to 13 Hz for increasing frequency chirps and 9-13 Hz for decreasing frequency chirps) stimulation was greater with synaptic transmission intact ($p < 0.05$, three-way ANOVA, Figure 3.8B). The effect of blocking I_h was larger with synaptic transmission intact. We interpret these results to indicate that the main effect of I_h on network resonance was dependent on synaptic transmission.

DISCUSSION

Oscillations cause time windows during which neuronal interaction is facilitated by synchronized depolarization of the membrane voltage (Steriade, Nunez, & Amzica, 1993); such a mechanism enables the emergence of dynamic cell assemblies that serve as the building block of neuronal processing (Harris, Csicsvari, Hirase, Dragoi, & Buzsaki, 2003; Womelsdorf, Valiante, Sahin, Miller, & Tiesinga, 2014). Emerging large-scale organization of neuronal firing directly correlates with cognition and behavior and therefore is a likely candidate for the mechanism that bridges brain activity and behavior (X. J. Wang, 2010). Therefore, understanding the causal mechanisms by which cortical oscillations are recruited will offer insights into how cellular and synaptic properties interact to enable information processing in cortex. Coupled harmonic oscillators become synchronized at a frequency which is dependent on the resonant frequencies and coupling strength of those oscillators. Here we have examined supra-threshold resonance of networks. In this approach the MU are oscillators which are coupled by synaptic transmission. This metric of resonance is different from those used for subthreshold oscillations. Subthreshold resonance measures the frequency response of membrane impedance of single cells in isolation as an indicator of how these cells may contribute to oscillations. Here we show I_M and I_h, which contribute to subthreshold resonance, also contribute to supra-threshold resonance on the scale of networks.

Optogenetic stimulation of networks with cell-type specificity offers the opportunity for causal interrogation of circuit dynamics (Cho et al., 2015; Scanziani & Hausser, 2009). We here utilized multielectrode array recordings of acute cortical slices to study the intrinsic and synaptic mechanisms of network resonance by supra-threshold optogenetic stimulation of L5 PYs. The cortical networks exhibited a frequency preference for delta and theta band stimulation of L5 PYs. Blockade of Kv7 or HCN channels boosted the response to low frequency stimuli. We further examined the interaction of I_M and I_h with

synaptic transmission. The blockade of Kv7 channels caused an increased response for low frequency stimuli regardless of the state of synaptic transmission. Conversely when synaptic transmission was suppressed, there was a minimal effect of blocking HCN channels. These results suggest that both Kv7 and HCN channels play a role in resonance of networks but the effect of HCN channels was largely dependent on synaptic interactions. Interestingly, the blockade of I_h, I_M, or suppression of synaptic transmission did not fully remove resonance from the network. These manipulations reduced the resonant frequency of the network, but did not completely change the response of the network to that of a low pass filter.

Importantly, both Kv7 and HCN channels enable subthreshold resonance in individual neurons; in particular, the time-constant of these channels mediate a suppression of slow input by effectively high pass filtering the input. Therefore, both types of channels are ideally situated to selectively amplify oscillations in the theta frequency band (Hutcheon & Yarom, 2000). Numerous studies have confirmed such resonance dynamics by application of low-amplitude (subthreshold), frequency-modulated current injection into different excitatory cell types in a range of brain structures including, most importantly for the discussion here, L5 PYs (Fellous et al., 2001; Hutcheon et al., 1996), but also hippocampus (Hu et al., 2002; Leung & Yu, 1998; Pike et al., 2000), subiculum (W. T. Wang et al., 2006), and entorhinal cortex (Alonso & Llinas, 1989; Dickson et al., 2000; Giocomo, Zilli, Fransen, & Hasselmo, 2007; Nolan, Dudman, Dodson, & Santoro, 2007). However, it has remained unclear if the extrapolation from intrinsic dynamics in disconnected hyperpolarized cells to active networks holds true. In particular, I_h dependent theta resonance was found to be absent for experimentally depolarized individual neurons *in vitro* (Erchova, Kreck, Heinemann, & Herz, 2004a; Halliwell & Adams, 1982; Hu et al., 2002; McCormick & Pape, 1990). Yet, theta peak frequency *in vivo* correlates with functional organization of grid cells in entorhinal cortex and with single-cell resonance peak frequencies, strongly supporting a direct link between intrinsic cellular resonance and network-level oscillations (Giocomo & Hasselmo, 2009). Furthermore, cellular resonance could provide a mechanism for frequency-specific filtering of incoming synaptic input in intact networks (Izhikevich, Desai, Walcott, & Hoppensteadt, 2003).

In the intact animal, mPFC networks may preferentially respond to stimuli in the high delta to low theta range from any one of multiple types of oscillatory inputs. For example, parvalbumin positive (PV^+)

interneurons can drive neocotortical and hippocampal theta oscillations *in vivo* (Stark et al., 2013). Local optogenetic stimulation was applied to small networks of 2 to 20 PV^+ cells (Royer et al., 2012; Stark, Koos, & Buzsaki, 2012), the resulting spiking activity of the pyramidal cells exhibited theta band resonance. Furthermore with I_h blocked, the resonant profile of the excitatory cells was removed. Conversely stimulation of all subtypes of excitatory cells (under the calmodulin-dependent protein kinase II promoter) resulted in a frequency response without resonance, in this case a more or less flat response across frequencies. Some methodological differences may explain the variance between these results and those presented here. Specifically, here we have directly stimulated only L5 PYs (under the Thy1 promotor) and have stimulated and recorded on a larger spatial scale. Stark and colleagues applied optogenetic stimulation in such a way as to record from the same cells which were directly stimulated. Conversely, here cells within layers outside of L5 did not express ChR2 in our preparation and were not directly activated by light stimulation.

Here, we have treated L5 PYs as a homogenous group, however there exist two subtypes based on axonal projections (for review: Shepherd, 2013). L5 PYs which project to the contralateral region of cortex and the striatum, so called intra-telencephalic cells, exhibit fewer HCN channels than those which project to other subcortical structures (Sheets et al., 2011). The magnitude of I_h is therefore lower in these cells (Dembrow et al., 2010; Gee et al., 2012; Sheets et al., 2011). The intra-telencephalic neurons, with lower magnitude I_h currents, exhibit a preference for low frequencies without a resonant peak in the theta band (Dembrow et al., 2010). Here, it is unlikely that the population that was optogentically stimulated was dominated by either subtype of L5 PYs. The intra-telencephalic neurons vary from pyramidal tract neurons in input impedance, spike threshold, and spike duration (Dembrow et al., 2010; Hattox & Nelson, 2007; Suter, Migliore, & Shepherd, 2013). However a previous study observed no significant difference in these metrics between L5 PYs that express ChR2 under the Thy1 promoter and those that do not (H. Wang et al., 2007). Additionally, in our patch experiments, we observed a variety of resonance profiles and magnitudes of I_h, as measured by sag ratio, in the eYFP (and thus ChR2) labelled cells.

Together, our data present a novel perspective on the role of L5 PYs in propagating delta and theta band resonance of networks. Our combined pharmacological and optogenetic manipulations support a

model where intrinsic excitability regulated by Kv7 and HCN channels represents a fundamental mechanism by which periodic input is translated into network-level frequency response.

FIGURES AND TABLES

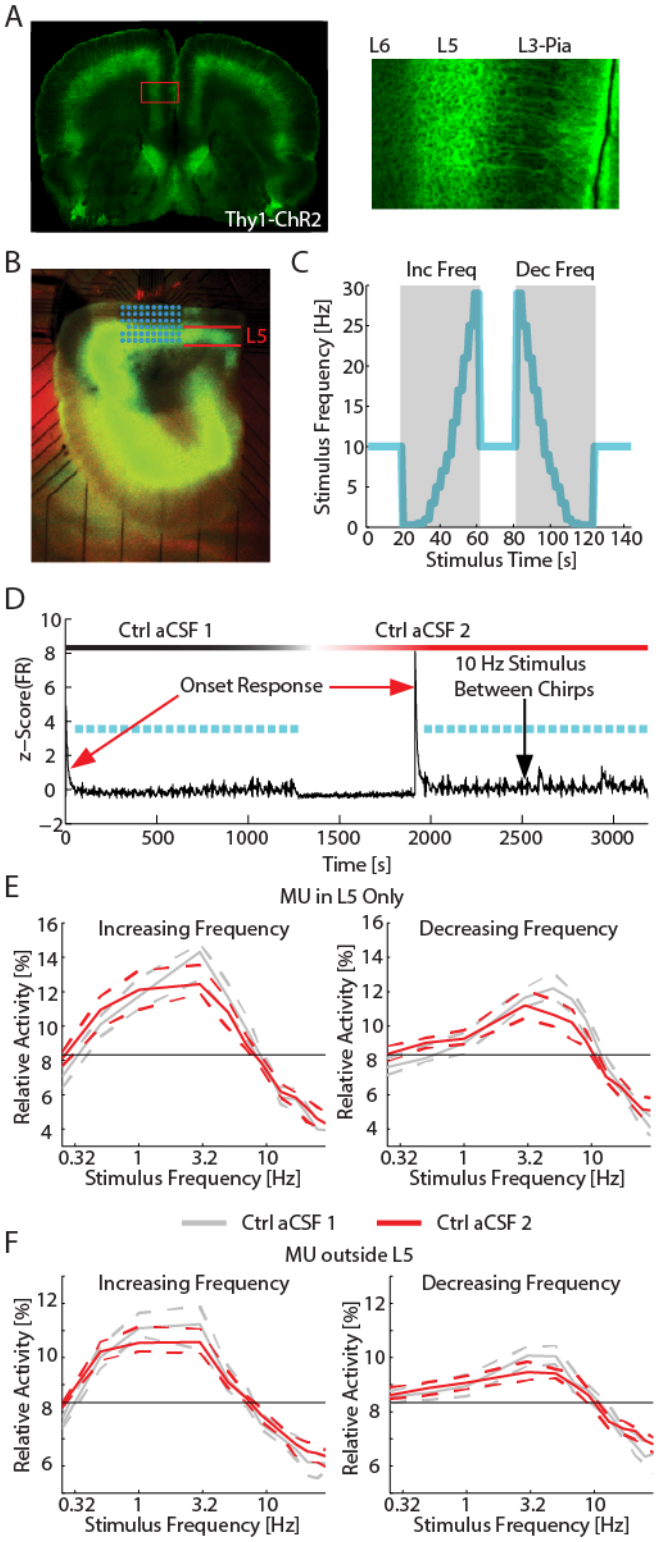

Figure 3.1. Network resonance by optogenetic activation of L5 PYs.

(A) Fluorescence images of a coronal section containing mPFC. Left: eYFP expression throughout a coronal section, all neocortical regions express eYFP in L5. Right: Zoom in of mPFC displaying eYFP in cell bodies and dendrites of cells originating in L5. (B) Fluorescence image of an experimental slice on the MEA. L5 indicated in red. MEA electrodes superimposed in cyan. (C) Frequency of optogenetic stimulation (cyan) for two sample trials denoted with gray background. 10 Hz conditioning stimulus is applied for 20 s between trials. Trials consisted of chirp stimuli ranging from 0.25 Hz to 29 Hz applied in either increasing (left) or decreasing (right) order. (D) The mean z-scored firing rate for all MU during an experiment (black). Frequency sweeps are indicated in cyan. After the completion of the first epoch of stimulation (approximately 1300 s), the perfusion was switched to another container of control aCSF. A second epoch of stimulation was applied 10 minutes after switching the aCSF (approximately 1900 s here). The red arrows illustrate the strong onset response to the start of stimulation epochs. Black arrow indicates the response during the 20s of 10 Hz stimulus between chirps. (E) The relative activity for each frequency of stimulation for increasing (left) and decreasing (right) frequency chirp stimuli for MU in L5. The response during the first epoch of stimulation is in gray. The response of the second epoch of stimulation is in red. The black line indicates chance level of activity. In both cases the network exhibited a resonant frequency in the high delta to low theta range. (F) The relative activity for each frequency of stimulation for increasing (left) and decreasing (right) frequency chirp stimuli for MU outside of L5 (including L1, L2/3, and L6). The response during the first epoch of stimulation is in gray. The response of the second epoch of stimulation is in red. In both cases the network exhibited a resonant frequency in the high delta to low theta range. Inc Freq: increasing frequency chirps. Dec Freq: decreasing frequency chirps. Ctrl aCSF: control aCSF. Dashed lines indicate the 95% confidence interval of the median.

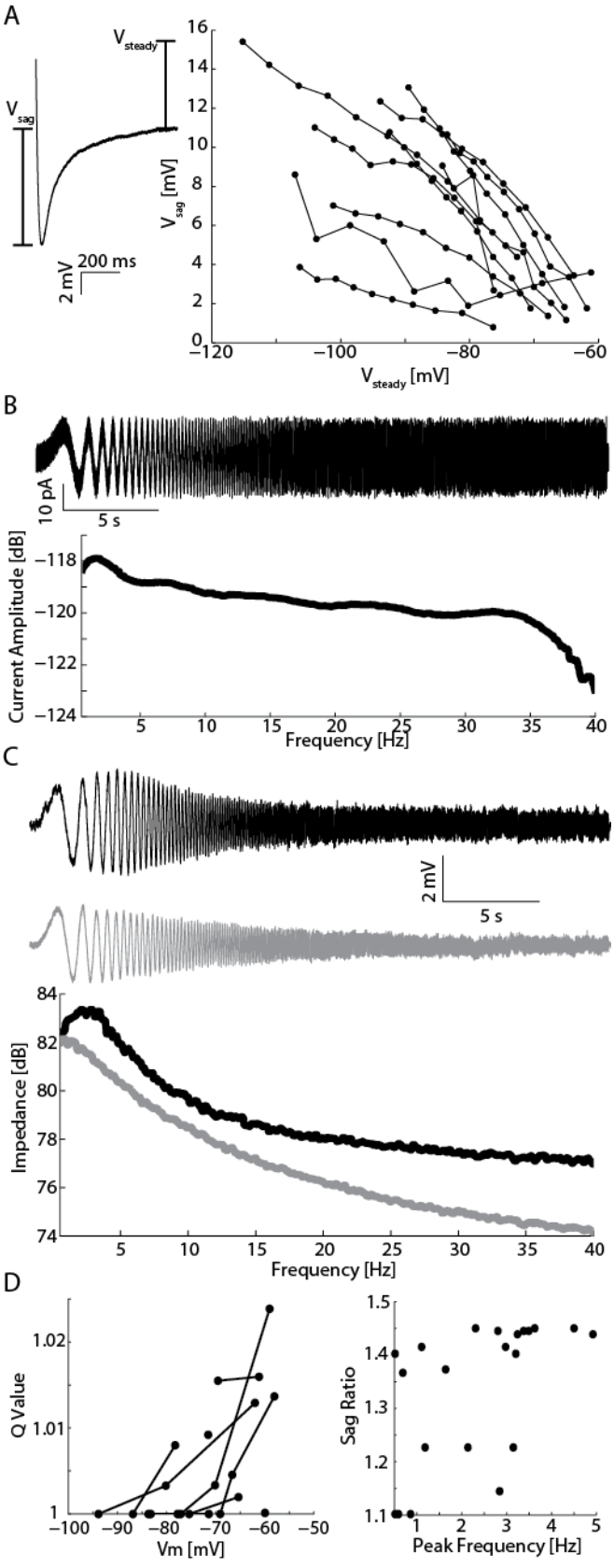
A
V_steady
V_sag
2 mV
200 ms
V_sag [mV]
V_steady [mV]
B
10 pA
5 s
Current Amplitude [dB]
Frequency [Hz]
C
2 mV
5 s
Impedance [dB]
Frequency [Hz]
D
Q Value
Vm [mV]
Sag Ratio
Peak Frequency [Hz]

Figure 3.2. Patch recordings of eYFP/ChR2 labelled cells.

(A) V_{sag}, as a measurement of I_h, in response to hyperpolarizing current injections versus the V_{steady}. The two values were highly correlated for all cells. (B) ZAP current injections in time (top) and frequency (bottom) domains. (C) Example recorded V_m (top) and calculated impedance spectra (bottom) for a cell with a resonant peak (black) and one with a preference for low frequency (gray) in response to ZAP stimulation. (D) Left: Q Value versus V_m for all ZAP stimuli. Right: Sag ratio versus the peak frequency for all cells. The peak frequency was correlated with sag ratio indicating that the resonant frequency was partially determined by the magnitude of I_h.

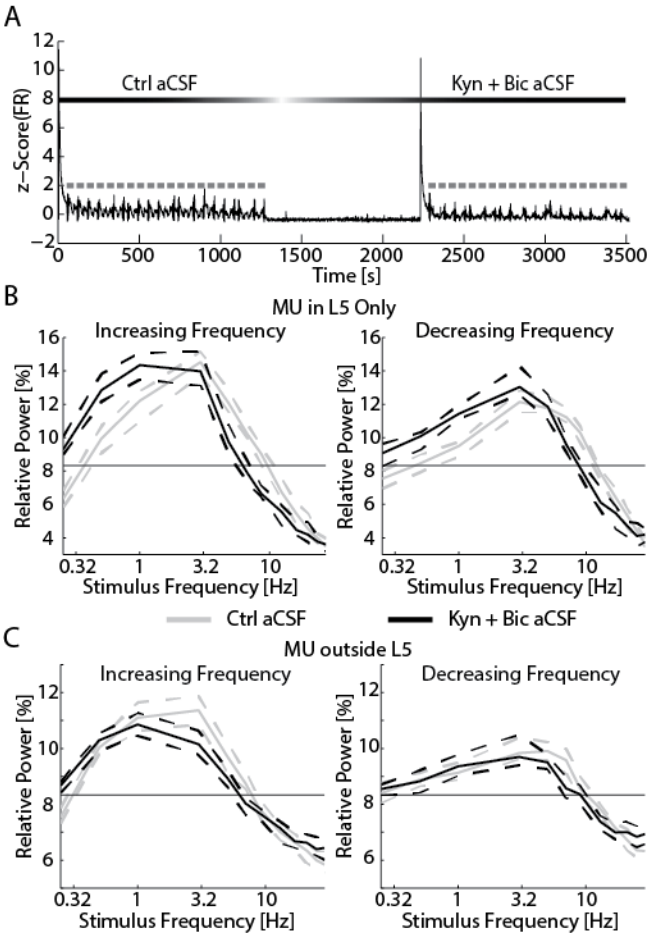

Figure 3.3. Suppression of synaptic transmission favors slower stimuli.

(A) The z-scored time course of the MU firing rate (black) for the duration of the experiment. Optogentic chirps are indicated in gray. After the first epoch of stimulation with control aCSF the perfusion was switched to Kyn + Bic aCSF. 10 minutes after the addition of synaptic blockers, a second epoch of stimulation was applied. The relative activity of MU recorded in L5 (B) and MU recorded outside of L5 (C) for increasing (left) and decreasing (right) frequency stimuli. For chirps in control aCSF (gray) and Kyn + Bic aCSF (black). The thin black line indicates chance activity levels. The addition of synaptic blockers caused a shift in the frequency response in favor of slow stimuli. Dashed lines indicate the 95% confidence interval of the median. Ctrl aCSF: control aCSF.

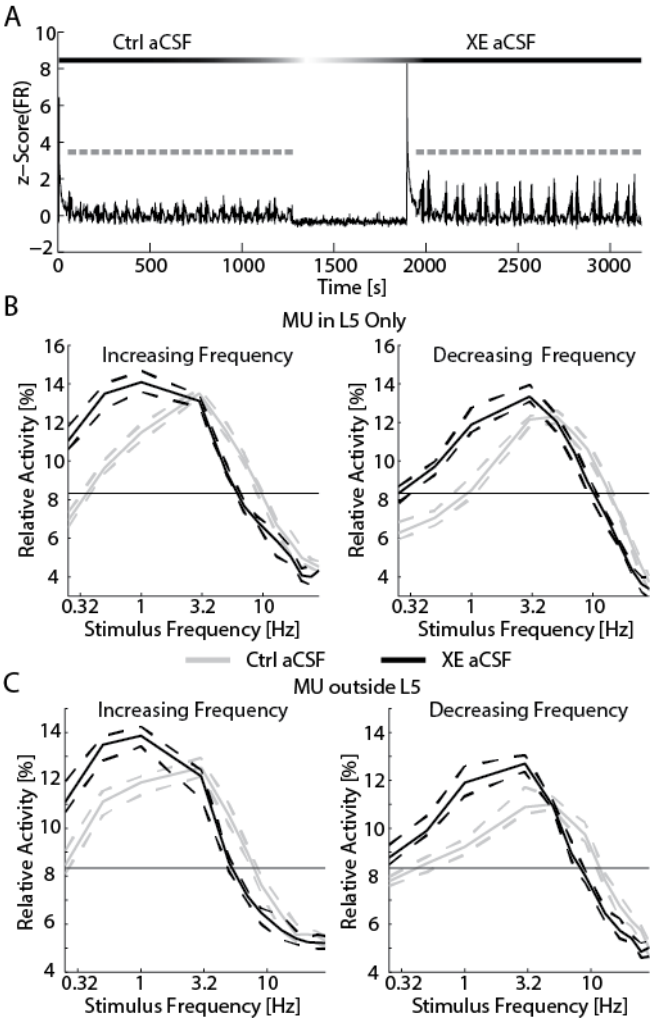

Figure 3.4 Addition of XE-991 reduced the resonant frequency of networks.

(A) The z-scored time course of the MU firing rate (black). Chirp trials are indicated in gray. After the first epoch of stimulation the perfusion was switched to XE aCSF. 10 minutes after the application of XE aCSF a second epoch of stimulation were applied. (B) The relative activity for each frequency of stimulation for increasing (left) and decreasing (right) frequency chirps for MU recorded within L5. (C) The relative activity for MU recorded outside of L5 for increasing (left) and decreasing (right) frequency chirp stimuli. For (B) and (C) response to optogenetic chirps in control aCSF is in gray while the response to chirps delivered in XE aCSF is in black. The thin black line indicates chance activity levels. With XE-991 in the bath the response to low frequency stimuli were increased. Ctrl aCSF: control aCSF. Dashed lines indicate the 95% confidence interval of the median.

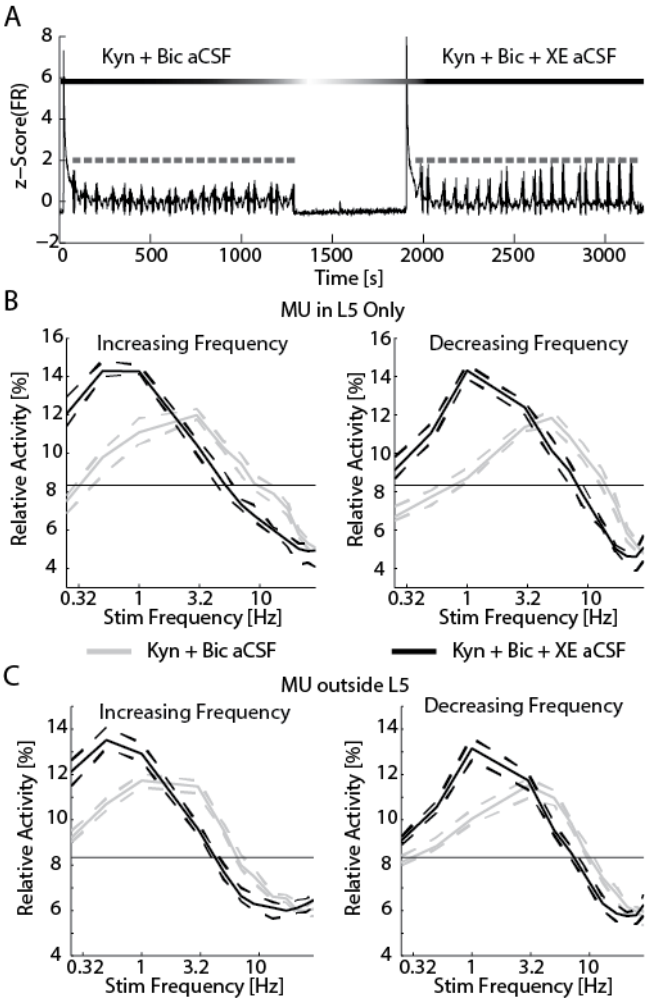

Figure 3.5. XE-991 remained effective in the presence of suppressed synaptic transmission.

(A). The z-scored time course of the MU firing rate (black). Optogenetic chirp trials are indicated in gray. Synaptic transmission was suppressed throughout the experiment, after the first epoch of trials the perfusion was switched to Kyn + Bic + XE aCSF. 10 minutes after the application of Kyn + Bic + XE aCSF a second epoch of optogentic chirp stimulation was applied to examine the effect of I_M when synaptic transmission was suppressed. (B) The relative activity for each frequency of stimulation for increasing (left) and decreasing (right) frequency chirps for MU within L5. (C) The relative activity for MU outside of L5. The blockade of I_M had a significant effect on the relative activity with synaptic transmission suppressed. Dashed lines indicate the 95% confidence interval of the median.

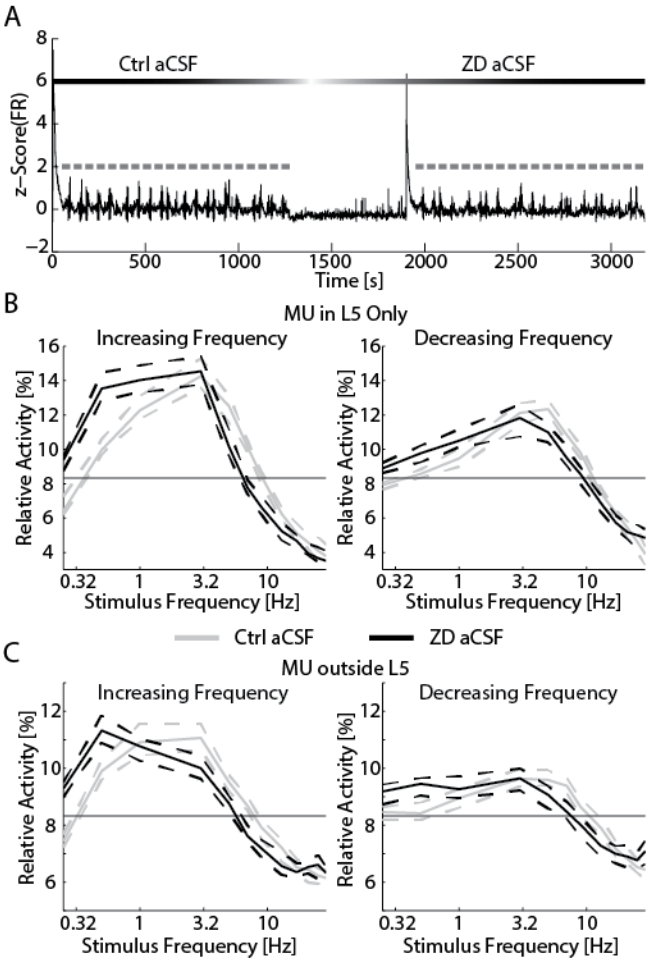

Figure 3.6. Blockade of I_h reduced the resonant frequency of networks.

(A) The z-scored time course of the MU firing rate for the duration of an experiment (black). Optogentic chirps are indicated in gray. After the first epoch of stimulation with control aCSF the perfusion was switched to ZD aCSF. 10 minutes after the addition of ZD-7288, a second epoch of stimulation was applied. The relative activity of MU recorded in L5 (B) and MU recorded outside of L5 (C) for increasing (left) and decreasing (right) frequency stimuli. For chirps in control aCSF (gray) and ZD aCSF (black). The thin black line indicates chance activity levels. With ZD-7288 in the bath, the responses to low frequency stimuli were increased. Ctrl aCSF: control aCSF. Dashed lines indicate the 95% confidence interval of the median.

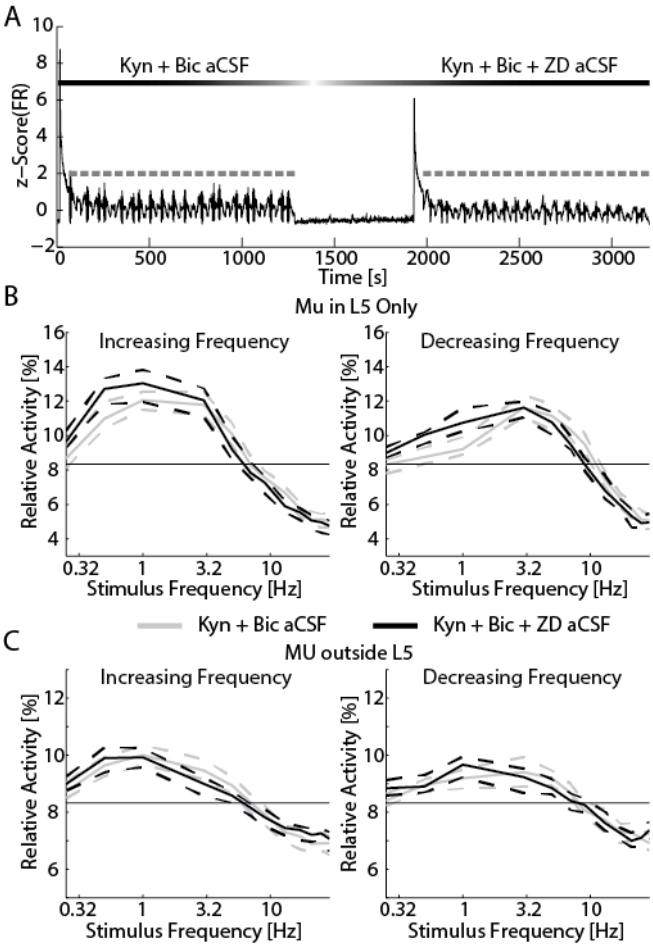

Figure 3.7. I_h played a limited role in resonance when synaptic transmission was suppressed.

(A) The z-scored time course of the MU firing rate for the duration of an experiment (black). Optogentic chirps are indicated in gray. After the first epoch of stimulation with Kyn + Bic aCSF the perfusion was switched to Kyn + Bic + ZD aCSF. 10 minutes after the addition of ZD, a second epoch of stimulation was applied. The relative activity of MU recorded in L5 (B) and MU recorded outside of L5 (C) for increasing (left) and decreasing (right) frequency stimuli. For chirps in Kyn + Bic aCSF (gray) and Kyn + Bic + ZD aCSF (black). The thin black line indicates chance activity levels. The addition of ZD-7288 caused a limited change in the frequency response, indicating that with synaptic transmission suppressed I_h played a small role in the frequency response. Dashed lines indicate the 95% confidence interval of the median. Blockade of I_h reduced the resonant frequency of networks. (A) The z-scored time course of the MU firing rate for the duration of an experiment (black). Optogentic chirps are indicated in gray. After the first epoch of stimulation with control aCSF the perfusion was switched to ZD aCSF. 10 minutes after the

addition of ZD-7288, a second epoch of stimulation was applied. The relative activity of MU recorded in L5 (B) and MU recorded outside of L5 (C) for increasing (left) and decreasing (right) frequency stimuli. For chirps in control aCSF (gray) and ZD aCSF (black). The thin black line indicates chance activity levels. With ZD-7288 in the bath, the responses to low frequency stimuli were increased. Ctrl aCSF: control aCSF. Dashed lines indicate the 95% confidence interval of the median.

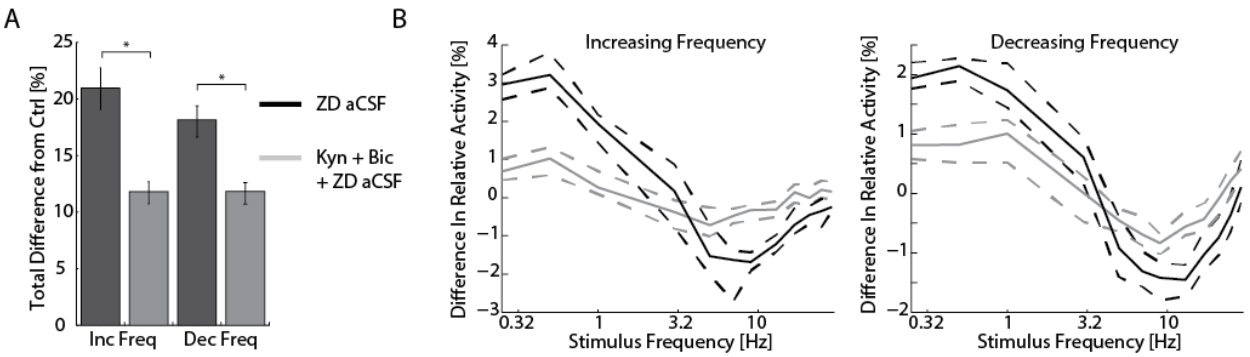

Figure 3.8. The effect of I_h depended on synaptic transmission.

(A) The sum of the absolute difference in relative activity caused by the addition of ZD-7288 to control aCSF (dark gray) and Kyn + Bic aCSF (light gray) across frequencies. For both increasing (left) and decreasing (right) frequency chirps the effect of adding ZD-7288 was greater without synaptic transmission suppressed. (B) The difference in relative activity by frequency across all MU for increasing (left) and decreasing (right) frequency chirps. Both the increased response to low frequency stimuli and the decreased response in the middle frequency band were greater with synaptic transmission intact. Ctrl: control aCSF. Inc Freq: increasing frequency chirps. Dec Freq: decreasing frequency chirps. * $p < 0.05$. Dashed lines indicate the 95% confidence interval of the median. Data presented here are a direct comparison of the results of experiments presented in Figure 3.6-7.

Stimulation Frequency [Hz]	Ctrl1 vs Ctrl2	Ctrl vs Kyn + Bic	Ctrl vs XE	Kyn + Bic vs Kyn + Bic + XE	Ctrl vs ZD	Kyn + Bic vs Kyn + Bic + ZD
0.25	0.153	$< 10^{-3}$	$< 10^{-3}$	$< 10^{-3}$	$< 10^{-3}$	0.166
0.5	0.532	$< 10^{-3}$	$< 10^{-3}$	$< 10^{-3}$	$< 10^{-3}$	0.004
1	1	$< 10^{-3}$	$< 10^{-3}$	$< 10^{-3}$	$< 10^{-3}$	0.949
3	0.145	1	1	$< 10^{-3}$	1	1
5	0.030	$< 10^{-3}$	$< 10^{-3}$	$< 10^{-3}$	$< 10^{-3}$	1
7	0.027	$< 10^{-3}$	$< 10^{-3}$	$< 10^{-3}$	$< 10^{-3}$	1
9	1	$< 10^{-3}$	$< 10^{-3}$	$< 10^{-3}$	$< 10^{-3}$	1
13	1	0.007	0.856	$< 10^{-3}$	0.001	1
17	1	1	1	$< 10^{-3}$	0.671	1
21	1	1	0.419	0.046	0.990	1
25	1	1	1	0.999	1	1
29	1	1	1	1	1	1

Table 3.1. ANOVA p values for MU within L5 for increasing frequency chirps.

Stimulation Frequency [Hz]	Ctrl1 vs Ctrl2	Ctrl vs Kyn + Bic	Ctrl vs XE	Kyn + Bic vs Kyn + Bic + XE	Ctrl vs ZD	Kyn + Bic vs Kyn + Bic + ZD
0.25	0.047	$< 10^{-3}$	$< 10^{-3}$	$< 10^{-3}$	$< 10^{-3}$	0.637
0.5	0.083	$< 10^{-3}$	$< 10^{-3}$	$< 10^{-3}$	$< 10^{-3}$	0.271
1	0.986	0.40	$< 10^{-3}$	$< 10^{-3}$	$< 10^{-3}$	0.016
3	1	0.853	0.004	0.143	0.964	1
5	0.789	$< 10^{-3}$	0.962	$< 10^{-3}$	0.538	1
7	0.061	$< 10^{-3}$	0.999	$< 10^{-3}$	$< 10^{-3}$	0.990
9	0.050	$< 10^{-3}$	$< 10^{-3}$	$< 10^{-3}$	$< 10^{-3}$	0.760
13	1	0.010	$< 10^{-3}$	$< 10^{-3}$	$< 10^{-3}$	1
17	1	1	$< 10^{-3}$	$< 10^{-3}$	0.014	0.999
21	1	1	0.012	$< 10^{-3}$	0.991	1
25	1	1	0.864	0.656	1	1
29	0.920	0.992	1	1	1	1

Table 3.2. ANOVA p values for MU within L5 for decreasing frequency chirps

Stimulation Frequency [Hz]	Ctrl1 vs Ctrl2	Ctrl vs Kyn + Bic	Ctrl vs XE	Kyn + Bic vs Kyn + Bic + XE	Ctrl vs ZD	Kyn + Bic vs Kyn + Bic + ZD
0.25	1	$< 10^{-3}$	$< 10^{-3}$	$< 10^{-3}$	$< 10^{-3}$	0.789
0.5	0.873	1	$< 10^{-3}$	$< 10^{-3}$	$< 10^{-3}$	1
1	0.217	1	$< 10^{-3}$	$< 10^{-3}$	1	1
3	1	$< 10^{-3}$	1	$< 10^{-3}$	0.131	1
5	0.925	$< 10^{-3}$	$< 10^{-3}$	$< 10^{-3}$	0.009	0.994
7	0.026	0.188	$< 10^{-3}$	$< 10^{-3}$	$< 10^{-3}$	0.544
9	1	1	$< 10^{-3}$	$< 10^{-3}$	0.099	1
13	1	1	0.994	0.998	0.525	1
17	1	1	1	0.999	1	1
21	1	0.994	1	1	1	1
25	1	0.485	1	1	1	1
29	1	0.056	1	1	1	1

Table 3.3. ANOVA p values MU outside L5 for increasing frequency chirps.

Stimulation Frequency [Hz]	Ctrl1 vs Ctrl2	Ctrl vs Kyn + Bic	Ctrl vs XE	Kyn + Bic vs Kyn + Bic + XE	Ctrl vs ZD	Kyn + Bic vs Kyn + Bic + ZD
0.25	0.657	0.998	0.002	0.092	$< 10^{-3}$	0.984
0.5	0.746	1	$< 10^{-3}$	$< 10^{-3}$	$< 10^{-3}$	1
1	1	1	$< 10^{-3}$	$< 10^{-3}$	0.327	0.984
3	1	1	$< 10^{-3}$	1	1	1
5	1	1	1	$< 10^{-3}$	0.430	0.867
7	0.301	0.505	0.011	$< 10^{-3}$	0.162	0.383
9	0.544	0.661	$< 10^{-3}$	$< 10^{-3}$	0.007	1
13	1	1	$< 10^{-3}$	$< 10^{-3}$	0.057	1
17	1	1	0.080	0.053	0.999	1
21	1	1	0.799	1	1	1
25	1	1	0.833	1	1	1
29	1	0.695	1	1	1	0.081

Table 3.4. ANOVA p values MU outside L5 for decreasing frequency chirps.

REFERENCES

Achermann, P., & Borbely, A. A. (1997). Low-frequency (< 1 Hz) oscillations in the human sleep electroencephalogram. *Neuroscience, 81*(1), 213-222.

Alonso, A., & Llinas, R. R. (1989). Subthreshold Na+-dependent theta-like rhythmicity in stellate cells of entorhinal cortex layer II. *Nature, 342*(6246), 175-177. doi:10.1038/342175a0

Arenkiel, B. R., Peca, J., Davison, I. G., Feliciano, C., Deisseroth, K., Augustine, G. J., . . . Feng, G. (2007). In vivo light-induced activation of neural circuitry in transgenic mice expressing channelrhodopsin-2. *Neuron, 54*(2), 205-218. doi:10.1016/j.neuron.2007.03.005

Bazhenov, M., Timofeev, I., Steriade, M., & Sejnowski, T. J. (2002). Model of thalamocortical slow-wave sleep oscillations and transitions to activated States. *The Journal of neuroscience : the official journal of the Society for Neuroscience, 22*(19), 8691-8704.

Beltramo, R., D'Urso, G., Dal Maschio, M., Farisello, P., Bovetti, S., Clovis, Y., . . . Fellin, T. (2013). Layer-specific excitatory circuits differentially control recurrent network dynamics in the neocortex. *Nature neuroscience, 16*(2), 227-234. doi:10.1038/nn.3306

Buzsáki, G. (2006). *Rhythms of the brain*. Oxford ; New York: Oxford University Press.

Chauvette, S., Volgushev, M., & Timofeev, I. (2010). Origin of active states in local neocortical networks during slow sleep oscillation. *Cerebral cortex, 20*(11), 2660-2674. doi:10.1093/cercor/bhq009

Cho, K. K., Hoch, R., Lee, A. T., Patel, T., Rubenstein, J. L., & Sohal, V. S. (2015). Gamma rhythms link prefrontal interneuron dysfunction with cognitive inflexibility in Dlx5/6(+/-) mice. *Neuron, 85*(6), 1332-1343. doi:10.1016/j.neuron.2015.02.019

Crochet, S., & Petersen, C. C. (2006). Correlating whisker behavior with membrane potential in barrel cortex of awake mice. *Nature neuroscience, 9*(5), 608-610. doi:10.1038/nn1690

Cuntz, H., Remme, M. W., & Torben-Nielsen, B. (2014). *The computing dendrite: from structure to function*. New York: Springer.

Dembrow, N. C., Chitwood, R. A., & Johnston, D. (2010). Projection-specific neuromodulation of medial prefrontal cortex neurons. *The Journal of neuroscience : the official journal of the Society for Neuroscience, 30*(50), 16922-16937. doi:10.1523/JNEUROSCI.3644-10.2010

Dickson, C. T., Magistretti, J., Shalinsky, M. H., Fransen, E., Hasselmo, M. E., & Alonso, A. (2000). Properties and role of I(h) in the pacing of subthreshold oscillations in entorhinal cortex layer II neurons. *Journal of neurophysiology, 83*(5), 2562-2579.

Engel, T. A., Schimansky-Geier, L., Herz, A. V., Schreiber, S., & Erchova, I. (2008). Subthreshold membrane-potential resonances shape spike-train patterns in the entorhinal cortex. *Journal of neurophysiology, 100*(3), 1576-1589. doi:10.1152/jn.01282.2007

Erchova, I., Kreck, G., Heinemann, U., & Herz, A. V. (2004a). Dynamics of rat entorhinal cortex layer II and III cells: characteristics of membrane potential resonance at rest predict oscillation properties near threshold. *The Journal of physiology, 560*(Pt 1), 89-110. doi:10.1113/jphysiol.2004.069930

Erchova, I., Kreck, G., Heinemann, U., & Herz, A. V. (2004b). Dynamics of rat entorhinal cortex layer II and III cells: characteristics of membrane potential resonance at rest predict oscillation properties near threshold. *The Journal of physiology, 560*(Pt 1), 89-110. doi:10.1113/jphysiol.2004.069930

Fellous, J. M., Houweling, A. R., Modi, R. H., Rao, R. P., Tiesinga, P. H., & Sejnowski, T. J. (2001). Frequency dependence of spike timing reliability in cortical pyramidal cells and interneurons. *Journal of neurophysiology, 85*(4), 1782-1787.

Fransen, E., Alonso, A. A., Dickson, C. T., Magistretti, J., & Hasselmo, M. E. (2004). Ionic mechanisms in the generation of subthreshold oscillations and action potential clustering in entorhinal layer II stellate neurons. *Hippocampus, 14*(3), 368-384. doi:10.1002/hipo.10198

Gee, S., Ellwood, I., Patel, T., Luongo, F., Deisseroth, K., & Sohal, V. S. (2012). Synaptic activity unmasks dopamine D2 receptor modulation of a specific class of layer V pyramidal neurons in prefrontal cortex. *The Journal of neuroscience : the official journal of the Society for Neuroscience, 32*(14), 4959-4971. doi:10.1523/JNEUROSCI.5835-11.2012

Gentet, L. J., Avermann, M., Matyas, F., Staiger, J. F., & Petersen, C. C. (2010). Membrane potential dynamics of GABAergic neurons in the barrel cortex of behaving mice. *Neuron, 65*(3), 422-435. doi:10.1016/j.neuron.2010.01.006

Giocomo, L. M., & Hasselmo, M. E. (2009). Knock-out of HCN1 subunit flattens dorsal-ventral frequency gradient of medial entorhinal neurons in adult mice. *The Journal of neuroscience : the official journal of the Society for Neuroscience, 29*(23), 7625-7630. doi:10.1523/JNEUROSCI.0609-09.2009

Giocomo, L. M., Zilli, E. A., Fransen, E., & Hasselmo, M. E. (2007). Temporal frequency of subthreshold oscillations scales with entorhinal grid cell field spacing. *Science, 315*(5819), 1719-1722. doi:10.1126/science.1139207

Haas, J. S., & White, J. A. (2002). Frequency selectivity of layer II stellate cells in the medial entorhinal cortex. *Journal of neurophysiology, 88*(5), 2422-2429. doi:10.1152/jn.00598.2002

Halliwell, J. V., & Adams, P. R. (1982). Voltage-clamp analysis of muscarinic excitation in hippocampal neurons. *Brain research, 250*(1), 71-92.

Harris, K. D., Csicsvari, J., Hirase, H., Dragoi, G., & Buzsaki, G. (2003). Organization of cell assemblies in the hippocampus. *Nature, 424*(6948), 552-556. doi:10.1038/nature01834

Hattox, A. M., & Nelson, S. B. (2007). Layer V neurons in mouse cortex projecting to different targets have distinct physiological properties. *Journal of neurophysiology, 98*(6), 3330-3340. doi:10.1152/jn.00397.2007

Hu, H., Vervaeke, K., & Storm, J. F. (2002). Two forms of electrical resonance at theta frequencies, generated by M-current, h-current and persistent Na+ current in rat hippocampal pyramidal cells. *The Journal of physiology, 545*(Pt 3), 783-805.

Hutcheon, B., Miura, R. M., & Puil, E. (1996). Subthreshold membrane resonance in neocortical neurons. *Journal of neurophysiology, 76*(2), 683-697.

Hutcheon, B., & Yarom, Y. (2000). Resonance, oscillation and the intrinsic frequency preferences of neurons. *Trends in neurosciences, 23*(5), 216-222.

Izhikevich, E. M., Desai, N. S., Walcott, E. C., & Hoppensteadt, F. C. (2003). Bursts as a unit of neural information: selective communication via resonance. *Trends in neurosciences, 26*(3), 161-167. doi:10.1016/S0166-2236(03)00034-1

Jameson, L. C., & Sloan, T. B. (2006). Using EEG to monitor anesthesia drug effects during surgery. *Journal of clinical monitoring and computing, 20*(6), 445-472.

Ke, H., Tinsley, M. R., Steele, A., Wang, F., & Showalter, K. (2014). Link weight evolution in a network of coupled chemical oscillators. *Physical review. E, Statistical, nonlinear, and soft matter physics, 89*(5), 052712. doi:10.1103/PhysRevE.89.052712

Kole, M. H., Hallermann, S., & Stuart, G. J. (2006). Single Ih channels in pyramidal neuron dendrites: properties, distribution, and impact on action potential output. *The Journal of neuroscience : the official journal of the Society for Neuroscience, 26*(6), 1677-1687. doi:10.1523/JNEUROSCI.3664-05.2006

Lea-Carnall, C. A., Montemurro, M. A., Trujillo-Barreto, N. J., Parkes, L. M., & El-Deredy, W. (2016). Cortical Resonance Frequencies Emerge from Network Size and Connectivity. *PLoS Comput Biol, 12*(2), e1004740. doi:10.1371/journal.pcbi.1004740

Leung, L. S., & Yu, H. W. (1998). Theta-frequency resonance in hippocampal CA1 neurons in vitro demonstrated by sinusoidal current injection. *Journal of neurophysiology, 79*(3), 1592-1596.

Lorincz, A., Notomi, T., Tamas, G., Shigemoto, R., & Nusser, Z. (2002). Polarized and compartment-dependent distribution of HCN1 in pyramidal cell dendrites. *Nature neuroscience, 5*(11), 1185-1193. doi:10.1038/nn962

Luczak, A., Bartho, P., Marguet, S. L., Buzsaki, G., & Harris, K. D. (2007). Sequential structure of neocortical spontaneous activity in vivo. *Proceedings of the National Academy of Sciences of the United States of America, 104*(1), 347-352. doi:10.1073/pnas.0605643104

Luthi, A., & McCormick, D. A. (1998). H-current: properties of a neuronal and network pacemaker. *Neuron, 21*(1), 9-12.

Magee, J. C. (2000). Dendritic integration of excitatory synaptic input. *Nat Rev Neurosci, 1*(3), 181-190. doi:10.1038/35044552

Marshall, L., Helgadottir, H., Molle, M., & Born, J. (2006). Boosting slow oscillations during sleep potentiates memory. *Nature, 444*(7119), 610-613. doi:10.1038/nature05278

McCormick, D. A., & Pape, H. C. (1990). Properties of a hyperpolarization-activated cation current and its role in rhythmic oscillation in thalamic relay neurones. *The Journal of physiology, 431*, 291-318.

Mitra, P., & Bokil, H. (2008). *Observed brain dynamics*. Oxford ; New York: Oxford University Press.

Nolan, M. F., Dudman, J. T., Dodson, P. D., & Santoro, B. (2007). HCN1 channels control resting and active integrative properties of stellate cells from layer II of the entorhinal cortex. *The Journal of neuroscience : the official journal of the Society for Neuroscience, 27*(46), 12440-12451. doi:10.1523/JNEUROSCI.2358-07.2007

Pike, F. G., Goddard, R. S., Suckling, J. M., Ganter, P., Kasthuri, N., & Paulsen, O. (2000). Distinct frequency preferences of different types of rat hippocampal neurones in response to oscillatory input currents. *The Journal of physiology, 529 Pt 1*, 205-213.

Rotstein, H. G. (2015). Subthreshold amplitude and phase resonance in models of quadratic type: Nonlinear effects generated by the interplay of resonant and amplifying currents. *Journal of computational neuroscience, 38*(2), 325-354. doi:10.1007/s10827-014-0544-2

Rotstein, H. G., & Nadim, F. (2014). Frequency preference in two-dimensional neural models: a linear analysis of the interaction between resonant and amplifying currents. *Journal of computational neuroscience, 37*(1), 9-28. doi:10.1007/s10827-013-0483-3

Rotstein, H. G., Pervouchine, D. D., Acker, C. D., Gillies, M. J., White, J. A., Buhl, E. H., . . . Kopell, N. (2005). Slow and fast inhibition and an H-current interact to create a theta rhythm in a model of CA1 interneuron network. *Journal of neurophysiology, 94*(2), 1509-1518. doi:10.1152/jn.00957.2004

Royer, S., Zemelman, B. V., Losonczy, A., Kim, J., Chance, F., Magee, J. C., & Buzsaki, G. (2012). Control of timing, rate and bursts of hippocampal place cells by dendritic and somatic inhibition. *Nature neuroscience, 15*(5), 769-775. doi:10.1038/nn.3077

Sanchez-Vives, M. V., & McCormick, D. A. (2000). Cellular and network mechanisms of rhythmic recurrent activity in neocortex. *Nature neuroscience, 3*(10), 1027-1034. doi:10.1038/79848

Santoro, B., Chen, S., Luthi, A., Pavlidis, P., Shumyatsky, G. P., Tibbs, G. R., & Siegelbaum, S. A. (2000). Molecular and functional heterogeneity of hyperpolarization-activated pacemaker channels in the mouse CNS. *The Journal of neuroscience : the official journal of the Society for Neuroscience, 20*(14), 5264-5275.

Scanziani, M., & Hausser, M. (2009). Electrophysiology in the age of light. *Nature, 461*(7266), 930-939. doi:10.1038/nature08540

Schmidt, S. L., Chew, E. Y., Bennett, D. V., Hammad, M. A., & Frohlich, F. (2013). Differential effects of cholinergic and noradrenergic neuromodulation on spontaneous cortical network dynamics. *Neuropharmacology, 72C*, 259-273. doi:10.1016/j.neuropharm.2013.04.045

Schmidt, S. L., Iyengar, A. K., Foulser, A. A., Boyle, M. R., & Frohlich, F. (2014). Endogenous Cortical Oscillations Constrain Neuromodulation by Weak Electric Fields. *Brain stimulation*. doi:10.1016/j.brs.2014.07.033

Sellers, K. K., Bennett, D. V., & Frohlich, F. (2014). Frequency-band signatures of visual responses to naturalistic input in ferret primary visual cortex during free viewing. *Brain research*. doi:10.1016/j.brainres.2014.12.016

Sheets, P. L., Suter, B. A., Kiritani, T., Chan, C. S., Surmeier, D. J., & Shepherd, G. M. (2011). Corticospinal-specific HCN expression in mouse motor cortex: I(h)-dependent synaptic integration as a candidate microcircuit mechanism involved in motor control. *Journal of neurophysiology, 106*(5), 2216-2231. doi:10.1152/jn.00232.2011

Shepherd, G. M. (2013). Corticostriatal connectivity and its role in disease. *Nat Rev Neurosci, 14*(4), 278-291. doi:10.1038/nrn3469

Stark, E., Eichler, R., Roux, L., Fujisawa, S., Rotstein, H. G., & Buzsaki, G. (2013). Inhibition-induced theta resonance in cortical circuits. *Neuron, 80*(5), 1263-1276. doi:10.1016/j.neuron.2013.09.033

Stark, E., Koos, T., & Buzsaki, G. (2012). Diode probes for spatiotemporal optical control of multiple neurons in freely moving animals. *Journal of neurophysiology, 108*(1), 349-363. doi:10.1152/jn.00153.2012

Steriade, M., Nunez, A., & Amzica, F. (1993). Intracellular analysis of relations between the slow (< 1 Hz) neocortical oscillation and other sleep rhythms of the electroencephalogram. *The Journal of neuroscience : the official journal of the Society for Neuroscience, 13*(8), 3266-3283.

Steriade, M., Timofeev, I., & Grenier, F. (2001). Natural waking and sleep states: a view from inside neocortical neurons. *Journal of neurophysiology, 85*(5), 1969-1985.

Suter, B. A., Migliore, M., & Shepherd, G. M. (2013). Intrinsic electrophysiology of mouse corticospinal neurons: a class-specific triad of spike-related properties. *Cerebral cortex, 23*(8), 1965-1977. doi:10.1093/cercor/bhs184

Tononi, G., & Cirelli, C. (2014). Sleep and the price of plasticity: from synaptic and cellular homeostasis to memory consolidation and integration. *Neuron, 81*(1), 12-34. doi:10.1016/j.neuron.2013.12.025

Ulrich, D. (2002). Dendritic resonance in rat neocortical pyramidal cells. *Journal of neurophysiology, 87*(6), 2753-2759.

Wang, H., Peca, J., Matsuzaki, M., Matsuzaki, K., Noguchi, J., Qiu, L., . . . Augustine, G. J. (2007). High-speed mapping of synaptic connectivity using photostimulation in Channelrhodopsin-2 transgenic mice. *Proceedings of the National Academy of Sciences of the United States of America, 104*(19), 8143-8148. doi:10.1073/pnas.0700384104

Wang, W. T., Wan, Y. H., Zhu, J. L., Lei, G. S., Wang, Y. Y., Zhang, P., & Hu, S. J. (2006). Theta-frequency membrane resonance and its ionic mechanisms in rat subicular pyramidal neurons. *Neuroscience, 140*(1), 45-55. doi:10.1016/j.neuroscience.2006.01.033

Wang, X. J. (2010). Neurophysiological and computational principles of cortical rhythms in cognition. *Physiological reviews, 90*(3), 1195-1268. doi:10.1152/physrev.00035.2008

Womelsdorf, T., Valiante, T. A., Sahin, N. T., Miller, K. J., & Tiesinga, P. (2014). Dynamic circuit motifs underlying rhythmic gain control, gating and integration. *Nature neuroscience, 17*(8), 1031-1039. doi:10.1038/nn.3764

Yoshida, M., Giocomo, L. M., Boardman, I., & Hasselmo, M. E. (2011). Frequency of subthreshold oscillations at different membrane potential voltages in neurons at different anatomical positions on the dorsoventral axis in the rat medial entorhinal cortex. *The Journal of neuroscience : the official journal of the Society for Neuroscience, 31*(35), 12683-12694. doi:10.1523/JNEUROSCI.1654-11.2011

Zhuchkova, E., Remme, M. W., & Schreiber, S. (2013). Somatic versus dendritic resonance: differential filtering of inputs through non-uniform distributions of active conductances. *PloS one, 8*(11), e78908. doi:10.1371/journal.pone.0078908

CHAPTER 4: ENDOGENOUS CORTICAL OSCILLATIONS CONSTRAIN NEUROMODULATION BY WEAK ELECTRIC FIELDS[1]

INTRODUCTION

Oscillatory activity in neocortex enables temporal organization of information during sensory processing, cognition, and memory (Buzsáki, 2006; Wang, 2010). Perturbing cortical oscillations with brain stimulation has become a key experimental approach to evaluate the functional, frequency-specific roles of cortical oscillations. Targeted enhancement of cortical oscillations may in the future also serve as a treatment for psychiatric disorders associated with impaired cortical oscillations such as schizophrenia and autism (Uhlhaas & Singer, 2012). Suprathreshold excitation of cortical networks with pulsed transcranial magnetic stimulation (TMS) can alter temporal structure of network activity and mediate changes in associated cognitive processes (Romei, Gross, & Thut, 2010; for example Sauseng et al., 2009; Thut et al., 2011). Recently, transcranial alternating current stimulation (tACS) has emerged as an alternative non-invasive brain stimulation approach for targeted modulation of cortical oscillations (Herrmann, Rach, Neuling, & Struber, 2013). TACS applies a weak, sine-wave electric field (EF) that targets neocortical networks. Several studies have demonstrated cognitive enhancement by tACS in humans (Kirov, Weiss, Siebner, Born, & Marshall, 2009; Marshall, Helgadottir, Molle, & Born, 2006; Polania, Nitsche, Korman, Batsikadze, & Paulus, 2012; Santarnecchi et al., 2013) and animals (Binder, Rawohl, Born, & Marshall, 2014) and enhancing effects of tACS on neuronal activity in animal models *in vitro* (Deans, Powell, & Jefferys, 2007; Frohlich & McCormick, 2010; Reato, Rahman, Bikson, & Parra, 2010) and *in vivo* (Ali, Sellers, & Frohlich, 2013; Ozen et al., 2010). However, very little is known about the interaction dynamics between endogenous cortical oscillations and the small, periodic changes in membrane voltage caused by tACS. In fact, differences in endogenous network activity alter the effects of

[1] This chapter previously appeared as an article in Brain Stimulation; doi: 10.1016/j.brs.2014.07.033 (http://www.sciencedirect.com/science/article/pii/S1935861X14002629). The original citation is as follows: **Stephen L. Schmidt**, Apoorva K. Iyengar, A. Alban Foulser, Michael R. Boyle, Flavio Frohlich, (2014). Endogenous Cortical Oscillations Constrain Neuromodulation. Brain Stimulation, 7(6): 878-889.

tACS on macroscopic brain activity measured by electroencephalography (EEG) and may explain the variability of behavioral effects for seemingly very similar stimulation paradigms (Neuling, Rach, & Herrmann, 2013). In the long term, elucidating the role of endogenous activity in shaping the response to non-invasive brain stimulation is crucial for the development of individualized, adaptive stimulation paradigms that take into account ongoing network activity and adjust stimulation accordingly.

Computational simulations suggest that cortical activity is preferentially enhanced by EFs at the frequency of the endogenous oscillation through network resonance (Ali et al., 2013; Reato et al., 2010). Network resonance in this contexts is defined as the preference of a network to oscillate in a narrow frequency band in response to periodic stimulation (for review of resonance see Hutcheon & Yarom, 2000), in this case centered on the frequency of the endogenous oscillation. Here, we combine optogenetic network activation with applied EF stimulation *in vitro* to determine how the relationship between the network oscillation and stimulation frequency determines the effect of periodic stimulation on cortical oscillations. Using optogenetic stimulation for generating an *in vivo*-like activity structure provided precise and simultaneous control of both the "endogenous" activity (Beltramo et al., 2013) and the applied EF stimulation to directly study the interaction dynamics. Specifically, we used optogenetic stimulation of layer 5 pyramidal cells in cortical slices of the Thy1-ChR2 mouse (Arenkiel et al., 2007) to induce a pronounced slow cortical oscillation (1 Hz) that we then targeted with applied EF stimulation. Layer 5 pyramidal cells play a central role in low-frequency cortical oscillations (Chauvette, Volgushev, & Timofeev, 2010) and their optogenetic activation *in vivo* induces network activity that closely mimics spontaneous slow cortical oscillations (Beltramo et al., 2013). Using this approach, we tested the hypothesis that intrinsically oscillating neocortical networks exhibit network resonance by preferentially responding to frequency-matched sine-wave EF stimulation.

METHODS

Slice Preparation and Data Acquisition

All procedures were approved by The University of North Carolina at Chapel Hill Institute of Animal Use and Care and were in compliance with the National Institute of Health guide for care and use of laboratory animals (NIH Publications No. 8023, revised 1978). Thy1-Chr2 mice (Jackson Laboratory, Bar

Harbor, ME), deeply anesthetized with Euthasol (0.5 mL/kg, Virbac, Fort Worth, TX), were decapitated and their brains extracted and quickly placed in ice-cold sucrose solution (mM: 83.0 NaCl, 2.5 KCl, 0.5 $CaCl_2$, 3.3 $MgSO_4$, 1 NaH_2PO_4, 26.2 $NaHCO_3$, 22.0 Dextrose Anhydrose and 72.0 Sucrose) bubbled with carbogen (95% O_2, 5% CO_2). 200 µm coronal sections containing V1 were cut using a vibratome (Leica Microsystems, Wetzlar, Germany) and allowed to recover in incubation solution (mM: 119.0 NaCl, 2.5 KCl, 1.0 NaH_2PO_4, 26.2 $NaHCO_3$, 22.0 glucose, 2 $MgSO_4$ and 2.0 $CaCl_2$) for at least 1 hr at 34 °C. After recovery, slices were placed on a MEA 2100 (Multichannel Systems, Reutligen, Germany) and perfused with artificial cerebrospinal fluid (aCSF, mM: 119.0 NaCl, 4.5 KCl, 1 NaH_2PO_4, 26.2 $NaHCO_3$, 22.0 glucose, 1.0 $MgSO_4$, and 1.0 $CaCl_2$), heated to 36 °C, at a rate of greater 4 mL per minute as in (Schmidt, Chew, Bennett, Hammad, & Frohlich, 2013). The calcium and magnesium concentrations in the aCSF were modeled after human CSF concentrations (Sanchez-Vives & McCormick, 2000). Data were recorded from 59 electrodes (30 µm diameter) in a 6 by 10 perforated array with 100 µm spacing between electrodes at a rate of 25 kHz.

Experimental Design

Experiments included continuous 1 Hz optogenetic stimulation by blue light (460 nm, 22 mW maximum, approximately 200 µW delivered at slice surface) from a LED 460 (Prizmatix, Givat Shmuel, Israel). EF was generated by applying a calibrated current from a stimulus isolator (World Precision Instruments, Sarasota, FL) between two AgCl wires in the bath. Slices were arranged on the MEA such that pia was in parallel to the stimulation wires and therefore approximately orthogonal to the somato-dendritic axes of the pyramidal cells in the slice preparation. Therefore, the EF was oriented from the wire close to layer 1 of visual cortex to the wire close to the ventral side of the slice such that the positive first half-wave and the negative second half wave caused a somatic membrane depolarization and hyperpolarization, respectively (Bikson et al., 2004; Tranchina & Nicholson, 1986). Experiments consisted of continuous 1 Hz optogenetic stimulation (square-wave, 50% duty cycle) for 64 trials of EF stimulation. Each trial of EF stimulation consisted of 10 s of optogenetic stimulation, 10 s of EF with optogenetic stimulation, followed by an additional 10 s of optogenetic stimulation. The order of trials was randomized for both stimulation frequency (0.8, 1.0, 1.2 or 2.0 Hz) and stimulation amplitude (1 or 2 mV/mm EF). The

EF was selected to be of similar amplitude to the estimated EF strength during tACS in humans (Datta et al., 2009; Marshall et al., 2006) and was below action potential threshold for cells at rest (Bikson et al., 2004; Frohlich & McCormick, 2010). For experiments without optogenetic stimulation, the same stimulation paradigm was used however the LED was disconnected from the power supply. In experiments with low intensity optogenetic stimulation, the intensity was decreased to an intensity of $1/10^{th}$ of the full intensity (approximately 20 μW at slice surface). For experiments with varied optogenetic stimulation, we first selected the length of each "UP/DOWN state" from a normal distribution (mean 500 ms, standard deviation 50 ms) for a total of 10 oscillation cycles. "UP" states here refer to the periods when the LED was on. Conversely, "DOWN" states refer to the inactive phase of the LED stimulation cycle.

Data Analysis

Multiunit traces and stimulation data were recorded using MC_Rack (Multichannel Systems, Reutligen, Germany). All data analysis was performed by custom-written Matlab (Mathworks, Natick, MA) scripts. Spikes were extracted at the time-points at which the recorded, high-pass filtered trace for each electrode crossed the threshold of -4 times the standard deviation of the trace with a 1 ms dead time. Application of the EF would occasionally cause a transient, stereotyped voltage spike on all electrodes at the onset, offset or zero-crossing of EF cycles; therefore artifact removal was performed by finding and removing voltage spikes that occurred on 10 or more electrodes within 1 ms. Following artifact removal, only electrodes in V1 were included for subsequent analysis. Single units (SU) were isolated using methods outlined in (Fee, Mitra, & Kleinfeld, 1996; Hill, Mehta, & Kleinfeld, 2011; Schmidt et al., 2013). Spike trains were binned with 1 ms resolution for each SU. The FR effect of EF stimulation was calculated as the FR during EF stimulation divided by the FR of the period without EF stimulation immediately preceding stimulation for each electrode for each trial. The activation ratio was calculated as the number of spikes while the LED was on divided by the total number of spikes. Whole-slice spike trains were constructed by summing spike trains across electrodes (1 ms bins). Frequency transforms were calculated by convolution with Morelet wavelets followed by temporal averaging, and subsequent whole-slice spectra were then normalized by dividing by the number of summed SU. Frequency preference was

calculated as the mean of the frequency spectra at the frequency ± 0.01 Hz subtracted by the mean of 1.5 times the frequency ± 0.01. This metric includes not only the enhancement of rhythmic structure at the frequency in question but the suppression of rhythmic structure at frequencies between the fundamental frequency and the first harmonic. Paired data were analyzed using a Wilcoxon signed rank test with a Bonferroni correction for multiple comparisons where appropriate. Confidence intervals were determined from 5% to 95% using bootstrapping with 1,000 iterations.

RESULTS

Optogenetic *in Vitro* Model of Slow Cortical Oscillations

To probe the interaction dynamics between neocortical network activity and EF stimulation, we developed an experimental approach that enabled precise control of endogenous network dynamics *in vitro*, application of EF stimulation, and simultaneous recording of neuronal activity in all layers of cortical networks. To this end, we first determined if full-field optogenetic stimulation in absence of EF stimulation robustly evoked activity in the entire network and not just pyramidal cells in layer 5 that express ChR2 (Figure 4.1A, left). We found that periodic stimulation with blue light (460 nm optogenetic stimulation, 1Hz, 500 ms of simulation followed by 500 ms without stimulation for each oscillation cycle) robustly evoked network activity (Figure 4.1A, right). Importantly, individual SU in all cortical layers responded to optogenetic stimulation to varying degrees (Figure 4.1B, activation ratio, long-tailed distribution). The spread of activation ratios demonstrates that the SU in the stimulated slices did not all exclusively fire in lockstep (activation ratio of 1.0) with the stimulation but maintained their ability to spike in absence of stimulation (activation ratio of 0.5 if optogenetic stimulation had no effect). The SU maintained sparse firing (activation ratio, median ± SEM: 0.907 ± 0.003 for all SU, 0.895 ± 0.004 for L 1-4, 0.917 ± 0.004 for L5&6; FR: 1.30 ± 0.038 Hz for all SU, 1.33 ± 0.053 Hz for L1-4, 1.29 ± 0.052 Hz for L5&6; n = 3840, 1536, 2304 SU*trials, respectively; correlation: $r = 0.125$, $p < 10^{-3}$ for all SU; Figure 4.1B). Thus, the optogenetic stimulation of the slices did not cause unphysiological firing rates. Despite the cell-to-cell variability, the overall network activity in individual slices exhibited a prominent peak at 1 Hz in most trials (1 Hz peak: 1.05 ± 0.027 spikes^2/Hz, n = 703 trials, trials sorted by power at 1 Hz, Figure 4.1C). These data demonstrate that our optogenetic stimulation paradigm provided a precisely tuned 1 Hz network

oscillation but preserved *in vivo*-like sparseness and cell-to-cell variability of the firing patterns of individual neurons.

Neocortex Responds to Weak EF stimulation with Network Resonance

TACS provides a weak EF that we modeled with an applied EF generated by a voltage-controlled current source. We simultaneously applied optogenetic stimulation to model endogenous network activity (Figure 4.2A, Experimental set-up and waveforms for optogenetic and EF stimulation). We hypothesized that the response to stimulation is guided by network resonance near the frequency of the endogenous oscillation. Accordingly, EF stimulation of equal amplitude at the frequency (or its first harmonic) of the ongoing network oscillation would have a greater effect than stimulation with waveforms at nearby, yet mismatched frequencies. To test this hypothesis, we examined the network response to EF stimulation with two different amplitudes (1 and 2 mV/mm) at stimulation frequencies matched to (1 Hz), twice (2 Hz), and nearby (0.8 and 1.2 Hz) the frequency of the endogenous network oscillation (1 Hz, induced by optogenetic stimulation). We first examined the raster plot of all SU for 1 Hz EF stimulation and determined that EF stimulation did not override the patterned network activity caused by optogenetic stimulation since oscillation cycles with and without EF closely resembled each other (Figure 4.2B, raster of all units for 1 Hz stimulation, n = 3840 SU*trials); peak activity occurred at the onset of the optogenetic stimulation during each oscillation cycle and low but detectable activity occurred in absence of optogenetic stimulation (second half of stimulation period). Therefore, stimulation with EF amplitudes similar to the ones estimated to occur in human neocortex during tACS (Datta et al., 2009; Marshall et al., 2006) failed to qualitatively alter the endogenous activity structure. In order to quantify the more subtle effects of EF stimulation on spontaneous cortical oscillations, we assessed the change in frequency structure of the overall network activity within individual slices by computing the change in frequency spectrum (Figure 4.2C). In agreement with our hypothesis of frequency-specific modulation, we found that these modulation profiles of oscillation structure exhibited distinct shapes for different stimulation frequencies (0.8, 1.0, 1.2, 2.0 Hz). Independent of the stimulation frequency, the only clear peaks of enhancement were localized at or very close to 1 Hz (and its integer multiples). Therefore, our data reject the alternative hypothesis that EF stimulation enables the selective enhancement of network activity at

the stimulation frequency. Rather, enhancement was strongly constrained by the endogenous oscillation, in particular in cases such as here where we induced a pronounced, in *vivo-like* slow oscillation by means of optogenetic stimulation. We quantified the modulation of the oscillatory activity by first determining the amount of enhancement at the EF stimulation frequency. For 1 mV/mm EF amplitude, we exclusively found an increase in frequency preference for EF stimulation frequencies of 1 and 2 Hz. However, for increased stimulation amplitude (2 mV/mm), the EF application significantly enhanced 1, 1.2, and 2 Hz oscillations respectively (Figure 4.2D; confidence intervals and statistics Table 4.1. Frequency preference for EF Stimulation Frequency.Table 4.1). These results show that cortex preferentially responded to EF stimulation at the frequency of endogenous oscillation and its first harmonic. We then examined the effect of the stimulation on the endogenous activity at 1 Hz. Indeed, EF stimulation at the frequency of the network oscillation (1 Hz), its first harmonic (2 Hz), and below the network frequency (0.8 Hz) all enhanced the rhythmic activity caused by optogenetic stimulation at 1 Hz for low amplitude stimulation. EF stimulation amplitude to 2 mV/mm caused an increase of 1 Hz oscillation for all EF stimulation frequencies (Figure 4.2E; Table 4.2). Again, we found that perturbations at the frequency of the ongoing oscillation and the first harmonic preferentially enhance the ongoing oscillation. However, EF stimulation at the frequency below that of the ongoing oscillation also enhanced the oscillation. We therefore concluded that cortical networks respond to sine-wave EF stimulation, and likely by extension, tACS, with the properties of network resonance. EF stimulation predominantly enhanced the endogenously present oscillation and shifts in frequency of the endogenous were unattainable in these experiments. We next probed for outlasting effects by comparing the 10 s after EF enhancement to that of the 10 s preceding stimulation. We did not find any outlasting effect for any amplitude or frequency EF stimulation; this lack of outlasting effect is most likely due to the short duration of the EF stimulation and the randomization of the different stimulation frequency conditions in our study.

EF Stimulation Increases Neuronal Activity Levels

Does EF stimulation only alter the temporal structure of network activity or does it also alter the net activity levels of individual neurons? To address this question, we next investigated how EF stimulation alters the overall activity levels of individual neurons by measuring firing rates (FR) of SU. We examined

modulation of FR during the UP state (500 msec activity caused by optogenetic stimulation), the DOWN state (500 msec of relative quiescence in absence of optogenetic stimulation), and the entire cycle while EF stimulation was applied compared to that of the preceding interval of optogenetic stimulation only (Figure 4.3). Indeed application of most EF stimulations tested here increased FR during the UP state of the 1 Hz cycle (Figure 4.3 left, Table 4.3). During the DOWN state, only EF stimulation that was matched to the frequency of the optogenetic stimulation (1 Hz EF stimulation) caused a FR decrease for both stimulation amplitudes (Figure 4.3A center, Table 4.4). When we compared the total FR with EF stimulation to the FR without EF, we observed that 2 mV/mm EF enhanced FR for most stimulation frequencies (Figure 4.3A right, Table 4.5). However the total FR was not significantly increased for all low amplitude (1 mV/mm) EF stimulation frequencies except for mismatched frequency (1.2 Hz) stimulation. Thus in agreement with the findings on network oscillation structure, matching the stimulation frequency to the endogenous network frequency caused differential modulation of the network activity in contrast to non-matching stimulation frequencies.

We next assessed the temporal profile of the FR modulation by applied EF stimulation. In absence of EF stimulation, a pronounced increase in FR occurred at the onset of optogenetic stimulation followed by decay in FR with a relatively abrupt transition to low activity levels when the stimulus was turned off at 500 ms (black traces in Figure 4.3B, left). Overall, this activity profile was maintained in presence of EF stimulation (blue and red traces in Figure 4.3B left; Top: 1 Hz EF; Bottom: 2 Hz EF). We then calculated the percent change caused by application of EF and fitted a sine-wave to this time-profile of FR modulation (Figure 4.3B, right). We found that enhancement of neural activity by EF lagged behind the stimulus waveform for 1 Hz EF stimulation (goodness of fit: R^2 = 0.71 for 1 mV/mm and 0.62 for 2 mV/mm; φ = -0.21 for 1 mV/mm at 1 Hz and -0.14 for 2 mV/mm at 1 Hz; Figure 4.3B, top). Similarly, EF stimulation at 2 Hz caused a temporal modulation profile that followed a 2 Hz sine-wave (R^2 = 0.45 for 1 mV/mm and 0.64 for 2 mV/mm, Fig 3B bottom). Again we observed a phase delay between the EF stimulation and the change in FR (φ = -0.58 for 1 mV/mm at 1 Hz and -0.74 for 2 mV/mm at 2 Hz; for results of 0.8 and 1.2 Hz EF). We then examined pairwise correlations between single units to determine if the increase in oscillatory structure was caused by an increase in similarity of firing patterns of individual neurons at a finer time-scale. Pairwise correlations on the 50 ms timescale were virtually unaltered (Table

4.6). The increased oscillatory structure did thus not depend on increased synchronization at faster time-scales. Together, these results demonstrated an overall increase in FR for EF stimulation (with the exception of low-amplitude, frequency-matched stimulation) and a temporal modulation of activity levels that closely followed the applied EF waveform.

Conditions That Limit Occurrence of Network Resonance

Our finding of endogenous network dynamics constraining the effect of stimulation is likely most prevalent in the case of pronounced endogenous activity and low-amplitude periodic perturbations. To experimentally delineate the conditions in which the above demonstrated interaction dynamics apply, we performed additional control experiments. First, we conducted control experiments with a 2 mV/mm EF in the absence of optogenetic stimulation. In these experiments, the network activity without EF stimulation did not exhibit any peak in the frequency spectrum (Figure 4.4A). In contrast to the results presented above, the EF application enhanced the oscillatory structure at the frequency of the EF stimulation (median enhancement at stimulation frequency: 0.102 [0.076 0.132] $spikes^2$/Hz for 0.8 Hz EF, 0.067 [0.032 0.101] $spikes^2$/Hz for 1.0 Hz EF, 0.073 [0.038 0.104] $spikes^2$/Hz for 1.2 Hz EF, and 0.059 of [0.043 0.071] $spikes^2$/Hz for 2.0 Hz EF; $p < 10^{-3}$ for each stimulation frequency; n = 144 trials; Figure 4.4B-C left). In further contrast to experiments with a strong oscillation evoked by the optogenetic stimulation, only EF stimulation of 1.0 and 2.0 Hz increased the frequency preference for 1.0 Hz oscillations (median enhancement at 1 Hz: 0.009 [-0.015 0.016] $spikes^2$/Hz for 0.8 Hz EF, 0.067 [0.039 0.103] $spikes^2$/Hz for 1.0 Hz EF, 0.015 [-0.010 0.027] $spikes^2$/Hz for 1.2 Hz EF, and 0.055 [0.034 0.075] $spikes^2$/Hz for 2.0 Hz EF; $p = 1$, $p < 10^{-3}$, $p = 1$, $p < 10^{-3}$ respectively; n = 144 trials; Figure 4.4C, right). Therefore, without an endogenous oscillation, EF stimulation increased oscillatory structure at all stimulation frequencies evaluated. In agreement with our overall hypothesis, these results suggest that the structure of the endogenous activity determines if and to what extent EF are constrained in their effect on network dynamics. Thus, we next investigated two other scenarios in which we reduced the strength of the endogenous oscillation modeled by optogenetic stimulation. We hypothesized that a reduction in endogenous rhythmic structure would enable even frequency-mismatched stimulation waveforms to enhance oscillations at the EF stimulation frequency.

First, we lowered the intensity of the optogenetic stimulation to 20 μW. With this lower intensity stimulation, the strength of the evoked oscillation was lower than that caused by the full intensity stimulation (1.15 [1.12 1.24] spikes^2/Hz for low intensity optogenetic stimulation, 3.49 [3.35 3.64] spikes^2/Hz full intensity, $p < 10^{-3}$ Wilcoxon ranked sum test, n = 640 and 703 trials respectively, Figure 4.5A). We then applied EF stimulation with 2 mV/mm amplitude. Similarly to the experiments with no optogenetic stimulation, EF stimulation was able to increase frequency preference at all stimulation frequencies evaluated (median enhancement for EF stimulation frequency: 0.068 [0.022 0.124] spikes^2/Hz for 0.8 Hz EF, 0.173 [0.097 0.260] spikes^2/Hz for 1.0 Hz EF, 0.107 [0.075 0.140] spikes^2/Hz for 1.2 Hz EF, and 0.047 [0.016 0.083] spikes^2/Hz for 2.0 Hz EF; $p < 0.005$ for each stimulation frequency; n = 160 trials; Figure 4.5B-C left). However, the increase in oscillatory structure at the EF stimulation frequency trended to be larger for 1.0 Hz stimulation (confidence that response to 1 Hz stimulation was different: $p = 0.0898$ for 0.8 Hz stimulation, $p = 0.0595$ for 1.2 Hz stimulation and $p = 0.0029$ for 2 Hz stimulation, Wilcoxon ranked sum test with a Bonferroni correction for 3 comparisons). The frequency preference for the ongoing cortical oscillation was only enhanced for frequency matched (1 Hz) stimulation (median enhancement for optogenetic stimulation frequency: -0.052 [-0.125 -0.009] spikes^2/Hz for 0.8 Hz EF, 0.173 [0.101 0.261] spikes^2/Hz for 1.0 Hz EF, -0.048 [-0.110 -0.009] spikes^2/Hz for 1.2 Hz EF, and 0.039 [-0.015 0.080] spikes^2/Hz for 2.0 Hz EF; $p = 0.026$, $p < 10^{-3}$, $p = 0.167$, and $p = 0.383$ respectively; n = 160 trials; Figure 4.5C right). Thus, with a less pronounced endogenous oscillation, EF stimulation provided the best enhancement when stimulating at the frequency of the ongoing oscillation. However mismatches stimulation also enhanced frequency preference for the EF stimulation frequency.

Second, we reduced the strength of the ongoing oscillation by using a optogenetic stimulation waveform with a broader spectral peak around 1 Hz. Specifically, we varied the length of each “UP” and “DOWN” state by randomly drawing 20 durations from a normal distribution around 500 ms (standard deviation 50 ms). We then compared the multiunit frequency response to optogenetic stimulation of the experiments shown in Figure 4.1-3 to the response to the variable duration optogenetic stimulation. The frequency structure of the stimulation waveform still exhibited a peak frequency of 1 Hz. However, the frequency content was spread over a broader band (Figure 4.6A). Due to this change in the optogenetic stimulation, the evoked cortical oscillation was also altered but still exhibited a peak frequency at 1.0 Hz

(Figure 4.6B). However, the cortical response at 0.8 and 1.2 Hz was relatively enhanced when normalized by the peak (1 Hz) amplitude (Figure 4.6B right, Table 4.7). We then applied 2 mV/mm EF stimulation to slices activated with this optogenetic stimulation paradigm. Similarly to the results in (Figure 4.2C), EF stimulation increased the frequency preference for 1.0 Hz using 1.0, 1.2 and 2.0 Hz stimulation, however EF stimulation at 0.8 Hz did not increase the frequency preference for 1.0 Hz (median enhancement at optogenetic stimulation frequency, 1 Hz: 0.003 [-0.044 0.048] spikes^2/Hz for 0.8 Hz EF, 0.199 [0.127 0.289] spikes^2/Hz for 1.0 Hz EF, 0.063 [-0.021 0.134] spikes^2/Hz for 1.2 Hz EF, and 0.148 [0.053 0.222] spikes^2/Hz for 2.0 Hz EF; $p = 1$, $p < 10^{-3}$, $p = 0.014$ and $p = 0.001$ respectively; n = 176 trials; Figure 4.6C-D left). With increased frequency structure at 0.8 and 1.2 Hz in the optogenetic stimulation, the EF stimulation was able to significantly enhance frequency preference for the applied EF frequency (median enhancement at EF stimulation frequency: .446 [0.348 0.532] spikes^2/Hz for 0.8 Hz EF, 0.198 [0.127 0.275] spikes^2/Hz for 1.0 Hz EF, 0.092 [0.038 0.161] spikes^2/Hz for 1.2 Hz EF, and 0.104 [0.040 0.157] spikes^2/Hz for 2.0 Hz EF; $p < 10^{-3}$ for all groups; n = 176 trials; Figure 4.6D right). Therefore, the ongoing variable oscillation also shaped the network response to EF stimulation.

Finally, we asked if increasing the strength of the EF stimulation would enable the EF stimulation to override the endogenous network dynamics. To answer this question, we performed experiments with 8 mV/mm field strength. At such high amplitude, the EF stimulation was indeed able to increase frequency preference for the EF frequency despite the ongoing oscillation at 1 Hz (median enhancement at EF stimulation frequency: 0.382 [0.258 0.560] spikes^2/Hz for 0.8 Hz EF, 0.471 [0.221 0.661] spikes^2/Hz for 1.0 Hz EF, 0.319 [0.173 0.441] spikes^2/Hz for 1.2 Hz EF, and of 0.185 [0.130 0.290] spikes^2/Hz for 2.0 Hz EF; $p < 10^{-3}$; n = 208 trials; Figure 4.7A-B left). Only EF stimulation at 1.0 Hz increased the frequency preference for 1.0 Hz while EF stimulation at 0.8 Hz suppressed the frequency preference for 1.0 Hz (median enhancement at optogenetic stimulation frequency: -0.142 [-0.209 -0.049] spikes^2/Hz for 0.8 Hz EF, 0.483 [0.223 0.661] spikes^2/Hz for 1.0 Hz EF, 0.0444 [0.000 0.126] spikes^2/Hz for 1.2 Hz EF, and 0.100 [-0.018 0.245] spikes^2/Hz for 2.0 Hz EF; $p = 0.017$, $p < 10^{-3}$, $p = 0.915$ and $p = 0.054$ respectively; n = 208 trials; Figure 4.7B right). From these data, we concluded that indeed a comparatively strong EF may override the response-dependence of EF stimulation on the ongoing cortical oscillation.

DISCUSSION

Targeted modulation of cortical oscillations with non-invasive brain stimulation has the potential to enable significant progress (1) in the study of the causal role of oscillations in cognition and behavior and (2) in the development of novel treatments for neurological and psychiatric disorders associated with deficits in the macroscopic cortical activity patterns. However, in absence of a direct demonstration of the underlying mechanism of action by which such stimulation interacts with ongoing network dynamics, this progress will be severely hampered.

Application of weak EFs by transcranial current stimulation represents one promising approach to non-invasive brain stimulation (Brunoni et al., 2014; M. F. Kuo, Paulus, & Nitsche, 2014; Reato, Rahman, Bikson, & Parra, 2013). The presence of endogenous activity is crucial for EFs to have an effect on network dynamics since the depolarization caused by the EF is too small to activate neurons at rest (Ali et al., 2013; Frohlich & McCormick, 2010; Radman, Ramos, Brumberg, & Bikson, 2009). In essence, neurons need to be close to firing threshold for the resulting sub-millivolt perturbation of the membrane voltage to be an effective modulator of endogenous network activity. Previous *in vitro* studies have shown enhancing effects of sinewave EF stimulation on ongoing network activity (Deans et al., 2007; Frohlich & McCormick, 2010; Reato et al., 2010). However, the direct assessment of the interaction dynamics has been limited to observational descriptions of the effects of weak EF due to limited control of spontaneous or pharmacologically induced oscillations. Here, we used optogenetic tools to directly assess these interaction dynamics by exercising precise temporal control of both the endogenous activity (induced by optogenetic stimulation) and the EF stimulation. We established that sine-wave EF patterns with very low amplitude can indeed enhance network dynamics even in presence of very pronounced, rhythmic neocortical network activity that resembles *in vivo* activity patterns. In agreement with predictions from previous experimental (Feurra et al., 2013; Reato et al., 2010) and computational work (Ali et al., 2013), we show that the choice of stimulation frequency relative to the endogenous oscillation frequency plays a key role in determining the effect of stimulation. Specifically, we found that a pronounced endogenous oscillation precluded the generation of activity patterns at other (nearby) frequencies and that the enhancement of the endogenous oscillation depended on the EF stimulation frequency. We then tested the apparent constraint endogenous network dynamics impose on modulatory effects of stimulation;

indeed, with no endogenous oscillation present or with application of higher amplitude EF stimulation, oscillations at the EF stimulation frequency could be enhanced. We also reduced the strength of the endogenous oscillation (by reduced optogenetic stimulation) and found that these dynamics still constrained the effects of stimulation at trend level. Finally, with a temporally varied endogenous oscillation, we again found that mismatched stimulation could increase the endogenous oscillation but also increased oscillatory structure at the EF stimulation frequency.

The field has yet to converge on whether application of EF increases the net average FR of networks. In our hands, the average FR over 10 s was increased for most of the 2 mV/mm EF stimulation frequencies. This result agrees with the previously reported increase in multiunit activity evoked by field strengths as low as 1 mV/mm in (Frohlich & McCormick, 2010). However other studies have observed that while EF stimulation increased FR during the positive going phase of the stimulation, during the negative-going phase of the stimulation the FR was decreased, thus resulting in no net change (Reato et al., 2010). This distinction may be important for future studies aimed at determining if tACS acts by synchronizing neural oscillators or evoking more activity as a function of the temporal structure of the stimulation waveform.

Our findings demonstrate that the state of the targeted networks plays an important role in determining the response to EF stimulation. Such state-dependent response of neuronal circuits is well known for sensory input that reaches sensory areas in cortex. For example, the neuronal representation of visual (Niell & Stryker, 2010) and auditory (Curto, Sakata, Marguet, Itskov, & Harris, 2009) inputs depends on overall brain state. Our results suggest that this “gating” by brain state (defined by the presence of specific network-level activity patterns) also applies to external stimuli directly provided to neuronal networks by brain stimulation. Matching the brain stimulation to the specific endogenous network dynamics of an individual at a given time-point may therefore be crucial for effectiveness and thus an appealing opportunity for individualized treatment. Indeed, in human motor cortex, the presence of a pronounced beta oscillation was found to determine whether beta (20 Hz) or theta (5 Hz) frequency tACS best facilitated motor-evoked potentials by transcranial magnetic stimulation (Feurra et al., 2013). Here we have performed EF stimulation in the presence and absence of a cortical oscillation and likewise observed different cortical response dependent on the cortical oscillation. In contrast, we used EF

stimulation frequencies within the same frequency band as the ongoing cortical oscillation since oscillations in different frequency bands are likely generated by different mechanisms and presently cannot be simultaneously modeled in a slice preparation. Importantly, a similar phenomenon has also been reported for alpha oscillations where the effect of tACS on macroscopic network dynamics depended on the strength of the ongoing oscillation (Neuling, Wagner, Wolters, Zaehle, & Herrmann, 2012). However, in this case, the presence of strong alpha oscillations precluded further enhancement by frequency-matched tACS. Yet, enhancement was successful for the case of weak endogenous alpha oscillations in the same participants. This difference in the effect of frequency-matched stimulation can have several causes, including the presence of ceiling effects. Taken together with the results presented here, the effect of EF stimulation may vary from enhancement at any frequency, to enhancement only of the endogenous oscillation, to no enhancement at the stimulation frequency, depending on the strength of the ongoing cortical oscillation.

Importantly, further studies will be needed to fully elucidate the mechanism of action of tACS for other cortical oscillations with different frequency structure such as the gamma oscillation (> 30 Hz). Since cortical oscillations at different frequencies are likely generated by distinct single cell and network mechanisms, it is as of now unclear if the work presented here will generalize to other cortical oscillations. For example, the gamma oscillation likely arises from the dynamic interaction of pyramidal cells and fast-spiking inhibitory interneurons that exhibit their own resonance profile (Cardin et al., 2009). Nevertheless, the overall approach taken in this study will likely be equally elucidating when applied to the study of tACS that targets other frequency bands and therefore lays the groundwork for a comprehensive understanding of tACS and its interaction with cortical network dynamics (Frohlich & Schmidt, 2013).

Our study focused on unraveling the interaction dynamics between periodic, weak EF and oscillatory network activity. Understanding tACS will require the study of other important aspects of stimulation delivery. In particular, we used a model system of tACS where we directly applied calibrated EF to cortical slices *in vitro* and recorded microscopic network dynamics measured by SU activity. Thus, our study does not provide any insight into the spatial patterning of the stimulation (i.e. EF distribution) as a result of the current application to the scalp in human tACS. Only the intersection of the mechanisms of temporal targeting (demonstrated here), spatial targeting (H. I. Kuo et al., 2013), and functional targeting

(Feurra et al., 2013) will provide the tools for developing highly specific stimulation paradigms. We also cannot, with only one slice, examine the mechanisms of applying anti-phase tACS to different brain regions. This type of stimulation has shown interesting behavioral results (Polania et al., 2012; Struber, Rach, Trautmann-Lengsfeld, Engel, & Herrmann, 2014), but cannot be probed with the methods used here. Likely, distinct mechanisms such as switching between multiple stable states may mediate such effects on coherence (Kutchko & Frohlich, 2013). Nevertheless, our *in vitro* approach provides essential advantages that can help build an important bridge between computational studies (that inherently lack biological plausibility) and *in vivo* studies in animals and humans that often do not provide the level of experimental access and control required to elucidate the interaction dynamics. Using optogenetic stimulation of layer 5 pyramidal cells causes naturalistic slow rhythmic activity *in vivo*; here we adapted this approach for *in vitro* stimulation. We found such stimulation to cause a clear network rhythm although individual cells continued to exhibit low, naturalistic firing rates in presence of stimulation. Given the known role of layer 5 pyramidal cell to greatly contribute to the genesis of slow (cortical) rhythms, our approach provided the opportunity to maintain *in vivo* like activity patterns *in vitro*.

Together, these results provide a mechanism of action of tACS at the network level and point towards next-generation tACS that provides individualized, state-dependent feedback tACS for the enhancement of cortical oscillations (Boyle & Frohlich, 2013). The most important next step towards this goal will be the successful recording of brain activity during stimulation as recently demonstrated for EEG combined with tACS (Helfrich et al., 2014).

FIGURES AND TABLES

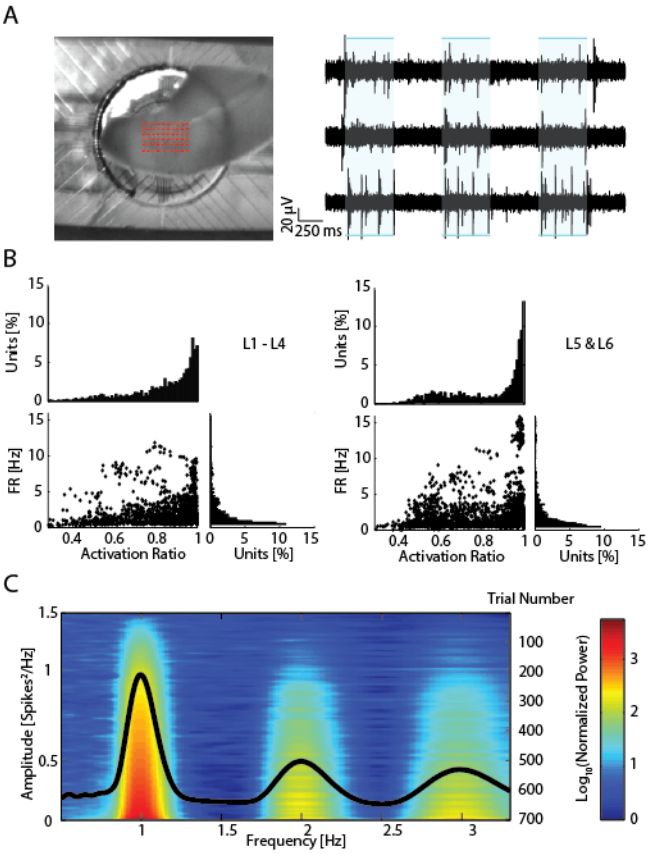

Figure 4.1. Optogenetic stimulation activates cortical networks *in vitro*.

(A) Left: Coronal slice positioned on multielectrode array with 100 mm spacing between electrodes. Right: Modulation of action potential firing by optogenetic stimulation (3 s trace of multiunit activity for three sample electrodes) (B) FR versus Activation Ratio for all SU in layers 1 through 4 (left) and layers 5 and 6 (right). (C) Frequency response to 10 s of optogenetic stimulation with mean response overlaid (black). Spontaneous activity was modulated by optogenetic stimulation and exhibited pronounced 1 Hz oscillation

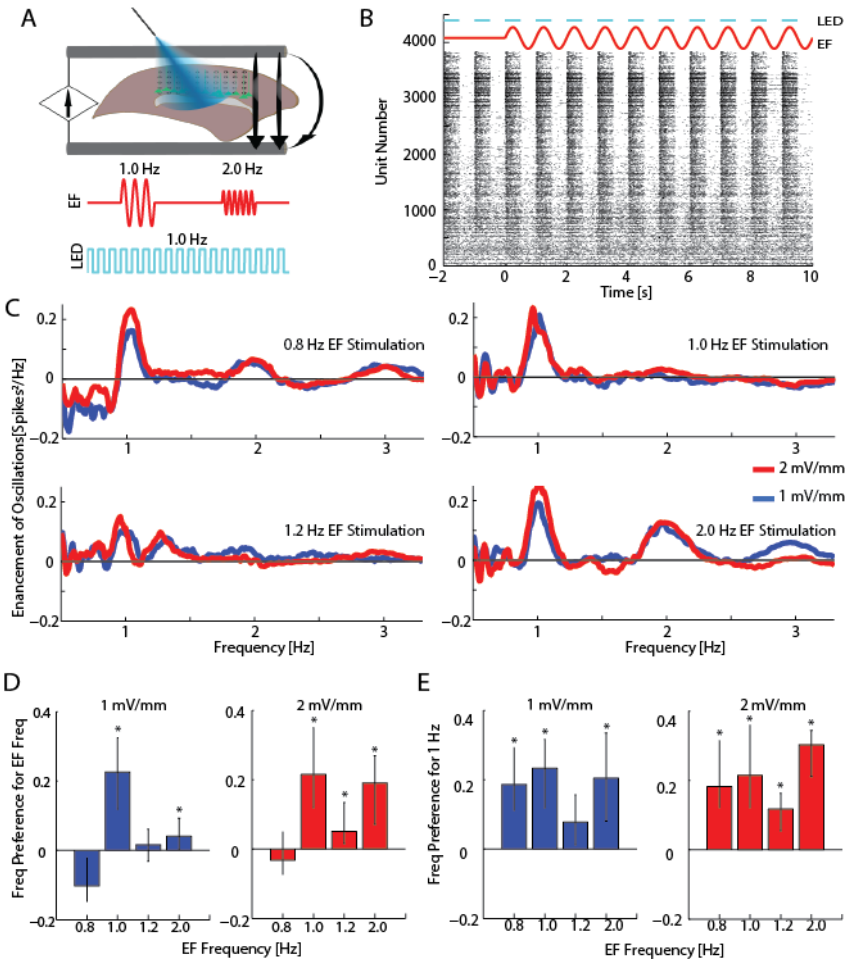

Figure 4.2. Interaction dynamics between endogenous oscillation and EF stimulation.

(A) Top: Optogenetic stimulation (cyan) is applied to L5 pyramidal neurons (green) while EF is applied between two AgCl wires (gray, example field lines in black) with the positive terminal nearest layer 1 of visual cortex. Bottom: Example trials (shortened to 3 s for visualization). (B) Raster plot for all SU for each trial with 1 Hz EF stimulation. (C) Difference spectra between activity during EF stimulation and the preceding 10 s for all EF stimulation frequencies and amplitudes. (D) Frequency preference for the stimulation frequency. (E) Frequency preference for 1 Hz. Error bars indicate 5 to 95% confidence interval. *P < 0.05.

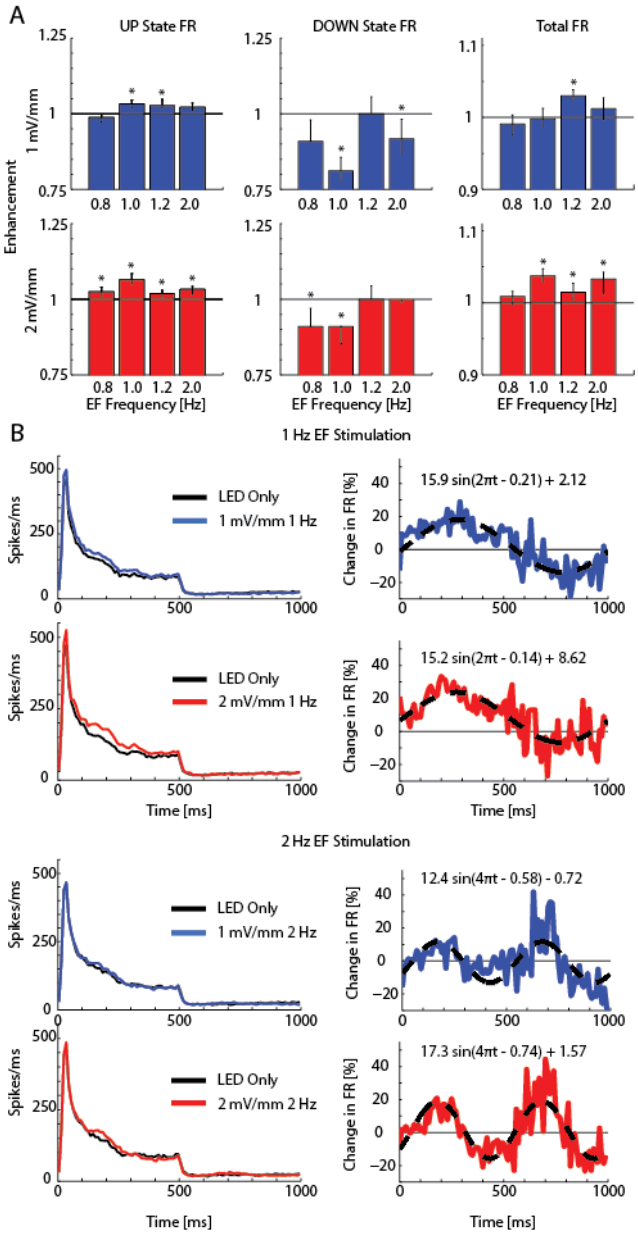

Figure 4.3. Firing rate modulation by EF stimulation.

(A) Left: Enhancement of FR during UP states. FR was enhanced by most EF stimulation amplitudes and frequencies during the UP state. Center: Enhancement of FR during the DOWN state. FR was significantly decreased for 1 Hz EF stimulation across stimulation amplitudes. Right: Total enhancement of FR by EF. In most cases application of 2 mV/mm EF increased total FR while only 1.2 Hz stimulation increased FR for 1 mV/mm EF. SU with an activation ratio of <1 (at least one spike during the DOWN state) shown. (B) Left: Spiking activity as a single cycle of the applied EF frequency for 1 and 2 Hz EF stimulation (color) with the averaged preceding 10 s of oscillatory activity (black). Right: Percent

change by application of EF (color) and fitted sine-waves (black, dashed). Phase delay (shown in radians) between the applied EF signal and resulting change in activity was observed for both conditions. Error bars indicate 5-95% confidence interval. *P < 0.05.

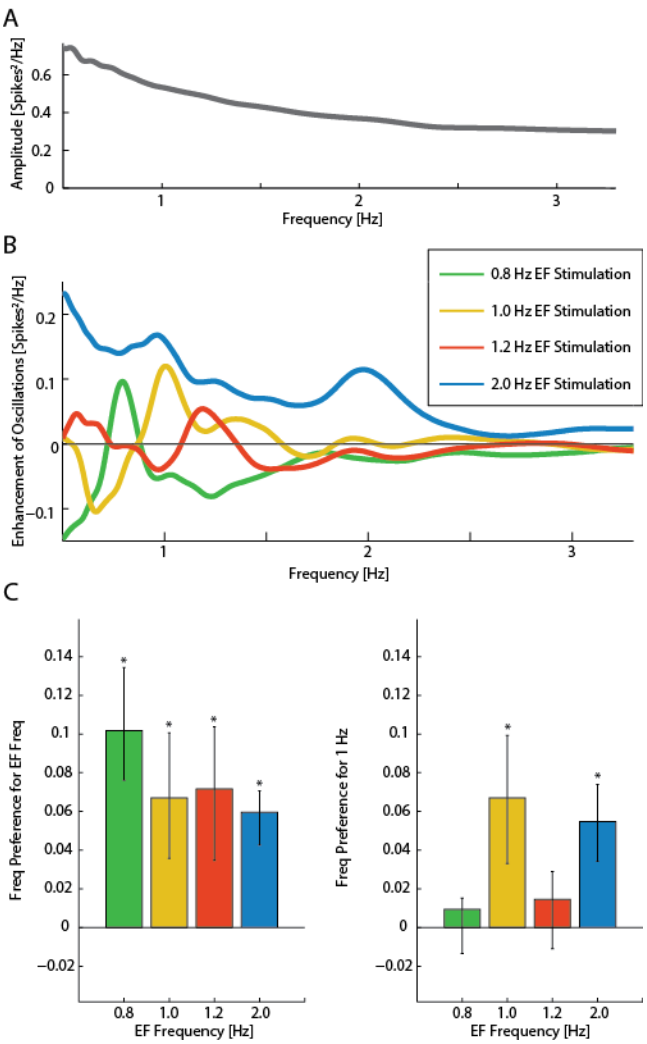

Figure 4.4. Modulation of frequency structure in absence of an endogenous oscillation.

(A) Frequency spectrum of spontaneous activity in cortical slices with neither optogenetic stimulation nor EF stimulation. (B) Enhancement of frequency structure by EF stimulation only. (C) Frequency preference for the EF stimulation frequency (left). Frequency preference for 1 Hz oscillations (right). In absence of strong cortical oscillations, all frequencies were enhanced and only 1 and 2 Hz EF stimulation enhanced preference for 1 Hz oscillations. Error bars indicate 5-95% confidence interval. *P < 0.05.

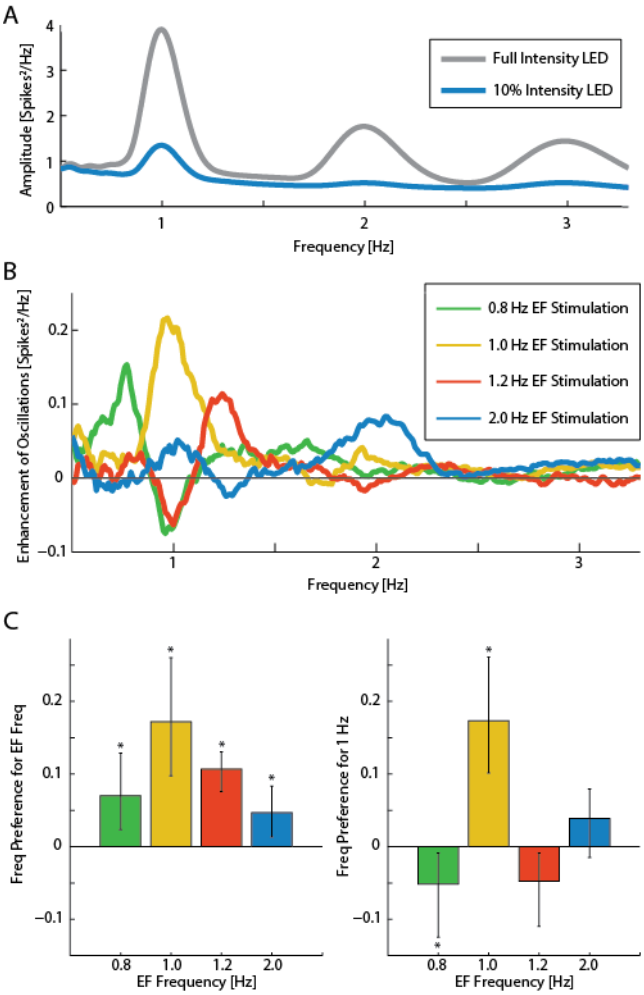

Figure 4.5. EF stimulation of networks exhibiting weak cortical oscillations.

EF stimulation of networks exhibiting weak cortical oscillations. (A) Spectra of the response to full intensity optogenetic simulation (gray) and 10% intensity optogenetic stimulation (blue). (B) Enhancement of cortical oscillations by EF stimulation. (C) Change in frequency preference for the EF stimulation frequency (left) and for the 1 Hz oscillation (right). Error bars indicate 5-95% confidence interval. *P<0.05.

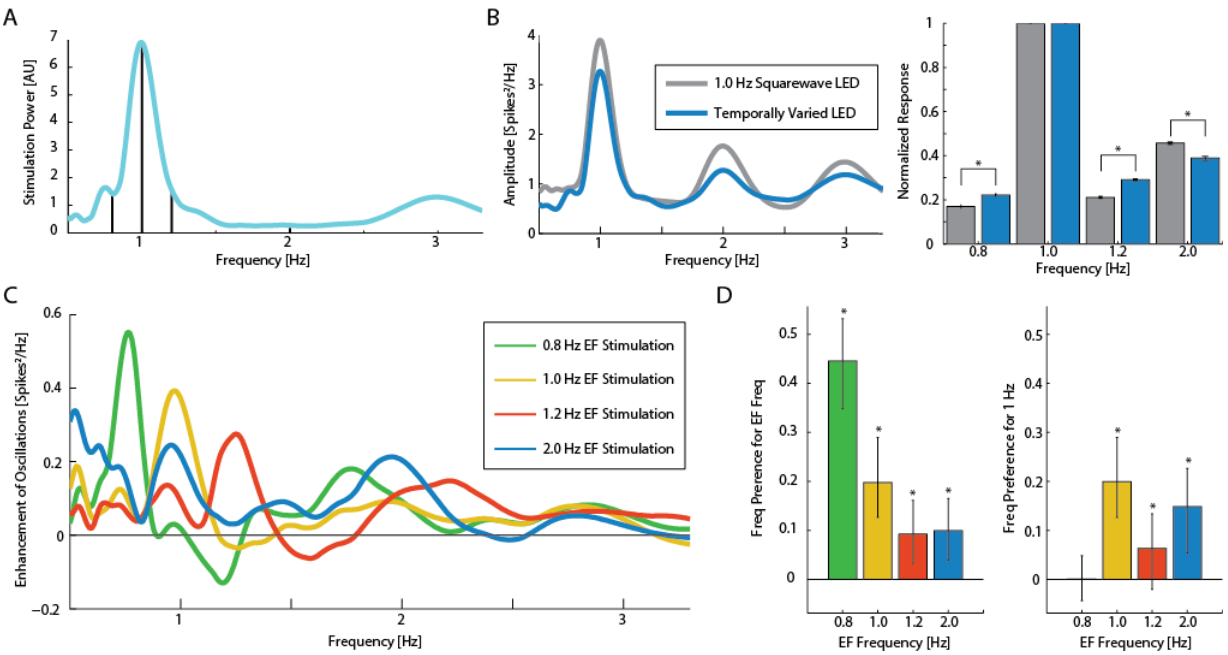

Figure 4.6. EF stimulation of networks exhibiting cortical oscillations with variable UP and DOWN state duration.

(A) Spectrum of the 10 s optogenetic stimulation waveform (cyan). EF stimulation frequencies are indicated in black. (B) Left: Spectra of the response to 1 Hz square-wave optogenetic stimulation (gray) and response to temporally variant optogenetic stimulation (blue). Right: Response optogenetic stimulation, normalized by the oscillation amplitude at 1 Hz. (C) Spectra of the enhancement of oscillations by EF stimulation for 0.8 (green), 1.0 (yellow), 1.2 (red), 2.0 (blue) Hz stimulation. (D) Left: Frequency preference for oscillations at the frequency of the EF stimulation. Right: Frequency preference for 1 Hz oscillations. Error bars indicate 5-95% confidence interval. *P < 0.05.

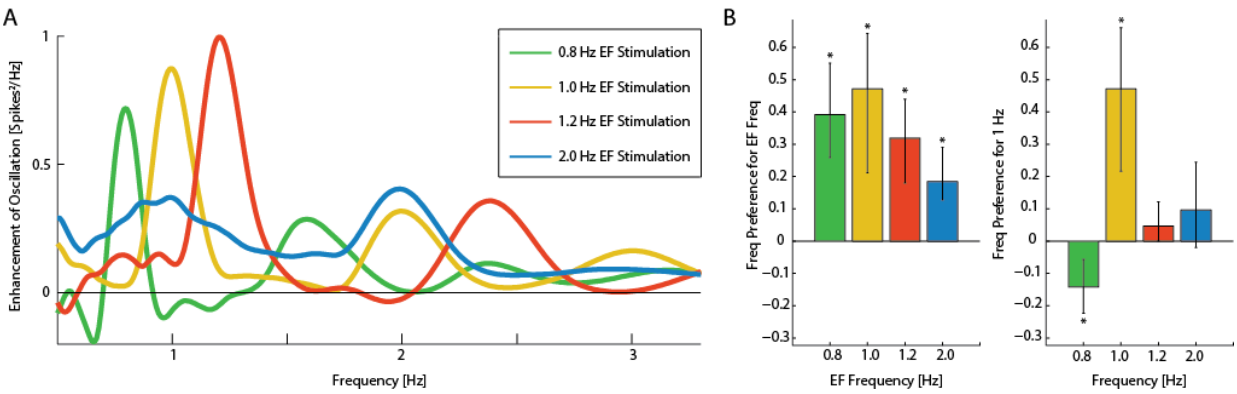

Figure 4.7. High amplitude EF stimulation.

(A) Difference spectra between 10 s of application of 8 mV/mm EF stimulation and the preceding 10 s. (B) Left: Frequency preference for the EF stimulation frequency. Right: Frequency preference for 1 Hz oscillation. Error bars indicate 5-95% confidence interval. *P < 0.05.

EF Amplitude [mV/mm]	EF Frequency [Hz]	Confidence Interval [spikes^2/Hz]	n [trials]	p (Wilcoxon signed rank with Bonferroni correction)
1	0.8	-0.148 to -0.021	88	1
1	1.0	0.119 to 0.325	88	< 10e^{-3}
1	1.2	-0.032 to 0.061	87	0.987
1	2.0	0.001 to 0.092	88	0.008
2	0.8	-0.073 to 0.049	88	1
2	1.0	0.119 to 0.349	88	< 10e^{-3}
2	1.2	0.015 to 0.135	88	< 10e^{-3}
2	2.0	0.071 to 0.269	88	< 10e^{-3}

Table 4.1. Frequency preference for EF Stimulation Frequency.

EF Amplitude [mV/mm]	EF Frequency [Hz]	Confidence Interval [spikes^2/Hz]	n [trials]	p (Wilcoxon signed rank with Bonferroni correction)
1	0.8	0.111 to 0.292	88	< 10e^{-3}
1	1.0	0.119 to 0.316	88	< 10e^{-3}
1	1.2	0.012 to 0.156	87	0.269
1	2.0	0.080 to 0.335	88	0.001
2	0.8	0.121 to 0.314	88	< 10e^{-3}
2	1.0	0.121 to 0.358	88	< 10e^{-3}
2	1.2	0.054 to 0.163	88	0.044
2	2.0	0.211 to 0.344	88	< 10e^{-3}

Table 4.2. Frequency Preference for 1 Hz.

EF Amplitude [mV/mm]	EF Frequency [Hz]	Confidence Interval	n [SU]	p (Wilcoxon signed rank with Bonferroni correction)
1	0.8	0.973 to 0.999	441	1
1	1.0	1.019 to 1.045	446	$< 10e^{-3}$
1	1.2	1.019 to 1.048	451	$< 10e^{-3}$
1	2.0	1.010 to 1.035	430	0.106
2	0.8	1.012 to 1.040	423	$< 10e^{-3}$
2	1.0	1.051 to 1.085	432	$< 10e^{-3}$
2	1.2	1.008 to 1.029	433	0.027
2	2.0	1.016 to 1.042	432	0.004

Table 4.3. Change in UP state FR.

EF Amplitude [mV/mm]	EF Frequency [Hz]	Confidence Interval	n [SU]	p (Wilcoxon signed rank with Bonferroni correction)
1	0.8	0.909 to 0.980	441	0.907
1	1.0	0.775 to 0.856	446	$< 10e^{-3}$
1	1.2	1.000 to 1.057	451	1
1	2.0	0.869 to 0.982	430	0.002
2	0.8	0.909 to 0.970	423	0.005
2	1.0	0.854 to 0.909	432	$< 10e^{-3}$
2	1.2	1.000 to 1.044	433	1
2	2.0	0.990 to 1.000	432	1

Table 4.4. Change in DOWN state FR.

EF Amplitude [mV/mm]	EF Frequency [Hz]	Confidence Interval	n [SU]	p (Wilcoxon signed rank with Bonferroni correction)
1	0.8	0.976 to 1.003	441	0.106
1	1.0	0.987 to 1.012	446	1
1	1.2	1.023 to 1.038	451	$< 10e^{-3}$
1	2.0	0.996 to 1.027	430	0.556
2	0.8	0.997 to 1.016	423	0.467
2	1.0	1.029 to 1.047	432	$< 10e^{-3}$
2	1.2	1.005 to 1.027	433	0.007
2	2.0	1.012 to 1.043	432	0.003

Table 4.5. Change in Total FR.

EF Amplitude [mV/mm]	EF Frequency [Hz]	Confidence Interval [10^{-3}]	n [SU pairs * trials]	p (Wilcoxon signed rank with Bonferroni correction)
1	0.8	-7.53 to -4.24	5737	< $10e^{-3}$
1	1.0	-1.35 to 1.43	6018	1
1	1.2	0.50 to 4.29	5884	0.011
1	2.0	-1.42 to 2.27	6066	1
2	0.8	0.59 to 4.16	5976	1
2	1.0	0.48 to 3.63	5860	< $10e^{-3}$
2	1.2	6.49 to 9.44	6159	< $10e^{-3}$
2	2.0	5.70 to 8.87	5931	< $10e^{-3}$

Table 4.6. Change in Correlation.

Optogenetic Stimulation Type	Frequency [Hz]	Confidence Interval [Spikes^2/Hz]	n [trials]	p (Wilcoxon ranked sum with Bonferroni correction)
1 Hz Square	0.8	0.162 to 0.177	703	< 10e^{-3}
Varied	0.8	0.214 to 0.227	704	
1 Hz Square	1.0	1	703	1
Varied	1.0	1	704	
1 Hz Square	1.2	0.206 to 0.215	703	< 10e^{-3}
Varied	1.2	0.286 to 0.295	704	
1 Hz Square	2.0	0.450 to 0.463	703	< 10e^{-3}
Varied	2.0	0.378 to 0.398	704	

Table 4.7. Normalized Optogenetic Response

REFERENCES

Ali, M. M., Sellers, K. K., & Frohlich, F. (2013). Transcranial alternating current stimulation modulates large-scale cortical network activity by network resonance. *The Journal of neuroscience : the official journal of the Society for Neuroscience, 33*(27), 11262-11275. doi:10.1523/JNEUROSCI.5867-12.2013

Arenkiel, B. R., Peca, J., Davison, I. G., Feliciano, C., Deisseroth, K., Augustine, G. J., . . . Feng, G. (2007). In vivo light-induced activation of neural circuitry in transgenic mice expressing channelrhodopsin-2. *Neuron, 54*(2), 205-218. doi:10.1016/j.neuron.2007.03.005

Beltramo, R., D'Urso, G., Dal Maschio, M., Farisello, P., Bovetti, S., Clovis, Y., . . . Fellin, T. (2013). Layer-specific excitatory circuits differentially control recurrent network dynamics in the neocortex. *Nature neuroscience, 16*(2), 227-234. doi:10.1038/nn.3306

Bikson, M., Inoue, M., Akiyama, H., Deans, J. K., Fox, J. E., Miyakawa, H., & Jefferys, J. G. (2004). Effects of uniform extracellular DC electric fields on excitability in rat hippocampal slices in vitro. *The Journal of physiology, 557*(Pt 1), 175-190. doi:10.1113/jphysiol.2003.055772

Binder, S., Rawohl, J., Born, J., & Marshall, L. (2014). Transcranial slow oscillation stimulation during NREM sleep enhances acquisition of the radial maze task and modulates cortical network activity in rats. *Frontiers in behavioral neuroscience, 7*, 220. doi:10.3389/fnbeh.2013.00220

Boyle, M. R., & Frohlich, F. (2013). EEG Feedback-Controlled Transcranial Alternating Current Stimulation. *2013 6th International Ieee/Embs Conference on Neural Engineering (Ner)*, 140-143.

Brunoni, A. R., Shiozawa, P., Truong, D., Javitt, D. C., Elkis, H., Fregni, F., & Bikson, M. (2014). Understanding tDCS effects in schizophrenia: a systematic review of clinical data and an integrated computation modeling analysis. *Expert review of medical devices, 11*(4), 383-394. doi:10.1586/17434440.2014.911082

Buzsáki, G. (2006). *Rhythms of the brain*. Oxford ; New York: Oxford University Press.

Cardin, J. A., Carlen, M., Meletis, K., Knoblich, U., Zhang, F., Deisseroth, K., . . . Moore, C. I. (2009). Driving fast-spiking cells induces gamma rhythm and controls sensory responses. *Nature, 459*(7247), 663-667. doi:10.1038/nature08002

Chauvette, S., Volgushev, M., & Timofeev, I. (2010). Origin of active states in local neocortical networks during slow sleep oscillation. *Cerebral cortex, 20*(11), 2660-2674. doi:10.1093/cercor/bhq009

Curto, C., Sakata, S., Marguet, S., Itskov, V., & Harris, K. D. (2009). A simple model of cortical dynamics explains variability and state dependence of sensory responses in urethane-anesthetized auditory cortex. *The Journal of neuroscience : the official journal of the Society for Neuroscience, 29*(34), 10600-10612. doi:10.1523/JNEUROSCI.2053-09.2009

Datta, A., Bansal, V., Diaz, J., Patel, J., Reato, D., & Bikson, M. (2009). Gyri-precise head model of transcranial direct current stimulation: improved spatial focality using a ring electrode versus conventional rectangular pad. *Brain stimulation, 2*(4), 201-207, 207 e201. doi:10.1016/j.brs.2009.03.005

Deans, J. K., Powell, A. D., & Jefferys, J. G. (2007). Sensitivity of coherent oscillations in rat hippocampus to AC electric fields. *The Journal of physiology, 583*(Pt 2), 555-565. doi:10.1113/jphysiol.2007.137711

Fee, M. S., Mitra, P. P., & Kleinfeld, D. (1996). Automatic sorting of multiple unit neuronal signals in the presence of anisotropic and non-Gaussian variability. *Journal of neuroscience methods, 69*(2), 175-188. doi:10.1016/S0165-0270(96)00050-7

Feurra, M., Pasqualetti, P., Bianco, G., Santarnecchi, E., Rossi, A., & Rossi, S. (2013). State-dependent effects of transcranial oscillatory currents on the motor system: what you think matters. *The Journal of neuroscience : the official journal of the Society for Neuroscience, 33*(44), 17483-17489. doi:10.1523/JNEUROSCI.1414-13.2013

Frohlich, F., & McCormick, D. A. (2010). Endogenous electric fields may guide neocortical network activity. *Neuron, 67*(1), 129-143. doi:10.1016/j.neuron.2010.06.005

Frohlich, F., & Schmidt, S. L. (2013). Rational design of transcranial current stimulation (TCS) through mechanistic insights into cortical network dynamics. *Frontiers in human neuroscience, 7*, 804. doi:10.3389/fnhum.2013.00804

Helfrich, R. F., Schneider, T. R., Rach, S., Trautmann-Lengsfeld, S. A., Engel, A. K., & Herrmann, C. S. (2014). Entrainment of brain oscillations by transcranial alternating current stimulation. *Current biology : CB, 24*(3), 333-339. doi:10.1016/j.cub.2013.12.041

Herrmann, C. S., Rach, S., Neuling, T., & Struber, D. (2013). Transcranial alternating current stimulation: a review of the underlying mechanisms and modulation of cognitive processes. *Frontiers in human neuroscience, 7*, 279. doi:10.3389/fnhum.2013.00279

Hill, D. N., Mehta, S. B., & Kleinfeld, D. (2011). Quality metrics to accompany spike sorting of extracellular signals. *The Journal of neuroscience : the official journal of the Society for Neuroscience, 31*(24), 8699-8705. doi:10.1523/JNEUROSCI.0971-11.2011

Hutcheon, B., & Yarom, Y. (2000). Resonance, oscillation and the intrinsic frequency preferences of neurons. *Trends in neurosciences, 23*(5), 216-222.

Kirov, R., Weiss, C., Siebner, H. R., Born, J., & Marshall, L. (2009). Slow oscillation electrical brain stimulation during waking promotes EEG theta activity and memory encoding. *Proceedings of the National Academy of Sciences of the United States of America, 106*(36), 15460-15465. doi:10.1073/pnas.0904438106

Kuo, H. I., Bikson, M., Datta, A., Minhas, P., Paulus, W., Kuo, M. F., & Nitsche, M. A. (2013). Comparing cortical plasticity induced by conventional and high-definition 4 x 1 ring tDCS: a neurophysiological study. *Brain stimulation, 6*(4), 644-648. doi:10.1016/j.brs.2012.09.010

Kuo, M. F., Paulus, W., & Nitsche, M. A. (2014). Therapeutic effects of non-invasive brain stimulation with direct currents (tDCS) in neuropsychiatric diseases. *NeuroImage, 85 Pt 3*, 948-960. doi:10.1016/j.neuroimage.2013.05.117

Kutchko, K. M., & Frohlich, F. (2013). Emergence of metastable state dynamics in interconnected cortical networks with propagation delays. *PLoS computational biology, 9*(10), e1003304. doi:10.1371/journal.pcbi.1003304

Marshall, L., Helgadottir, H., Molle, M., & Born, J. (2006). Boosting slow oscillations during sleep potentiates memory. *Nature, 444*(7119), 610-613. doi:10.1038/nature05278

Neuling, T., Rach, S., & Herrmann, C. S. (2013). Orchestrating neuronal networks: sustained after-effects of transcranial alternating current stimulation depend upon brain states. *Frontiers in human neuroscience, 7*, 161. doi:10.3389/fnhum.2013.00161

Neuling, T., Wagner, S., Wolters, C. H., Zaehle, T., & Herrmann, C. S. (2012). Finite-Element Model Predicts Current Density Distribution for Clinical Applications of tDCS and tACS. *Frontiers in psychiatry, 3*, 83. doi:10.3389/fpsyt.2012.00083

Niell, C. M., & Stryker, M. P. (2010). Modulation of visual responses by behavioral state in mouse visual cortex. *Neuron, 65*(4), 472-479. doi:10.1016/j.neuron.2010.01.033

Ozen, S., Sirota, A., Belluscio, M. A., Anastassiou, C. A., Stark, E., Koch, C., & Buzsaki, G. (2010). Transcranial electric stimulation entrains cortical neuronal populations in rats. *The Journal of neuroscience : the official journal of the Society for Neuroscience, 30*(34), 11476-11485. doi:10.1523/JNEUROSCI.5252-09.2010

Polania, R., Nitsche, M. A., Korman, C., Batsikadze, G., & Paulus, W. (2012). The importance of timing in segregated theta phase-coupling for cognitive performance. *Current biology : CB, 22*(14), 1314-1318. doi:10.1016/j.cub.2012.05.021

Radman, T., Ramos, R. L., Brumberg, J. C., & Bikson, M. (2009). Role of cortical cell type and morphology in subthreshold and suprathreshold uniform electric field stimulation in vitro. *Brain stimulation, 2*(4), 215-228, 228 e211-213. doi:10.1016/j.brs.2009.03.007

Reato, D., Rahman, A., Bikson, M., & Parra, L. C. (2010). Low-intensity electrical stimulation affects network dynamics by modulating population rate and spike timing. *The Journal of neuroscience : the official journal of the Society for Neuroscience, 30*(45), 15067-15079. doi:10.1523/JNEUROSCI.2059-10.2010

Reato, D., Rahman, A., Bikson, M., & Parra, L. C. (2013). Effects of weak transcranial alternating current stimulation on brain activity-a review of known mechanisms from animal studies. *Frontiers in human neuroscience, 7*, 687. doi:10.3389/fnhum.2013.00687

Romei, V., Gross, J., & Thut, G. (2010). On the role of prestimulus alpha rhythms over occipito-parietal areas in visual input regulation: correlation or causation? *The Journal of neuroscience : the official journal of the Society for Neuroscience, 30*(25), 8692-8697. doi:10.1523/JNEUROSCI.0160-10.2010

Sanchez-Vives, M. V., & McCormick, D. A. (2000). Cellular and network mechanisms of rhythmic recurrent activity in neocortex. *Nature neuroscience, 3*(10), 1027-1034. doi:10.1038/79848

Santarnecchi, E., Polizzotto, N. R., Godone, M., Giovannelli, F., Feurra, M., Matzen, L., . . . Rossi, S. (2013). Frequency-dependent enhancement of fluid intelligence induced by transcranial oscillatory potentials. *Current biology : CB, 23*(15), 1449-1453. doi:10.1016/j.cub.2013.06.022

Sauseng, P., Klimesch, W., Heise, K. F., Gruber, W. R., Holz, E., Karim, A. A., . . . Hummel, F. C. (2009). Brain oscillatory substrates of visual short-term memory capacity. *Current biology : CB, 19*(21), 1846-1852. doi:10.1016/j.cub.2009.08.062

Schmidt, S. L., Chew, E. Y., Bennett, D. V., Hammad, M. A., & Frohlich, F. (2013). Differential effects of cholinergic and noradrenergic neuromodulation on spontaneous cortical network dynamics. *Neuropharmacology, 72C*, 259-273. doi:10.1016/j.neuropharm.2013.04.045

Struber, D., Rach, S., Trautmann-Lengsfeld, S. A., Engel, A. K., & Herrmann, C. S. (2014). Antiphasic 40 Hz oscillatory current stimulation affects bistable motion perception. *Brain topography, 27*(1), 158-171. doi:10.1007/s10548-013-0294-x

Thut, G., Veniero, D., Romei, V., Miniussi, C., Schyns, P., & Gross, J. (2011). Rhythmic TMS causes local entrainment of natural oscillatory signatures. *Current biology : CB, 21*(14), 1176-1185. doi:10.1016/j.cub.2011.05.049

Tranchina, D., & Nicholson, C. (1986). A model for the polarization of neurons by extrinsically applied electric fields. *Biophysical journal, 50*(6), 1139-1156. doi:10.1016/S0006-3495(86)83558-5

Uhlhaas, P. J., & Singer, W. (2012). Neuronal dynamics and neuropsychiatric disorders: toward a translational paradigm for dysfunctional large-scale networks. *Neuron, 75*(6), 963-980. doi:10.1016/j.neuron.2012.09.004

Wang, X. J. (2010). Neurophysiological and computational principles of cortical rhythms in cognition. *Physiological reviews, 90*(3), 1195-1268. doi:10.1152/physrev.00035.2008

CHAPTER 5: MODULATION OF CORTICAL OSCILLATIONS BY LOW-FREQUENCY DIRECT CORTICAL STIMULATION IS STATE-DEPENDENT[1]

INTRODUCTION

Oscillations in a wide range of frequencies represent a ubiquitous organizational pattern of cortical network dynamics (Buzsaki & Draguhn, 2004). In particular, oscillations in the alpha frequency band are pronounced activity patterns routinely observed in posterior leads of electroencephalograms (EEGs) of healthy human participants with closed eyes (Berger, 1929). This alpha rhythm was originally considered to reflect an "idling" state of cortex in the absence of sensory input (Pfurtscheller, Stancak, & Neuper, 1996). However, it has become clear that alpha oscillations dynamically regulate processing of sensory input and mediate long-range cortical interaction dynamics (Klimesch, 2012; Sauseng et al., 2009). These roles of alpha oscillations in cognition and behavior have been demonstrated by the use of non-invasive brain stimulation to modulate alpha oscillations. Repetitive transcranial magnetic stimulation (repetitive TMS) in the alpha frequency range modulates sensory detection (Romei, Gross, & Thut, 2010; Thut, Veniero, et al., 2011), likely by entraining alpha oscillations. Similarly, transcranial alternating current stimulation (tACS), which applies a weak, sine-wave electric current to the scalp, alters cognitive processes by targeting alpha oscillations (Cecere, Rees, & Romei, 2015; Helfrich, Schneider, et al., 2014; Zaehle, Rach, & Herrmann, 2010). In addition to the causal role of alpha oscillations in mediating behavior, oscillations in this frequency band are selectively impaired in psychiatric illnesses such as major depressive disorder, autism, and schizophrenia (L. Sun et al., 2012; Uhlhaas & Singer, 2010; Woltering, Jung, Liu, & Tannock, 2012). As a result, alpha oscillations have recently emerged as a potential target for therapeutic intervention with non-invasive brain stimulation. The FDA has approved repetitive TMS

[1] This chapter previously appeared as an article in PLoS Biology; doi: 10.1371/journal.pbio.1002424 (http://journals.plos.org/plosbiology/article?id=10.1371%2Fjournal.pbio.1002424). The original citation is as follows: Sankaraleengam Alagapan, **Stephen L. Schmidt**, Jeremie Lefebvre, Eldad Hadar, Hae Won Shin, and Flavio Frohlich. (2016). Modulation of Cortical Oscillations by Low-Frequency Direct Cortical Stimulation Is State-Dependent. PLoS Biology, 14(3):e1002424.

with 10 Hz stimulation frequency as a treatment for major depressive disorder (George, 2010). Of note, the 10 Hz patterning was the result of an attempt to develop repetitive TMS paradigms with outlasting effects, and considerations of the possible effect on alpha oscillations emerged later (Fröhlich, 2015). Furthermore, other non-invasive stimulation modalities that target alpha oscillations for the treatment of major depressive disorder are under active investigation (Frohlich, 2015; Leuchter et al., 2015; Leuchter, Cook, Jin, & Phillips, 2013).

Despite the confluence of evidence for modulation of alpha oscillations and promising clinical applications, the network mechanisms by which brain stimulation modulates alpha oscillations have remained unclear. Therefore, computational modeling efforts have remained limited. In contrast, both low frequency (< 4 Hz) and fast cortical oscillations have been investigated as a target of weak periodic perturbations. Both computer simulations (Ali, Sellers, & Frohlich, 2013; Kutchko & Frohlich, 2013; Reato, Rahman, Bikson, & Parra, 2010) and slice experiments (Frohlich & McCormick, 2010; Schmidt, Iyengar, Foulser, Boyle, & Frohlich, 2014) have provided mechanistic hypotheses on the interaction dynamics of endogenous activity and stimulation. First, periodic stimulation matched to the endogenous frequency allows weak stimulation amplitudes to entrain endogenous oscillation (Ali et al., 2013). Second, stimulation frequencies that differ from the endogenous frequency cause enhancement of oscillation power at the endogenous frequency in case of high-amplitude endogenous oscillations (Schmidt et al., 2014). Yet, it remains unclear if and how these principles apply to stimulation that targets alpha oscillations, which are of thalamo-cortical origin (Hughes & Crunelli, 2005; Hughes et al., 2004; Lorincz, Kekesi, Juhasz, Crunelli, & Hughes, 2009). In humans, concurrent tACS and EEG showed enhanced activity at the stimulation frequency (10 Hz) possibly caused by entrainment of endogenous alpha oscillators (Helfrich, Schneider, et al., 2014). Also, stimulation at individual alpha frequencies produced enhancement when the participants had their eyes open, but not when the participants had their eyes closed (Neuling, Rach, & Herrmann, 2013). In contrast, brief epochs of tACS failed to cause entrainment determined by a lack of phase synchronization (Struber, Rach, Neuling, & Herrmann, 2015; Vossen, Gross, & Thut, 2015), suggesting plasticity as an alternative mechanism for the observed increase in oscillation power. Thus, there is no clear consensus on the mechanism underlying the effects of periodic brain stimulation that targets alpha oscillations (Fröhlich, 2015).

To fill this gap, we aimed to develop models that would help elucidate the effect of periodic stimulation on alpha oscillations and demonstrate the experimental validity of the models using neurophysiological effect of stimulation in the alpha frequency in human cortex. The combination of direct cortical stimulation with electrocorticography (ECoG) serves as an ideal approach since it allows for the simultaneous manipulation and recording of oscillations at a finer spatial scale. We derived our approach from the direct cortical stimulation with high stimulation amplitude and frequency, which is clinically used during invasive monitoring to determine 'eloquent cortex' for surgical planning in patients with pharmacoresistant epilepsy (Gallentine & Mikati, 2009; Ojemann, Ojemann, Lettich, & Berger, 1989).

Here, we developed a simple summation model to explain the state-dependent effects of stimulation and a network model to explain the outlasting effects of stimulation. The nature of periodic perturbation was chosen to match the stimulation used in the ECoG experiment. We applied 10 Hz periodic pulse stimulation and recorded directly from the parietal region of the brain in three patients. Grid electrodes for electrocorticography (ECoG) had been implanted in these patients before resective epilepsy surgery.

METHODS

ECoG Data Collection and Direct Cortical Stimulation

All procedures in this study were approved by the Institutional Review Board of the University of North Carolina at Chapel Hill, and informed consent was obtained from the participants. The participants underwent temporary implantation of subdural electrodes for pre-surgical localization of seizure focus in the Epilepsy Monitoring Unit at the UNC Neurosciences Hospital. Electrode grids were implanted over the different cortical regions as described in Table 5.1.

The electrodes were made of platinum-iridium alloy, were 4 mm in diameter (2.5 mm exposed), and were embedded in silicone (Ad-Tech Medical, Racine, WI, USA). The inter-electrode distance in each grid was 10 mm. Four electrodes in a separate set placed distant from the recording grids were chosen to be reference electrodes. ECoG signals were recorded using a 128-channel Aura LTM 64 acquisition system and the corresponding TWin software (Grass Technologies, Warwick, RI, USA) at 800 Hz sampling rate.

Electrical stimulation consisted of a train of biphasic pulses 2 mA in amplitude and 200 μs in duration with a pulse every 100 ms (10 Hz) generated by a S12x cortical stimulator (Grass Technologies, Warwick, RI, USA) and applied between a pair of adjacent electrodes for 5 seconds. The stimulations were spaced at about 15 s between trials to enable safety monitoring for the occurrence of after-discharges.

Behavioral Tasks

The experimental paradigm consisted of three conditions. In the first condition, the participants were asked to close their eyes and relax. This was called the eyes-closed state. In the second condition, the participants were asked to open their eyes and relax without focusing on anything. This was named the eyes-open state. In the third state, the task-engaged state, the participants performed a visual working memory task based on the task developed by Luck and Vogel (Luck & Vogel, 1997). Data was acquired from participants P005 and P008 in both the eyes-closed and eyes-open conditions but not during the working memory task. Participant P001 completed the eyes-closed task and the working memory task. The task was programmed in Matlab using Psychophysics Toolbox. The task required the participant to look at a set of colored dots for 1.5 s and indicate with a key press whether or not there was any change in color in the set of dots presented in a second test set 0.9 s later (memory period with no stimuli on the screen). This task required considerable cognitive effort from the participant. The participant was able to detect the change accurately in 71% of trials with a reaction time of 909.80 ± 61.52 ms.

Data Analysis

The collected ECoG data was transferred from the clinical acquisition system to a research workstation in EDF format (Kemp, Varri, Rosa, Nielsen, & Gade, 1992) . Switching circuits designed to protect amplifier during stimulation prevented recording of data from stimulating electrodes and hence data from stimulating electrodes were not included in the analysis. Electrodes over epileptogenic tissue were identified from clinical seizure traces and then excluded from further analysis. Additionally, electrodes that showed significant noise were also excluded (four electrodes in P001). Each stimulation trial was identified (manually by visual inspection for stimulation artifacts) and marked in the open source

software EDFBrowser. Later, the data were processed to remove stimulation artifacts and line noise using custom scripts written in Matlab (Mathworks Inc.). A detailed description of the stimulation artifact removal algorithm is provided below. Following artifact removal, line noise was removed using a second order IIR notch filter. Then, the signals were re-referenced to a common average reference. Signal power spectra were calculated at 0.1 Hz resolution between 0.5 Hz and 20 Hz and at 1 Hz resolution between 21 Hz and 80 Hz by convolving with Morlet wavelets of corresponding frequencies. Modulation indices were computed to quantify changes in power at specific frequency bands in different epochs. Mathematically,

$$Modulation\ Index\ = \frac{(S_b^2 - S_b^1)}{(S_b^2 + S_b^1)}$$

where S_b^1 and S_b^2 are average power in frequency band *b* in epochs 1 and 2. In the analysis, the 5-second window before stimulation was chosen as epoch 1, and the 5-second windows during stimulation and after stimulation were chosen as epoch 2. A symmetric 3 Hz band was chosen around the peak of the spectra for the endogenous frequency, and a symmetric 2 Hz band was chosen around 10 Hz for the stimulation frequency. The resulting measure was bounded between -1 and 1 and amenable to comparison.

Statistics

Statistics included 1 sample t-tests to determine the significance of modulation indices and 2 sample t-tests for determining significance of differences in modulation indices between the two states under investigation. All statistical analysis was performed using Matlab Statistics Toolbox (Mathworks Inc).

Stimulation Artifact Removal

Stimulation artifacts appeared as transient deflections (~ 10 ms in duration) in traces recorded from electrodes near the stimulating electrodes. A template matching algorithm was used to remove these artifacts. First, the waveforms were up-sampled to 3200 samples/second (anti-alias filtering followed by linear interpolation), as this allowed more robust estimation of these deflections' peaks at later steps. The next step involved determination of the artifacts' temporal location. By comparing the power around 100

Hz (corresponding to the artifact waveform), the electrode with the highest stimulation artifact amplitude was determined. Then, the trace recorded from the chosen electrode was high pass filtered to remove low frequency biological signals using a cubic polynomial fitting algorithm (Wagenaar & Potter, 2002). Artifacts were detected using a threshold crossing approach and corresponding times were collected. The artifacts corresponding to a stimulation trial occurred at all electrodes at the same time point. Hence, the times collected from the single channel provided the temporal location of artifacts in all electrodes. The next step of the algorithm was to remove the detected artifacts. Waveforms of artifacts were extracted in a temporal segment around the detected location and aligned to their peaks. For each artifact, a template was constructed by averaging the waveforms of five artifacts (the current waveform, two preceding waveforms, and two following waveforms). Next, the template was scaled to the amplitude of the artifact and subtracted from the trace. This resulted in offsets at the edges of the temporal segments. These abrupt discontinuities were removed by subtracting the linear interpolation between the offsets from the segment, which resulted in a continuous waveform. Finally, the signals were downsampled back to 800 Hz after anti-alias filtering.

Extraction of Electrode Location from Neuroimaging Data

3D Slicer (Fedorov et al., 2012) was used to analyze and extract electrode locations from CT images obtained after implantation of subdural electrodes. A multistep procedure was followed to generate images showing activation of cortical surface. The post-operative MRI was co-registered to post-operative CT in Slicer. Skull stripping was performed using ROBEX (Iglesias, Liu, Thompson, & Tu, 2011), and the gray matter and white matter were then segmented using ITK-Snap (Yushkevich et al., 2006). The surface model was generated using Slicer, and the model was imported into Matlab. The anatomical locations of the electrodes were determined by co-registering the MRI Image to the MNI Atlas (Fonov et al., 2011), recomputing electrode locations in the MNI space, transforming these locations to Talairach space, and using the Talairach Client (Lancaster et al., 2000) to obtain the label of the gray matter nearest to the coordinate representing electrode location. The shape and anatomical landmarks of Participant P005's brain deviated significantly from the atlas MRI. So we estimated the anatomical locations based on patient MRI directly instead of patient MRI co-registered to atlas MRI.

Computational Model

To generate mechanistic hypotheses that can explain our experimental findings, we used a population-scale neural oscillator network model, which combines essential components of cortical anatomy as well as interactions between cortical and subcortical areas. To propose a functional mechanism underlying the effect after termination of stimulation, we deliberately chose a simplified network model inspired and adapted from existing population-scale cortical network models (Amari, 1977; Wilson & Cowan, 1972) where we concentrated our attention on the role of feedback connections as opposed to local recurrent dynamics. It was designed primarily to investigate the influence of recurrence and feedback on both endogenous and stimulation-induced oscillations. The model consisted of N recurrently connected neural oscillators composed of excitatory (*e*) and inhibitory (*i*) units that spontaneously expressed oscillatory alpha activity due to delayed thalamo-cortical feedback. The membrane potential proxy vectors $\boldsymbol{V_e}(t)$ and $\boldsymbol{V_i}(t)$ obeyed the dimensionless equations

$$\tau_e \, \dot{\boldsymbol{V}}_e(t) = a\boldsymbol{V_e}(t) + \boldsymbol{G_{e\to e}} + \boldsymbol{G_{i\to e}} + I_{bias}\boldsymbol{F_1} + \boldsymbol{F_2} + \boldsymbol{I}_{task} + \boldsymbol{S} + \sqrt{2D}\boldsymbol{\xi_e}(t)$$

$$\tau_i \, \dot{\boldsymbol{V}}_i(t) = a\boldsymbol{V_i}(t) + \boldsymbol{G_{e\to i}} + \boldsymbol{G_{i\to i}} + \boldsymbol{S} + \sqrt{2D}\boldsymbol{\xi_i}(t)$$

The terms $\boldsymbol{\xi_{e,i}}$ referred to independent, zero mean Gaussian white noise processes. The synaptic time constants of excitatory and inhibitory populations were given by τ_e and τ_i respectively, and the membrane leakage coefficient was a. Recurrent inputs from population $n = e, i$ to population $m = e, i$ were defined by the following:

$$\boldsymbol{G}_{n\to m} = g_{nm}\,\boldsymbol{W}_{nm} \cdot f[\boldsymbol{V_n}(t)]$$

where $f[V] = (1 + \exp[-35(V-h)])^{-1}(1 + \exp[-150(V-h)])^{-1}$was a non-linear saturating response function with threshold h.

Thalamo-cortical feedback, through which endogenous oscillatory activity emerged in the eyes-closed and eyes-open conditions, was defined as

$$F_1 = g_1\boldsymbol{W}_1 \cdot f[\boldsymbol{V_e}(t - D_1)].$$

Cortico-cortical feedback mediated by more distant cortical nets was defined as

$$F_2 = g_2\boldsymbol{W}_2 \cdot f[\boldsymbol{V_e}(t - D_2)]$$

For each of those components, $\boldsymbol{W}_{nm} = (\rho N)^{-1} \cdot \mathbf{1}$, $\boldsymbol{W}_1 = (\rho N)^{-1} \cdot \mathbf{1}$, and $\boldsymbol{W}_2 = (\rho N)^{-1} \cdot \mathbf{1}$ represented sparse synaptic connectivity matrices with connection probability ρ. Feedback delays, representing conduction latencies to and from sub-cortical and other cortical areas were given by D_1 and D_2, respectively. These were adjusted to fit the spectral features expressed by the experimental data. Task-dependent input to the excitatory units was scaled as a function of the condition: it was minimal in the eyes-closed condition, intermediate for the eyes-open state, and maximal in the task-engaged state. The stimulation $\boldsymbol{S}$ is applied to all neurons, defined as a biphasic pulse train with frequency of 10 Hz, intensity S for 200μs and –S for another 200μs, and then set to zero until the next cycle. Numerical integration was performed using an Euler-Maruyama scheme with time step of dt=0.1=1 ms. Spectral analysis was performed over a synthetic ECoG signal defined by the network-wide potential average i.e. $ECoG = N^{-1} \sum_N [V_e + V_i]$. The parameter values used in the model are listed in Table 5.2.

RESULTS

The first model we developed was inspired by the finding that alpha oscillations reflect periodic modulation of cortical excitability (Jensen & Mazaheri, 2010; Klimesch, Sauseng, & Hanslmayr, 2007; Mathewson et al., 2011). We hypothesized that the strength of the oscillation (quantified by the amplitude) determines the excitability and only stimulation pulses that coincide with the excitable intervals (as determined by alpha oscillation phase) would produce a change in the ongoing oscillation. We modeled ongoing oscillation as a sine wave (Figure 5.1) and the stimulation response as a linear summation of this sine wave and the cortical response to pulse stimulation. The cortical response was modeled to be the convolution between the pulse train and a response function $f(t) = t.e^{-0.01t}$ (t denotes time in milliseconds; Figure 5.1B-C). The response function was motivated by the time course of response (direct and indirect) of neurons to stimulation. To account for our hypothesis, we required the response to cross a threshold (denoted by dotted horizontal line in Figure 5.1A) before including it in the stimulus response. As a result, the phases of the sine wave at which stimulation induced a response were restricted by the amplitude of the sine wave as denoted in Figure 5.1D. The black dotted line denotes the ongoing oscillation while the orange solid line denotes the effect of stimulation on the oscillation. The red lines at the bottom denote the times at which pulses were delivered and the gray line denotes the neural

response to the pulse train. The frequency of the oscillation was set at 7 Hz and the stimulation frequency was set at 10 Hz. The orange line is a linear summation of the black and gray lines subjected to the condition only summation values greater than 0 are incorporated in the orange line. In situations where the summation failed to reach 0, the values of black line were used. With this condition, it can be seen in Figure 5.1D that only pulses that coincided with phases where the amplitude of the oscillation is greater than 0 produced a change in the oscillation (e.g. pulses close to 0.1 s, 0.4 s and 0.7 s).

Eyes-closed state was modeled as a state with oscillation of large amplitude as alpha oscillations are known to be more pronounced in this state. In this case, the phases at which stimulation produced a response were most heavily constrained due to the threshold condition (denoted by a blue band in Figure 5.1A). Also, the relative change in amplitude as a result of the response to stimulation was minimal given the large amplitude of the oscillation (Figure 5.1E). The eyes-open state was modeled as a state with oscillations of intermediate alpha oscillations. Although the strength of the oscillation was weakened in comparison to the eyes-closed state, the phases at which stimulation can induce a response were still somewhat restricted (magenta band in Figure 5.1A) such that the effect of stimulation was an enhancement of the endogenous oscillation (Figure 5.1E). The task-engaged state was modeled as the state with lowest oscillation amplitude as task-engagement is often associated with a marked suppression of the power of alpha oscillations. In this last case, stimulation was able to induce a response at all phases (yellow band in Figure 5.1A), hence increasing the power at stimulation frequency (Figure 5.1E) and causing entrainment (Thut, Schyns, & Gross, 2011). Therefore, this model can explain the enhancement at the endogenous frequency instead of the stimulation frequency in the presence of a sufficiently strong endogenous oscillation. We parameterized this simple static model by oscillation strength (relative amplitude of the sine-wave) and stimulation strength (relative amplitude of the response function). We found that the normalized power at the stimulation frequency strongly and monotonically depended on these two parameters (Figure 5.1F bottom). Enhancement at the stimulation frequency requires low oscillation strength and high stimulation strength. In contrast, power at the endogenous oscillation frequency depended less on these parameters as long as the oscillation and stimulation strength exhibited some minimal value. Of particular note, the enhancement of power at the oscillation frequency as a function of the two parameters was non-monotonic. For example, the strongest

enhancement occurred for an intermediate level of oscillation strength, since, for high levels of oscillation strength, the relative contribution of the stimulation was limited to a small range of oscillation phases where the response of the perturbation reaches threshold.

Establishing outlasting effects of stimulation is crucial for non-invasive brain stimulation approaches to be translated from basic science research to clinical applications. The minimalistic mathematical model (Figure 5.1) explained the instantaneous effects of stimulation but did not provide insight into what may cause experimentally observed outlasting effects. We hypothesized that the outlasting effects are the result of multistable dynamics caused by recurrent neuronal loops. To test this hypothesis, we built a reduced network-level computational model to examine if we could reproduce the main experimental effects without including any plasticity mechanism. In particular, we aimed to reproduce (1) outlasting enhancement of alpha oscillations and (2) state-dependent stimulation effects. To this end, we performed numerical simulations of a cortical oscillator network model subjected to external stimulation and investigated its responses during three different simulated states: eyes-open, eyes-closed, and task-engaged. The model included (1) a thalamo-cortical loop as the main circuit involved in the generation and maintenance of alpha oscillations and (2) a long-range cortico-cortical loop to replicate the distributed topography of ECoG with grid electrodes (Figure 5.2A). The network model included the essential features of thalamo-cortical networks and yet was simplistic enough to provide insights about what mechanism could underlie the state-dependent and outlasting effects observed in the data. The eyes-closed, eyes-open, and task-engaged states were defined as states of increasing afferent inputs. The input to the excitatory neurons in the eyes-closed and eyes-open condition was assumed to be minimal; as a result, neural oscillatory dynamics were dominated by local recurrent interactions in cortex and feedback interactions in the thalamo-cortical loop. In the task-engaged condition, however, the input to the excitatory neurons was increased to represent their recruitment and engagement in the task-related cognitive processes.

Using this modeling strategy, we found that task-dependent input to the neurons acted as a gain control mechanism. Specifically, during the eyes-closed condition, the endogenous oscillations were too robust for modulation of the spectral peak frequency (Figure 5.2B, top trace): self-sustained, high-amplitude, alpha-like oscillations governed the network dynamics. Tightly stabilized in an oscillatory

attractor, the neurons were fully driven by the feedback inputs conveyed by the thalamo-cortical loop (no alpha oscillations were observed in absence of a thalamic model component), which effectively masked the drive provided by the stimulation at 10 Hz. On the other hand, in the eyes-open condition, amplification of endogenous oscillations occurred due to stimulation-induced recruitment of cortico-cortical feedback, which in turn also mediated the sustained effect after termination of stimulation. Indeed, our model predicts that damped oscillations at the endogenous frequency were amplified through cortical feedback loops and gave rise to the post-stimulation dynamics observed in the eyes-open condition. We found enhancement both at the endogenous frequency and at the stimulation frequency. Lastly, during the task-engaged state, increased input to the excitatory neuronal population destabilized the local oscillatory attractor, suppressing endogenous alpha rhythmic activity and making the neurons more susceptible to the stimulation. As a result, the stimulation was more effective, and a clear spectral signature of the stimulation became apparent (Figure 5.2B, bottom trace). Cortico-cortical feedback, recruited by the stimulation, provided the basis for the outlasting effect of stimulation (spectra in Figure 5.2C). Our model predicts that the maintenance of stimulation-induced dynamics after stimulation termination was due to reverberation of input-driven responses through cortical recurrence and not to resonance. Our computational model suggests that the effect of exogenous stimulation depends on the robustness of the ongoing oscillatory cortical dynamics, whereas task-related inputs tune the network to enhance susceptibility to perturbations and therefore enable frequency-matched responses to brain stimulation. Therefore, no synaptic plasticity was required to qualitatively reproduce state-dependent enhancement of oscillations that outlasted the stimulation.

To validate the observations from the models described above, we performed intracranial stimulation experiments in epilepsy participants with sub-dural electrodes implanted for surgical planning. We applied 2 mA biphasic current pulse (200 μs per phase) trains of 10 Hz frequency for 5 seconds to the cortical surface through pairs of neighboring ECoG electrodes (Figure 5.3A-B). We simultaneously recorded ECoG signals on all other electrodes during three different conditions (eyes closed, eyes open, and task-engaged; see methods for details) that altered cortical dynamics determined by the strength of alpha-band activity. We divided stimulation trials into 15-second segments comprised of a 5-second epoch before stimulation onset, a 5-second epoch during stimulation, and a 5-second epoch after

stimulation offset. Stimulation artifacts were removed using a template matching algorithm (Figure 5.3B-E; see methods).

Power spectral densities were computed in the three epochs, and modulation of power at the endogenous frequency and the stimulation frequency were quantified. A modulation index (MI) was defined as the difference in power at specific frequency bands between two epochs normalized by the sum of the power at the frequency bands in the two epochs. Figure 5.4A shows the average power spectra in the three epochs for each of the three participants under two different conditions, while Figure 5.4B shows a summary of the modulation indices at the endogenous and stimulation frequency bands for the three participants.

In three participants, we found spectral peaks that we interpreted as a sign of the dominant endogenous oscillation. In participants P001 and P005, the stimulation frequency (10 Hz) did not match the endogenous frequency. For patient P008, the peak we identified was below the classical alpha frequency, but there was an associated peak at the first harmonic frequency which approximately matched the stimulation frequency. Given this mismatch in frequencies, we considered the power at the endogenous frequency and the power at the stimulation frequency separately in our analysis.

Participant P001 completed the eyes-closed and working-memory tasks. Alpha oscillations were successfully enhanced both during and after stimulation. During stimulation, activity was enhanced at the stimulation frequency of 10 Hz (eyes closed: MI = 0.034 ± 0.011; $p = 0.002$; task: MI = 0.0414 ± 0.011; $p < 0.001$; one sample t-tests) but not at the endogenous frequency (eyes closed: MI = 0.011 ± 0.01; $p = 0.275$; task: MI = -0.0042 ± 0.013; $p = 0.747$). We found no difference in power modulation as a function of state (endogenous frequency: $p = 0.354$, stimulation frequency: $p = 0.650$). However, only in the task-engaged state, there was an acceleration of oscillation frequency from the endogenous peak (7.1 Hz) towards 10 Hz with a median peak frequency at 9 Hz ($p = 0.010$; Wilcoxon rank-sum test). This change in oscillation frequency was evident in the time-domain signal and was confirmed not to be the result of stimulation artifacts. Interestingly, in the epoch after stimulation, we found state-dependent modulation of oscillation power (endogenous frequency: $p < 0.001$; stimulation frequency: $p = 0.022$). After stimulation, the peak at the endogenous frequency was enhanced in the eyes-closed state (MI = 0.0279 ± 0.0117; $p = 0.018$) but decreased in the task-engaged state (MI = -0.031 ± 0.011; $p = 0.006$). In conjunction with the

shift of the alpha frequency towards the stimulation frequency during the task-engaged state, the peak at the stimulation frequency was increased in the task-engaged state (MI = 0.030 ± 0.010; p = 0.002) but not in the eyes-closed state (MI = -0.0017 ± 0.010; p =0.867). The shift in peak frequency persisted at a median of 8.95 Hz (p = 0.014) in the task-engaged state. In summary, the results from Participant P001 confirmed the modulation of alpha oscillations by stimulation at 10 Hz both during and after stimulation. A pronounced state-dependent effect was observed after stimulation; the stimulation boosted power at the endogenous frequency or at the stimulation frequency as a function of state.

Participant P005 completed the eyes-open and eyes-closed tasks. Endogenous oscillation power was successfully enhanced only in the eyes-open state both during and after stimulation. This enhancement was limited to the power at the endogenous frequency both during stimulation (eyes-open: MI = 0.034 ± 0.011; p = 0.002; eyes-closed MI = -0.006 ± 0.016; p = 0.693; one sample t-tests; difference: p = 0.04; 2 sample t-test) and after stimulation (eyes-open: MI = 0.035 ± 0.012; p = 0.006; eyes-closed: MI = -0.071 ± 0.016; p < 0.001; difference: p < 0.001). The power at the stimulation frequency either decreased or did not change both during stimulation (eyes-open: MI = -0.023 ± 0.010; p = 0.031; eyes-closed: MI = -0.031 ± 0.015; p = 0.043) and after stimulation (eyes-open: MI = 0.010 ± 0.001; p = 0.280; eyes-closed: MI = -0.048 ± 0.014; p < 0.001).

Participant P008 completed the eyes-open and eyes-closed tasks. Endogenous oscillation power was also successfully enhanced in this patient. During stimulation, the power increased at the endogenous frequency (eyes-closed state: MI = 0.046 ± 0.014; p = 0.001; eyes-open state: MI = 0.041 ± 0.010; p < 0.001, one sample t-tests; difference: p = 0.802; 2 sample t-test) and increased again at the stimulation frequency (eyes- closed state: MI = 0.083 ± 0.017; p < 0.001; eyes-open state: MI = 0.061 ± 0.020; p = 0.002; difference: p = 0.397). After stimulation, there was only a significant modulation of the power at the stimulation frequency, which was state-dependent (eyes-closed state MI = 0.043 ± 0.015; p = 0.005; eyes-open state MI = -0.014 ± 0.013; p = 0.282, difference p = 0.005).

Together, the data from the three participants demonstrate modulation of endogenous cortical oscillations by 10 Hz stimulation during and after stimulation, depending on behavioral state. In particular, the effects on endogenous oscillation that outlasted stimulation followed the predictions of the network model as well as the summation model. In agreement with entrainment of cortical oscillations by periodic

brain stimulation, we found a shift towards the stimulation frequency for P001 in the task-engaged state. However, we also found enhancement of power at the endogenous frequency, which is hard to reconcile with entrainment (for example, in P001 after stimulation and in P005 during and after stimulation).

The effect of stimulation on endogenous oscillations, during stimulation in particular, observed in participants P001 and P005 support the observations from the static summation model. In the eyes-closed state where alpha oscillations are strongest, stimulation produced little change while in the eyes - open state, stimulation enhanced oscillation power in the endogenous frequency. In contrast, in the task-engaged state, stimulation enhanced power in the stimulation frequency suggesting stimulation produced entrainment (or 1:1 frequency locking). The data from P008 does not fully agree with the summation model as enhancement was observed in the stimulation frequency in both the eyes-open and eyes-closed states; the stimulation frequency being close to the first harmonic of the endogenous frequency is a potential confounding variable that could explain this difference.

The predictions from the network model are confirmed by the results from participants P001 and P005. However, in contrast to the model which predicts enhancement in power at stimulation as well as endogenous frequencies in the eyes-open state, the data from participant P005 showed no change in power at stimulation frequency. There are multiple possible reasons for this discrepancy between the experimental data and model. For example, the specific locations of stimulation electrodes in the experiment were more wide-spread and not just limited to the recording site as it was in our model by definition. Indeed, we found that enhancement at 10 Hz was present in average across the participants but that it was only observed local to the stimulation electrodes and reflected in the statistics of modulation indices as well (Figure 5.4B) .

DISCUSSION

We elucidated the effects of 10 Hz stimulation on cortical network dynamics to advance the mechanistic understanding of interaction between cortical oscillations and periodic brain stimulation. We leveraged the unique access to human cortex in patients with medication-refractory epilepsy to provide experimental support. We attribute the effects that outlast stimulation to cortico-cortical network synchronization and the state-dependent effect to the thalamo-cortical network. Previous simulations of

large-scale cortical networks with physiological propagation delays have demonstrated outlasting effects resulting from inherent multistable behavior mediated by the propagation delays in the long-range connections (Kutchko & Frohlich, 2013; Zaehle et al., 2010). Similar cortico-cortical interactions may play a further role in the dynamics reported here. The choice of components in our model was motivated by biological plausibility. The thalamo-cortical network is the generator of alpha oscillations, and the cortico-cortical network involvement is motivated by the abundance of recurrent connections in the cortex. Although our model is a simplistic approximation of these circuits, the behavior of the model successfully reflected the dynamics observed in ECoG data. Moreover, the dynamics of the recurrent loop determines the frequency of oscillation exhibited by the network. Hence this model can be applicable to oscillations other than alpha oscillations and networks other than the thalamo-cortical network provided there exists a loop that mediates recurrent excitation. It is important to note that, although our model supports the experimental observations based only on network interactions, other studies have suggested the possibility that synaptic plasticity also plays a role (Reato et al., 2010; Vossen et al., 2015). It is possible that the stimulation duration was not long enough to recruit plasticity in our study. Typically, stimulation is applied in the order of minutes in studies where outlasting effects are observed in stark contrast to the short 5 second segments used here. Thus the time scale of observation is likely shorter than the time scale where plasticity induced changes could be observed. This restricts the comparison with models and experiments that study plasticity in the context of transcranial current stimulation.

In contrast to previous experimental studies, we recorded from the cortical surface while directly stimulating the cortical tissue. This approach helped us avoid issues of spatial filtering and artifact contamination observed in non-invasive stimulation and recording approaches. In agreement with previously postulated mechanisms (Neuling et al., 2013; Schmidt et al., 2014), we found differential modulation of cortical oscillations by 10 Hz stimulation as a function of the endogenous state of the stimulated networks. In the eyes-closed state, stimulation had little effect on the oscillation dynamics. In the eyes-open state, the stimulation altered power at the endogenous frequency. In contrast, in the task-engaged state, the reduced endogenous peak permitted a response matched to the stimulation frequency. Our data demonstrate that cortical oscillations can indeed be enhanced by rhythmic

stimulation and that even short periods of stimulation can have effects that, at least briefly, outlast stimulation.

Our results contribute to an ongoing debate about whether network entrainment or plasticity mediates the outlasting effects of periodic brain stimulation. The former hinges on the idea that periodic stimulation causes a realignment of phase of the oscillators resulting in an increase in oscillation strength at the stimulation frequency (Thut, Schyns, et al., 2011). Our observation that the oscillation was power was enhanced at the stimulation frequency and not at the endogenous frequency during the task-engaged state demonstrates the presence of entrainment. The entrainment hypothesis has been explored in studies which employed tACS stimulation and EEG (Helfrich, Knepper, et al., 2014; Helfrich, Schneider, et al., 2014; Neuling et al., 2013) and results with varying degree of support for this hypothesis have been obtained. In contrast, recent studies failed to find evidence of entrainment as a mechanism for oscillation power increases (Struber et al., 2015; Vossen et al., 2015). The studies employed short duration stimulation (comparable to the duration used in our study) and found that there was no evidence for entrainment despite the observed outlasting effects. Hence the studies argue plasticity to be the underlying mechanism. In our study we found signs of entrainment (during the task-engaged state) as well as signs of enhancement of the endogenous oscillation (eyes-open condition). Therefore, the debate on the presence of entrainment could potentially be resolved by recasting it in the framework of state-dependent effects that we have demonstrated here. In fact, state-dependent effects have also been observed in tACS studies employing stimulation at frequency bands other than alpha band (Feurra et al., 2013). Our summation model proposes that the strength of the stimulation relative to the strength of the oscillation is an important contributing factor for the state-dependent effect. An alternate explanation for this effect is that weak network oscillations are generally more malleable to weak stimulation than strong network oscillations due to a ceiling effect. Specifically, strong oscillations have been suggested to correspond to a scenario in which all endogenous oscillators are already synchronized and, accordingly, no further entrainment by stimulation would be possible (Neuling et al., 2013).

Our findings demonstrate that stimulation in the alpha frequency band may differ in its effect as a function of the endogenous state during stimulation. Of note, the functional implications of such differential modulation at varying frequencies within the alpha frequency band remain unclear.

Furthermore, stimulation at matched frequencies, as used in individualized alpha frequency stimulation (IAF) for tACS, may reveal different response dynamics. Data from P008 supports this hypothesis where an endogenous oscillation was observed at a frequency that was a subharmonic of stimulation frequency. Enhancement was observed at stimulation frequency as well as at the endogenous frequency irrespective of whether the participant had her eyes closed or open.

The fact that power at 10 Hz increased locally (< 20 mm) suggests that it is indeed possible to enhance oscillation power at the stimulation frequency. It is likely that the strength of stimulation relative to endogenous oscillation was higher locally and this resulted in a scenario similar to task-engaged state predicted by the simple summation model. The strength of stimulus relative to ongoing oscillation is an important parameter in designing studies and is seldom studied in humans due to various limitations. Our dataset is limited to a single stimulation strength which makes such analysis difficult and further studies incorporating multiple stimulation strengths are required. Additionally, the spatial effect of stimulation is important for studies that attempt to address functions that are localized anatomically. Many tACS studies utilize large electrodes to produce an effect over a wide region. When the function under investigation is localized to anatomically specific regions, it might be advisable to utilize electrode configuration that produces a localized electric field as close as possible to the anatomical region.

Direct cortical stimulation is widely used in clinical settings, albeit in a different context. Developed by Wilder Penfield in the 1950s, it is generally used for localizing language areas and sensorimotor cortex (eloquent cortex) for surgical resection planning in patients suffering from seizures (Gallentine & Mikati, 2009; Ojemann et al., 1989). The approach involves using biphasic pulses at frequencies higher than were used in this study (50 Hz vs 10 Hz) to produce reversible, temporary microlesions in the stimulated site. These microlesions help to identify the functions associated with the areas (Borchers, Himmelbach, Logothetis, & Karnath, 2012; Cervenka et al., 2013; Koubeissi, Bartolomei, Beltagy, & Picard, 2014; Parvizi et al., 2012; Parvizi, Rangarajan, Shirer, Desai, & Greicius, 2013; Rauschecker et al., 2011). However, the electrographic data obtained during stimulation are seldom analyzed due to severe stimulation artifacts. Alternately, using low frequency stimulation allows for analysis of stimulation effects. Utilizing this strategy, cortico-cortical evoked potentials (CCEPs) induced by low frequency stimulation (1 Hz) have been used to map functionally connected areas (Entz et al., 2014; Keller et al., 2011; Keller et

al., 2014; Kunieda, Yamao, Kikuchi, & Matsumoto, 2015; Matsumoto et al., 2007; Matsumoto et al., 2004). Apart from these, chronically implanted devices that use electrical stimulation for termination of seizures have also been developed (F. T. Sun & Morrell, 2014). In the future, this approach can be extended to study the neural and behavioral responses to different frequencies. An added advantage of direct cortical stimulation (at low amplitudes) is that there are no perceptual effects that may confound the effect of stimulation in studies of non-invasive brain stimulation.

Despite the clear advantages of our approach based on ECoG recordings and stimulation, there are also important technical limitations. First, the actual waveforms of repetitive TMS and tACS, even though both have a 10 Hz structure, differ from the pulsed waveform used in our study. Consequently, the effects of stimulation on neuronal tissue are different. tACS is believed to produce sub-threshold modulation with stimulation current flowing perpendicular to the cortical surface. In contrast, repetitive TMS produces supra-threshold modulation with current flowing tangential to the cortical surface (Hallett, 2007). Like repetitive TMS, biphasic stimulation produces a local supra-threshold modulation. Our choice of biphasic pulses was motivated by the stimulator hardware and stimulation waveforms approved for direct cortical stimulation in human participants. As a benefit of the waveform used in our study, artifact removal was simplified. Only a brief period of the raw signal during and immediately after the pulse was contaminated with a stimulation artifact. In spite of the above differences, we argue that the key shared feature between all stimulation waveforms is the periodic, 10 Hz structure. Second, as for any ECoG study, our results were obtained from patients with severe epilepsy a few days after head surgery for electrode implantation. Although we excluded electrodes that were in proximity to the clinically determined epileptic focus, the responses obtained may differ from the healthy intact brain as patients with focal seizures often exhibit abnormal global oscillation patterns (Walker, 2008). Finally, given the small sample sizes and variability in electrode locations and stimulation locations in these patients, ECoG data tends to be more heterogeneous than data from other electrophysiology techniques. This was also the case here. Nevertheless, as argued before, the opportunity to measure directly from cortical surface help us to elucidate interaction between stimulation and endogenous dynamics at a finer spatial and temporal scale.

In conclusion, we provide new mechanistic models supported by invasive human electrophysiological recordings for the modulation of endogenous oscillations by periodic brain stimulation. Despite the limitations discussed above, our findings carry important implications for the design and interpretation of brain stimulation studies. This is of heightened importance, given the emergence of novel therapeutic brain stimulation paradigms that target alpha oscillations (Frohlich, 2015; Leuchter et al., 2015). First, it is highly recommended that the state of the participant is uniform within a study and that there is independent verification of whether the according instructions to the participant were followed. Second, if an enhancement of endogenous alpha oscillations is (clinically) desired, stimulation during the eyes-open state may be the most effective approach. Third, if an increase (or likely change in general) of the alpha frequency is desired, stimulating in a state of suppressed alpha oscillations (e.g. state of heightened behavioral arousal or attention) likely provides the best state for stimulation. Fourth, the response to stimulation may vary from participant to participant and (ideally simultaneous) electrophysiological monitoring is essential. We argue that the study of these principles, together with the further development of computational and mathematical models, will advance brain stimulation towards becoming a clinically effective modality for the restoration of functional alpha oscillations, perhaps the most fundamental electric activity pattern generated by the brain (Berger, 1929).

FIGURES AND TABLES

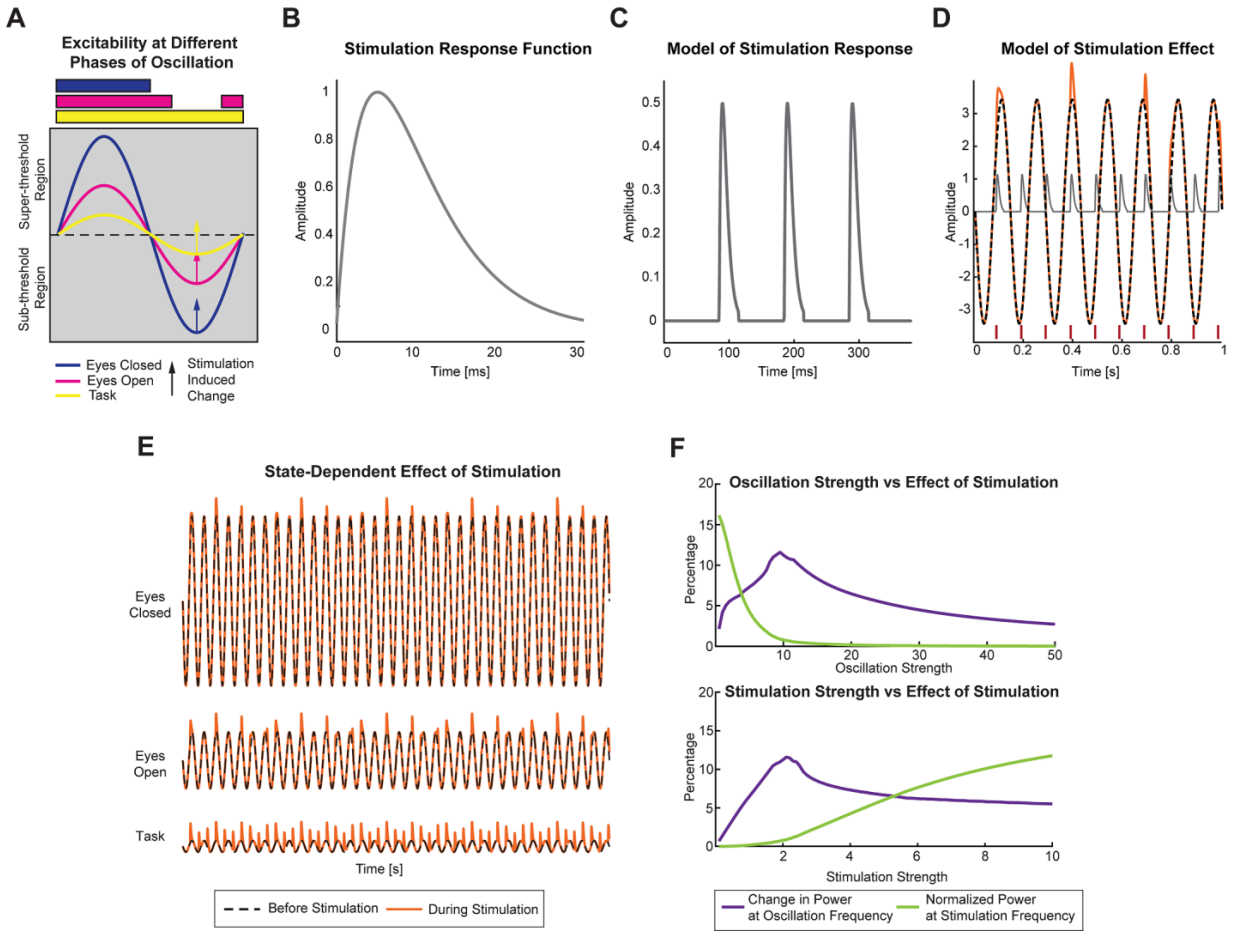

Figure 5.1. Simple Static Model Explains State-Dependence.

(A) The endogenous oscillation is denoted as a pure sine wave, and the amplitude of the sine wave represents the strength of oscillation in the three states studied here. Dotted line denotes the threshold above which stimulation produces a change (denoted by arrow). When the change produced by stimulation is below the threshold, no change in the oscillation is observed. However, when the threshold is crossed, stimulation produces a response that decays with time. The bands denote the phases of the oscillation at which stimulation produces a change in the oscillation. For stronger oscillations (eyes-closed), the phases at which stimulation produces change are minimal. For very weak oscillations (task engaged), stimulation produces change at all phases. (B) The function used to model the stimulation response. The stimulation response is modeled as the linear convolution between the stimulation pulse and this response function. (C) Convolution between stimulation pulses and stimulation response function. (D) Example traces illustrating the model behavior. The red lines at the bottom denote the timing

of the stimulation pulses. The gray line denotes the stimulation response that is added to the oscillation waveform (black dashed line) to produce the stimulation effect (orange solid line). (E) Example traces produced using the model described in (A). In the eyes-closed state, stimulation-induced changes are minimal. In the eyes-open state, the stimulation induced change is still constrained by the endogenous frequency. In the task-engaged state, stimulation produces change at all phases resulting in entrainment. Black dashed line represents the endogenous oscillation. Red solid line represents the waveform resulting from the addition of the stimulation waveform to the endogenous oscillation. (F) Top: Effect of varying endogenous oscillation strength. The change in power at the endogenous frequency increases until a certain limit and then decreases when the strength of oscillation relative to stimulation strength is high (violet line). The power at stimulation frequency (green line) decreases with increasing oscillation strength as stimulation effect is observed in a restricted range of phases. Bottom: Effect of varying stimulation strength for a given oscillation strength. As stimulation strength increases, the power at oscillation frequency increases until the strength relative to oscillation strength is high enough to cause increase in power at stimulation frequency. Beyond this, the increase in power at oscillation frequency is minimal, and power at stimulation frequency increases monotonically.

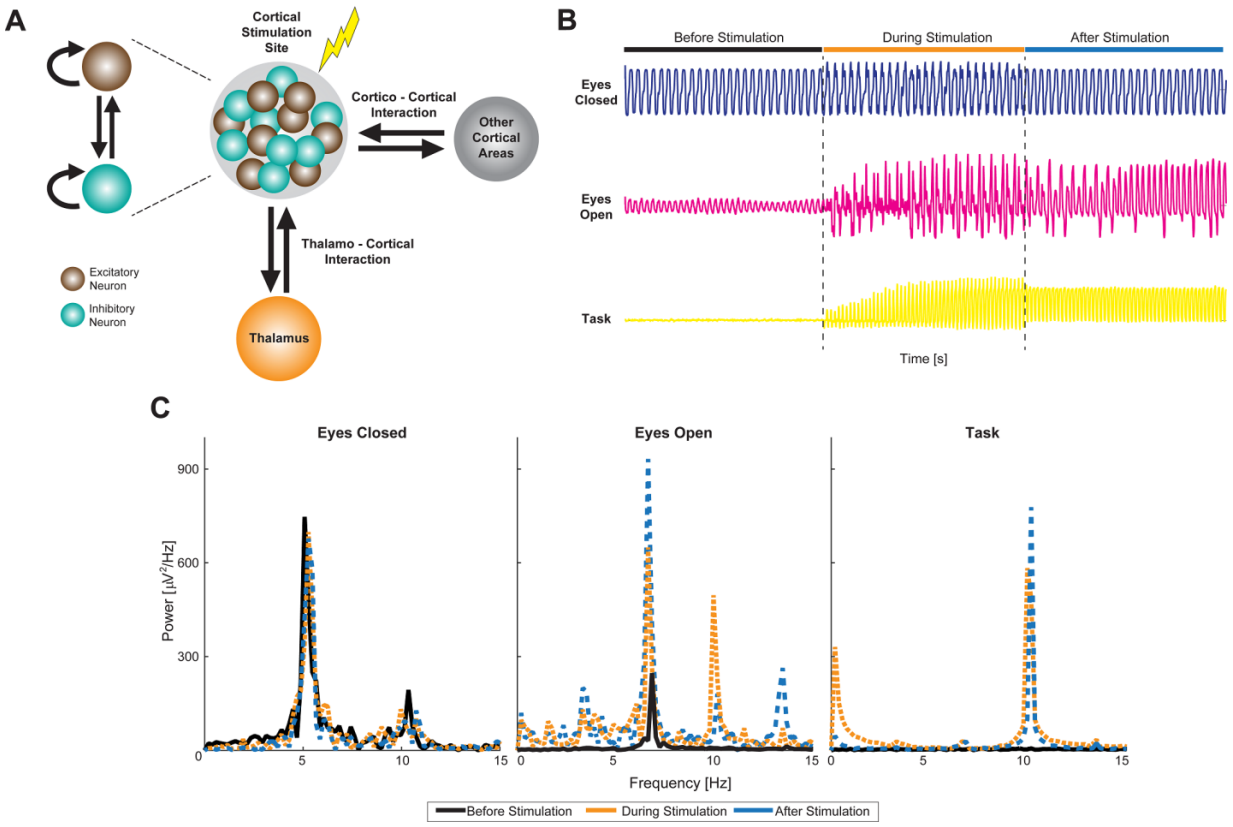

Figure 5.2. Computational Model Explains Outlasting Effects of Periodic Stimulation.

(A) Schematic of computational model that includes the different components and interactions among them. The region of the cortex being stimulated is denoted by a gray circle encompassing excitatory and inhibitory neurons. The model neurons exhibit reciprocal as well as recurrent connections. The cortico-thalamic and cortico-cortical interactions are also modeled to be reciprocal. (B) Membrane potential observed from excitatory neurons in the model shows task-dependent differences in stimulation effect. During the eyes closed state (blue trace), a strong oscillation is observed in the alpha frequency range. Stimulation onset does not alter the dynamics significantly. In the eyes-open state (magenta trace), an oscillation is still observed in the alpha frequency range. However, the strength is decreased compared to the eyes closed state. Stimulation onset causes the amplification of this oscillation, which persists after stimulation offset and then slowly decays. In the task-engaged state (yellow trace), no strong oscillation is observed due to the external inputs that model task-related input. In this state, stimulation causes the network to oscillate at the stimulation frequency, which persists and decays in the

epoch after stimulation. (C) Spectral analysis of membrane potential reveals state-dependent effect of stimulation.

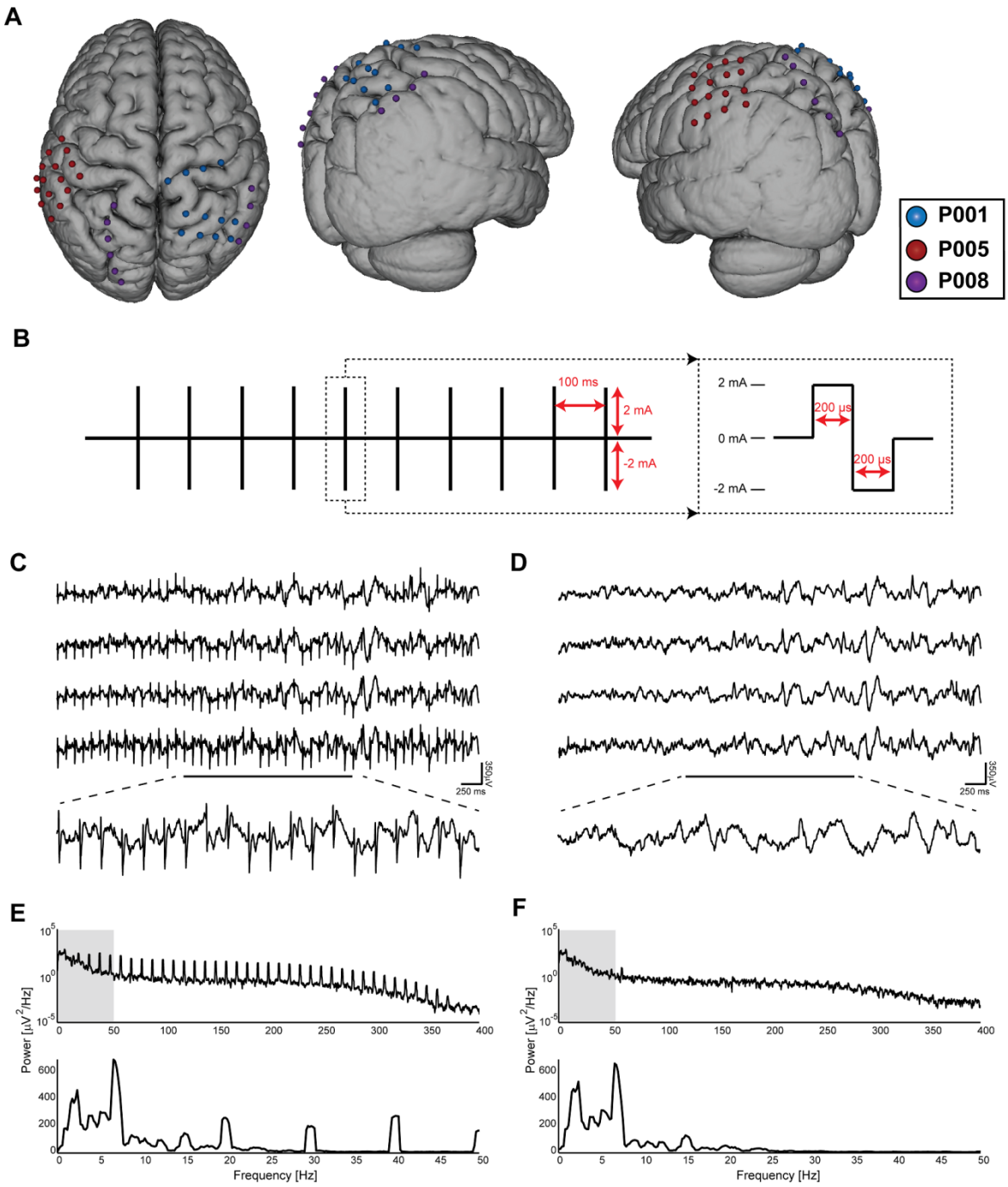

Figure 5.3. Electrode Locations and Artifact Suppression.

(A) Surface model of an atlas brain showing locations of electrodes over the parietal regions in each of the three patients. Signals measured from only these electrodes were used in the analysis. (B) Schematic of stimulation waveform used. Stimulation consisted of one biphasic pulse 400 µs in duration every 100 ms for 5 s. (C) Stimulation artifacts in representative sample traces from four electrodes (top).

Enlarged portion denoted by the black line (bottom). Artifacts appear as periodic sharp deflections with stereotyped waveforms. (D) Traces from the same four electrodes as in (B) after the artifact suppression procedure. The artifacts are suppressed compared to the signal amplitude. (E) Spectrum of the fourth waveform in (B) showing peaks at 10 Hz and harmonics of 10 Hz corresponding to artifact waveform. Top: Full frequency range. Bottom: Zoom-in on low frequencies. (F) Spectra of the same waveform after artifact suppression confirming the effectiveness of the algorithm. The only remaining exogenous peak is at 60 Hz, caused by electric line noise.

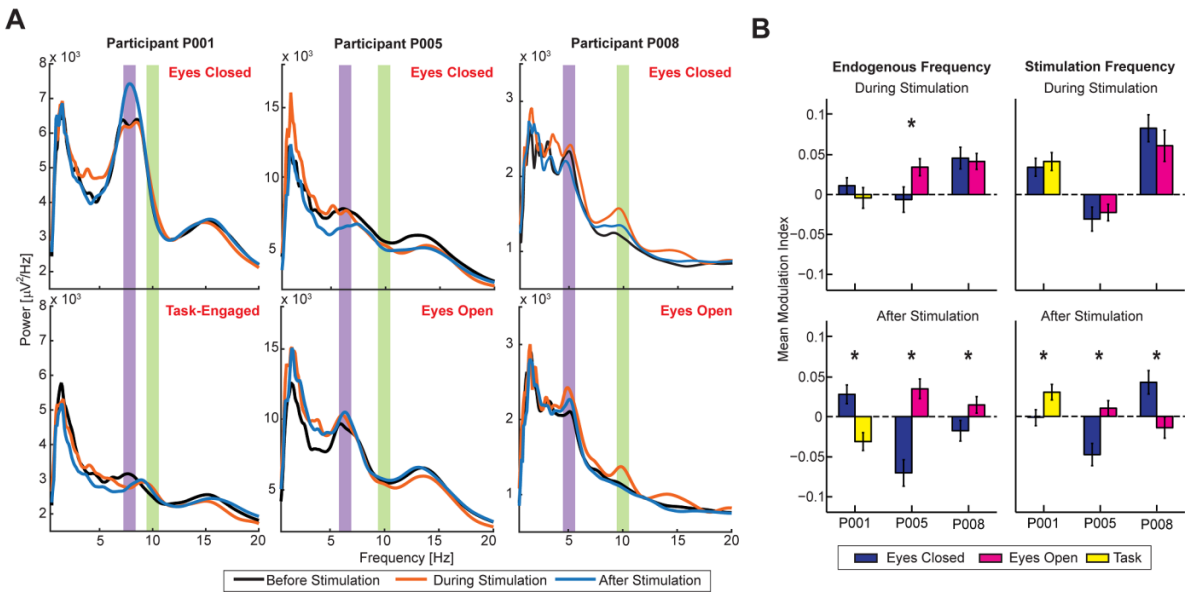

Figure 5.4. State-Dependent Modulation by Periodic Stimulation

(A) Power spectra in the epochs before stimulation (black trace), during stimulation (orange trace), and after stimulation (blue trace) for the three participants during the different states. Participant P001's spectra showed no appreciable change in the eyes-closed state in the endogenous frequency band (violet shaded region) and minimal change in the stimulation frequency band (green shaded region) in eyes-closed state during stimulation. However, there was a change in dominant oscillation frequency from endogenous frequency to stimulation frequency in the task-engaged state. P005 showed no change in power at endogenous frequency in the eyes-closed state, while there was an increase in the eyes-open state. Power at stimulation frequency was decreased in both states. P008 showed an increase in both states in the endogenous and stimulation frequencies. (B) Mean modulation indices at the endogenous frequency (left) and the stimulation frequency (right) in the epochs during stimulation (top) and after stimulation (bottom) for each of the three participants. Bars denote standard error of mean. * denotes statistical significance ($p < 0.05$) from a paired t test.

Participant	Age	Sex	Handedness	Clinical Seizure Focus	Grid Locations (Number of Electrodes)	Location of Stimulation Electrodes (Number of Electrode Pairs Stimulated)	Total Number of Stimulations (Stimulation per Electrode Pair per Condition)
P001	21	F	R	Right Frontal Lobe	Right Frontal Lobe (29), Right Parietal Lobe (24), Right Limbic Lobe (3)	Right Anterior Frontal Lobe (8), Right Parietal Lobe (6)	28 (1)
P005	30	F	R	Unknown Seizure Focus	Left Frontal Lobe (40), Left Temporal Lobe (38), Left Parietal Lobe (12), Left Limbic Lobe (3)	Left Frontal Lobe (2), Left Parietal Lobe (1), Left Temporal Lobe (1)	18 (2)
P008	23	F	R	Bitemporal Lobe	Bilateral Parahippocampal Gyrus (16), Left Frontal Lobe (12), Right Frontal Lobe (12), Left Parietal Lobe (6), Right Parietal Lobe (4), Left Temporal Lobe (14), Right Temporal Lobe (4)	Left Parietal Lobe (3), Right Parietal Lobe (2)	20 (2)

Table 5.1. Clinical Information of Participants.

Symbol	Value	Definition
τ_e	10.0 ms	Excitatory synaptic time constant
τ_i	6.6 ms	Inhibitory synaptic time constant
a	1.5	Membrane leak constant
g_{ee}	1.0	Synaptic gain $e \rightarrow e$
g_{ei}	1.0	Synaptic gain $e \rightarrow i$
g_{ie}	-1.0	Synaptic gain $i \rightarrow e$
g_{ii}	-1.0	Synaptic gain $i \rightarrow i$
g_1	-0.5	Thalamo-cortical feedback gain
g_2	0.85	Large-scale cortico-cortical feedback gain
h_o	-0.50	Recurrent interactions threshold
h_1	-0.30	Thalamo-cortical feedback threshold
h_2	0.1	Cortico-cortical feedback threshold
D_1	65 ms	Thalamo-cortical delay
D_2	290 ms	Cortico-cortical delay
I_{Bias}	-0.25	Baseline input
$I_{Resting}$	0.00	Resting state input
$I_{Eyes-open}$	0.30	Input in the eyes-open condition
I_{task}	0.55	Task-related input
S	0.20	Stimulation amplitude
D	0.01	Noise intensity

Table 5.2. Model Parameters.

REFERENCES

Ali, M. M., Sellers, K. K., & Frohlich, F. (2013). Transcranial alternating current stimulation modulates large-scale cortical network activity by network resonance. *J Neurosci, 33*(27), 11262-11275. doi:10.1523/JNEUROSCI.5867-12.2013

Amari, S. (1977). Dynamics of pattern formation in lateral-inhibition type neural fields. *Biol Cybern, 27*(2), 77-87.

Berger, H. (1929). Uber das Elektrenkephalogramm des Menschen. *Archiv für Psychiatrie und Nervenkrankheiten, 87*(1), 527-570.

Borchers, S., Himmelbach, M., Logothetis, N., & Karnath, H. O. (2012). Direct electrical stimulation of human cortex - the gold standard for mapping brain functions? *Nat Rev Neurosci, 13*(1), 63-70. doi:10.1038/nrn3140

Buzsaki, G., & Draguhn, A. (2004). Neuronal oscillations in cortical networks. *Science, 304*(5679), 1926-1929. doi:10.1126/science.1099745

Cecere, R., Rees, G., & Romei, V. (2015). Individual differences in alpha frequency drive crossmodal illusory perception. *Curr Biol, 25*(2), 231-235. doi:10.1016/j.cub.2014.11.034

Cervenka, M. C., Corines, J., Boatman-Reich, D. F., Eloyan, A., Sheng, X., Franaszczuk, P. J., & Crone, N. E. (2013). Electrocorticographic functional mapping identifies human cortex critical for auditory and visual naming. *Neuroimage, 69*, 267-276. doi:10.1016/j.neuroimage.2012.12.037

Entz, L., Toth, E., Keller, C. J., Bickel, S., Groppe, D. M., Fabo, D., . . . Mehta, A. D. (2014). Evoked effective connectivity of the human neocortex. *Hum Brain Mapp, 35*(12), 5736-5753. doi:10.1002/hbm.22581

Fedorov, A., Beichel, R., Kalpathy-Cramer, J., Finet, J., Fillion-Robin, J. C., Pujol, S., . . . Kikinis, R. (2012). 3D Slicer as an image computing platform for the Quantitative Imaging Network. *Magn Reson Imaging, 30*(9), 1323-1341. doi:10.1016/j.mri.2012.05.001

Feurra, M., Pasqualetti, P., Bianco, G., Santarnecchi, E., Rossi, A., & Rossi, S. (2013). State-dependent effects of transcranial oscillatory currents on the motor system: what you think matters. *J Neurosci, 33*(44), 17483-17489. doi:10.1523/JNEUROSCI.1414-13.2013

Fonov, V., Evans, A. C., Botteron, K., Almli, C. R., McKinstry, R. C., Collins, D. L., & Brain Development Cooperative, G. (2011). Unbiased average age-appropriate atlases for pediatric studies. *Neuroimage, 54*(1), 313-327. doi:10.1016/j.neuroimage.2010.07.033

Frohlich, F. (2015). Tuning out the Blues - Thalamo-Cortical Rhythms as a Successful Target for Treating Depression. *Brain Stimul*. doi:10.1016/j.brs.2015.07.040

Fröhlich, F. (2015). Experiments and models of cortical oscillations as a target for noninvasive brain stimulation. *Prog Brain Res*.

Frohlich, F., & McCormick, D. A. (2010). Endogenous electric fields may guide neocortical network activity. *Neuron, 67*(1), 129-143. doi:10.1016/j.neuron.2010.06.005

Gallentine, W. B., & Mikati, M. A. (2009). Intraoperative electrocorticography and cortical stimulation in children. *J Clin Neurophysiol, 26*(2), 95-108. doi:10.1097/WNP.0b013e3181a0339d

George, M. S. (2010). Transcranial magnetic stimulation for the treatment of depression. *Expert Rev Neurother, 10*(11), 1761-1772. doi:10.1586/ern.10.95

Hallett, M. (2007). Transcranial magnetic stimulation: a primer. *Neuron, 55*(2), 187-199. doi:10.1016/j.neuron.2007.06.026

Helfrich, R. F., Knepper, H., Nolte, G., Struber, D., Rach, S., Herrmann, C. S., . . . Engel, A. K. (2014). Selective Modulation of Interhemispheric Functional Connectivity by HD-tACS Shapes Perception. *PLoS Biol, 12*(12), e1002031. doi:10.1371/journal.pbio.1002031

Helfrich, R. F., Schneider, T. R., Rach, S., Trautmann-Lengsfeld, S. A., Engel, A. K., & Herrmann, C. S. (2014). Entrainment of brain oscillations by transcranial alternating current stimulation. *Curr Biol, 24*(3), 333-339. doi:10.1016/j.cub.2013.12.041

Hughes, S. W., & Crunelli, V. (2005). Thalamic mechanisms of EEG alpha rhythms and their pathological implications. *Neuroscientist, 11*(4), 357-372. doi:10.1177/1073858405277450

Hughes, S. W., Lorincz, M., Cope, D. W., Blethyn, K. L., Kekesi, K. A., Parri, H. R., . . . Crunelli, V. (2004). Synchronized oscillations at alpha and theta frequencies in the lateral geniculate nucleus. *Neuron, 42*(2), 253-268.

Iglesias, J. E., Liu, C. Y., Thompson, P. M., & Tu, Z. (2011). Robust brain extraction across datasets and comparison with publicly available methods. *IEEE Trans Med Imaging, 30*(9), 1617-1634. doi:10.1109/TMI.2011.2138152

Jensen, O., & Mazaheri, A. (2010). Shaping functional architecture by oscillatory alpha activity: gating by inhibition. *Frontiers in human neuroscience, 4*, 186. doi:10.3389/fnhum.2010.00186

Keller, C. J., Bickel, S., Entz, L., Ulbert, I., Milham, M. P., Kelly, C., & Mehta, A. D. (2011). Intrinsic functional architecture predicts electrically evoked responses in the human brain. *Proc Natl Acad Sci U S A, 108*(25), 10308-10313. doi:10.1073/pnas.1019750108

Keller, C. J., Honey, C. J., Megevand, P., Entz, L., Ulbert, I., & Mehta, A. D. (2014). Mapping human brain networks with cortico-cortical evoked potentials. *Philos Trans R Soc Lond B Biol Sci, 369*(1653). doi:10.1098/rstb.2013.0528

Kemp, B., Varri, A., Rosa, A. C., Nielsen, K. D., & Gade, J. (1992). A simple format for exchange of digitized polygraphic recordings. *Electroencephalogr Clin Neurophysiol, 82*(5), 391-393.

Klimesch, W. (2012). alpha-band oscillations, attention, and controlled access to stored information. *Trends Cogn Sci, 16*(12), 606-617. doi:10.1016/j.tics.2012.10.007

Klimesch, W., Sauseng, P., & Hanslmayr, S. (2007). EEG alpha oscillations: the inhibition-timing hypothesis. *Brain Res Rev, 53*(1), 63-88. doi:10.1016/j.brainresrev.2006.06.003

Koubeissi, M. Z., Bartolomei, F., Beltagy, A., & Picard, F. (2014). Electrical stimulation of a small brain area reversibly disrupts consciousness. *Epilepsy Behav, 37*, 32-35. doi:10.1016/j.yebeh.2014.05.027

Kunieda, T., Yamao, Y., Kikuchi, T., & Matsumoto, R. (2015). New Approach for Exploring Cerebral Functional Connectivity: Review of Cortico-cortical Evoked Potential. *Neurol Med Chir (Tokyo), 55*(5), 374-382. doi:10.2176/nmc.ra.2014-0388

Kutchko, K. M., & Frohlich, F. (2013). Emergence of metastable state dynamics in interconnected cortical networks with propagation delays. *PLoS Comput Biol, 9*(10), e1003304. doi:10.1371/journal.pcbi.1003304

Lancaster, J. L., Woldorff, M. G., Parsons, L. M., Liotti, M., Freitas, C. S., Rainey, L., . . . Fox, P. T. (2000). Automated Talairach atlas labels for functional brain mapping. *Hum Brain Mapp, 10*(3), 120-131.

Leuchter, A. F., Cook, I. A., Feifel, D., Goethe, J. W., Husain, M., Carpenter, L. L., . . . George, M. S. (2015). Efficacy and Safety of Low-field Synchronized Transcranial Magnetic Stimulation (sTMS) for Treatment of Major Depression. *Brain Stimul, 8*(4), 787-794. doi:10.1016/j.brs.2015.05.005

Leuchter, A. F., Cook, I. A., Jin, Y., & Phillips, B. (2013). The relationship between brain oscillatory activity and therapeutic effectiveness of transcranial magnetic stimulation in the treatment of major depressive disorder. *Front Hum Neurosci, 7*, 37. doi:10.3389/fnhum.2013.00037

Lorincz, M. L., Kekesi, K. A., Juhasz, G., Crunelli, V., & Hughes, S. W. (2009). Temporal framing of thalamic relay-mode firing by phasic inhibition during the alpha rhythm. *Neuron, 63*(5), 683-696. doi:10.1016/j.neuron.2009.08.012

Luck, S. J., & Vogel, E. K. (1997). The capacity of visual working memory for features and conjunctions. *Nature, 390*(6657), 279-281. doi:10.1038/36846

Mathewson, K. E., Lleras, A., Beck, D. M., Fabiani, M., Ro, T., & Gratton, G. (2011). Pulsed out of awareness: EEG alpha oscillations represent a pulsed-inhibition of ongoing cortical processing. *Frontiers in psychology, 2*, 99. doi:10.3389/fpsyg.2011.00099

Matsumoto, R., Nair, D. R., LaPresto, E., Bingaman, W., Shibasaki, H., & Luders, H. O. (2007). Functional connectivity in human cortical motor system: a cortico-cortical evoked potential study. *Brain, 130*(Pt 1), 181-197. doi:10.1093/brain/awl257

Matsumoto, R., Nair, D. R., LaPresto, E., Najm, I., Bingaman, W., Shibasaki, H., & Luders, H. O. (2004). Functional connectivity in the human language system: a cortico-cortical evoked potential study. *Brain, 127*(Pt 10), 2316-2330. doi:10.1093/brain/awh246

Neuling, T., Rach, S., & Herrmann, C. S. (2013). Orchestrating neuronal networks: sustained after-effects of transcranial alternating current stimulation depend upon brain states. *Frontiers in human neuroscience, 7*, 161. doi:10.3389/fnhum.2013.00161

Ojemann, G., Ojemann, J., Lettich, E., & Berger, M. (1989). Cortical language localization in left, dominant hemisphere. An electrical stimulation mapping investigation in 117 patients. *J Neurosurg, 71*(3), 316-326. doi:10.3171/jns.1989.71.3.0316

Parvizi, J., Jacques, C., Foster, B. L., Witthoft, N., Rangarajan, V., Weiner, K. S., & Grill-Spector, K. (2012). Electrical stimulation of human fusiform face-selective regions distorts face perception. *J Neurosci, 32*(43), 14915-14920. doi:10.1523/JNEUROSCI.2609-12.2012

Parvizi, J., Rangarajan, V., Shirer, W. R., Desai, N., & Greicius, M. D. (2013). The will to persevere induced by electrical stimulation of the human cingulate gyrus. *Neuron, 80*(6), 1359-1367. doi:10.1016/j.neuron.2013.10.057

Pfurtscheller, G., Stancak, A., Jr., & Neuper, C. (1996). Event-related synchronization (ERS) in the alpha band--an electrophysiological correlate of cortical idling: a review. *Int J Psychophysiol, 24*(1-2), 39-46.

Rauschecker, A. M., Dastjerdi, M., Weiner, K. S., Witthoft, N., Chen, J., Selimbeyoglu, A., & Parvizi, J. (2011). Illusions of visual motion elicited by electrical stimulation of human MT complex. *PLoS One, 6*(7), e21798. doi:10.1371/journal.pone.0021798

Reato, D., Rahman, A., Bikson, M., & Parra, L. C. (2010). Low-intensity electrical stimulation affects network dynamics by modulating population rate and spike timing. *J Neurosci, 30*(45), 15067-15079. doi:10.1523/JNEUROSCI.2059-10.2010

Romei, V., Gross, J., & Thut, G. (2010). On the role of prestimulus alpha rhythms over occipito-parietal areas in visual input regulation: correlation or causation? *The Journal of neuroscience : the official journal of the Society for Neuroscience, 30*(25), 8692-8697. doi:10.1523/JNEUROSCI.0160-10.2010

Sauseng, P., Klimesch, W., Heise, K. F., Gruber, W. R., Holz, E., Karim, A. A., . . . Hummel, F. C. (2009). Brain oscillatory substrates of visual short-term memory capacity. *Curr Biol, 19*(21), 1846-1852. doi:10.1016/j.cub.2009.08.062

Schmidt, S. L., Iyengar, A. K., Foulser, A. A., Boyle, M. R., & Frohlich, F. (2014). Endogenous cortical oscillations constrain neuromodulation by weak electric fields. *Brain stimulation, 7*(6), 878-889. doi:10.1016/j.brs.2014.07.033

Struber, D., Rach, S., Neuling, T., & Herrmann, C. S. (2015). On the possible role of stimulation duration for after-effects of transcranial alternating current stimulation. *Front Cell Neurosci, 9*, 311. doi:10.3389/fncel.2015.00311

Sun, F. T., & Morrell, M. J. (2014). Closed-loop neurostimulation: the clinical experience. *Neurotherapeutics, 11*(3), 553-563. doi:10.1007/s13311-014-0280-3

Sun, L., Grutzner, C., Bolte, S., Wibral, M., Tozman, T., Schlitt, S., . . . Uhlhaas, P. J. (2012). Impaired gamma-band activity during perceptual organization in adults with autism spectrum disorders: evidence for dysfunctional network activity in frontal-posterior cortices. *The Journal of neuroscience : the official journal of the Society for Neuroscience, 32*(28), 9563-9573. doi:10.1523/JNEUROSCI.1073-12.2012

Thut, G., Schyns, P. G., & Gross, J. (2011). Entrainment of perceptually relevant brain oscillations by non-invasive rhythmic stimulation of the human brain. *Frontiers in psychology, 2*, 170. doi:10.3389/fpsyg.2011.00170

Thut, G., Veniero, D., Romei, V., Miniussi, C., Schyns, P., & Gross, J. (2011). Rhythmic TMS causes local entrainment of natural oscillatory signatures. *Current biology : CB, 21*(14), 1176-1185. doi:10.1016/j.cub.2011.05.049

Uhlhaas, P. J., & Singer, W. (2010). Abnormal neural oscillations and synchrony in schizophrenia. *Nat Rev Neurosci, 11*(2), 100-113. doi:10.1038/nrn2774

Vossen, A., Gross, J., & Thut, G. (2015). Alpha Power Increase After Transcranial Alternating Current Stimulation at Alpha Frequency (alpha-tACS) Reflects Plastic Changes Rather Than Entrainment. *Brain stimulation, 8*(3), 499-508. doi:10.1016/j.brs.2014.12.004

Wagenaar, D. A., & Potter, S. M. (2002). Real-time multi-channel stimulus artifact suppression by local curve fitting. *J Neurosci Methods, 120*(2), 113-120.

Walker, J. E. (2008). Power spectral frequency and coherence abnormalities in patients with intractable epilepsy and their usefulness in long-term remediation of seizures using neurofeedback. *Clin EEG Neurosci, 39*(4), 203-205.

Wilson, H. R., & Cowan, J. D. (1972). Excitatory and inhibitory interactions in localized populations of model neurons. *Biophys J, 12*(1), 1-24. doi:10.1016/S0006-3495(72)86068-5

Woltering, S., Jung, J., Liu, Z., & Tannock, R. (2012). Resting state EEG oscillatory power differences in ADHD college students and their peers. *Behav Brain Funct, 8*, 60. doi:10.1186/1744-9081-8-60

Yushkevich, P. A., Piven, J., Hazlett, H. C., Smith, R. G., Ho, S., Gee, J. C., & Gerig, G. (2006). User-guided 3D active contour segmentation of anatomical structures: significantly improved efficiency and reliability. *NeuroImage, 31*(3), 1116-1128. doi:10.1016/j.neuroimage.2006.01.015

Zaehle, T., Rach, S., & Herrmann, C. S. (2010). Transcranial alternating current stimulation enhances individual alpha activity in human EEG. *PloS one, 5*(11), e13766. doi:10.1371/journal.pone.0013766

CHAPTER 6: TARGET ENGAGEMENT WITH TRANSCRANIAL CURRENT STIMULATION1

MECHANISTIC INSIGHTS FROM ANIMAL STUDIES

Although tCS is non-invasive stimulation modality with an outstanding safety track record for the use in humans, studies in animal models are of high importance. Animal studies play a crucial role in understanding the mechanisms by which tCS modulates brain activity. First, animal experiments allow for the use of invasive electrophysiology such as the insertion of recording microelectrodes into the brain. Such recordings overcome the technical difficulties of simultaneously stimulating and recording electric activity since action potential signals occur in a different frequency band (typically 300 - 5000 Hz) than the stimulation artifacts, which exhibit a spectral peak at the stimulation frequency (typically below 100 Hz). Therefore, the stimulation artifact can be removed by high-pass filtering for the study of neuronal firing. Second, reduced *in vitro* preparations such as the slice preparation offer the opportunity to study the effects of weak electric fields under controlled experimental conditions.

EFFECT OF ELECTRIC FIELDS ON INDIVIDUAL NEURONS

One of the first observations of the effect of electric fields on neurons goes back many decades when Terzuolo and Bullock (Terzuolo & Bullock, 1956) applied a 1 mV/mm field to spontaneously active cardiac ganglion neurons of a lobster. The spontaneous firing rate of the cells was increased by the electric field. Similar modulation of neuronal firing rates by constant electric fields was also reported for other species (Creutzfeldt, Fromm, & Kapp, 1962; Purpura & McMurtry, 1965). In 1988, Chan and colleagues (Chan, Hounsgaard, & Nicholson, 1988) demonstrated that an applied electric field depolarizes the membrane voltage even when action potentials were blocked with the sodium-channel blocker tetrodotoxin. This demonstrated that the membrane depolarization caused by electric fields was a

[1] This chapter previously appeared as part of a book chapter in Transcranial Direct Current Stimulation in Neuropsychiatric Disorders: Clinical Principals and Management; doi: 10.1007/978-3-319-33967-2_11 The original citation is as follows: Andre Russowski Brunoni, Michael A. Nitsche and Colleen Loo. Target Engagement with Transcranial Current Stimulation. Transcranial Direct Current Stimulation in Neuropsychiatric Disorders: Clinical Principals and Management. Springer. *In Press*.

passive event, i.e. no opening or closing of ion channels was required. Rather, the ions within neurons change position in the presence of an external electric field. As the charge carriers redistribute within the cell to compensate for the applied field, the intracellular potential changes. The two distal poles of the structure aligned with electric field exhibit a depolarization and a hyperpolarization, respectively. This process is called *polarization* and depends on the overall length of the neuron as measured along the direction of the applied electric field (Figure 6.1). Therefore the orientation and size of the cell play a role in the response to the application of electric fields.

In addition, the change in the membrane voltage also depends on both the amplitude and frequency of the applied field. To demonstrate that the change in membrane voltage is dependent on the strength of the electric field, fields ranging from -40 to +60 mV/mm were applied along the somato-dendritic axis of CA1 cells and the change in membrane voltage at somata recorded in acute hippocampal slices (Bikson et al., 2004). The resulting polarization linearly depended on the strength of the applied electric field. This work was then extended to sine-wave (AC) electric fields in CA3 pyramidal cells (Deans, Powell, & Jefferys, 2007). The change in membrane potentials resulting from AC electric fields were less than those of DC fields of the same strength. The relationship between the field strength and the membrane depolarization was still linear but the slope, which quantifies the change in membrane voltage for every V/m of electric field, was decreased with increased frequency. Frequencies ranging from 5 to 100 Hz were applied and the change in the slope exponentially decay with the frequency of the applied electric field. This frequency dependence is caused by the low-pass filtering property of the passive cell membrane.

INTERACTIONS OF NETWORK OSCILLATIONS AND ELECTRIC FIELDS

The change in membrane voltage of a single neuron by tCS electric fields is too small to evoke action potentials in a cell at its resting potential in absence of synaptic input. Therefore, the effects of tDCS and tACS depend on the interaction of the applied stimulation and the endogenous network dynamics. *In vitro*, a DC electric field changed the timing of action potentials; this effect correlated with the strength of the electric field (Radman, Su, An, Parra, & Bikson, 2007). In contrast, AC fields increase the likelihood of spikes to occur during the first quarter cycle (0 to 90 degrees) of the sinewave. Two

mechanisms of recruiting the dynamics of neuronal networks have been suggested (Thut, Schyns, & Gross, 2011; Vossen, Gross, & Thut, 2015): plasticity and entrainment. First, the temporal grouping of neuronal firing imposed by AC fields may boost spike-timing dependent plasticity. Second, the AC field may impose its rhythmic structure on the neuronal dynamics such that at very cycle, the active neuron fire at a specific time of the oscillation cycle. Human studies (see below) provide early evidence for both mechanism and likely a combination of the two may be eventually determined as the underlying mechanism of the modulation of neuronal networks with AC fields.

Here, we now consider the effects of weak electric fields on network of neurons in animal model systems. In particular, slice experiments have provided important insights on the interactions between the ongoing network activity and the applied electric fields. Few slice preparations exhibit spontaneous network oscillations, presumably because of (1) the relative lack of synaptic inputs due to the differentiation inherent to this preparation and (2) impaired neuromodulatory in tissue slices tone in comparison to the intact brain. However, oscillations may occur spontaneously in the slice preparation in more *in vivo*-like ionic conditions (Sanchez-Vives & McCormick, 2000) and in response to pharmacological activation (Williams & Kauer, 1997). More recently, optogenetic stimulation has uncovered *in vivo*-like activity patterns in the slice preparation (Beltramo et al., 2013). Therefore, these experimental strategies can be combined with the application of external electric fields for the study of the mechanisms of tCS. For example, pharmacological activation of hippocampal slices caused the emergence of gamma oscillations that were susceptible to weak DC electric fields (Reato, Rahman, Bikson, & Parra, 2010). Interestingly, the effect of the DC field was asymmetry with regards to the polarity. Hyperpolarizing fields were more effective at suppressing this network oscillation than depolarizing fields were at enhancing the same activity pattern. In case of AC fields, for sufficiently low stimulation frequency, the amplitude of the gamma oscillation was periodically modulated, reminiscent of the theta-nested gamma oscillation (Canolty et al., 2006). The most complex effect occurred if the stimulation frequency was similar to the frequency of the endogenous oscillation. In this case, three simultaneous frequencies were observed. The endogenous oscillation was reduced (but still present) while oscillations half a harmonic above and below the endogenous frequency appeared. Thus, the effects of AC stimulation can be highly nonlinear since in linear systems the observed output exhibits the same

frequency as the input signal. In other words, neuronal networks may act as an energy transfer filter whereby energy in one frequency may be shifted into different frequency bands.

The interaction of electric field stimulation and endogenous oscillation appears to not only depend on the frequencies of both but their relative amplitudes. In a study of low frequency (1 Hz) oscillations evoked by optogenetic stimulation, it was observed that electric fields of a mismatched frequency would enhance the power of the endogenous oscillation often without increasing power at the frequency of the electric field (Schmidt, Iyengar, Foulser, Boyle, & Frohlich, 2014). This occurred when the optogenetic drive and therefore the "endogenous" oscillations were strong and the electric field was relatively weak. However the power of the oscillations at the stimulation frequency was enhanced when the magnitude of the endogenous oscillation was reduced (lower light intensity for optogenetic stimulation) or the strength of the electric field was increased. Taken together, the response of neural networks depends both on the frequency and the power (relative to the endogenous oscillation) of the electric field used for stimulation. Furthermore, these results demonstrate that the response of cortical networks to tCS may be non-linear in nature.

So far, we have focused on the response to stationary stimulation waveforms; however endogenous neural activity is not stationary. To this end endogenous activity may be better manipulated with feedback control algorithms than with static pre-programmed stimulation waveforms. One such example is the modulation of seizure-like, epileptiform electric events in slices. The application of DC fields can suppress epileptiform activity in hippocampal slices, which exhibit spontaneous seizure-like activity, however the network quickly adapted to the stimulation and epileptiform activity returned (Gluckman et al., 1996). In a follow-up study, non-stationary electric stimulation was applied to suppress seizure-like activity (Gluckman, Nguyen, Weinstein, & Schiff, 2001). The authors were able to suppress seizure activity for 16 minutes using a negative feedback stimulation paradigm on a hippocampal slice which exhibited seizure events every 40 seconds. Critically, spontaneous activity still occurred while epileptiform activity was suppressed. Thus, in the case of suppression of epileptiform activity with tCS, these studies show that adaptive feedback stimulation may have greater effect on network dynamics than constant stimulation. Indeed, there is also evidence that feedback stimulation has uses outside of suppression of aberrant activity. In spontaneously oscillating slices of ferret visual cortex, positive

feedback stimulation with electric field was shown to decrease the length of time between cortical up states and increase the strength of the endogenous oscillation (Frohlich & McCormick, 2010). Conversely, the application of negative feedback stimulation to the slices reduced strength of the endogenous oscillation. Interestingly, this effect was accomplished with stimulation amplitudes similar to the amplitude of endogenous electric fields recorded *in vivo* (1 mV/mm).

OUTLASTING EFFECTS OF ELECTRIC FIELDS

One of the most exciting aspects of tCS is that the effects of stimulation can outlast the stimulation as demonstrated by sustained modulation of motor-evoked potentials after completion of stimulation (Nitsche & Paulus, 2000). This "outlasting effect" of tDCS has been studied in animal models and slice preparations. Most *in vitro* studies have reported no outlasting effects of weak electric fields however the stimulation duration in these studies was typically short. With a longer stimulation duration, outlasting effects were observed more than 10 minutes after the end of 10 minute DC stimulation with higher field amplitudes (i.e. 10 V/m and higher) than what can be expected to occur with tCS in humans (Reato, Bikson, & Parra, 2015). *In vivo*, tDCS over somatosensory cortex applied to rabbits modulated eyeblink conditioning; however, an outlasting effect of tDCS only occurred for cathodal stimulation (Marquez-Ruiz et al., 2012). The underlying mechanism was probed by paired pulse experiments which revealed that spike-time dependent long-term depression (LTD) was activated by tDCS. Moreover the resulting LTD was suppressed by pharmacological blockade of adenosine receptors by a local injection. Both long-term potentiation (LTP) and paired-pulse facilitation (PPF) was increased after DC field application in hippocampal slices (Rohan, Carhuatanta, McInturf, Miklasevich, & Jankord, 2015). Intriguingly, LTP (but not PPF) was also enhanced in hippocampal slices of rats which had received anodal tDCS 24 hours earlier. Application of an NMDA antagonist prevented LTP induction but not paired pulse facilitation. In slices of mouse motor cortex, the application of DC field enhanced synaptic strength when paired with a low-frequency electric stimulation of afferent pathways (Fritsch et al., 2010). Importantly, this observed form of LTP depended on NMDA receptors and brain-derived neurotrophic factor (BDNF). Today's limited evidence therefore suggests that tDCS activate multiple, diverse plasticity mechanisms, both pre- and

postsynaptic, depending on the brain region, polarity (anodal vs cathodal) of stimulation, and other poorly understood factors.

INTERACTION OF CELLULAR AND NETWORK MECHANISMS

The main target of tCS is cortical networks due to their positions closest to the stimulation electrodes. The circuits in neocortex are composed of different cell types that exhibit distinct morphology and electrophysiological properties. Importantly, not all cell types respond equally to weak electric fields. This was demonstrated by the combination of patch recordings of the somatic membrane voltage with careful reconstruction of cell morphology (Radman, Ramos, Brumberg, & Bikson, 2009). Layer 5 (L5) pyramidal cells were shown to have the largest change in membrane voltage in response to externally applied electric fields due to their morphology and orientation within cortex. These cells exhibit an elongated somato-dendritic axis that spans from L5 to L1. In addition, the somato-dendritic axis is approximately perpendicular to the surface of the brain meaning that the cells are properly aligned to receive energy from an external electric field orthogonal to the skull. Note that the folding of cortex introduces additional complexity, which for the purpose of this section we do not further discuss. Because L5 pyramidal neurons are the likely primary targets of tCS, we can expect that their response to stimulation play a critical role in the modulation of cortical network dynamics. Therefore, considering the intrinsic dynamics of this cell type will provide clues with regards to the network-level effects of stimulation. The response of L5 pyramidal cells to subthreshold changes in membrane voltages, particularly in the prefrontal cortex, has been well studied by current-clamp whole-cell patch clamp experiments; these cells respond best to subthreshold perturbations in the theta frequency (4-8 Hz) band (Hu, Vervaeke, & Storm, 2002; Hutcheon & Yarom, 2000). This suggests that electric fields of a given strength will cause the largest subthreshold oscillations in the theta band and that AC field stimulation preferentially modulates low frequency oscillation in cortex. However, direct experimental evidence confirming this link between single cell excitability, cell morphology, and network level effects have not yet been reported.

FIGURES

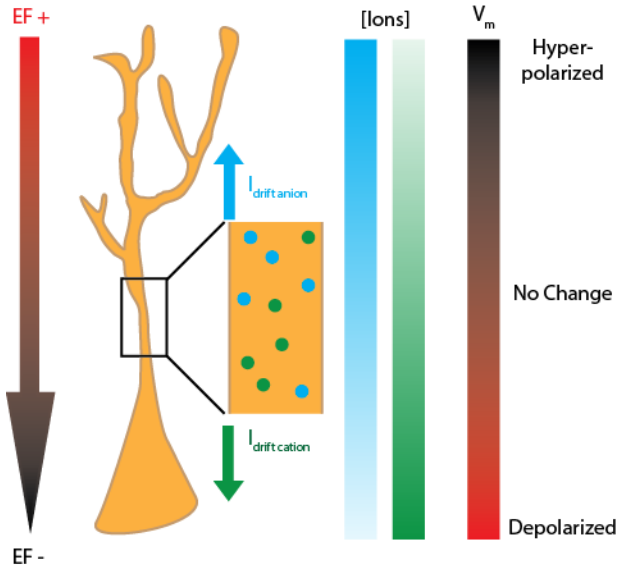

Figure 6.1. Schematic illustration of how an electric field changes the membrane voltage of a neuron.

The electric field (EF) is indicated with the *arrow* to the left of the neuron. When an electric field is applied (parallel to the somato-dendritic axis of a neuron), cations and anions move in opposite direction to cancel out the electric potential gradient imposed by the field within the neuron. The membrane voltage is defined as the difference between the electric potentials inside and outside the cell. Therefore, the gradient in the extracellular potential leads to a net depolarization of one end of the neuron (cell body) and a hyperpolarization of the other end of the neuron (distal apical dendrites).

REFERENCES

Beltramo, R., D'Urso, G., Dal Maschio, M., Farisello, P., Bovetti, S., Clovis, Y., . . . Fellin, T. (2013). Layer-specific excitatory circuits differentially control recurrent network dynamics in the neocortex. *Nature neuroscience, 16*(2), 227-234. doi:10.1038/nn.3306

Bikson, M., Inoue, M., Akiyama, H., Deans, J. K., Fox, J. E., Miyakawa, H., & Jefferys, J. G. (2004). Effects of uniform extracellular DC electric fields on excitability in rat hippocampal slices in vitro. *The Journal of physiology, 557*(Pt 1), 175-190. doi:10.1113/jphysiol.2003.055772

Canolty, R. T., Edwards, E., Dalal, S. S., Soltani, M., Nagarajan, S. S., Kirsch, H. E., . . . Knight, R. T. (2006). High gamma power is phase-locked to theta oscillations in human neocortex. *Science, 313*(5793), 1626-1628. doi:10.1126/science.1128115

Chan, C. Y., Hounsgaard, J., & Nicholson, C. (1988). Effects of electric fields on transmembrane potential and excitability of turtle cerebellar Purkinje cells in vitro. *The Journal of physiology, 402*, 751-771.

Creutzfeldt, O. D., Fromm, G. H., & Kapp, H. (1962). Influence of transcortical d-c currents on cortical neuronal activity. *Exp Neurol, 5*, 436-452.

Deans, J. K., Powell, A. D., & Jefferys, J. G. (2007). Sensitivity of coherent oscillations in rat hippocampus to AC electric fields. *The Journal of physiology, 583*(Pt 2), 555-565. doi:10.1113/jphysiol.2007.137711

Fritsch, B., Reis, J., Martinowich, K., Schambra, H. M., Ji, Y., Cohen, L. G., & Lu, B. (2010). Direct current stimulation promotes BDNF-dependent synaptic plasticity: potential implications for motor learning. *Neuron, 66*(2), 198-204. doi:10.1016/j.neuron.2010.03.035

Frohlich, F., & McCormick, D. A. (2010). Endogenous electric fields may guide neocortical network activity. *Neuron, 67*(1), 129-143. doi:10.1016/j.neuron.2010.06.005

Gluckman, B. J., Neel, E. J., Netoff, T. I., Ditto, W. L., Spano, M. L., & Schiff, S. J. (1996). Electric field suppression of epileptiform activity in hippocampal slices. *Journal of neurophysiology, 76*(6), 4202-4205.

Gluckman, B. J., Nguyen, H., Weinstein, S. L., & Schiff, S. J. (2001). Adaptive electric field control of epileptic seizures. *The Journal of neuroscience : the official journal of the Society for Neuroscience, 21*(2), 590-600.

Hu, H., Vervaeke, K., & Storm, J. F. (2002). Two forms of electrical resonance at theta frequencies, generated by M-current, h-current and persistent Na+ current in rat hippocampal pyramidal cells. *The Journal of physiology, 545*(Pt 3), 783-805.

Hutcheon, B., & Yarom, Y. (2000). Resonance, oscillation and the intrinsic frequency preferences of neurons. *Trends in neurosciences, 23*(5), 216-222.

Marquez-Ruiz, J., Leal-Campanario, R., Sanchez-Campusano, R., Molaee-Ardekani, B., Wendling, F., Miranda, P. C., . . . Delgado-Garcia, J. M. (2012). Transcranial direct-current stimulation modulates synaptic mechanisms involved in associative learning in behaving rabbits. *Proceedings of the National Academy of Sciences of the United States of America, 109*(17), 6710-6715. doi:10.1073/pnas.1121147109

Nitsche, M. A., & Paulus, W. (2000). Excitability changes induced in the human motor cortex by weak transcranial direct current stimulation. *The Journal of physiology, 527 Pt 3*, 633-639.

Purpura, D. P., & McMurtry, J. G. (1965). Intracellular Activities and Evoked Potential Changes during Polarization of Motor Cortex. *Journal of neurophysiology, 28*, 166-185.

Radman, T., Ramos, R. L., Brumberg, J. C., & Bikson, M. (2009). Role of cortical cell type and morphology in subthreshold and suprathreshold uniform electric field stimulation in vitro. *Brain stimulation, 2*(4), 215-228, 228 e211-213. doi:10.1016/j.brs.2009.03.007

Radman, T., Su, Y., An, J. H., Parra, L. C., & Bikson, M. (2007). Spike timing amplifies the effect of electric fields on neurons: implications for endogenous field effects. *The Journal of neuroscience : the official journal of the Society for Neuroscience, 27*(11), 3030-3036. doi:10.1523/JNEUROSCI.0095-07.2007

Reato, D., Bikson, M., & Parra, L. C. (2015). Lasting modulation of in vitro oscillatory activity with weak direct current stimulation. *Journal of neurophysiology, 113*(5), 1334-1341. doi:10.1152/jn.00208.2014

Reato, D., Rahman, A., Bikson, M., & Parra, L. C. (2010). Low-intensity electrical stimulation affects network dynamics by modulating population rate and spike timing. *The Journal of neuroscience : the official journal of the Society for Neuroscience, 30*(45), 15067-15079. doi:10.1523/JNEUROSCI.2059-10.2010

Rohan, J. G., Carhuatanta, K. A., McInturf, S. M., Miklasevich, M. K., & Jankord, R. (2015). Modulating Hippocampal Plasticity with In Vivo Brain Stimulation. *The Journal of neuroscience : the official journal of the Society for Neuroscience, 35*(37), 12824-12832. doi:10.1523/JNEUROSCI.2376-15.2015

Sanchez-Vives, M. V., & McCormick, D. A. (2000). Cellular and network mechanisms of rhythmic recurrent activity in neocortex. *Nature neuroscience, 3*(10), 1027-1034. doi:10.1038/79848

Schmidt, S. L., Iyengar, A. K., Foulser, A. A., Boyle, M. R., & Frohlich, F. (2014). Endogenous cortical oscillations constrain neuromodulation by weak electric fields. *Brain stimulation, 7*(6), 878-889. doi:10.1016/j.brs.2014.07.033

Terzuolo, C. A., & Bullock, T. H. (1956). Measurement of Imposed Voltage Gradient Adequate to Modulate Neuronal Firing. *Proceedings of the National Academy of Sciences of the United States of America, 42*(9), 687-694.

Thut, G., Schyns, P. G., & Gross, J. (2011). Entrainment of perceptually relevant brain oscillations by non-invasive rhythmic stimulation of the human brain. *Frontiers in psychology, 2*, 170. doi:10.3389/fpsyg.2011.00170

Vossen, A., Gross, J., & Thut, G. (2015). Alpha Power Increase After Transcranial Alternating Current Stimulation at Alpha Frequency (alpha-tACS) Reflects Plastic Changes Rather Than Entrainment. *Brain stimulation, 8*(3), 499-508. doi:10.1016/j.brs.2014.12.004

Williams, J. H., & Kauer, J. A. (1997). Properties of carbachol-induced oscillatory activity in rat hippocampus. *Journal of neurophysiology, 78*(5), 2631-2640.

CHAPTER 7: DISCUSSION

The work presented here falls into two categories: (1) dissection of how ion channels affect network dynamics and (2) the effect of electrical stimulation on network dynamics. As basic science, the first category can be incorporated into the RDoC framework. The RDoC framework rests on the assumption that network activity can be used to identify mental illness but that the underlying cause is biomolecular (Insel et al., 2010). To begin to reconcile data from studies based on molecular methods with aberrant activity at the network level, I have presented two studies which addressed the gap between ion channels and network activity. The second category, the study of the effect of electrical stimulation, also falls under the RDoC framework. Electrical stimulation interacts with network activity making it an attractive intervention for manipulation of targets identified as network level correlates of mental illness. The works presented here have focused on the mechanisms by which electrical stimulation interacts with ongoing network activity. Such mechanistic studies are critical for the rational design of brain stimulation for targeting psychiatric disease.

Chapters 2 and 3 focused on the dissection of networks dynamics as a function of the activation of ion channel species. Such work represents a first step to begin to relate network activity to molecular change by relating network activity to ion channels and receptors. In Chapter 2, I presented a study of the effect two types of metabotropic receptors on network dynamics. Specifically, I examined the effects of cholinergic and noradrenergic activation on the network dynamics of slices of V1. Such neuromodulators bind to metabotropic receptors which cause biomolecular changes within the cells. *In vivo*, these two neuromodulators play key roles in the regulation of wakefulness and memory. In this study, agonists were applied for 30 minutes and the activity compared to baseline. Application of agonists increased the average FR of the network and increased the network complexity. Slices bathed in cholinergic agonist CCh slowly returned to baseline FR after the washout began and CCh was removed from the bath. However, the effect of application of NE on FR was found to outlast the application of NE by at least 30

minutes when applied in 10 or 50 μM concentrations. Future studies will be needed to determine the cause of the outlasting effect of NE on the FR, however I hypothesize that this outlasting effect of NE was due to long term potentiation of synapses based on previous research on the effect of NE on spike-time dependent plasticity. Of specific interest, no temporally patterned stimulus was given here. Network activity was maintained by the ionic concentrations of the aCSF before addition of the agonists and further increased by the addition of neuromodulators. Any long term potentiation induced by the application of NE arose from the temporal pattern of spontaneous activity. This result indicates that in networks, long term potentiation may be induced without periodic stimulus, but rather given sufficient neuromodulatory tone, the endogenous network dynamics alone may induce plastic mechanisms.

In Chapter 3 I presented a study on the frequency response of networks of mPFC driven by oscillatory input to L5 PYs. This study related the activity of voltage gated ion channels to the frequency response of networks. Successful execution of this study critically depended on the ability of oscillatory input to L5 PYs is able to recruit low frequency oscillations similar to those found *in vivo* (Beltramo et al., 2013). However in this work, I have examined to what extent rhythmic stimulation can recruit the network at frequencies ranging from slow oscillations (0.25 Hz) to the upper edge of the beta band (29 Hz). Stimulation of L5 PYs was best able to recruit the network to fire with stimuli in the delta and theta bands (1 to 7 Hz). Pharmacological blockade of ion channels isolated the effects of synaptic transmission, I_h and $I_{M,}$ on the frequency response of networks. The blockade or synaptic transmission, I_h or I_M, reduced the resonant frequency of the network by increasing the response to low frequency stimulus relative to other frequencies. The interaction of I_h and I_M with synaptic transmission was then observed by suppressing synaptic transmission and further blocking I_h or I_M. Interestingly, the effect of I_h on the frequency response was dependent on synaptic transmission however that of I_M was not. When combined with the result that stimulation of GABAergic neurons produced I_h-dependent resonance in networks (Stark et al., 2013), it is possible that resonance due to I_M was caused by dynamics of excitatory synaptic transmission while resonance due to I_h was critically dependent on GABA transmission. This hypothesis was not directly tested due to concerns of excitotoxicity when applying strong depolarizing stimulus during the suppression of GABAergic synaptic transmission.

Chapters 4 through 6 focused on electrical stimulation as a method for perturbing the network level activity in the brain with the ultimate goal of treatment of mental illness. Chapter 4 examined the hypothesis that electric field stimulation necessarily entrains network oscillations. This entrainment hypothesis is the underlying assumption of many behavioral interventions by electrical brain stimulation. However, tACS contaminates simultaneous EEG recordings, and so the hypothesis that tACS entrains network oscillations has not been directly tested in human participants. To begin to address this I have tested this hypothesis in cortical slice. Due to the expression of ChR2 in many L5 PYs, stimulation with blue light applied to acute slices of V1 evoked a continuous oscillation which modeled oscillatory drive from other brain networks. Electric field stimulation was then applied as a model of tACS. The EF stimulation enhanced the endogenous oscillation at 1 Hz regardless of the EF frequency when the amplitude of the endogenous oscillation was larger. However when the optogenetically evoked oscillation was reduced to low amplitude by reducing the intensity of the light stimulation, EF stimulation increased power at the frequency of the EF stimulation rather than the endogenous oscillation. These results indicate that stimulation may not entrain networks in all cases. Instead in the case of large magnitude endogenous oscillations, stimulation may enhance the ongoing oscillation. This result is particularly applicable to the occipital alpha oscillation. Occipital alpha oscillations are a high amplitude oscillation in healthy human participants. The amplitude of the alpha oscillation can be easily modulated by the participants, when the participants' eyes are closed the alpha oscillation is very high magnitude, when the participants' eyes are open the oscillation is lower magnitude but still identifiable. Indeed a recent study found that tACS could not increase the amplitude of alpha oscillations in participants with their eyes closed (Neuling, Rach, & Herrmann, 2013). Together these results suggest that the occipital alpha oscillation, particularly in the eyes closed state, may be a particularly difficult target for tACS. Due to its high stationarity compared to other cortical oscillations, the occipital alpha oscillation is often targeted with tACS. However the results of the study presented in chapter 4 challenge the assumption that tACS entrains the high amplitude, eyes closed occipital alpha oscillation in all cases.

In Chapter 5, I presented work examining the interaction of brain stimulation and cortical oscillations in human participants. This study utilized direct electrical stimulation of the cortical surface through ECoG electrodes implanted on patients in the epilepsy monitoring unit prior to tissue resection for

treatment of epilepsy. Stimulation was applied while the participants were in two distinct states based on network activity, namely high and low levels of alpha activity. The network state, the amplitude of occipital alpha oscillations, was modulated by the participant changing behavioral state. High levels of occipital alpha were recorded with eyes closed, while low occipital alpha levels were recorded when the participant was either in eyes open resting state or task-engaged state. As predicted by *in vitro* results and computational models, in the presence of high amplitude alpha oscillations, stimulation was unable to change the frequency of the ongoing alpha oscillation. However, when the amplitude of the endogenous alpha oscillation was relatively low, stimulation was able to increase oscillatory power at the stimulation frequency. Despite the short duration of the stimulus (5 s), the effect of stimulation was significant even after the offset of the stimulation. Of particular interest, in one participant the endogenous oscillation was a subharmonic of the stimulation frequency; in this case, stimulation increased power at both the endogenous and stimulation frequencies. This result implies that, as with Arnold tongues, entrainment may occur at rational fractions of the stimulation frequency. This implication has been further suggested by a follow-up computational study demonstrating entrainment of both harmonic and subharmonic frequencies (Herrmann, Murray, Ionta, Hutt, & Lefebvre, 2016). Such harmonic entrainment may be useful for activation of high frequency oscillations. Due to the capacitance of the cell membrane, high frequency electric fields cause a smaller depolarization of the membranes of the cells in the network (Deans, Powell, & Jefferys, 2007). Therefore, it may be useful to use a 15 Hz sinusoid to entrain 30 Hz activity; however this remains to be tested in human participants.

In Chapter 6, I reviewed animal studies which focused on the mechanisms of tCS. Such studies fall into two main categories: (1) the study of the acute effects of stimulation and (2) the outlasting effects of stimulation. The studies in the first category are often performed in cortical slice with spatially uniform electric fields. Such studies have formed the basis for our understanding of the acute effects of TCS but fail to account for complications which arise from the spatial inhomogeneity of the electric field in living animals with a convoluted neocortex (Rahman et al., 2013). The study of the outlasting effects of stimulation has been performed both *in vivo* and *in vitro*. To observe an outlasting effect of direct current stimulation *in vitro*, the strength of the electric field was increased to roughly ten times that used *in vivo* (Reato, Rahman, Bikson, & Parra, 2013). This finding supports the hypothesis that brain stimulation by

electric fields causes a small change in membrane potential and requires large populations of neurons for a significant effect. *In vitro* there are fewer cells and activity is sparser than *in vivo*, therefore there are fewer cells close to action potential threshold. This indicates that the magnitude of the stimulation must be increased to reach the critical point where outlasting effects are recruited. Conversely, when performed *in vivo*, the effect of tDCS may be driven by glia rather than the neurons directly (Monai et al., 2016). This proposed mechanism depends on noradrenergic and NMDA activation as a product of increased BDNF expression. That NMDA activity and BDNF expression is enhanced by tDCS agrees with recent animal studies (Fritsch et al., 2010; Podda et al., 2016; Rohan, Carhuatanta, McInturf, Miklasevich, & Jankord, 2015). Indeed the response to tDCS of human participants with the BDNF Val66Met polymorphism differs from those without this polymorphism (Antal et al., 2010). Compared to tDCS, the mechanism of the outlasting effect of tACS remains unclear. It is possible that tACS also causes noradrenergic activation of NMDA receptors. Indeed there is no proposed mechanism of glial activation by tDCS and so it is not yet possible to determine if tACS also activates glia based on current evidence. Indeed to date, there is no study demonstrating that the outlasting effect tACS is caused by a similar mechanism as tDCS. There is an alternative to the hypothesis that tACS and tDCS share mechanisms of action. Specifically when tACS entrains the oscillators across large regions of the brain, the phases of the oscillators become aligned and slowly desynchronize after the stimulation stops. The proposed time course of this desynchronization remains unspecified. These mechanisms are not mutually exclusive. It is possible that entrainment facilitates communication between regions in such a way to strengthen synapses between the regions. However it is crucial to determine the underlying mechanism of the outlasting effect of tACS for the development of treatment paradigms.

The RDoC framework provides a new, network centered view of psychiatric disease. Despite network level activity being the focus, it stresses that underlying biomolecular activity must be determined for network level disease traits. There is much work remaining to reconcile network activity with biomolecular traits. One such example is the case of cognitive deficits from schizophrenia. One hypothesis rests on the idea that the hippocampus, which is involved in memory recall, cannot appropriately communicate with the prefrontal cortex, which is involved in executive function. Molecular studies have demonstrated aberrant mRNA expression within fast-spiking GABAergic neurons in patients

with schizophrenia (Lewis, Hashimoto, & Volk, 2005). Such fast-spiking GABAergic interneurons have a resonant frequency in the gamma band (Cardin et al., 2009). Together these data provide a mechanism for aberrant gamma band oscillations in patients with schizophrenia (Uhlhaas & Singer, 2010). Deficits in the gamma band make an attractive target for treatment of cognitive symptoms of schizophrenia because synchrony in the gamma band between regions facilitates cognition (Fries, 2009). It therefore seems likely that activation of the gamma rhythm should treat cognitive symptoms of schizophrenia. Indeed a preliminary study of eleven patients with schizophrenia observed that gamma band tACS over dorsolateral prefrontal cortex was found to improve working memory compared to sham (Hoy, Whitty, Bailey, & Fitzgerald, 2016). In addition to in interneurons and gamma activity, the theta band offers a promising target for treatment of cognitive symptoms in patients with schizophrenia. The prefrontal cortex, hippocampus and ventral tegmental area are synchronized by theta band activity (Fujisawa & Buzsaki, 2011). Here I have presented a study which suggests that theta band synchrony depends on I_h (mediated by HCN channels) and GABAergic synaptic transmission. In patients with schizophrenia, the expression of proteins which constitute neuronal HCN channels and the ligand which gates the channels may also be dysregulated (Funk, McCullumsmith, Haroutunian, & Meador-Woodruff, 2012; Paspalas, Wang, & Arnsten, 2013). These results indicate that HCN channels are less effective in patients with schizophrenia. Applied here, it is therefore necessary for both physiological GABAergic activity and HCN channel expression for mPFC to best respond to theta band input from hippocampus and facilitate information transfer between the two regions. Therefore it is possible that increasing theta power by exogenous theta-band stimulus may restore function in patients with cognitive deficits from schizophrenia. Indeed a recent case study of three patients with clozapine-resistant schizophrenia found that theta band tACS negative and general symptoms of the disease (Kallel, Mondino, & Brunelin, 2016). The tACS studies referenced here are preliminary studies with low numbers of participants (11 and 3 participants respectively) however such work is a promising first step. These studies demonstrate how rational design of stimulation paradigms based on network level targets of disease can arise from understanding the neurobiology of disease.

The NIMH has recently begun to use RDOC which focuses on pathological network level activity as quantifiable measure of mental illness. As a network intervention brain stimulation with electric currents is

an attractive intervention for treatment of mental illness. However the rational design of brain stimulation paradigms for treatment of mental illness requires both an understanding of how brain stimulation interacts with ongoing activity and how such network level activity arises from cellular and synaptic components. The studies presented here contribute to our understanding of how network activity arises from cellular and synaptic components or how such activity interacts to brain stimulation. While much work remains, brain stimulation offers direct interaction with network level disease targets.

REFERENCES

Antal, A., Chaieb, L., Moliadze, V., Monte-Silva, K., Poreisz, C., Thirugnanasambandam, N., . . . Paulus, W. (2010). Brain-derived neurotrophic factor (BDNF) gene polymorphisms shape cortical plasticity in humans. *Brain stimulation, 3*(4), 230-237. doi:10.1016/j.brs.2009.12.003

Beltramo, R., D'Urso, G., Dal Maschio, M., Farisello, P., Bovetti, S., Clovis, Y., . . . Fellin, T. (2013). Layer-specific excitatory circuits differentially control recurrent network dynamics in the neocortex. *Nature neuroscience, 16*(2), 227-234. doi:10.1038/nn.3306

Cardin, J. A., Carlen, M., Meletis, K., Knoblich, U., Zhang, F., Deisseroth, K., . . . Moore, C. I. (2009). Driving fast-spiking cells induces gamma rhythm and controls sensory responses. *Nature, 459*(7247), 663-667. doi:10.1038/nature08002

Deans, J. K., Powell, A. D., & Jefferys, J. G. (2007). Sensitivity of coherent oscillations in rat hippocampus to AC electric fields. *The Journal of physiology, 583*(Pt 2), 555-565. doi:10.1113/jphysiol.2007.137711

Fries, P. (2009). Neuronal gamma-band synchronization as a fundamental process in cortical computation. *Annual review of neuroscience, 32*, 209-224. doi:10.1146/annurev.neuro.051508.135603

Fritsch, B., Reis, J., Martinowich, K., Schambra, H. M., Ji, Y., Cohen, L. G., & Lu, B. (2010). Direct current stimulation promotes BDNF-dependent synaptic plasticity: potential implications for motor learning. *Neuron, 66*(2), 198-204. doi:10.1016/j.neuron.2010.03.035

Fujisawa, S., & Buzsaki, G. (2011). A 4 Hz oscillation adaptively synchronizes prefrontal, VTA, and hippocampal activities. *Neuron, 72*(1), 153-165. doi:10.1016/j.neuron.2011.08.018

Funk, A. J., McCullumsmith, R. E., Haroutunian, V., & Meador-Woodruff, J. H. (2012). Abnormal activity of the MAPK- and cAMP-associated signaling pathways in frontal cortical areas in postmortem brain in schizophrenia. *Neuropsychopharmacology : official publication of the American College of Neuropsychopharmacology, 37*(4), 896-905. doi:10.1038/npp.2011.267

Herrmann, C. S., Murray, M. M., Ionta, S., Hutt, A., & Lefebvre, J. (2016). Shaping Intrinsic Neural Oscillations with Periodic Stimulation. *The Journal of neuroscience : the official journal of the Society for Neuroscience, 36*(19), 5328-5337. doi:10.1523/JNEUROSCI.0236-16.2016

Hoy, K. E., Whitty, D., Bailey, N., & Fitzgerald, P. B. (2016). Preliminary investigation of the effects of gamma-tACS on working memory in schizophrenia. *J Neural Transm (Vienna)*. doi:10.1007/s00702-016-1554-1

Insel, T., Cuthbert, B., Garvey, M., Heinssen, R., Pine, D. S., Quinn, K., . . . Wang, P. (2010). Research domain criteria (RDoC): toward a new classification framework for research on mental disorders. *The American journal of psychiatry, 167*(7), 748-751. doi:10.1176/appi.ajp.2010.09091379

Kallel, L., Mondino, M., & Brunelin, J. (2016). Effects of theta-rhythm transcranial alternating current stimulation (4.5 Hz-tACS) in patients with clozapine-resistant negative symptoms of schizophrenia: a case series. *J Neural Transm (Vienna)*. doi:10.1007/s00702-016-1574-x

Lewis, D. A., Hashimoto, T., & Volk, D. W. (2005). Cortical inhibitory neurons and schizophrenia. *Nat Rev Neurosci, 6*(4), 312-324. doi:10.1038/nrn1648

Monai, H., Ohkura, M., Tanaka, M., Oe, Y., Konno, A., Hirai, H., . . . Hirase, H. (2016). Calcium imaging reveals glial involvement in transcranial direct current stimulation-induced plasticity in mouse brain. *Nat Commun, 7*, 11100. doi:10.1038/ncomms11100

Neuling, T., Rach, S., & Herrmann, C. S. (2013). Orchestrating neuronal networks: sustained after-effects of transcranial alternating current stimulation depend upon brain states. *Frontiers in human neuroscience, 7*, 161. doi:10.3389/fnhum.2013.00161

Paspalas, C. D., Wang, M., & Arnsten, A. F. (2013). Constellation of HCN channels and cAMP regulating proteins in dendritic spines of the primate prefrontal cortex: potential substrate for working memory deficits in schizophrenia. *Cerebral cortex, 23*(7), 1643-1654. doi:10.1093/cercor/bhs152

Podda, M. V., Cocco, S., Mastrodonato, A., Fusco, S., Leone, L., Barbati, S. A., . . . Grassi, C. (2016). Anodal transcranial direct current stimulation boosts synaptic plasticity and memory in mice via epigenetic regulation of Bdnf expression. *Sci Rep, 6*, 22180. doi:10.1038/srep22180

Rahman, A., Reato, D., Arlotti, M., Gasca, F., Datta, A., Parra, L. C., & Bikson, M. (2013). Cellular effects of acute direct current stimulation: somatic and synaptic terminal effects. *The Journal of physiology, 591*(10), 2563-2578. doi:10.1113/jphysiol.2012.247171

Reato, D., Rahman, A., Bikson, M., & Parra, L. C. (2013). Effects of weak transcranial alternating current stimulation on brain activity-a review of known mechanisms from animal studies. *Frontiers in human neuroscience, 7*, 687. doi:10.3389/fnhum.2013.00687

Rohan, J. G., Carhuatanta, K. A., McInturf, S. M., Miklasevich, M. K., & Jankord, R. (2015). Modulating Hippocampal Plasticity with In Vivo Brain Stimulation. *The Journal of neuroscience : the official journal of the Society for Neuroscience, 35*(37), 12824-12832. doi:10.1523/JNEUROSCI.2376-15.2015

Stark, E., Eichler, R., Roux, L., Fujisawa, S., Rotstein, H. G., & Buzsaki, G. (2013). Inhibition-induced theta resonance in cortical circuits. *Neuron, 80*(5), 1263-1276. doi:10.1016/j.neuron.2013.09.033

Uhlhaas, P. J., & Singer, W. (2010). Abnormal neural oscillations and synchrony in schizophrenia. *Nature Reviews Neuroscience, 11*(2), 100-113.